THE HYDRATION CHEMISTRY OF BLENDED PORTLAND BLASTFURNACE SLAG CEMENTS FOR RADIOACTIVE WASTE ENCAPSULATION

Mark Tyrer

Doctor of Philosophy

THE UNIVERSITY OF ASTON IN BIRMINGHAM

July 1991

THE HYDRATION CHEMISTRY OF BLENDED PORTLAND BLASTFURNACE SLAG CEMENTS FOR RADIOACTIVE WASTE ENCAPSULATION

Mark Tyrer

Doctor of Philosophy

THESIS SUMMARY

Blended Portland-blastfurnace slag cements provide a suitable matrix for the encapsulation of low and intermediate level waste due to their inherantly low connective porosity and provide a highly alkaline and strongly reduced chemical environment.

The hydration mechanism of these materials is complex and involves several competing chemical reactions. This thesis investigates three main areas:

1) The developing chemical shrinkage of the system shows that the underlying kinetics are dominantly linear and estimates of the activation energy of the slag made by this method and by conduction calorimetry show it to be c.53 kJ/mol.

2) Examination of the solid phase reveals that calcium hydroxide is initially precipitated and subseqently consumed during hydration. The absolute rate of slag hydration is investigated by chemical and thermal methods and an estimation of the average silicate chain length (3 silicate units) by NMR is presented.

3) The developing pore solution chemistry shows that the system becomes rapidly alkaline (pH 13 - 13.5) and subsequently strongly reduced. Ion chromatography shows the presence of reduced sulphur species which are associated with the onset of reducing conditions.

In the above studies, close control of the hydration temperature was maintained and the operation of a temperature controlled pore fluid extration press is reported.

KEYWORDS Slag, Cement, Hydration, NMR, Kinetics.

This work is dedicated to the memory of
Iain McNaught Shaw 1959-1991

Acknowledgement

Grateful thanks are extended to the following for their help and support during this work:

Prof. C.L.Page, for his help, enthusiasm and encouragement throughout

Dr. M. Perry, for production of the NMR spectra

Prof. W.S. McWhinnie, for valuble advice about the above technique

Mr. C.J.Thompson, for maintaining the laboratory facilities and his help in repairing and calibrating the equipment

Dr. D.J. Lee, (UKAEA) for his advice and interest

Dr. R. Simmonds (UKAEA) for producing some high temperature thermograms

UKAEA Research Establishment Winfrith for the funding of this project

Particularly to my parents for their incalculable support and ecouragement

In addition, thanks are due to many friends and collegues, both in the Civil Engineering department and at the University Village whose encouragement was much appreciated.

List of contents

List of figures

List of Tables

Chapter 1

Introduction and Literature review

1.1 Introduction

Cementitious materials have been in use since ancient times and the oldest surviving concrete is thought to be that found in Yugoslavia (c.5600 B.C.) whilst examples from Egyptian (c.2500 B.C.) and Roman (c.300 B.C.) workings are well preserved. Indeed, the etymology of our modern words 'cement' and 'concrete' shows them to be from the Latin *'caementum'* (rough stone or chipping) and *'concretus'* (grown together,compounded). It was however, the work of Joseph Aspdin of Leeds which in 1824, founded the basis of the cement we know today. Aspdin's patented process involved the crushing and mixing of clay and limestone, which was subsequently fired in a kiln and ground to a fine powder. The resulting hydraulic cement he called 'Portland' cement, as it resembled the fine building stone quarried on the Isle of Portland and much prized by builders and architects over several centuries. Although Aspdin's procedure has been constantly refined and subjected to much tighter controls, the process has not essentially changed in the intervening years.

Blast furnace slag (BFS) has been used as a cementitious material for around 100 years. Emil Langen discovered the potential hydraulicity of glassy blast furnace slag in 1862 and the blended, Portland cement - blast furnace slag materials used today have been developed from this early work. Before the advent of sulphate resisting cement (SRPC), super - sulphated cement (1) was being produced in Scunthorpe during the 1950's, based upon 85% blast furnace slag. As the demand for this product declined following the development of SRPC, separately ground BFS became available from the same source in the 1960's.In comparison, Portland - blast furnace slag cement with a fixed BFS

content, has been produced in Ravenscraig, Glasgow for some sixty years.

Blast furnace slag is an industrial by - product of the steel industry and is the result of the addition of flux to the furnace during the production of pig iron. Limestone is added in the furnace charge to (principally) dissolve silicates present in the ore. The resulting molten mixture floats above the iron and may periodically, be extracted as necessary. This molten product has a high level of thermal energy, which, if dissipated by slow cooling, gives rise to a stable crystalline system of calcium and magnesium silico - aluminates, without hydraulic properties. It is necessary to prevent the slag attaining this low energy level by rapid chilling (granulation) to produce vitreous slag. The product so formed is in a higher energy state than if it were crystalline and shows latent hydraulic properties and a suitable chemistry for use as a cementitious material.

The history, production and utilization of blast furnace slag is well documented (2 - 8) and BFS production in the countries of "Cembureau" (European Cement Association) accounts for about 40 million Tonnes annually - approximately 20% of the total cement production (9).

It has long been a subject of heated debate how best to store non - heat generating radioactive waste. Various proposals have been evaluated (such as encapsulation in synthetic glasses, polymers and even bitumen) the most promising of which is encapsulation of the waste forms in cement . Before considering the rôle of cement in radioactive waste management, the source and nature of the various waste types is presented:

High level waste: Typically heat generating, α - emitting, long half - lives. (Mainly re-processing waste from depleted fuel elements, Actinides and fission products)

Intermediate level waste: Typically non - heat generating, some long

lived isotopes.(Fuel hulls,ion exchange/filter media, raffinates and borax waste).

Low level waste: Non - heat generating, isotopes of predominantly short half lives. (High bulk / low activity waste from a variety of sources i.e. research, industry, medicine).

Figure 1 (below) shows the principal stages in the nuclear fuel cycle. It is at the chemical processing and fuel reprocessing stages that the bulk of the intermediate level radioactive waste is generated and this may take a variety of forms.

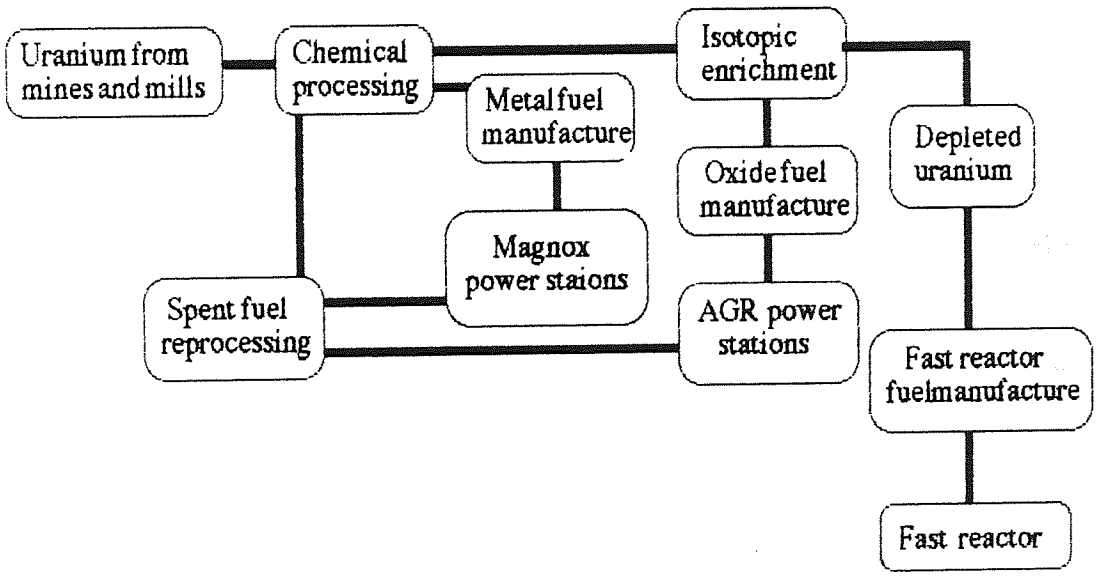

N.B. Some plutonium is recovered during reprocessing and is subsequently used in the fast reactor cycle. Oxide fuel is also used in pressurized water reactors.

Figure 1 *The nuclear fuel cycle showing the relationship between processing of nuclear materials and their use in power generation.*

Spent fuel from the thermal reactors is stored in cooling ponds to allow the decay of short - lived isotopes after which the fuel is transferred to the

reprocessing plant pond. Inside the reprocessing plant, the fuel pins are opened and the hulls are removed. The fuel pellets are then dissolved and the plutonium is separated by solvent extraction with tributyl phosphate in a mixture of alkanes.The unfissioned uranium and generated plutonium may be processed and subsequently used again. The high level fission product waste must then be concentrated and removed for long term storage.

The materials used in this processing, along with ion exchange and filter media used to clean the storage ponds (and heat exchanger waters) and the used fuel pin hulls, constitute the bulk of the intermediate level waste in the U.K. Typical examples are as follows:

Sodium nitrate / sulphate from evaporation of acid digests used in reprocessing.

Iron, from ferrous sulphamate used in solvent extraction

Aluminium nitrate (acid deficient) from reprocessing uranium - aluminium fuels in MTR (materials testing reactors).

SGHWR sludge (Steam generating heavy water moderated reactor). This contains fine 'Powdex' type resins, 'Metasil' (diatomaceous earth) type filter media, transition metal oxides and other inorganics.

Ion exchange resins - possibly with some tributyl phosphate from solvent extraction.

The above shows the wide range of materials which require encapsulation before ultimate disposal. Low level waste has, until recently, been buried in engineered shallow trenches (for example at the Drigg site in Cumbria) without encapsulation. Recent policy reviews suggest that future disposal will include some primary containment in addition to the geological barriers relied on so far. The 1986 House of Commons Environment committee chaired by Sir Hugh Rossi, on the management of radioactive waste, proposed that all intermediate level waste should ultimately be subject to deep burial.

The variety of low level waste material is extremely variable. The common feature of low level wastes is that by their nature they are high bulk

materials - items of industrial and laboratory equipment which have become contaminated, protective clothing, tissues and other cleaning material and a number of items which are suspected of being contaminated. Generally, low level waste is subjected to some form of volume reduction before encapsulation.

The rôle of cements in radioactive waste encapsulation is to act as both a physical and chemical barrier to the movement of the radionuclides, to provide some physical integrity to the waste and to resist the ingress of ground water, should the waste container be damaged. The advantages which cements offer over other media (such as bitumen) are that they are easily worked at room temperatures, are not very susceptible to radiolytic decomposition, are reasonably inexpensive and maintain a highly alkaline environment around the waste. This last property is of great importance as the actinide metals exhibit low aqueous solubility under conditions of high pH.

Initial trials with a range of cement types suggested that blast furnace slag blends would be the most suitable for a number of reasons . First, as slag is normally slightly finer than portland cement, the paste will compact more readily than in other types. This, coupled with the fine grained nature of the hydrates, results in a matrix with a very low connective porosity.The chemical environment in slag cements is known to be substantially different to that found in other types[10]. The pH of the pore solution is slightly reduced in comparison to portland cement (12.5 as opposed to 13) but significantly, the redox potential of the slag matrix is noticeably lower.The implications of this in terms of actinide chemistry are that uranium would exist as U^{4+} as opposed to the more soluble U^{6+} and that ruthenium would exist as the insoluble sulphide. Although the total available buffering capacity of slag cements is slightly less than that of portland cement, the advantages of its reducing environment and low permeability are seen to out weigh this.

The work done on slag cements until recent years has mainly concentrated on their physical properties as building materials and the chemistry of their production as by-products in steel manufacture. This project

was developed to examine the hydration chemistry of the slag cements likely to be used in radioactive waste encapsulation. These materials differ to those used in the construction industry in two important respects: Firstly they do not contain any aggregate or filler material and secondly they may contain a significantly higher proportion of blast furnace slag than that which would provide the high strengths required in building applications. Their strength requirement is limited to simply maintaining their physical integrity as the loads to which they will be subjected are low and the matrix is surrounded by a waste drum.

1.2 Objectives of project

The aims of this project are to elucidate some of the physico - chemical changes which occur during the hydration of slag cements. The principal objectives can be summarized as follows:

1) To attempt to characterize some of the rate determining steps in the kinetics of the hydration reactions.

2) To analyze isolated phases, both solid and liquid during the course of hydration.

3) To relate the chemical changes to the kinetic measurements made in 1)

The project is presented as a literature review followed by experimental work in the above order and includes in chapter two, observations made on the raw materials. The implications of the results are discussed in the final chapter and are presented with reference to the major changes in properties over the hydration period.

1.3 Literature review

Literature sources in this subject area are varied and spread between chemistry, construction and materials science publications. In the first instance, the abstracting journal "Cements Research Progress" revealed a large number of

primary sources which was complemented by an on line search of the "Chemical abstracts" data base. This preliminary review of the published work revealed extensive literature on the composition, hydration and particularly physical properties of Portland cement. Blast furnace slags, by comparison, despite their now wide acceptance, have attracted relatively little attention to anything other than their physical properties.

The literature of direct relevance can be grouped into two broad categories: First, that concerning slag and OPC composition and structure and secondly work on the hydration chemistry of blended portland - slag cements, including the microscopy of the developing hydrate structure and studies of the changing physical properties such as porosity and permeability.

1.3.1 The structure and composition of blast furnace slags.

Slag cements are essentially glassy materials which may contain small, euhedral crystalline domains. The bulk chemistry and mineralogy of slags have been reviewed extensively, most recently by Smolczyk (11). He classifies the potential minerals formed from the re - crystallization of basic glassy slags and includes potential minor phases obtained from a comparable acid slag. A similar review by Lea (5) complements this work as does a more fundamental study on the phase chemistry of the CaO -MgO - Al_2O_3 -SiO_2 system by Prince (12). The possible mineral compositions are shown in table 1.

It is important to remember that these mineral compositions have been obtained by slow recrystallization of a melt and that it is unlikely that they would comprise more than a small fraction of cementitious slag as this material is almost wholly glassy.

The previously held view that slag hydraulicity was proportional to, or at least dominated by glass content (13), prompted a number of papers (14,15,16,17,) concerned with the determination of glass content. In addition to this, The view that the Ca / Si ratio in part governs strength was found not always to be true. Frearson *et al* (15,16) and Smolczyk (11) explain these incongruities in terms of

phase chemistry during granulation. They identify essentially three types of particle in ground granulated blast furnace slag: The wholly glassy phase, the wholly crystalline phase and a phase containing dendritic merwinite with interstitial glass. It is this last, partially crystalline phase (now known to be highly reactive) which was formerly considered to be unreactive crystals.

Table 1 *Possible mineral composition of blast furnace slag*

Melilite (Gehlenite, C_2AS - Akermanite, C_2MS_2 solid solution series)	
Merwinite (C_3MS_2)	
Pyroxenes (in acid slags only) ie Diopside	
Dicalcium silicates (C_2S) $\alpha,\alpha',\beta,\gamma$. Polymorphs (Basic slags only)	
Monticellite (CMS)	
Rankinite (C_3S_2)	
Wollastonite / Pseudo wollastonite (CS)	
Oldhamite (CS)	
Anorthite (CAS_2)	(acid slags only)
Forsterite (M_2S)	
Enstatite (MS)	(acid slags only)
Perowskite (CT)	
Spinel (MA)	

Previous work by Van Loo (18) suggested that merwinite was unfavorable to the hydration of slag. Better knowledge of glass reactivity supercedes this belief and it is now thought (15,16) that a small degree of crystallization may enhance hydration. The mechanism for this anomalous behavior is not well understood but it is speculated that the residual strain energy in the glass is higher in these inter-grown phases and that dissolution in this situation may be aided by its release, perhaps analogously to stress corrosion cracking.

The crystallization of melilite at 1350° - 1450°C is almost totally

suppressed by rapid chilling during granulation. A very slight increase of the calcium content of a melilitic melt would cause merwinite to be the dominant species on recrystallization. As merwinitic crystallization occurs between 1450°C and 1600° C it is reasonable to expect some degree of incipient crystallization of this mineral within the blast furnace (1500°C). Consequently relatively small changes in the composition of the blast furnace charge, can cause significant changes in the mineralogy, and hence hydraulicity of the granulated slag.

N.B. "Cemsave" slag used in this project is of a composition which, if re-crystallized would yield dominantly melilite.

The glassy components in comparison with the above are of a much more complex nature. Lea (5) discusses two theories describing the structure of slag glasses, the latter (19) having attracted little attention in recent years. This postulates a micro-heterogeneity where domains of short range order ("embryos of crystallization") containing most of the cations are linked to poorly ordered regions, rich in anions.

The more popular view (11,20) is that of Zachariasen's network theory (21) which although long established and frequently modified, is still considered to be a useful model. The glass structure is considered to be a network of oxide poyhedra which, although they do not contain sufficient long range order to be distinguished by diffraction methods, have short range order comparable to crystals of similar composition. The disordered polyhedra (i.e. SiO_4^{4-}) exhibit low co-ordination numbers (tetrahedra and / or triangles) joined at the vertices by bridging oxygens. These are known as network formers and the elements suitable for forming these monomers have small ionic radii and the highest possible valencies. Other polyhedra with higher co-ordination numbers (six or eight) exist as network modifiers which introduce disorder into the system.The presence of these network modifiers results in variation of bond sequence (configurational change) and bond angle (conformational change). Figure 2 shows a somewhat stylized view of the glassy state which is approaching the structure of a silicate crystal lattice but is both highly strained and lacks long range order:

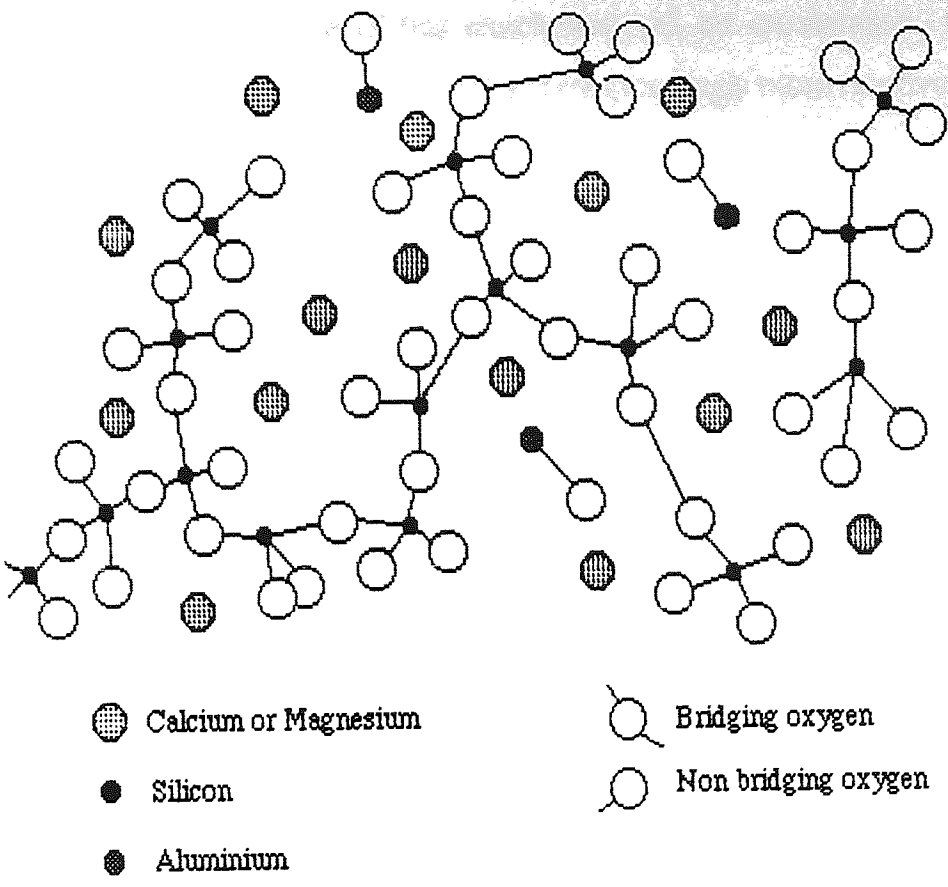

Figure 2 *Glass structure according to Zachariasen's network theory (After Dron)*

Figure 2 (21) can be interpreted in terms of Zachariasen's network theory of glasses such that the SiO_4^{4-} monomer is the dominant network former and calcium and magnesium are the major network modifiers.

Scott *et al* (22) Have produced a detailed study of the microstructure and phase relations of slag glasses and have examined the inter-growth of melilite and merwinite. The triangular plot in figure 3 shows the likely range of mineral compositions in BFS with Frodingham "Cemsave" occupying the upper half of the melilite field. These authors have identified tabular melilite crystals with inclusions of oldhamite in granulated slags and suggest that oldhamite is the first mineral to solidify from the melt.

Frearson and Uren (23) observe that merwinite contains no aluminium and suggest that as this mineral depletes the melt of calcium, magnesium and silicon it will, on crystallization, leave the residual melt relatively enriched in

aluminium. The consequence of this enrichment will be an increase in the abundance of network modifiers (Al) and a correspondingly more reactive glass.

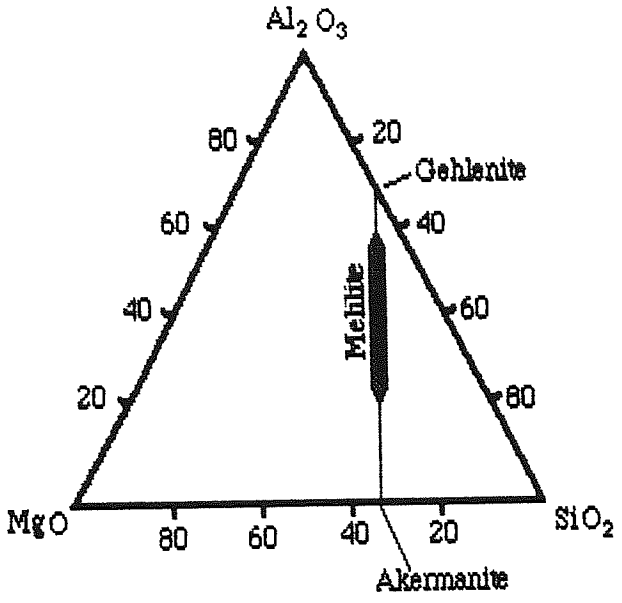

Figure 3 *Al - Mg - Si oxide ternary diagram showing melilite domain. (After Scott et al)*

In BFS, the tetrahedron SiO_4^{4-} is the monomer and network former, whilst octahedrally co-ordinated Ca^{2+} is the network modifier. As a network modifier, calcium depolymerizes the system in proportion to its concentration. Aluminium and magnesium may exist as either network formers (MeO_4) or modifiers (MeO_6) or both, and the redistribution of of Mg^{2+} and Al^{3+} into tetrahedral and octahedral sites depends on the composition of the slag and, for similar compositions, the thermal history of the melt. Aluminium may exist as a network former as AlO_4^{5-} or more advantageously as Al^{3+}, increasing the reactivity of the glass by depolymerization and, if in tetrahedral co-ordination,by the relatively weak Al-O bond. Magnesium has an analogous behavior in that slag reactivity increases when Mg^{2+} replaces Ca^{2+} in agreement with the lower ratio between charge and ionic radius of magnesium. Sersale (24) and Satarin (25) remark that in some slags of similar composition where the ratio between Al^{3+} and Mg^{2+}

octahedrally co-ordinated has been changed, the optimum strength (and it is assumed reactivity) is obtained at an MeO_6 / MeO_4 ratio of 0.35 and that the magnesium and aluminium ions remain mainly in the tetrahedral sites.

Regourd (26,27) reviews several papers concerned with the relationships between slag glass structure and its hydraulicity. She describes Roiak's work on electron paramagnetic resonance and infra-red spectroscopy (28) which concludes that slag reactivity is a function of the degree of depolymerization of the metal oxide - silica complexes. This work suggests that the observed differences in activity between slags of identical elemental composition is likely to be due to the energy of the metal - oxygen bond of the depolymerizing cation and to its co-ordination.

Regourd describes silicon atoms with one, two, or three singly bonded oxygen atoms in terms of a set of structural elements shown in figure 4 (overleaf). In a silicate glass, the structure deviates from the crystalline form by the weakening of some Si-O-Si bonds:

$$Si \text{ --- } O \text{ --- } Si \; + \; O^{2-} \; \rightarrow \; Si \text{ --- } O^{-} \; + \; Si \text{ --- } O^{-}$$

The resulting negative charges are neutralized by the incorporation of metal cations (structure modifiers) into the matrix of the glass. The connectivities "Q" (figure 5) of the SiO_4 tetrahedra range from Q=1 to Q=4 as the structure deviates from the crystalline state. In some of the tetrahedral sites atoms other than silicon are located (especially aluminium). Each such replacement of Si^{4+} by Al^{3+} is equivalent to one of SiO_2 by AlO_2^- and thus introduces a negative charge which is balanced by further introduction of metal cations (29). Similarly, at least some of the magnesium is in tetrahedral sites replacing silicon and this introduces two negative charges.

Calcium however, leads only to ionic bonds. It is the oxygen atom provided by the CaO which, in forming covalent bonds with the chain elements, in order of their affinity, determines the degree of chain branching. This idea diverges from Zachariasen's theory in that the limitation of chain branching is not strictly the degree of depolymerization, she argues, since monomers of the type SiO^{4-} and more surely AlO_4^{5-} are not thought to occur in

blast furnace slag. Regourd also makes the observation that Al and Mg are not found in octahedral co-ordination.

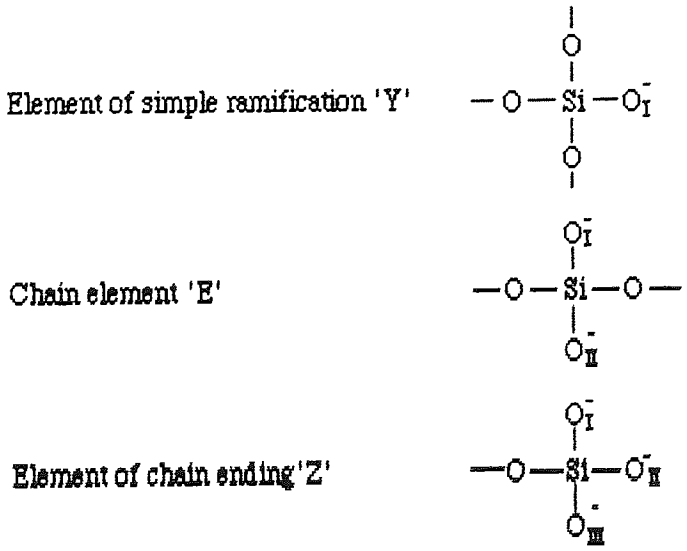

Because of its more metallic character, aluminium would be surrounded by four doubly bonded oxygens i.e:

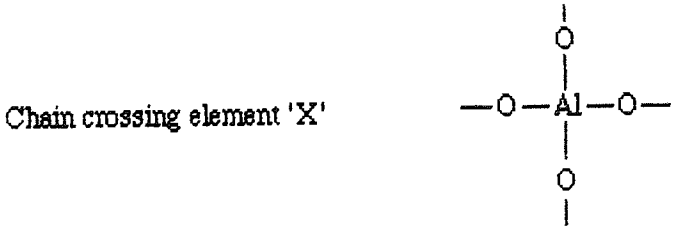

Figure 4 *Structural elements postulated for slag glass* *(After Dron)*

The minor components in BFS (Mn,Ti, S) (28) are thought to play similar rôles to the alkali cations. Manganese and titanium are usually network modifiers in six fold co-ordination but in high concentration become network modifiers in their own right. Sulphur is probably homogeneously distributed being incorporated as S^{2-} in place of oxygen in low concentration but when in excess of 3% wt. may crystallize out as free sulphides.

Extensive literature exists in this area and is critically reviewed in references 11, 24, 26 & 27. The original ideas of Zachariasen have been developed using the structural elements described by Regourd and the two have been combined by Dron (30) as a diagram (figure 5, below) which has been

subsequently shown by several authors.

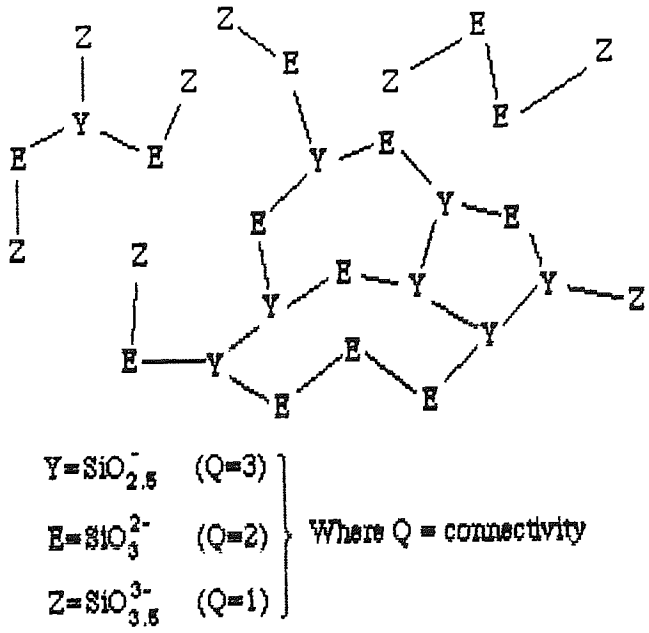

Figure 5 *Probable network structure in glassy blast furnace slag (After Dron)*

Recent work by infra red laser Raman spectroscopy - microscopy (31) and selective dissolution (32) suggests that spinoidal decomposition occurs to produce several glassy phases. Sersale (24) points out that slag is "not homogeneous, being constituted of at least two phases with different composition, one rich in network formers, the other in network modifiers, with consequently different reactivities according to the microzones".

1.3.2 The structure and composition of portland cement

The mineral chemistry of portland cement in comparison to slag, is much better characterized and the bulk chemistry of the materials is compared to other cement types in figure 6.

Lea(5), Bogue (33), Ghosh (34) Bye (35) Czernin (36) and many others have published thorough reviews of Portland cement composition. The subject is reviewed regularly during the "International Congress On The Chemistry Of Cement" and is the subject of numerous papers each year. The essential mineralogy of Portland cement focuses on the four major constituents di- and

tri-calcium silicates, tri-calcium aluminate and the so called 'ferrite' phase.

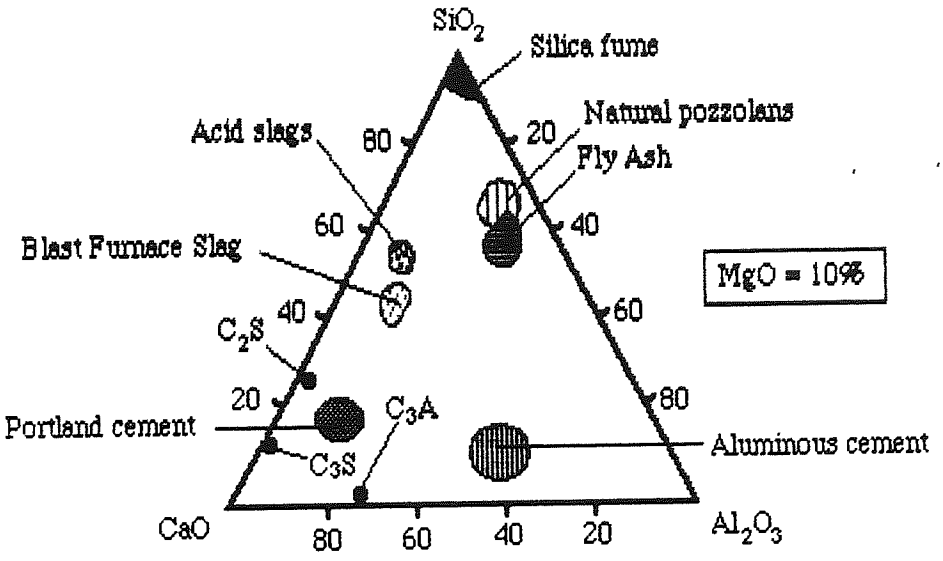

Figure 6 *Ternary Si - Al - Ca oxide plot of major cement types and minerals.*

Tricalcium silicate: ['C_3S'] $Ca_3\ SiO_5$ c.50% by wt. Pseudo trigonal / triclinic. Gribenshikov (37) considers C_3S is a solid solution of CaO in dicalcium silicate proposing the formula $Ca_2(SiO_4(CaO))$ and suggests layers of orthosilicate C_2S, parted by layers rich in CaO. That the fine details of this, the principal cementing mineral are still in doubt, explains the vast amount of literature on its structure.

Dicalcium silicate: ['C_2S'] $Ca_2\ SiO_4$ c.20% by wt.

Five polymorphs of this mineral are recognized of which the γ (orthorhombic) is the stable form at room temperature. The others may be stabilized by impurities in the lattice which accounts for the monoclinic symmetry of the (β) form found in OPC. The stabilizing impurities are K_2SO_4 (38) with Ba,P,Cr,V and minor constituents (39).

Tricalcium Aluminate: ['C_3A'] $Ca_3\ Al_2O_6$ c.15% by wt.

This is the only cement compound not to show polymorphic transformations with temperature, however, group I metal substitution

(for Ca) does cause changes in symmetry from the essentially cubic lattice. Five compositional polymorphs have been identified. In practice,Fe,Mg,Si,Ti,Na,&K can constitute as much as 10% by weight in this phase. Tarte (40) has determined the limiting composition of these components and Lea (5) estimates the probable iron content in this phase at around 4.1% by weight (as Fe_2O_3).

Alumino-Ferrite phase. $Ca_2 (Fe_{1-P} Al_P)_2 O_5$ Where $0 \leq P \leq 0.7$ or 0.52 (38,39). c.10% by wt. Orthorhombic. This is a solid solution between C_6AF_2 and C_6A_2F with commonly occuring compositions of C_4AF and C_6A_2F present in Portland cement. This mineral contains the bulk of the transition metals, and especially Mg, Si, Ti, Mn & Cr are incorporated into the lattice. MgO & SiO_2 substitute for $(Al\ Fe)_2\ O_3$ up to about 10% (molar) (41).

Gypsum: $CaSO_4.2H_2O$ (variable moisture content) up to 10%
Monoclinic, perfect cleavage and common twinning on {100} plane. Occursas lozenge shaped fragments with distinctive 114° angle between cleavage planes. Gypsum is added to retard the rapid hydration of the aluminate phase by the ultimate formation of ettringite.

In Portland cement clinker these minerals are distributed between euhedral 'alite' and 'belite', subhedral aluminate and anhedral interstitial phases. The relationships between pure minerals and the actual phases found in portland cement are described variously by Regourd (42), Lea(5), Ghosh (34) and Bye (35):

Alite: Essentially C_3S. May appear as sub hexagonal (pseudomorphic remnants of high temperature trigonal) polymorphic, zoned crystals of generally lighter appearance than belite. Refractive index= 1.719 - 1.724

Belite: Essentially C_2S, belite can be considered to be an oxygen defective solid solution with silicon substitution (43). C_2S in clinker is a complex material containing point defects, which undergoes inversions on cooling, resulting in an accumulation of strain in the lattice which

induces twinning.The grains are darker and more rounded than for alite, and often distinctively yellow in transmitted light. R.I= 1.714 - 1.735. Bogue(33) recognizes four other phases in portland cement clinker:

	Symmetry	Refractive index
1) C_3A: Rectangular, Dark, interstitial prisms.	Cubic	1.710
2) NC_8A_3: Prismatic, Dark interstitial.	Monoclinic	1.710 - 1.717
3) Glassy Aluminoferrite: Dark interstitial.	Amorphous	>1.72
4) C_4AF: Light interstitial.	Orthorhombic	1.92 - 2.08

Practically, identification of individual cement grains after grinding is both difficult and time consuming. Optical microscopy is limited to microchemical tests and to measurements of refractive index. Electron microscopy is similarly limited to qualitative use of the elemental x-ray spectrometry.

In addition to the above, much work has been done on the minor components (periclase, free-lime etc.) which is out of the scope of this review. Mention is made to work by Boikova (44) which considers the solid solutions of cement minerals and the rigorous experimental synthesis and subsequent analysis contained therein.

In conclusion, the slag - portland cement - water system is one of high complexity and care must be exercised when treating the composition quantitively. It is not practical to define exactly the nature of the starting materials in most experiments, hence generalizations must be made in the presentation of compositional data.

1.3.3 The hydration chemistry of Portland and Portland-blast furnace slag cements.

Primary references were Lea (5) and Bogue (33) which document the work up to the early 1970's. This 'classical' interpretation considers relatively little of the detailed chemistry and like their contemporary workers, direct their

attention to the study of microstructure and strength development. Similarly Czernin (35) concerns himself with early calorimetric studies (Ros.,M.) and Keil's hydraulic index: The "F" factor, an empirical relationship between slag hydration and hydraulicity. Lea correctly identifies (in the light of later knowledge) the hydration products produced by OPC - BSF blended cements:

1) C-S-H gel phase containing group I (and possibly group II) metals.This tends to be of a more complex structure than that of OPC.

2) Hexagonal C_4AH or its solid solution intergrowth with $3CaO.(Al_2O_3.Fe_2O_3).CaSO_4.12H_2O$ ('monosulphate')

3) An ettringite phase $3CaO.(Al_2O_3.Fe_2O_3).CaSO_4.31H_2O$

4) $Ca(OH)_2$ This phase is not common in hydrated blast furnace slag as it is consumed during hydration.

He also notes minor phases reported by Locher:

5) C_2ASH_8 (hydrated gehlenite)

6) C_3ASH_4 (hydrogarnet) - more accurately: $(C_3(A.F)S_nH_{(6-2n)})$

7) C_2AH_8 (rarely found)

Locher believes that hydrated Gehlenite is a transitional phase which reacts with calcium hydroxide to produce more hydrogarnet. Early work by Smolczyk and by Sersale note that hydrated gehlenite is not present after a year's hydration and Smolczyk has observed only one phase per sample - either hydrogarnet or hydrated gehlenite.

Before considering in detail the hydration chemistry of Portland - blast furnace slag cements, it is important to have a clear appreciation of the chemistry of hydrating Portland cement in isolation. This is best presented in terms of the hydration of the individual minerals in isolation and then as the hydration of Portland cement.

Hydration of tricalcium silicate: This mineral reacts rapidly with water to produce a gelatinous mass of calcium silicate hydrate gel. The core of the mineral grains may continue a slow reaction over a period of several years. Initially, dissolution of silica and calcium, accompanied by hydrolysis of the water, releases calcium hydroxide into solution. The original orthosilicate ions

(SiO_4 tetrahedra) present in the lattice, are converted to disilicate ions (SiO_7^{6-}) and subsequently into higher polymeric forms (45). The layer of first hydrate so formed prevents further rapid reaction and is thought to be responsible for the onset of the 'dormant' period. During this period, suprsaturation of the solution with respect to calcium hydroxide occurs up to the nucleation of portlandite crystals. The end of the dormant period and the subsequent increase in the hydration reactions are a matter of some debate between authors. Jennings and Pratt (46) suggest that the low amount of water or low local pH in the first hydrate region limits the rate of hydration during this period and propose that the situation is overcome by the continued uptake of water by the quasi-solid (the first hydrate).

They (46) go on to say:

"When finally conditions become favourable for the formation of C-S-H, the induction period comes to an end and a quasi solid state reaction takes place. Unlike the surface reaction which continually (and slowly) heals the rupturing membrane, this reaction forms a colloidal gel which is much less effective at slowing the transportation of water to the interior."

Figure 7 shows schematically their model of C_3S hydration (below)

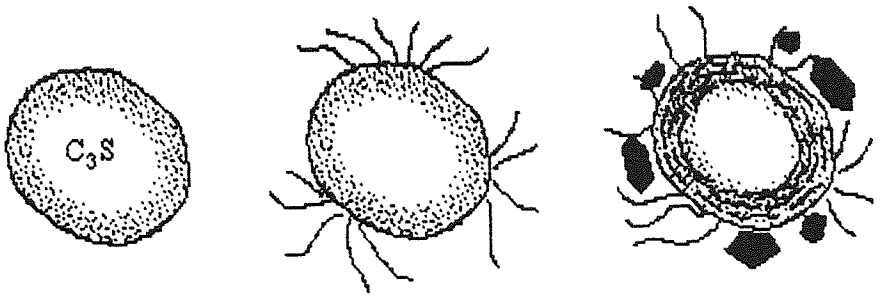

Initial reaction forming C-S-H coating Ca^+ & OH^- go into solution.

Induction period: Exfol--iating C-S-H membrane and formation of new membrane.

End of induction period. Formation of C-S-H gel and portlandite.

Figure 7 *Hydration of tricalcium silicate grain (After Jennings and Pratt)*

Several workers subscribe to the theories proposed by Double and Hellawell (47) concerning the mechanism by which the dormant period is ended. The concept of an osmotic model in cement hydration is not new (48) but has received much attention in the last decade (49,50,51,52). The idea is that the layer of first hydrate limits ion mobility to a large extent and maintains its physical integrity over the surface of the grain. The resulting concentration gradient across the membrane, is the driving force for an osmotic mechanism, which transfers water to the unhydrated side of the hydrate layer. The subsequent increase in pressure is accommodated by the membrane until it reaches a value sufficient to rupture it. The mobile, water rich hydrate is then free to be ejected into the surrounding solution where it is thought to react with highly alkaline species to form tubules in a similar way to the formation of the structures seen in 'silicate garden' experiments. Skalny and Young (53) propose a different mechanism for the early stage of hydration.

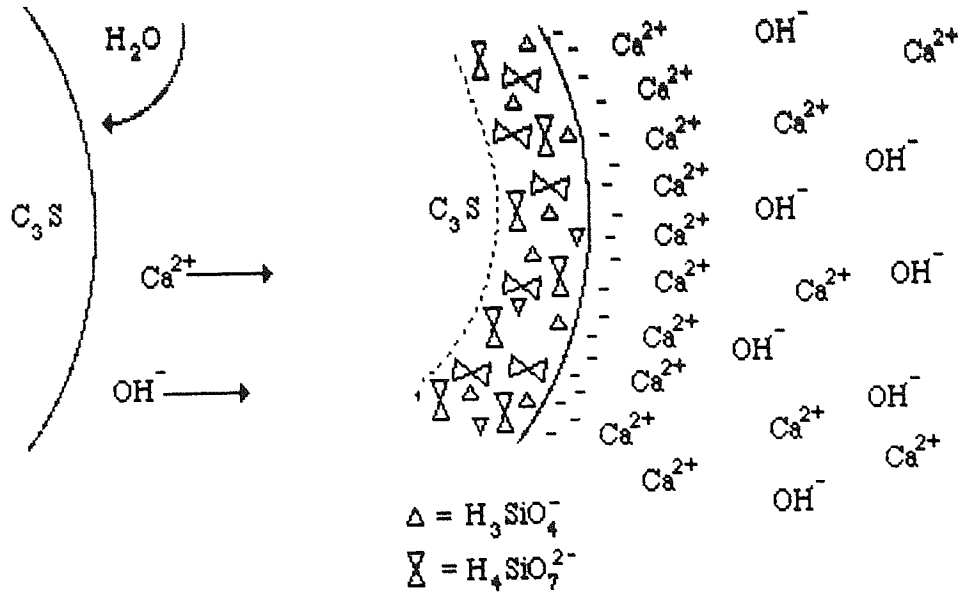

Figure 8 *Surface charge layer on hydrating C_3S grain (After Skalny and Young)*

They consider the initial dissolution to be incongruent and that calcium and hydroxyl move rapidly into solution leaving the surface layers rich in silica. In doing so the surface layer adopts a negative zeta potential which strongly

adsorbscalcium ions to it as shown in figure 8. These authors go on to suggest that this adsorbed layer and its correspondingly low silicate concentration, account for the lack of immediate hydration products seen on the surface.

These models have been summarized diagrammatically and are shown in figure 9. Stage 'A' shows the formation of the first hydrate layer causing the onset of the induction period and its subsequent termination by the nucleation and growth of C-S-H as a second layer of hydrates as suggested by Stein and Stevels (54) and shown to the right. Although Skalny and Young's adsorbed layer is not in the strictest sense a hydrate, it could be considered as an electrostatic barrier in this position. The hydrolysis of water and dissolution of calcium at 'B' may result in exfoliation of the hydrates, as supported by Jennings and Pratt, shown as 'C' (see figure 7 also). Alternatively, the hydrous gel may be ejected into the surrounding solution (situation 'D') to form tubules as favored by Double and co workers. Each of these mechanisms attracts its exponents and many very convincing micrographs have been published of both types of structure. If both mechanisms occur, as the literature suggests they do, then the reason why one should be favored to the other remains unclear.

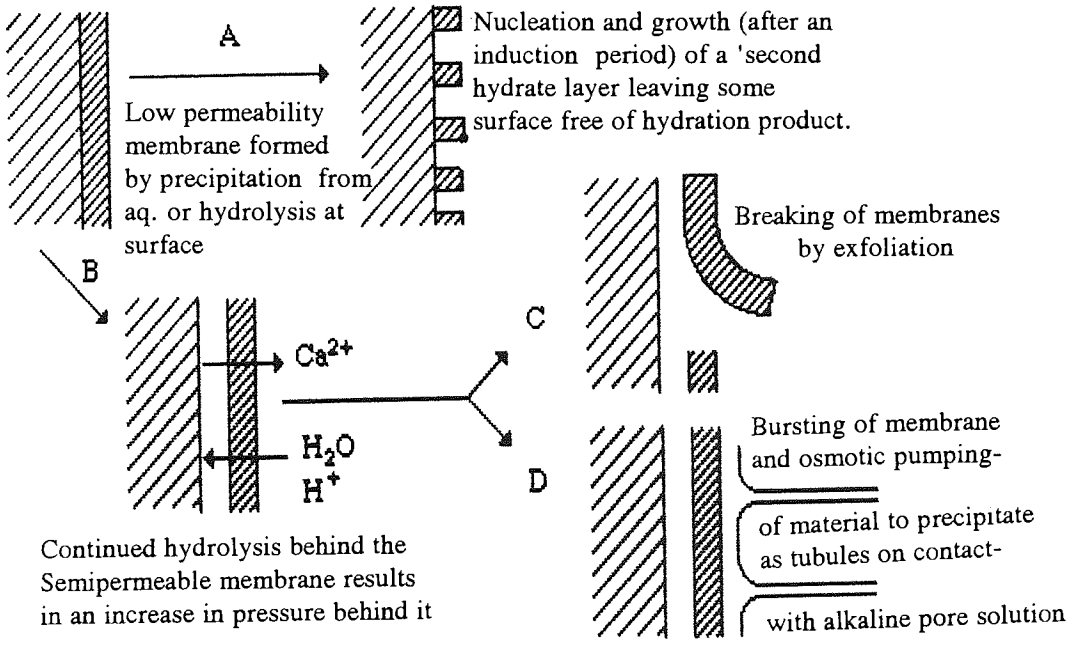

Figure 9 *Possible mechanisms for the hydration of C_3S (After Bye)*

Most recently, Taylor (55) has addressed this question and discusses previous models. He proposes that there is no diffusion of water molecules through either the inner or outer product layers and suggests that hydrogen ions are transferred from one oxygen atom (probably water molecules) to another until they reach the C_3S surface .....

....."which is attacked much as if it were in contact with an aqueous solution." He proposes that a narrow zone exists as an interface where atomic rearrangements convert C_3S into C-S-H gel. As this zone moves into the hydrating grain, calcium and silicate ions move through the product and into the surrounding liquid to be precipitated ultimately in the outer product layers or (for calcium) as portlandite. Taylor is quite definite in saying that there is no long range movement of oxygen atoms and suggests that the migration of silicon is by a series of movements through the faces of the tetrahedra, from sites initially filled to those initially empty. He similarly proposes this as a mechanism for the change of silicate anion type both during and after C-S-H formation. These ideas are presented in figure 10, below:

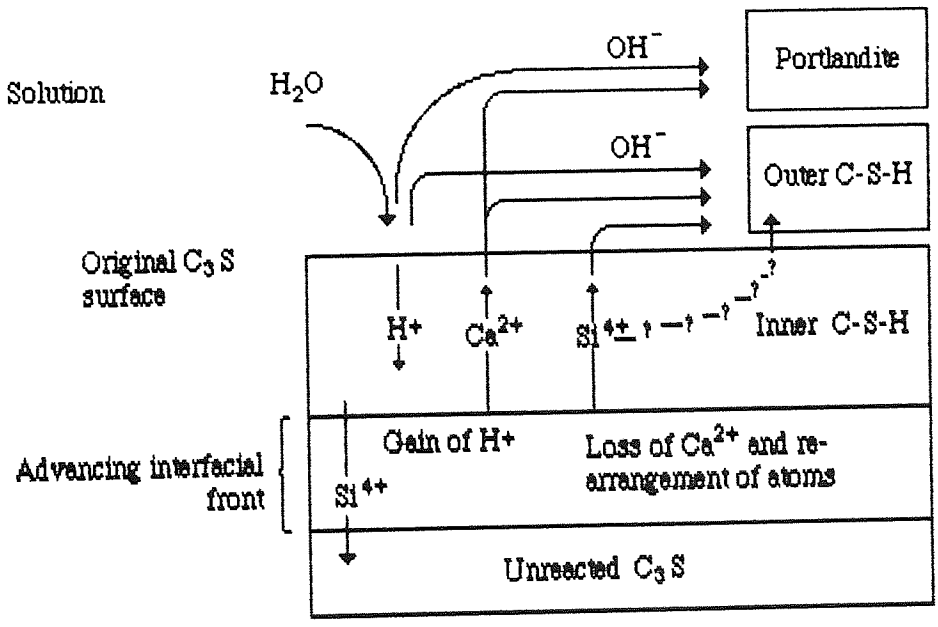

Figure 10 *Migration of hydration front through grain of C_3S (After Taylor)*

In conclusion, the hydration mechanisms for tricalcium silicate are not

fully understood but the models proposed so far are not mutually exclusive. There is little disagreement however that this mineral reacts in at least four stages, as revealed by conduction calorimetry, and that the overall chemistry of hydration can be summarized thus:

$$2C_3S + 7H \text{ ----> } C_3S_2H_4 + 3CH \qquad \Delta H = -1114 \text{ kJ mol}^{-1} \qquad (56)$$

Hydration of dicalcium silicate: This mineral reacts slowly to produce the same reaction products as above but only results in approximately one third of the portlandite produced by C_3S. The rate of reaction is much reduced when compared with C_3S although this mineral does make a significant contribution to the late strength if hydration is allowed to continue . Overall the hydration is around twenty times slower than for C_3S and the reaction can be summarized as:

$$2C_2S + 5H \text{ ---> } C_3S_2H_4 + CH \qquad \Delta H = -43 \text{ kJ mol}^{-1} \qquad (56)$$

The mechanism of hydration is thought to be similar to that for C_3S although the morphology of its hydrates are more variable. Young and Tong (57) note that during fracture, C_2S hydrates may be completely separated from the anhydrous core, a phenomenon rarely seen in C_3S. The significance of this is uncertain, but it suggests that there is a structural difference in the nature of the hydrates between the two species. Relatively little work has been done on the hydration chemistry of C_2S, which is perhaps not surprising given the relatively minor contribution to early strength afforded by C_2S.

Hydration of tricalcium aluminate: Of the cement minerals considered here, C_3A is the most reactive towards water and its rapid dominance of the rheological properties of cement paste require the intergrinding of gypsum to control this immediate hydration. The reaction of C_3A with water has been studied in isolation by Breval (57) who reports the initial formation of a gel hydrate which increases in crystallinity to form hexagonal hydrates of the

composition C_2AH_8 and C_4AH_{19}. These hydrates are thought to have a structure consisting of sheets of $Ca_2Al(OH)_6^+$ with $Al(OH)_4^-$ or OH^- in the interlayer region, which balance the net positive charge of the layer, together with water.

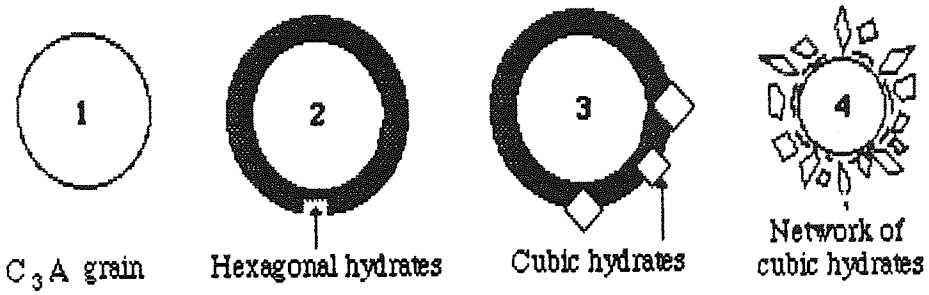

Figure 11 *Hydration of tricalcium aluminate in the absence of sulphate. (After Jawed et al)*

The hexagonal hydrates which form initially are converted to icosahedra of the cubic hydrate C_3AH_6. The hydration shown in figure 11 can be summarized as follows:

$2C_3A + 27H$ ----> C_4AH_{19} (or C_4AH_{13}) + C_2AH_8 [C_xAH_y = hexagonal hydrates]

(The C_4AH_{19} loses bound water at R.H. < 88% to become C_4AH_{13})

Then: $C_4AH_{19} + C_2AH_8$ ----> $2C_3AH_6$ [C_3AH_6 = cubic hydrate]

The conversion from the metastable hexagonal form to the stable cubic, is accompanied by a volume change which may have (very) detrimental effects if it occurs in a loaded structure. In cements with a high C_3A content, the heat of hydration is ordinarily sufficient to ensure conversion occurs quickly (before setting) from nucleated crystals of the cubic C_3AH_6. This ensures the continued growth of cubic hydrates even at temperatures which would not otherwise ensure complete conversion. In the presence of calcium hydroxide the formation of C_4AH_{19} (or C_4AH_{13}) is favoured, the hydration rate is

generally slower and the conversion to C_3AH_6 is inhibited.

Bye (45) notes that : ..." the reaction is sufficient,even at the level of C_3A present in cement (commonly 5-10%) to induce flash set unless gypsum is added as a controller."

The hydration of tricalcium silicate in the presence of sulphate follows a different route as shown in figure 12:

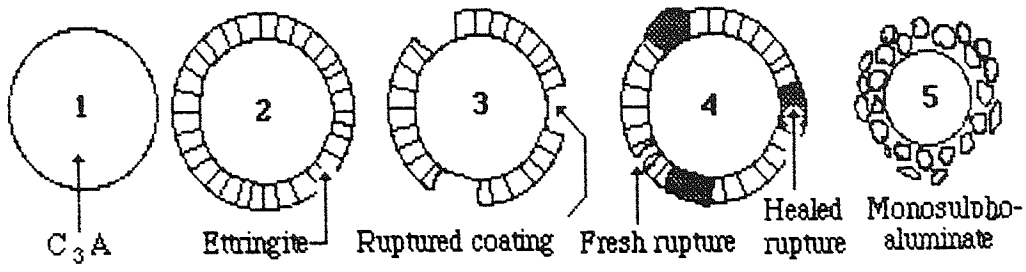

Figure 12 *Hydration of tricalcium aluminate in the presence of sulphate (After Jawed et al)*

Assuming that an adequate supply of sulphate ions is available, the first hydrate to form is ettringite ($C_6AS_3H_{32}$) producing a membrane around the hydrating grain which impedes the diffusion of ions from the solution to the unreacted C_3A, again resulting in a dormant period. This reaction will continue slowly by the repeated rupture and fresh reaction of this coating until the surrounding solution is depleted in both calcium and sulphate ions. An osmotic mechanism has also been proposed for the end of the dormant period in this mineral. Eventually, the stage is reached where formation of further ettringite is not stoichiometrically favoured and a second, related mineral begins to precipitate, monosulpho- aluminate hydrate (the so-called 'monosulphate'). Associated with this precipitation, is the gradual transformation of ettringite to monosulphate by reaction with the pore solution. Solid solution (particularly of Al^{3+} for Fe^{3+}) is common in these minerals to produce two phases of variable composition: "AFt" is the phase formed during the hydration of Portland cement which is thought to derive from ettringite, (the 't' indicates tri-sulphate although substitution for other

anions is thought to occur). Morphologically, this phase is present as prismatic and/or accicular crystals of hexagonal cross section. Similarly the "AFm" phase is thought to derive from pure monosulphate with partial substitution of Al^{3+} for Fe^{3+} and sulphate for other ions. These phases dissolve in pure water to reprecipitate as calcium hydroxide, gypsum and alumina gel.

Hydration of the aluminoferrite phase: Essentially, the hydration products of this mineral are similar to those of C_3A, but forming much more slowly and with substantial substitution of Fe^{3+} for Al^{3+}. If the unhydrated composition is considered to be $xC_2A.(1-x)C_2F$, then reactivity of the phase increases with x (45). Assuming, as is the case in OPC hydration, calcium hydroxide is available, then hexagonal hydrates of the form $C_4(AF)H_{13}$ and $C_2(AF)H_8$ precipitate, (which are essentially iron substituted varieties of those associated with C_3A). Hydrogarnets are reported to form by Copeland *et al* (58), an observation made by other workers only in pastes cured at high temperature. Like C_3A, aluminoferrite reacts with sulphates to produce ettringite and related phases, which ultimately convert to monosulphate. Thus, it is reasonable to expect some competition for the available sulphate occurs between this phase and C_3A. Rogers and Aldridge (59) have examined (amongst other compositions) the hydration of C_2F and report that this composition yields C_4FH_{13}, initially forming as C_4FH_{19} and converting to C_4FH_6 within a day. This product is metastable and ultimately decomposes to calcium hydroxide and haematite. Taylor (55) concludes the most recent review: ..."the existing evidence seems to favour the view that, when the ferrite phase hydrates in a cement, the space it occupied is filled with a mixture of C-S-H, an AFm phase low in Fe, a hydrated phase high in Fe, and often, another one high in Mg. Such a mixture can have a bulk composition quite close to that of the hydrogarnet that has sometimes been found"..."which could thus form from,or instead of it under favourable conditions".

Hydration of Portland cement paste: To some extent at least, hydration of Portland cement can be considered as essentially those reactions described above with relatively little interaction between the separate hydrating phases. It is important, before considering the extent of these interactions to establish two classical mechanisms of hydration. The significance of doing so is in relation to chapters 3 & 4 and involves isolating the processes which prove to be the rate determining steps.

Consider figure 13A. This describes the "through solution " model which involves the dissolution of the mineral phases and subsequent precipitation of hydrates at points remote from the dissolution sites. The liquid phase in this case must be saturated with respect to the hydration products and, assuming that the rate of dissolution is high, the rate determining process will be the nucleation and growth of the hydrates. The second process is known as the "topochemical" model because of the close proximity of the reactant to its hydrate and is considered to be subject to diffusion control . Figure 13B shows this situation for the formation of C-S-H gel on the surface of hydrating C_3S and a through solution precipitation of calcium hydroxide.

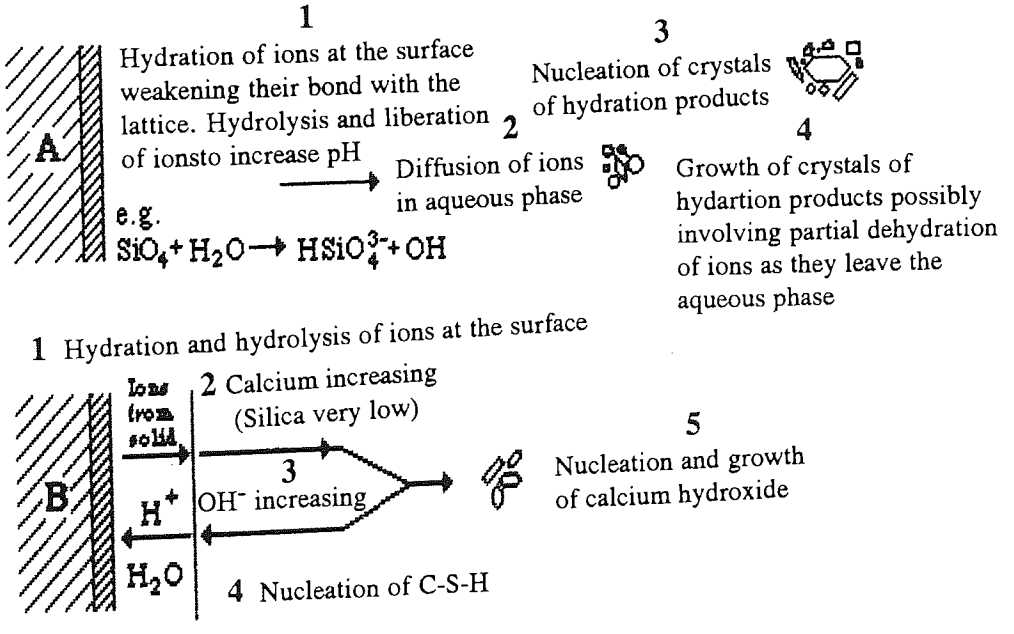

Figure 13 *Through solution and topochemical models of cement hydration*

It is interesting to note that Bye (45) criticizes the use of such definitive descriptions:

" The low solubility of silica and the very high supersaturation with respect to C-S-H, which is rapidly established in the hydration of C_3S would ensure that the product was formed close to the surface even if a through solution mechanism operated. Consequently distinction between the two mechanisms is virtually impossible..."

Regourd (60) has noted the existence of silico-aluminates in the hydration products of OPC, which is evidence for some reaction between the individual phases and Bye (45) discusses the acceleration of C_3S by gypsum. Jennings and Pratt (44) discuss the hydration of C_3A and C_3S in the presence of gypsum. They suggest that a membrane of composition approaching AFt replaces the initial C-S-H as aluminium becomes available in solution and that the chemistry of this membrane changes with time. They go on to propose that this membrane (see figure 14) continues to grow during hydration (as it does not rely on soluble silicates) to envelop adjacent particles thus forming agglomerations and contributing to the 'set' in the early stages of hydration.

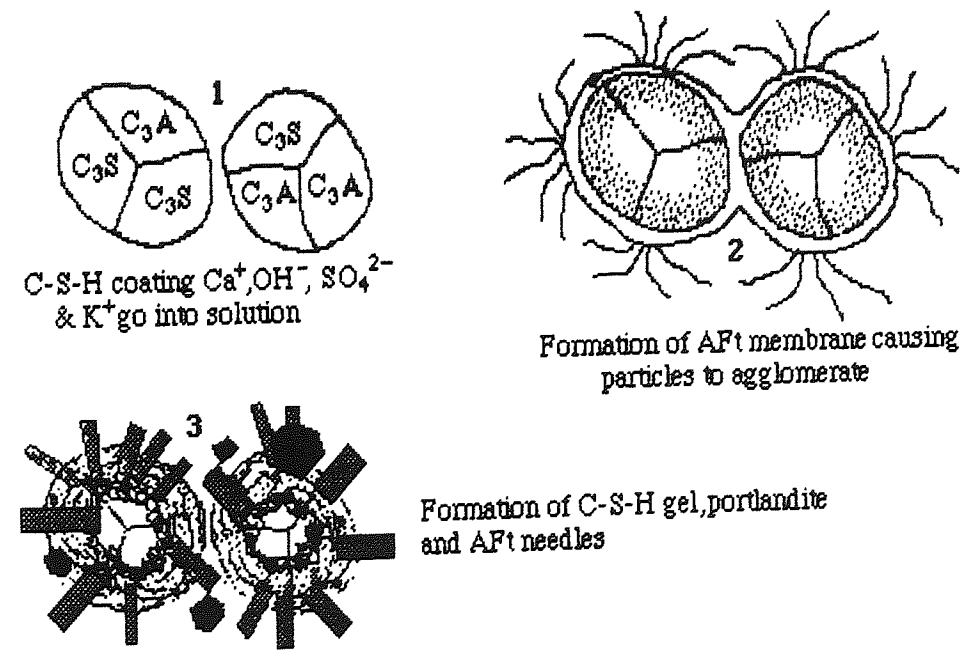

Figure14 *Reaction of C_3S and C_3A with gypsum (After Jennings and Pratt)*

In addition to the above, dissolution and reprecipitation of minor components such as periclase (MgO), free lime (CaO) and group Ia metal oxides further modify the system. These components ultimately are incorporated in the C-S-H gel and are discussed more fully in the next section.

In conclusion, the hydration of Portland cement can be considered as a set of complimentary reactions producing, (at different rates) C-S-H gel, Portlandite and a solid solution series of calcium aluminoferrite hydrates.

Hydration of blended blastfurnace slag - Portland cement: The mechanism of slag hydration is poorly understood and is frequently described in terms of a free energy diagram as described by Roy and co-workers (61,62) and shown in figure 15. Slag has 'latent' properties in as much as its hydration is rapidly promoted by the use of an 'activator'. If mixed with water, slag will react very slowly to produce a hydrate structure of low strength and consequently, it is not used in this condition. The 'activation' of slag is its direct reaction with aqueous hydroxyl and/or sulphate ions (alkali or sulphate activation) to produce hydration products simmilar to those formed by Portland cement. The term 'activator' is an unfortunate one as it implies something less than the formation of products from reactants. As the activators are most certainly consumed during hydration and become incorporated in the hydration products it is now realized that the activators are true reactants in their own rights.

In figure 15, ΔGa is essentially the apparent activation energy which must be overcome before reactions can proceed by releasing the energy from the slag glass. In the case of crystallization from a melt, the energy available would be equal to ΔG_1, once this activation energy barrier has been overcome. In comparison, the hydration reaction involves a larger energy transition (ΔG_2) resulting in products with lower free energies than those associated with the crystalline state.

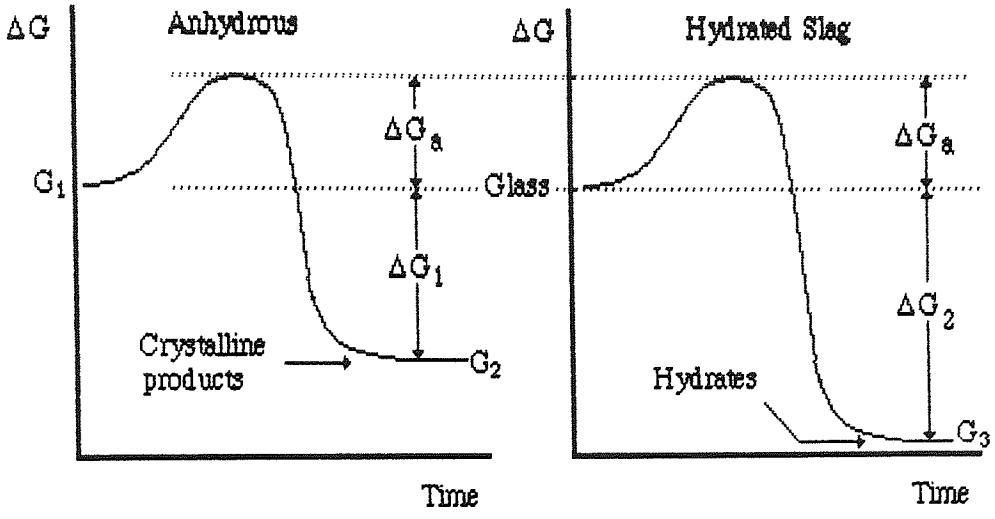

Figure 15 *Free energy diagrams for blast furnace slag (After Roy et al)*

Much work has been done on the study of heat evolution during reaction as a means of following the hydration of slag cements. Original work by Regourd (62) and others (63,64,65,66) and reviews by Daimon (67) Lee (68) and Regourd (26) suggest the following:

1 Portland cement hydrates to liberate a total heat of reaction of c.400 $kJ.Kg^{-1}$

2 An increase in temperature greatly increases the rate of reaction.

3 OPC-BSF hydrates more slowly and liberates a lower amount of heat than Portland cement alone.

Wu *et al* (65) develop Courtault and Briand's earlier work (67) which cautions that homogeneous reaction kinetics are inappropriate to multi-component glasses. They develop an effective "E", known as the thermal increment, analogous to activation energy, but determined using another parameter such as degree of reaction or heat evolution. "E" is determined from an Arrhenius relation, which describes the degree of advancement of this parameter. Complimentary work by Roy and Idorn (68), which was carried out at a range of temperatures up to 60°c, reports that the position and magnitude of the individual stages of heat evolution, depend on the composition of the mix and the temperature of hydration.

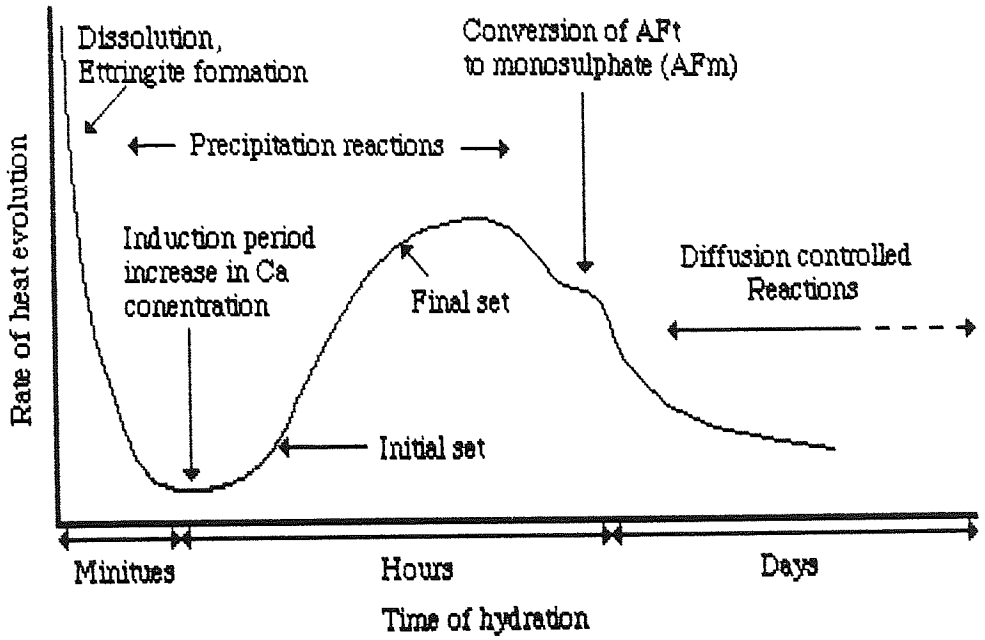

Figure 16 *Heat evolution profile from hydrating cement (After Skalny and Brophy)*

Regourd (62) has also published work on elevated temperature calorimetry in connexion with the characterization of French slags. Lee and Palmer (69) have investigated hydration at high levels of slag replacement and compared the results to electrical impedance measurements whilst Totani *et al* (70) have used the method to investigate the hydration of slags with OPC or cement minerals. Investigations using this technique to characterize slags are reported regularly usually in support of other methods (71). Variations on the calorimetric method are published and the measurement of adiabatic temperature rise provides complimentary data (72). Skalny and Brophy (73) present a schematic diagram for the heat evolution during hydration of slag cements as part of their work and this is shown in figure 16. Complimentary to these studies is the work on many other physical parameters which change during slag hydration. Volume changes (bulk and chemical shrinkage) are reported (62, 63,73) and are related to calorimetric work in that high heat evolution is associated with high shrinkage.

Studies of chemical shrinkage have concentrated on Portland cements although the method readily lends itself to applications in slag hydration. The method (74) relies on measuring the change in volume associated with hydration, such that the volume of unhydrated material, hydrates and remaining water is measurably less than the volume of original reactants. This change in volume has been the subject of a recent thesis (75) which uses chemical shrinkage to determine kinetic parameters for the hydrating system. The method has been reported in a number of publications (76, 77, 78, 79, 80) and the experimental technique has been adapted to investigate other causes of volume change (81) such as those associated with alkali-silica reaction.

X-ray diffraction has been used to study the dissolution of the crystalline components during slag hydration (82) but is of limited value in the study of blast furnace slag as the bulk of the material is glassy and the C-S-H gel displays only short range order. The method has, however been used successfully by Atkins *et al* (83) to identify minor phases in the hydration products of slag cements. This work has subsequently been used to model the likely hydration products in slags of greater ages than those attainable in the laboratory. Teoreanu *et al* (84) have employed XRD in the examination of hydrated phases in various slag-water-activator systems identifying ettringite and hydrated gehlenite under varying conditions. Much work has been done on the microscopy of slag hydration products. Regourd has made valuable contributions using SEM-EDS and XPS methods. Her recent surface analysis (85) confirms her earlier work (86,87,88) in describing a "pseudomorphic layer" surrounding hydrating slag particles, which shows a low degree of crystallinity. The layer of slag hydrate is essentially a C-S-H gel but is richer in magnesium and aluminium than that produced by OPC clinker. X-ray photoelectron spectroscopy was used to examine Ca, Al, Mg, and Si on the surface of the hydrating slag grains. She reports that the surface of the slag is modified as soon as it makes contact with the aqueous phase, showing a marked depletion of calcium, and that alkali metals in part replace calcium in the gel. To a meeting of the Royal Society (89), Regourd presented XPS results showing the ratio of

Ca_{2p} to Si_{2p} binding energy for the surface hydrates of the slag, which displayed a decrease in this ratio during the first few minutes of hydration. The stable ratio of between 1.5 and 2 reached after fifteen minutes, she concludes, suggests that only the very first step of hydration is affected by the incongruent dissolution of slag reported by Dron and Brivot (90).

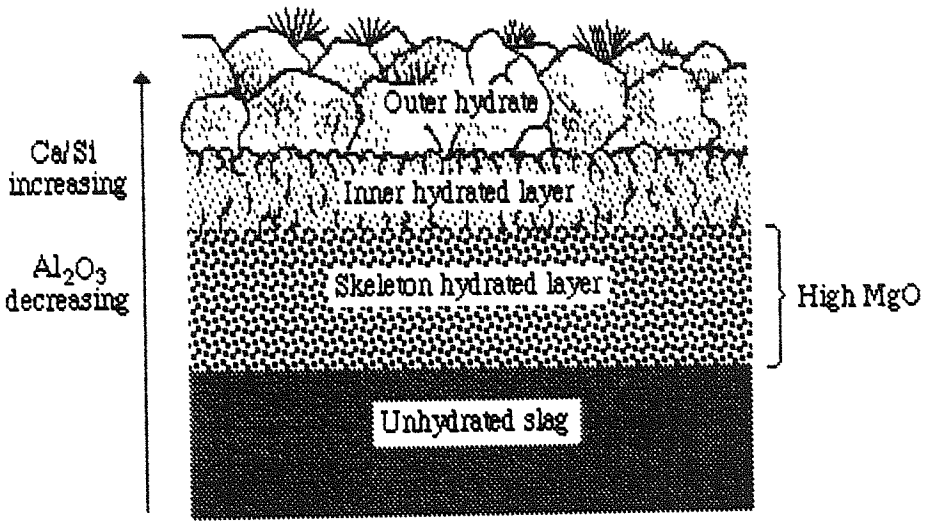

Figure 17 *Compositional variations at the surface of hydrating slag (After Tanaka et al)*

Studies on the rôle of magnesium during slag hydration suggest that at least 29% by weight can be incorporated in slags without detrimental effects (92) although the hydration of these materials is retarded. The magnesium bearing hydrates have been investigated by Schwiete *et al* (93) who reacted vitreous gehlenite and/or akermanite and found magnesium incorporated in both C-S-H and C_2ASH_8. Mascolo and Marino (94) identified brucite - $Mg(OH)_2$, Gibbsite-$Al(OH)_3$ and a double Mg-Al hydroxide in the hydration products of a reaction between MgO, CaO and alumina gel. Tanaka *et al* (91) examined the distribution of magnesium and found a magnesium rich layer below the level of the inner hydrates suggesting that magnesium is preferentially concentrated in the skeletal hydrated layer. Atkins (83) records the (well documented)

presence of a hydrotalcite-like phase (M_4AH_{10} - M_6AH_{14}),the chemical significance of which is that this phase is that it shows a marked anion exchange capacity (for the loosely bound hydroxyls) which may have implications if a high magnesium slag were to be used for waste encapsulation.

Of the many other publications relating to the microscopy of the hydrating slag system, a few are worthy of special mention. Satarin (95) reviewed seventy eight publications for the 1974 Moscow congress (ICCC) and concluded that the early stages of hydration involved slag grains as centers around which the aluminate sulphate hydrates and amorphous silicate hydrates were formed. Ben-Dor relates studies on both blended and Portland cements and reviews the many morphologies reported by other workers. Regourd (97) observes that up to 28 days both the clinker and slag grains in a hydrating blend are coated with hydrates derived from the clinker, after which time the hydration of the slag itself becomes visible. In her report to the 1980 Paris congress (26) she presented micrographs of the hydrates associated with slag cement and noted that at six months hydration, the slag hydrates are richer in aluminium and magnesium than those associated with the clinker. Sersale *et al* (98) have presented a detailed study of the developing microstructure of slag cements and Lou (99) has examined the growth and morphology of ettringite during the development of non shrinking or slightly expansive slag cements. Although much debate has taken place concerning the detailed variations in composition and morphology of the gel phase, there is full agreement that both slag and OPC contribute to gel formation. In general it can be taken that the gel phase produced by the slag displays a lower Ca/Si ratio than that of the OPC, commensurate with the different ratios found in the parent material.

The degree of slag hydration is usually inferred from other parameters such as the combined water content of a paste. Several workers have attempted to develop a method by which this can be attempted directly by selective dissolution. The method developed by Kondo and Oshawa (100) has been used by several authors (20, 65 & 101) and involves the dissolution of the unhydrated OPC and hydration products by a salicylic acid-acetone-methanol process.

Unfortunately, the method leaves some residue from the OPC/hydrates and does attack the remaining slag. Demoulian (102) *et al* reported a titrimetric study of the dissolution of various phases using a triethanolamine, EDTA and sodium hydroxide formula. Luke and Glasser (103) reviewed some published methods along with formulations of their own and concluded that the most promising technique was a formulation similar to that reported by Demoulian. The method has been somewhat refined recently (104) and published results show that the hydration of slag does not obey simple kinetics and that at least 40% is unreacted after one year's hydration.

The hydration chemistry of slag in various media has been treated theoretically by Voinovitch and Dron (105, 106) who have proposed the overall stoichiometries shown overleaf. They consider activation of slag with both sodium and calcium oxide and subsequently with sulphate to produce the following:

$$C_5S_3A + 12H_2O \rightarrow 1/3\,C_4AH_{13} + 7/3\,CSH + 2/3\,C_2ASH_8$$

(slag + water → aluminate hydrate + CSH gel + gehlenite hydrate)

and

$$C_5S_3A + 2CaO + 16H_2O \rightarrow C_4AH_{13} + 3\,CSH$$

(slag + lime + water → aluminate hydrate + CSH gel)

In the presence of sulphate:

$$C_5S_3A + 2CaSO_4 + 76/3\,H_2O \rightarrow 3CSH + 2/3\,C_3A.3CaSO_4.32H_2O + 2/3\,Al(OH)_3$$

(slag + calcium sulphate + water → CSH + ettringite + sodium sulphate)

Combining the above:

$$C_5S_3A + 4CaSO_4 + 2NaOH + 34H_2O \rightarrow 3CSH + C_3A.3CaSO_4.32H_2O + Na_2SO_4$$

(slag + sulphate + sodium hydroxide + water → CSH gel + ettringite + sodium sulphate)

This is now considered to be something of an oversimplification, not least that it disregards the reduced environment in slag cements. A paper by Dron and Brivot (107), develops thermodynamic work by Masson (108) to describe slag hydration in terms of the chain elements described by Regourd (26). In the initial phase of hydration, before CSH precipitation, it is the more basic species in the glass which preferentially go into solution:

$$(SiO_{3,5})^{3-} : 2SiO_{3,5} + 3H_2O) \rightarrow 2SiO_4H_2^{2-} + 2OH^-$$

$$(AlO_2)- : AlO_2^- + 2H_2O \rightarrow AlO_4H^{4-}$$

and similarly for $^1/_2 (Si_2O_7)^{6-}$

Stade and Wieker (109) have shown that for reasonably young precipitates stored at 0°C this is the principal silicate dimer [$(Si_2O_7)^{6-}$] on precipitation, with Ca^{2+} and H^+ providing electrical neutrality when the Ca/Si ratio is between 1.2 and 1.5. If however, this ratio lies in the range 1.0 to 1.2 some oligomer is reportedly also present. Regourd (26, 85) describes these reactions as hydrolytic and non hydroxylic. Dron and Brivot's work (90) employed a chemical reactor purged of carbon dioxide in which a suspension of reacting slag was recirculated by a peristaltic pump. Analysis of the aqueous phase shows that following the dissolution-CSH precipitation reactions, the Ca/Si ratio falls below that of the slag and the solution is therefore relatively enriched in calcium. To maintain a constant solubility product, silicon comes out of solution as precipitating gel. The concentration of aluminium however, is seen to gradually increase in solution up to the point of aluminate hydrate precipitation. Verenet *et al* (107) have employed a similar technique to examine ionic species in dilute aqueous solution during slag cement hydration. They detected pH, Na^+, K^+, S^{2-} and Cl^- electrochemically and also measured thermal flux and bulk conductivity in order to produce composite diagrams of these determinands against time. concentrations of aluminium sulphate and silicate were also measured (on aliquots removed from the suspension) and glass content determinations were

made by XRD during the the course of hydration. They identify four phases of chemical change which are in broad agreement with the findings of calorimetric studies.

The work above (109) is reviewed by Glasser *et al* (10) in their studies on the nature of C-H-S gel structure and solubility. They present calculations concerning the thermodynamics of dissolution and propose the formula below to describe the gel phase in slags:

$$Ca_X\ H_Y\ Si_2O_7 \cdot Z\,Ca(OH)_2$$

where $(X+Z)/2 = Ca/Si$

and $X = 2(Ca/Si) - Z$

$Y = 6 - 4(Ca/Si) - Z$

enabling the general formula to be re-written to eliminate Y, thus:

$$Ca_X\ H_{6-2X}\ Si_2O_7 \cdot Z\,Ca(OH)_2$$

They make the assumptions that the thermodynamic state of the water associated with the gel is similar to that of the aqueous phase and that the layered structure is homogeneous with regard to its bulk thermodynamic properties. This model is based on dimeric silicate species which will increasingly not be the case as hydration progresses. They go on to establish solubility equilibria for this system, where Ca/Si in the gel is in the range 1.0 to 1.5:

$$Ca_XH_{6-2X}\ Si_2O_7 \cdot Z\,Ca(OH)_2 + (2X-3)\ H_2O = (X+Z)Ca^{2+} + 2H_2SiO_4 + (2X+2Z-4)OH^-$$

For this reversible process the equilibrium position is determined thus:

$$K_{SP} = [Ca^{2+}]^{(X+Z)}\,[OH^-]^{(2X+2Z-4)}\,[H_2SiO_4^{2-}]^2 \cdot \gamma^{\pm(3X+3Z-2)}$$

$$\therefore K_{SP} = K'_{SP} \cdot \gamma^{\pm(3X+3Z-2)}$$

where K_{SP} is the concentration solubility product and $\gamma\pm$ is the mean activity coefficient.

This work is a development of that published by Stade and Wieker (109) who suggest a repeating layer structure for C-S-H gel as shown in figure 18. Both groups of authors (10,109) suggest that X,Y & Z are free to vary within limits and observe that it is difficult to write balanced equations for gel dissolution / precipitation.

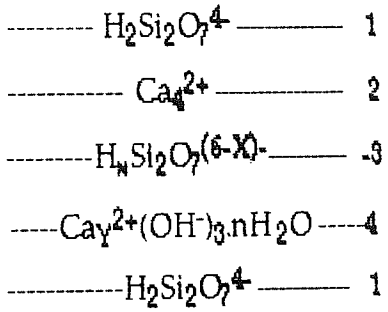

Figure 18 *Repeating layers in C-S-H gel structure (After Stade and Wieker)*

Glasser's group have done much valuable work on the pore solution chemistry of slag cements.Their method is a development of a design popularized by Longuet (111,112) and subsequently used by most workers in this field. (A full description is given in chapters 2 & 6). This group have extracted pore solutions (10, 83, 113, 114) with the exclusion of oxygen from the system, but make little reference to the temperatures at which the extractions have been performed. They have attempted to identify the chemical environment in slag cement matrices and have particularly been concerned with electro-active species in the system such as S^{2-}, $S_2O_3^{2-}$, Mn^+ and metallic iron. They consider pH and buffering capacity and perhaps more interestingly, E_H and poising capacity. (Poising capacity is the E_H analogue of buffering capacity). The greater

significance of these results is the ability to predict the speciation of trans-uranic metals in radioactive waste studies. Their method currently involves the electrometric back titration of excess cerium IV with iron II after oxidizing all the electo-active species with acidified cerium IV. This gives a relative poising capacity in equivalents per gramme of cement. Related work (113,114) involving the development of actinide speciation models, has resulted in the recalculation of the Pourbaix diagram (115) for sulphur in order to incorporate meta-stable species such as thiosulphate and polysulphides. Their modification is shown in figure 19, below:

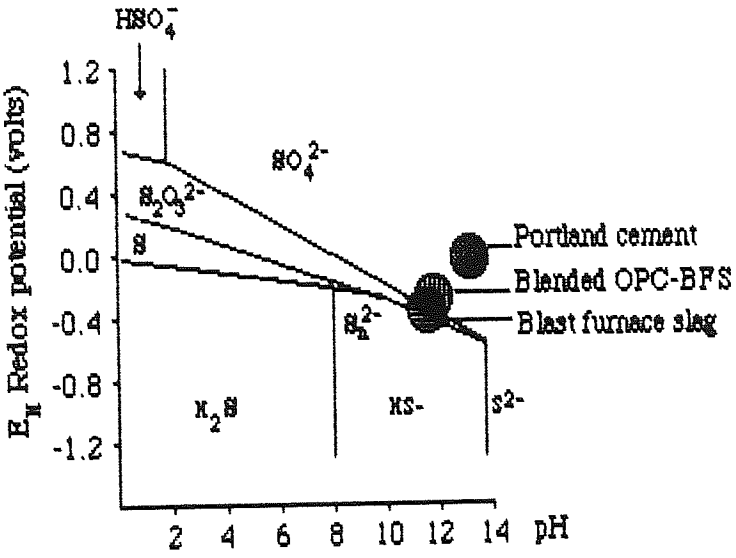

Figure 19 *Modified Pourbaix diagram for sulphur (After Glasser et al)*

The development of a model for long term slag durability unifies the work of this group (116-120) and consequently, findings related to the hydration of slag are published. Of particular interest is their surface analysis of slag grains by XPS (110) which suggests that magnesium is preferentially incorporated in the gel from slag hydration rather than that associated with OPC. The rôle of sulphur in slag hydration has been questioned in the literature (107) but little published work is available on this subject. By employing a selective dissolution method (103,104,) to estimate the degree of hydration of an 85% slag cement, Luke *et al* (121) have estimated the maximum potential sulphide concentration available to the pore solution. The actual (25 day) concentration of sulphide (measured by

Ag/AgS electrode) indicates that only around 2% of the available sulphur is present in solution. As sulphide makes up over 50% of the total oxidizable content (with thiosulphate accounting for some of the remainder) most of the oxidizable content of the cement must be concentrated in the solid phase after 25 days. Tutti (122) reported similar concentrations of sulphide in pore fluids extracted during corrosion studies. Berner (123) has presented a model for long term hydration of cements which, although it makes reference to slag cement, assumes all sulphur is present as sulphate and does not, as yet, account for the strongly reduced matrix found in slags. This phenomenon is perhaps best demonstrated by considering the redox potential of the pore solutions such as in figure 20:

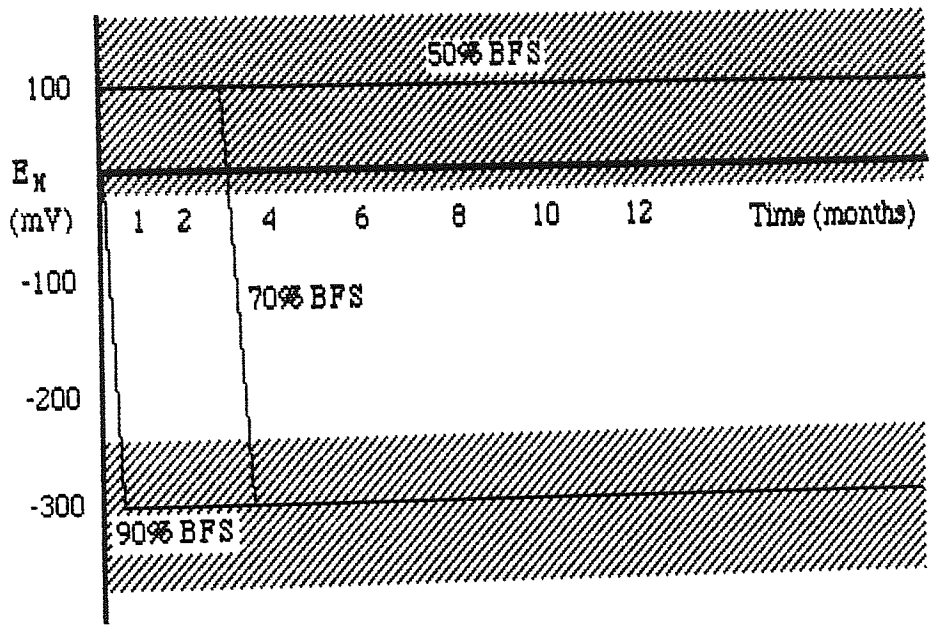

Figure 20 *Variation of redox potential with time for slag cements (After Atkins et al)*

It can be seen from the above that the change from oxidized to reduced conditions in the matrix is not a smooth transition but occurs as a switch between the two states. The poising capacity depends on the composition of the initial mix and it is only when the oxidizable content associated with the OPC is exhausted that the onset of reducing conditions rapidly occurs. It is interesting

to note that the absolute redox potential does not depend on the slag content, all compositions producing results within the shade area. The authors (83) suggest that for the 50% slag, reducing conditions prevail after c, 18 months.

Contributions to the study of pore solution chemistry from other sources use some of the methods described above and essentially confirm these findings. Kittl *et al* (124) have examined the products formed after slow drying of OPC pore solutions, to reveal Ca, K, & Na hydroxides, gypsum, ettringite and minor phases but no similar work is published on slags.

Dron (125) has presented a hydration model to predict the composition of slag hydrates formed with and without gypsum, which has been reproduced by other authors.

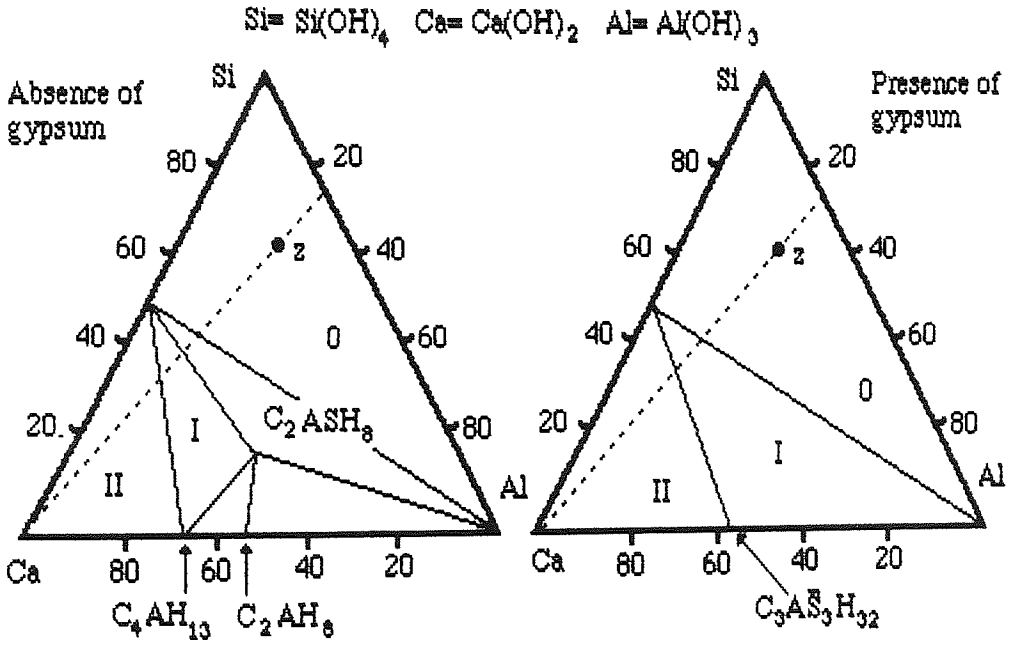

Figure 21 *Hydration models to predict the composition of hydrates (After Dron)*

This is shown above in figure 21 and is based on the thermodynamics of the $CaO - Al_2O_3 - SiO_2 - H_2O$ system. If the slag has a composition represented by point 'Z', that of the slag - 'lime' system lies on the Ca - Z line. The hydration products will have the same overall composition and so will also be on this line. Thus, if $Ca(OH)_2$ is present it will lie in area II and other hydration products will be calcium silicate hydrate and tetracalcium aluminate hydrate.In the presence of sulphates the system is modified to that shown on the right. Note that monosulphate (AFm) is only produced when the calcium sulphate initially added has reacted to form ettringite and the system is depleted in sulphate. Although this model does not account for sulphur contributed by the slag, nor does it account for the reducing conditions, it does however, provide a useful visualization of the developing hydrate chemistry.

Hinrichs (126) and Oder (127) have published work on the hydration of slag using the Kondo and Ohsawa (100) technique criticized by Luke and Glasser (103) Their work has shown the rates of slag hydration as a function of particle size and curing regime. Supporting techniques have involved the measurement of compressive strength, free 'lime' (measured as hydroxide) pore size distribution and permeability. Their pore size distribution data is in broad agreement with previous work (62, 64, 128) showing a large skew in the distribution towards finer pores. They measure between 60% and 90% of the pores are less than 10 nm after one year's hydration. Feldman (129) suggests that mercury intrusion alters the microstructure of cement pastes and suggests that the results should be treated with caution. Roy (62) and others (8,9) employ Bakker's model (130) to account for the fine pore size of slag cements (figure 22). This proposes that the difference in porosity between OPC and slag cement porosity can be accounted for in terms of their different hydration mechanisms. Bakker reasons that in addition to the hydrates formed around the slag and clinker grains, there are additional (and identical or related) hydrates formed in the gaps between adjacent particles, as shown below.

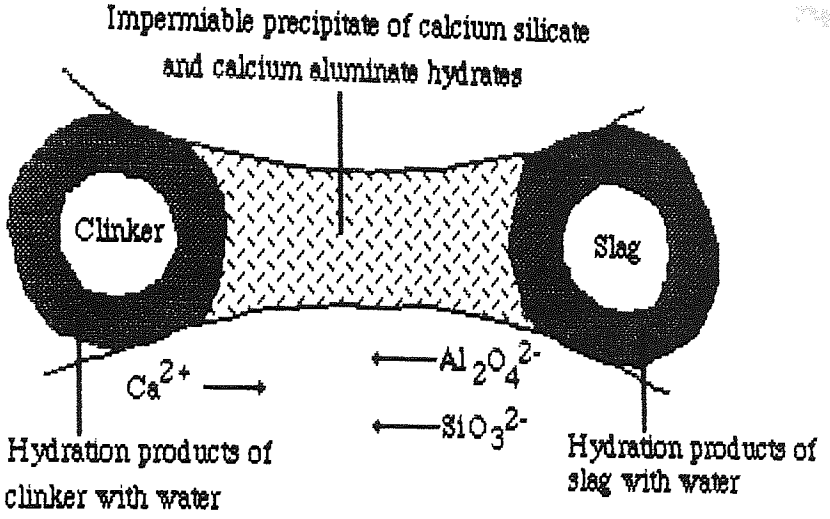

Figure 22 *Infilling of pores during long term slag hydration (After Bakker)*

His conclusions are drawn from measurements of permeability and his findings that the low permeability state is maintained in pastes cured at elevated temperature are confirmed by other workers (62,64,128,131). A thorough treatment of the developing porosity and permeability in slag cements has been made by Roy and co-workers at the Pennsylvania State University (62,64,128,131). Their work has, in addition, considered the physical and chemical development of hydrating slags and includes calorimetric investigations (62,64), mass transport studies (131), and pore solution chemistry work (132). Silsbee *et al* (132) have examined the fractionation of slag pore solution during extraction by taking samples at intervals of 14 MPa pressure up to a maximum of 275 MPa. Their results show a decrease in Na, K and Ca with pressure of between 20% and 50% above a limiting pressure of c.25 MPa. The anion analyses only consider sulphate, even though they have used ion chromatography for their determination. No mention of extraction temperature is made or whether oxygen was excluded from the pore extraction system. At this first stage a mechanism for fractionation is not presented. This work also presents results for the pore fluid chemistry at early ages which is

complimented by their physical data (65).

Roy and Idorn (62,68) propose a model for slag hydration, (figs 23 & 24) which has been reviewed by other authors. In the short term, they presuppose sufficient heat of hydration for the initial hydration of the slag and make the following observations (68):

(1) Dilution of portland cement by slag reduces proportionally the $Ca(OH)_2$ to be precipitated in the pore space.

(2) Slag hydration occurs along with OPC hydration.

(3) The OPC fraction releases alkali metals and calcium hydroxide whilst the slag fraction retains these in the developing C-S-H.

(4) The lower the calcium hydroxide concentration, the more alkali metals can be accommodated by the C-S-H.

(5) The combined OPC-BSF hydration results in a paste of greater density with smaller average pore size and correspondingly lower permeability than pure OPC.

The long term hydration of Portland cement continues to precipitate crystalline calcium hydroxide in the pore spaces whilst diffusion controlled gel formation occurs as an inward growing reaction rim. The lamellae of this rim are often annual, being associated with yearly wetting and drying cycles. The liberated calcium hydroxide reacts, in the presence of moisture, with the hydrating slag grains to produce more C-S-H of a finer, denser microstructure than that of OPC, Because of the increasing thickness of hydrate cover, the diffusion rate and hence the rate of hydration gets progressively slower. Samples exposed to the weather for tens of years show some unreacted material in the center of grains when viewed in thin section. (The arboreal analogy is less than ideal in as much as the youngest hydrates are those closest to the core of the grain, unlike the cambium layer of a tree).

The question of early hydration of slag is the one point on which there is some reasonable disagreement between authors. Roy and Idorn (62, 68) suggest that the formation of the first hydrates is rapid, which is in direct opposition to the findings of Regourd (97),who claims that both the slag and clinker are

covered with hydrates originating from the OPC. Regourd suggests that the slag does not appreciably hydrate for about 28 days but work on the absolute amount of slag hydrated (83,126,134) supports the view of Roy an Idorn (62,68) that between 20% and 40% of the original glass does indeed react within two days.

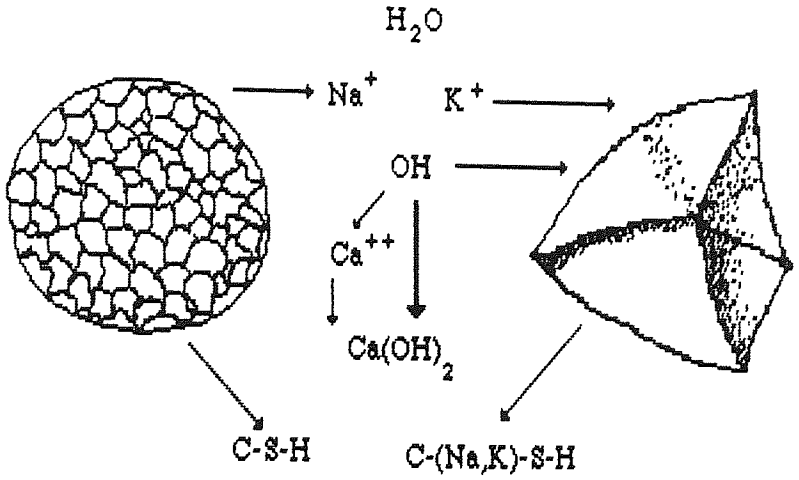

Figure 23 *Short term model of hydration (After Roy and Idorn)*

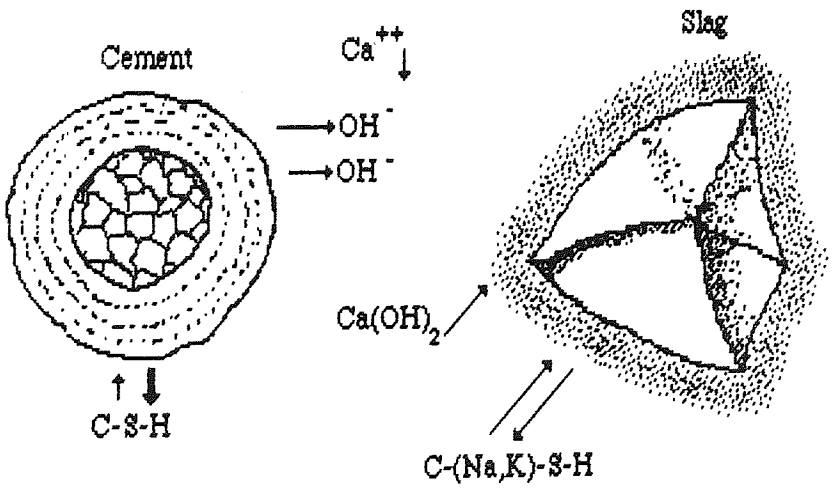

Figure 24 *Long term model of hydration (After Roy and Idorn)*

The most recent large scale review of slag hydration chemistry is that presented by Uchikawa (135) to the 1986 Rio de Janeiro congress (8th ICCC). He acknowledges the contribution of Daimon (136) to the Paris congress in 1980 (7th ICCC) and discusses the hydration of slag in the presence of various cement minerals. Uchkawa refers in particular to the acceleration of alite hydration in

the presence of slag (66) and draws attention to his own work on slag dissolution (*op.cit* 137) which suggests that the amount of Ca, Si and Al in solution are directly related to the amount of monomer present in the original glass. This is discussed more thoroughly in chapter 5.

In conclusion, it would appear that slag hydration occurs concurrently with clinker hydration, reacting with hydroxyl and sulphate ions in solution to produce hydrates similar to those of OPC hydration. Continued reaction produces a fine grained matrix of low porosity and permeability around the slag grains, at least in part, by the consumption of calcium hydroxide in the course of slow authigenic hydration. The local environment is strongly reducing and the matrix formed is chemically able to resist changes to both this reduced state and to its alkalinity. The implications for radioactive waste encapsulation are that slag cement offers a well poised and well buffered system of low permeability and connective porosity. There is much published work on the radiolytic oxidation (of water) in cements and other radiolysis effects which are essentially out of the scope of this review. Published material from the USA (138) and Scandinavia (139) suggest that from the yield of the radiolytic oxidation species produced, the most significant will be molecular hydrogen and work continues in this field. No work has so far been published on the interaction between aggressive re-combined species (from radiolysis of water) and the hydrating cement system. This subject is currently being investigated by the UKAEA (Harwell) but has not yet been published.

Chapter 2
Materials and Experimental Methods

2.1 Examination of raw materials

In developing an experimental approach to the analysis of slag hydration chemistry, it was seen as important to examine the constituent raw materials. The materials used in these experiments were both commercially supplied products. The Portland cement used was a Blue circle "Westbury" ordinary Portland cement and the slag was "Cemsave" produced by the Frodingham cement company of Scunthorpe.

The materials were stored as received, in 200 l steel drums containing the double bagged material wrapped to exclude moisture. Visual inspection of each drum on arrival confirmed that the materials had been received in a dry condition and the drums were stacked in the laboratory store room until required for use.

On opening each drum, the surface layer was carefully removed and discarded to eliminate any hydrated grains at the surface and any foreign matter which may have fallen in during handling.

Examination of the Portland cement Powder by optical microscopy suggested that no hydration had occurred during storage and this was confirmed by DTA (chapter 5.3) before casting. The unhydrated samples were examined extensively by scanning electron microscopy, both to determine the particle size and structure and to attempt to identify the phases present. Because the manufacturing process involves grinding of the material, little information can be gained on the crystallinity of the material other than from occasional fracture and cleavage fragments. Phase analysis was consequently difficult and time consuming, and relied on comparing variations in elemental composition as revealed by x-ray emission spectrometry.

Although over a dozen thermodynamically stable species are theoretically possible (chapter 1), many of which exist as allotropes (pseudomorphs), identification of slag particles under the electron microscope is not a simple task. Poorly developed crystals and amorphous glass fragments cannot readily be identified by morphology alone.

Examinations were made by scanning electron microscopy of powder samples mounted on SEM stubs by double sided tape. The samples were made conducting by vacuum deposition of carbon onto the surface. At 20kV anode voltage, the zone of excitation in the sample is approximately one micron in diameter, producing fluorescent x-rays which are collected by a detector at 45° to the sample surface. This data was processed in a "Link Systems" spectrometer which combined a data processor with a multichannel and twin, single channel analyzers. The accumulated spectra were then stored on floppy disk until required for analysis. The results from this system were used in two ways; qualitatively, as a display of counts against x-ray energy thus giving an immediate impression of the elements present or quantitatively after certain corrections had been made to the data. Quantitative energy dispersive x-ray spectrometry requires the calibration of the instrument against an internal standard target (cobalt) and the data collected to be corrected as follows:

1) Atomic number correction - The efficiency of the x-ray generation by an electron beam incident on a target increases with the atomic number 'Z' of the target.

2) Absorption correction - The absorption 'A' of x-rays generated within a target increases with the electron density and hence atomic number of that target.

3) Fluorescence correction - There is a statistical probability of leaving the target atoms in an excited state from which they will emit a photon by fluorescence 'F'

4) Dead time correction - The detector has a finite recovery time after detecting a photon, during which it cannot resolve another event. Dead time correction is proportional to count rate.

The first three corrections give a acronym to the range of software used in processing the data; "ZAF". Two programs were used, "ZAF-4" is the commonly used energy dispersive spectrometry (EDS) correction which requires a flat target surface hence its use on hard, polished, non-porous materials. "ZAF-PB" is a similar program which is intended for particle analysis and incorporates corrections for surface morphologies. This was rejected after several trials in favor of "ZAF-4" for two reasons: First, the assessment of surface correction is very subjective and susceptible to operator error and secondly, the microscope was unable to resolve surface detail at high magnification (see later micrographs) so further further assumptions about the target surface had to be made.

The problem of providing a surface flat enough to use "ZAF-4" was overcome by painting a ring of epoxy resin around the edge of an SEM stub and, after hardening, forcing the powdered sample (moistened with a little propan-2-ol) into the shallow depression so formed. The surface was pressed flat with a clean microscope slide to form a powder compact and the sample was then carbon coated. The surface was electrically connected to the stub by lines of conducting (colloidal silver) paint bridging the epoxy.

Counts were made for 500 seconds scanning the spot over an area of c.230 x 300µm to accumulate spectra which were converted to compositional data. The software determines the last element (oxygen) by stoichiometry hence table 2 is presented as relative oxide compositions.

Unfortunately, the nature of the barrier detector does not allow the detection of the lightest elements (lower than fluorine) so traces of Li, Be, and naturally H, O and C are omitted. As oxygen is likely to be the most significant of these, and

inline with current practice, the results are presented as weight - oxide - percent. It is important to note that blast furnace slag is not fully oxidized and that oxidation of free sulphides and free iron may occur some time after manufacture. This can be shown as a slight weight gain on ignition

Table2 *Percentage oxide composition of raw materials*

Oxide	BFS	OPC
CaO	42.3	64.5
SiO_2	36.7	19.8
Al_2O_3	10.1	6.8
Fe_2O_3	0.4	2.1
MgO	6.4	1.0
MnO	0.3	0.1
Na_2O	0.5	0.4
K_2O	0.6	0.5
TiO_2	0.3	0.4
SO_3	2.2	2.9
Total	100.5	99.4
LOI	+2.9%	-1.1%

The loss/gain on ignition was performed in a silica crucible over a Bunsen burner to dull red heat for two hours with the lid partially open. The weight gain of the BFS is a minimum value as sulphurous fumes were evolved during heating.

The high iron content of blast furnace slag was investigated independently as it proved to be a problem in NMR spectroscopy and needed to be removed (chapter 5.5). Hydrated samples intended for NMR studies were passed through a magnetic separator to remove any strongly magnetic phases present. It was

decided to attempt a comparative separation of the unhydrated slag in order to determine the nature of the iron rich phase.

Surprisingly high amounts of a magnetic phase were recovered from blast furnace slag (c.0.5%) whilst 1kg of Portland cement yielded insufficient material to analyze. Electron microscopy showed the phase recovered from the slag to be dominantly iron with trace amounts of barium, aluminium, silicon, calcium and manganese. Assuming that the trace elements were of sufficiently low concentration to indicate that they were not alloying components incorporated in the iron intentionally, it would seem reasonable to suggest that the iron was not a product of grinding, as had at first been supposed. Given then, that the iron is a remnant of the blast furnace, it seems likely to be free iron as it is easily removed by magnetic separation. The only other ferromagnetic phase is magnetite (Fe_3O_4) which seems an unlikely component, in view of the reduced nature of the slag (the sulphides and wüstite (FeO) are not ferromagnetic).

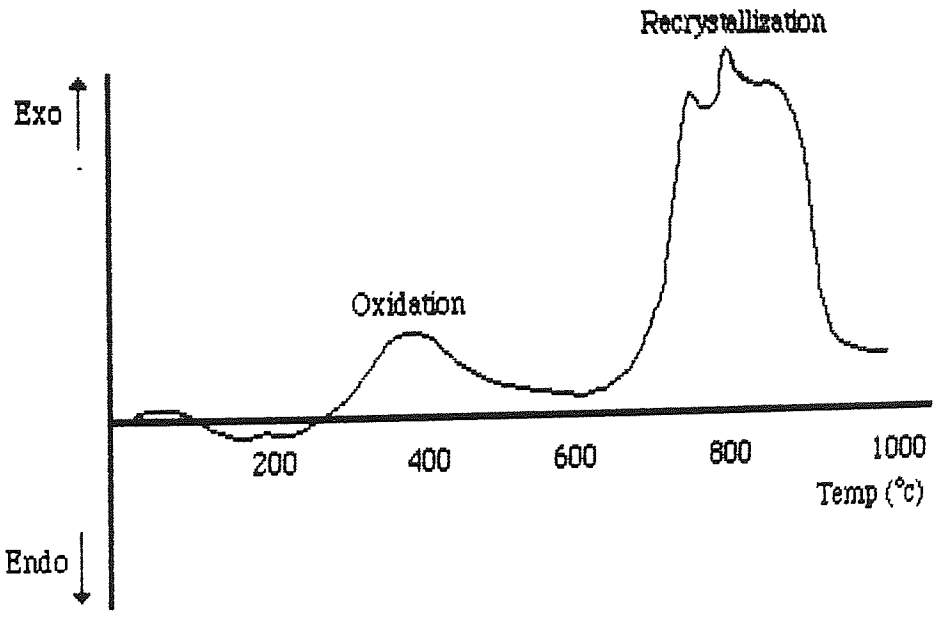

Figure25 *DTA thermogram of iron phase from unhydrated BFS*

Glasser (110) mentions free iron as a possible electroactive species but makes no

reference to having identified it *per se*. Differential thermal analysis showed an endotherm at 300°C suggesting oxidation of either Fe or FeO to Fe_2O_3 and a strong exotherm at about 650°C as shown in figure 25.

The likely reaction scheme during DTA analysis is as follows:

$$4Fe + 3O_2 \xrightarrow{\text{oxidation 300-400 °C}} 2\gamma Fe_2O_3 \xrightarrow{\text{recrystallization 600-900 °C}} 2\alpha Fe_2O_3$$

The phase was also examined by x-ray diffraction which suggested that the material is dominantly α - iron. To determine the origin of this phase, an elemental analysis was performed after dissolution. The materials used in grinding and milling both blastfurnace slag and cement are dominantly manganese - iron alloys. A low manganese concentration in this phase would suggest that its origin is the blastfurnace and not from the wear of milling components. Typically these hard brittle alloys contain tens of percent manganese by weight.

Two small samples of the metallic powder were dried over P_2O_5 for several days and approximately 0.2g was accurately weighed into two silica crucibles. The samples were intimately mixed, one with sodium carbonate, the other with sodium tetraborate. The salts were fused at red heat for two hours and then allowed to cool in a desiccator. Dissolution in aqua-regia was done with care and the covered samples were allowed to stand overnight. The solutions were diluted with water to one litre and the crucibles were re-weighed. Loss of silica was 0.12 & 0.17g, which is to be tolerated given the aggressive environment to which the crucibles were exposed. The solutions were filtered through sintered crucibles which were washed, dried and weighed to show, in both cases a 98% dissolution. The solutions were diluted by a factor of 100 and analyzed by

inductively coupled plasma emission spectroscopy at the British Geological Survey laboratories, Keyorth Nottingham.

The results show that the material is 97.4% iron with 1.1% manganese and 1.4% aluminium. (It was assumed that all the sodium, silicon and/or boron were from the fusion). The only other element present above detection level was barium, an order of magnitude lower concentration than manganese. Given these results it would seem reasonable to suggest that the iron is syngenetic with the slag and is not a product of grinding.

As discussed in chapter 1, a great deal of interest has been shown recently concerning the determination of glass content in blast furnace slags. In order to determine this for 'Frodingham Cemsave' several x-ray diffraction traces were produced using a *'Philips'* diffractometer .

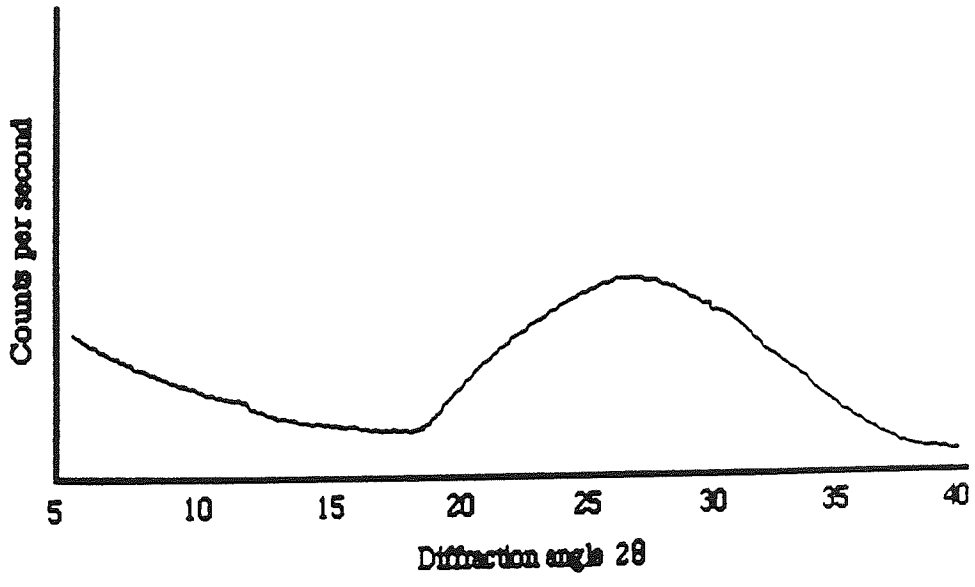

Figure 26 *X-ray diffraction of unhydrated BFS showing amorphous region between 22° and 38° 2θ*

The sample was loaded into the sample holder and flattened, again using a clean microscope slide and the sample holder height adjusted to the focus of the

instrument. Using a scan speed of 2° per minute (2θ), diffraction angles from 4° to 55° could be measured and the resulting spectra of angle against count rate were plotted by a chart recorder. The results show that the material does not have any domains of long range order producing peaks in the diffraction diagram but shows a gradual increase in count rate between 22° and 30° 2θ, described in the literature as the "glass hump" (16), which falls back to background at 38° 2θ.

This can be interpreted as localized domains of short range order (Porai-Koshit's (19) "embryos of crystallization" or Zachariasen's (21) "network formers") producing weak reflections.

Examination of the unhydrated materials under the scanning electron microscope shows that BFS is generally finer than OPC and produces fragments of ill-defined shape which display occasional conchoidal fracture surfaces typical of a glass, (figure 27). Portland cement, by comparison, produces cleavage fragments with many straight edges. Identification of the larger particles as either slag or Portland cement can be effected by comparison of their calcium to silicon ratios. In blast furnace slag, $CaO : SiO_2$ ratios average about 1.2 : 1, whilst those for Portland cement are much higher, typically 3.3 : 1. A secondary check can be made by comparing the manganese and magnesium contents. Magnesium is about six times more concentrated in BFS than in OPC and manganese is easily detectable in BFS but in very low concentration in OPC.

For reference, Lee (69) has estimated the mineral composition of Westbury cement and his results are shown in table 3 overleaf.

Table3 Mineral composition of 'Westbury' cement (After Lee (69))

Mineral	wt.% composition	symbol
Tricalcium silicate	53.3	C_3S
Dicalcium silicate (β)	16.9	C_2S
Tricalcium aluminate	13.9	C_3A
Teteracalcium alumino-ferrite*	6.6	C_4AF
Gypsum ($CaSO_4\ 2H_2O$)†	2.8	CS
Free lime (CaO)	0.9	C
Periclase (MgO)	1.2	M

* So called "ferrite" phase solid solution series between C_6AF_2 and C_6A_2F.

† Gypsum occurs with varying moisture content.

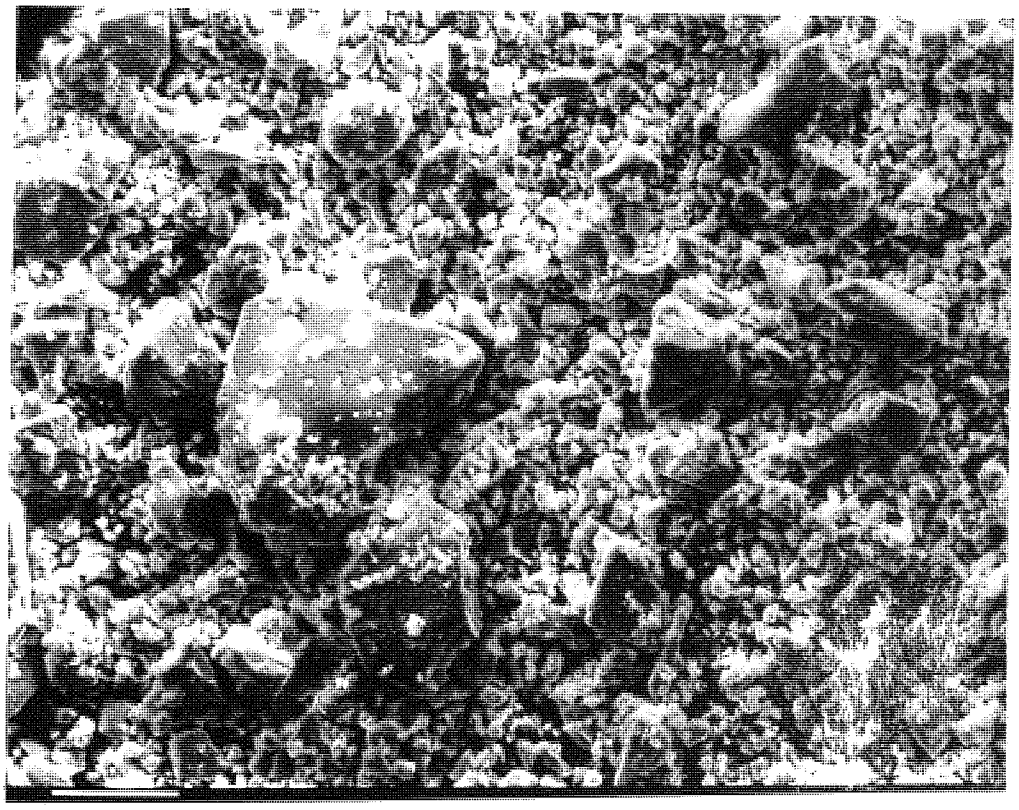

Figure 27 Scanning electron micrograph of unhydrated BFS
(Scale bar represents 40 μm)

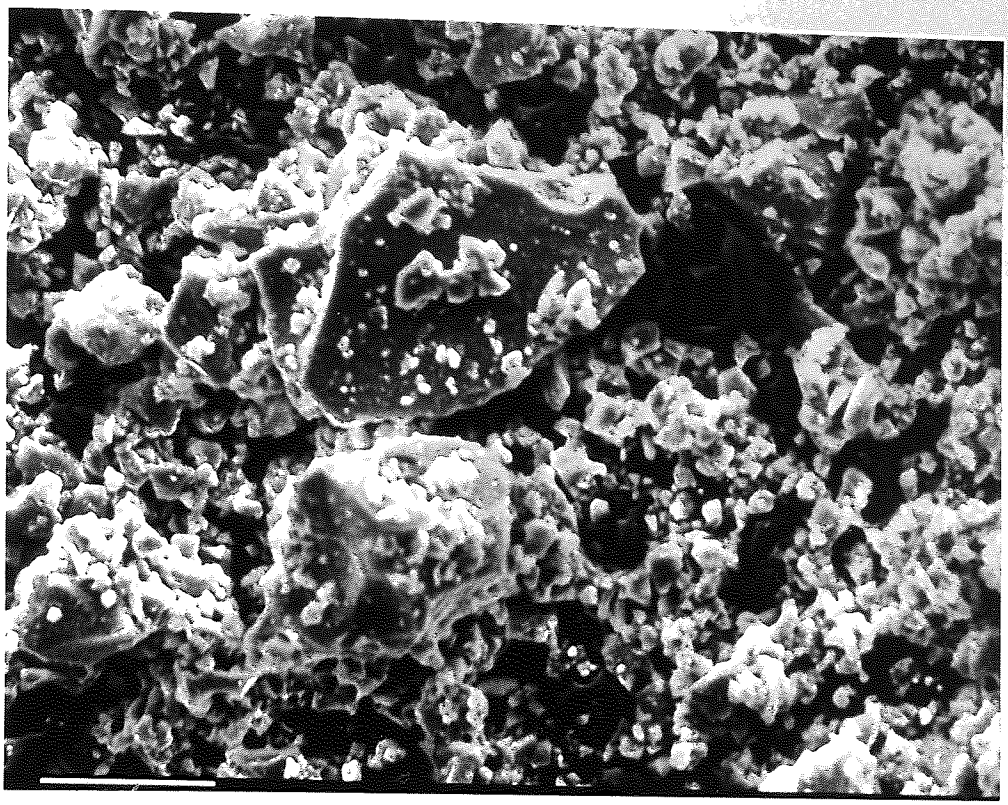

Figure 28 Scanning electron micrographs of unhydrated OPC
(Scale bar represents 40 µm)

2.2 Hydration studies - sample preparation

In designing the experimental programme for investigating the hydration chemistry of slag cements, a standard method of sample preparation was considered of high priority. To make best use of previously published work, a scheme used by UKAEA Winfrith was adopted, thus enabling direct comparison of results. This consisted of weighing the individual components (to 0.1g) into a 125µm sieve and sieving the solids together to attain a high degree of mixing and to break up any agglomerations of grains present in the dry materials.

This powder was then added over a period of five minutes to the deionized water which had previously been measured into a mixing bowl. Mixing in all cases was carried out with a "Hobart" industrial mixer operating at 90 rpm. Each batch was mixed for twenty minutes in total, including the initial five minutes during which the solids were added to the liquid.

The resulting cement paste was cast into a number of air tight plastic cylinders (45mmø x 65mm) which were vibrated to remove air bubbles, capped with a film of elastomer sealing film and finally sealed with push on lids. These cylinders were then rotated for twelve hours after casting to reduce settlement

and bleeding of pastes before being stored in environmental cabinets until required for use.

The mix compositions which were finally chosen were all of high slag content , namely 50, 70 & 90% BFS mixed at either 0.3 or 0.4 water to solids ratio. The prepared cylinders were divided into three batches for storage at 25, 50 & 70°C, thus producing eighteen possible combinations of composition and curing temperature. The relatively high curing temperatures were chosen to represent the core temperatures obtained on an industrial scale in a 200 l waste drum. Although the heat of hydration of blended BFS - OPC is substantially lower than that of pure Portland cement, the heat of hydration is still sufficient to raise the core temperature of a large cast substantially above ambient conditions. Thus a maximum temperature of 70°C was chosen to represent the upper temperature limit acceptable in an industrial application. The two water / solids ratios were chosen to be complimentary to previous work (140) and because the higher water content is slightly beyond the limit at which the paste will bleed on standing, whilst the lower will not.

2.3 Examination of the Hydrating system: Experimental methods

Investigations into the hydration chemistry of a complex system such as this can progress in three possible ways:

1) Examination of the hydrating system as a whole, through some change of the bulk properties of the material

2) Examination of the solid phase in isolation

3) Examination of the liquid phase in isolation

In the latter cases it is important to realize that the separation of any part of the system from the others must change the chemistry of that system to an unknown extent. Consequently, whilst every effort has been made to cause as little change as possible, it is important to consider the slag - cement - water - hydrates system as a composite and not as a simple mixture of its components.

This is particularly important in simple operations such as drying (see below) where it is possible to introduce a wide range of avoidable uncertainties.

2.3.1 Examination of the hydrating system as a whole

2.3.1.1 Conduction calorimetry The measurement of the development of the heat of hydration has been used extensively both in hydration studies (62 -69) and quality control in the cement industry. The method employs a cell containing a sample of cement paste in intimate contact with an aluminium heatsink. The heatsink base is maintained at a constant temperature by a water bath in which the whole cell is immersed. Thermopiles measure the flow of heat from the sample to the bath through the heatsink and the potential they produce is amplified and recorded with respect to time. This method allows us to follow the hydration of the sample over the first few days of hydration typically around 100 hours.

The mathematical interpretation of the calorimeter data requires a reference amount of heat to be applied to the cell, which permits each individual experiment to be calibrated after the heat evolution has fallen to a very small rate. This is effected by an electrical heating element inside the sample can which is in contact with both the sample bag and the can through a known quantity of 'transformer' oil. By applying a known current through the heater and measuring the voltage across the heater it is possible to determine the power dissipated.

By measuring the calorimeter output whilst the heater is conducting, it is possible to calibrate the output curve in terms of Watts per gramme of cement paste with respect to time. A more thorough treatment of the mathematics of the calibration is presented in chapter 3.

The choice of instruments centered on two basic types: In the former, the dry cementitious materials are loaded into the cell, which is sealed and placed in the

water bath to equilibrate for temperature. When this has occurred, a measured amount of water is injected, mixing with the solids by capillarity. This method was rejected in favor of the "Wexham" - type instrument which permits investigation of pastes mixed outside the cell. This latter type of instrument has been modified to operate also by the water injection method, thus allowing studies of a very early age hydration to be made.

Data collection is by chart recorder and digital serial transfer to a 'BBC model B' microcomputer, which was also used to process the results. The chart recorder provides immediate hard copy and acts as a backup incase of power failure or data corruption.

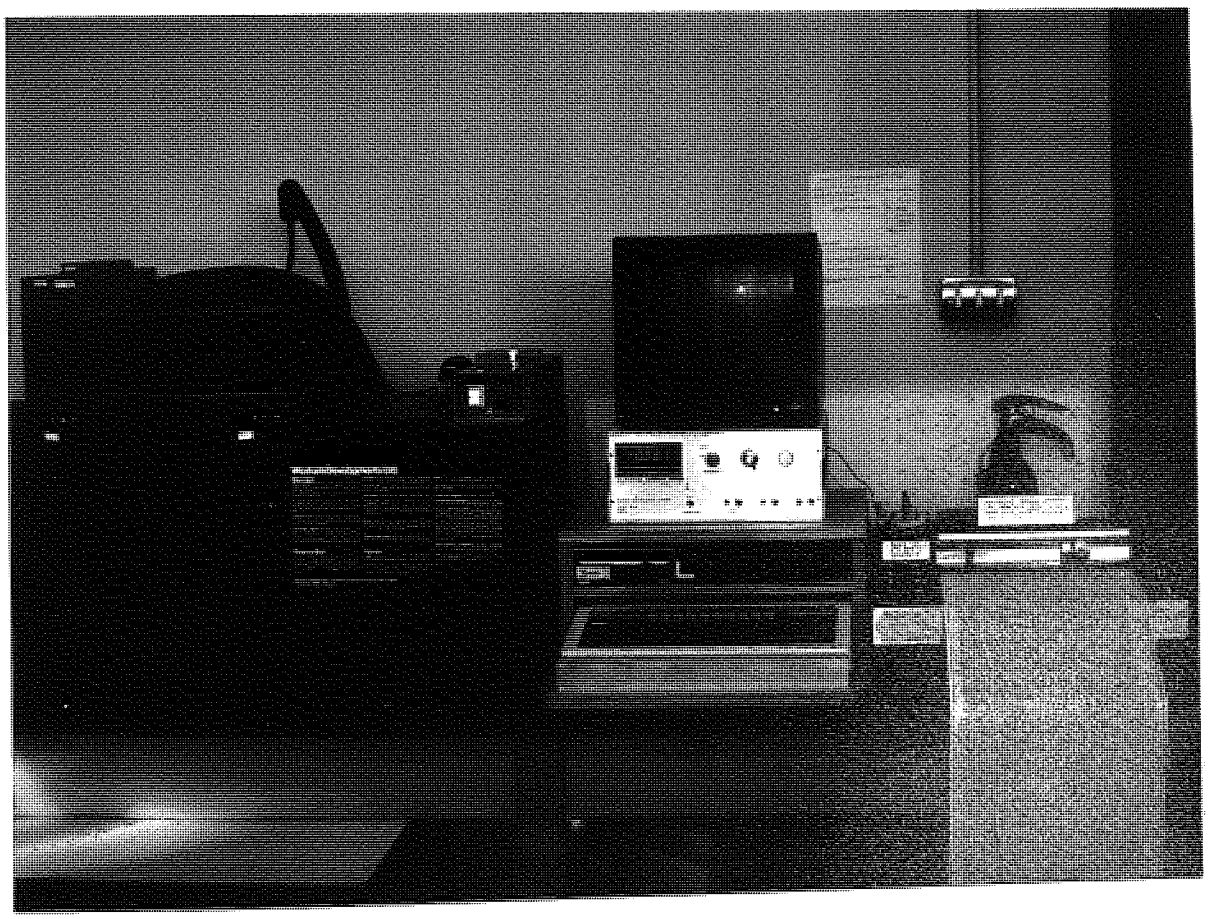

Figure29 *Conduction calorimeter in use. To the left is the main water bath containing the sample cells and the controll unit is on the right, below the monitor*

2.3.1.2 Kinetic studies by chemical shrinkage Chemical shrinkage is the phenomenon of dimensional change associated with the development of connective porosity during the hydration of a cement. The volume of the unhydrated cement materials plus hydrates and remaining water is measurably less than the volume of the original solid and liquid components. By measuring the volume change with respect to time, it is possible to determine chemical kinetic data regarding hydration reactions.

In this work, the dilatometry method has been used, following its successful deployment in Portland cement hydration studies (62, 63, 74-79). The apparatus consists of a test tube containing the cement paste sample into which a rubber stopper containing a graduated pipette is fitted (figure 30). The pipette holds a column of water overlying the sample which is held at constant temperature by immersing the assembly in a water bath. As the paste hydrates, water from the pipette fills the pores between the solids causing the column of water to fall. By measuring the height of water with respect to time, it is possible to follow the development of connective porosity as hydration progresses.

This method was chosen as it complements the data obtained by isothermal calorimetry and extends the time scale for the measurement of reaction kinetics to over one thousand hours.

The results obtained by this method are interpreted with respect to the "Powers" model (143) of cement hydration and their mathematical treatment is shown in chapter 4.

The method may be criticized for allowing water from the dilatometer to enter the hydrating paste, thus increasing the the effective water : solids ratio of the sample. In addition, Geike (75) postulates that the strongly alkaline pore solution will react to some extent with the glass test tube. Microscopic examination suggests that these effects are minimal as shown in figure 153, in chapter 7.

Together, conduction calorimetry and chemical shrinkage offer the

opportunity to study the hydration of cement paste without introducing chemical change into the system. There is a degree of overlap between the time scale on which the methods operate allowing some correlation of the results obtained. These independent methods may then be used as an aid in interpreting the results of chemical methods described below.

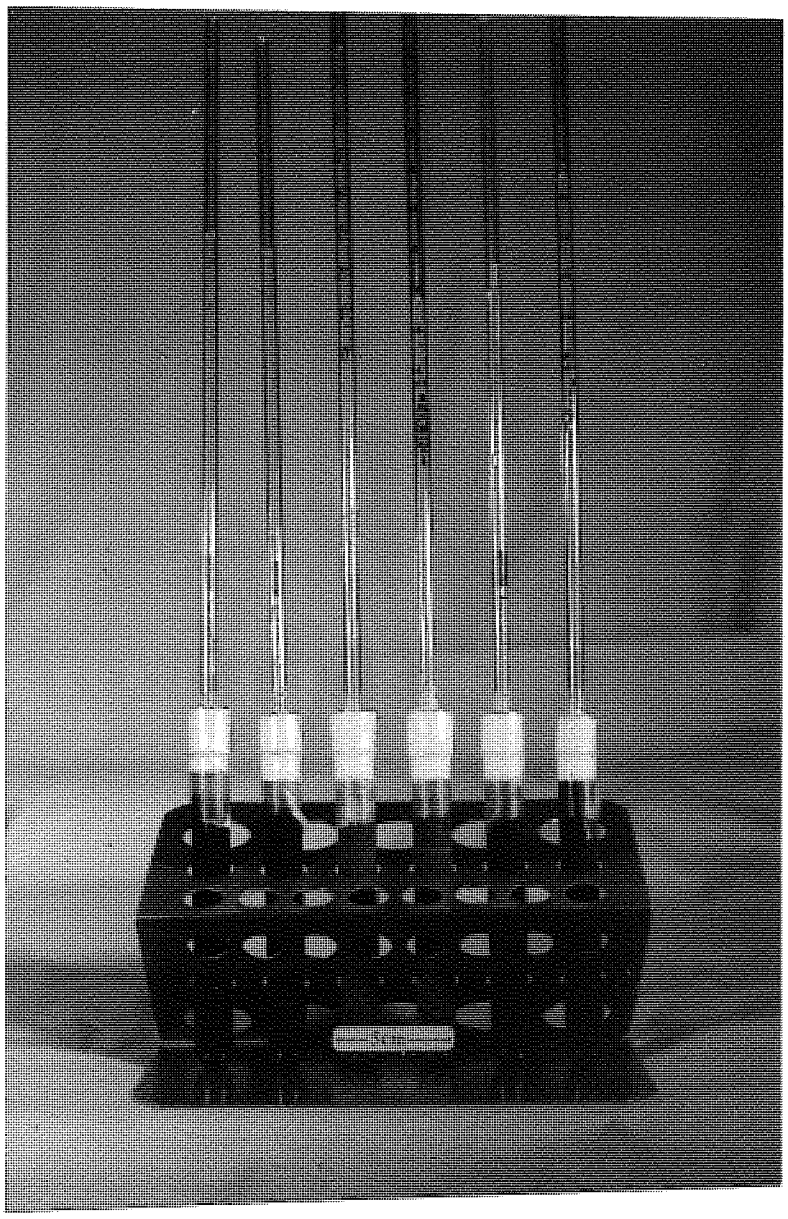

Figure 30 *Dilatometer assembly before submersion in water bath*

Note elastomer sealing tissue around top of each tube

2.3.2 Examination of the solid phase

In the examination of the solid phase chemistry, it was considered important to be able to stop the hydration of the cement paste promptly, because at early ages, the drying time may represent a reasonable proportion of the time of hydration. Oven drying was dismissed for two reasons: First, the method of drying to constant mass at a standard temperature of 105°c introduces the difficulty of defining the point at which sufficient water has been removed to consider the hydration reactions have stopped. This would be of particular importance when considering young pastes, as discussed above. Secondly, increasing the temperature to dry the samples would increase the rate of the hydration reactions, causing the properties measured to correspond to a later (and unknown) hydration time. In addition, Taylor (144) is critical of oven drying for a reason applicable to pastes of all ages; that some of the hydrates decompose at this temperature. In the light of these arguments, an alternative method of drying was seen to be desirable.

Four methods were investigated:

1) Vacuum drying. This method was rejected as it would not stop the hydration reactions sufficiently rapidly.

2) Freeze drying. This was potentially a good method although time consuming. The freezing of the pore solution, for example, in liquid nitrogen, would certainly arrest the hydration reactions rapidly but the method was (unfortunately) rejected owing to the limited availability of suitably large apparatus. The extent of disruption of the microstructure during rapid freezing was consequently not investigated.

3) Critical point drying. Generally, this is an excellent method of drying which relies for its operation on the replacement of water by a liquid of low critical point. In practice, an intermediate solvent is normally used to replace the water which is itself, replaced by the final solvent. This is then raised

above its critical point thus drying the sample. The great advantage of this method is that as the final stage involves a change of state above the temperature and pressure at which the liquid and gas are in equilibrium, there is no meniscus of liquid moving through the pores. The obvious consequence of this is that the fine structure of the sample will not be destroyed by the surface tension of the liquid meniscus moving through the pores. As several percent of the porosity in slag cements (62) is in the range 5-10nm, the surface tension associated with an aqueous meniscus of c.0.03Nm^{-1} in this region would result in forces of the order tens of tonnes acting in the fine pores. Critical point drying prevents the formation of a meniscus and therefore preserves the fine structures which are destroyed by other drying methods.

The requirements for the use of the method on cements are as follows: The two (or more) solvents used must be miscible with each other and water must be miscable with the first used of these. Naturally, none of the liquids used must react with the cement sample and the critical point of the of the final solvent must only be slightly above room temperature and pressure.

For biological samples, (the most common samples dried by this method) primary solvents are commonly amyl acetate or acetone and the secondary liquid carbon dioxide. For cements, carbon dioxide is wholly unacceptable owing to the potential for carbonation reactions. This effectively also excludes the use of acetone because of the high solubility of carbon dioxide in this compound. Initial experiments using amyl acetate and carbon dioxide showed a marked carbonation of the cement (revealed by DTA - endotherm at 900°c) which suggested that an alternative secondary solvent needed to be identified. Two compounds with critical points low enough to be used in commercially available apparatus are xenon and Freon-13. Both these liquified gasses are obtainable in the UK but are

expensive and disposal of Freon was considered prohibitively difficult. As neither was available for trial experiments the method was eventually abandoned, though this was with some regret as the method would appear to offer a significant advantage for microstructural studies.

4) Solvent replacement & vacuum drying. In this method the cement paste sample is crushed (to approximately 5 mm dia.) and dispersed in approximately ten times its own volume of an organic solvent in which water is soluble. The choice of solvents was made by rejecting compounds which are known to react with cement minerals or their hydrates (ie methanol, ethanol) or compounds in which carbon dioxide is very soluble (ie acetone). Propan-2-ol was chosen as it has no reported reactions with the sample material and is very volatile. The sample was ultrasonically dispersed in the alcohol, allowed to settle out and the supernatant liquid decanted off. This was replaced by a second, similar volume and the flask shaken for five minutes in a mechanical flask shaker. The process was repeated and the flask shaken for half an hour. The resulting slurry was then filtered and washed with 10 - 20 ml of anhydrous propan-2-ol after which the filter paper was folded and transferred to a vacuum desiccator. The alcohol was removed as a vapor by a two stage rotary pump over a period of 5 - 8 hours. Determination of the final dry stage was determined empirically by the use of self indicating silica gel. If slightly moist (pink) silica gel was used in the desiccator as an indicator, the system could be left pumping until the absorbed moisture in the gel was removed. This was shown by the characteristic deep blue colour. As no reverse of this colour change was seen during storage, it was assumed that the samples had been adequately dried.

As an additional precaution during desiccator storage, a container of 'Carbosorb', self indicating soda lime, was also kept in the desiccator to absorb any carbon dioxide.

The dried samples were finally ground by mortar and pestle and then seived through a standard 75μm seive before being transferred to sample bottles. These were then stored in a desiccator until required for use.

2.3.2.1 Selective dissolution

A number of papers (100, 103, 104) have been published in recent years which have described methods of following slag hydration by dissolution of the hydrates and unreacted Portland cement. A preliminary set of experiments using the method reported by Kondo and Oshawa (100) yielded erroneous results (Ch. 5) from dissolution in salicylic acid and methanol. A review of these methods by Luke and Glasser (103) proposed dissolution with sodium carbonate and EDTA which was adopted as an alternative. The method is a development of that published by Demoulian *et al* (102) and uses alkaline EDTA / Na_2CO_3 solution containing triethanolamine to dissolve the non-slag fraction which is recovered, after shaking, on a glass fiber / asbestos filter supported in a Gooch crucible. This method has very recently been modified by the authors (104) by coating the reaction vessel with a silane to reduce the possibility of fine particles remaining on the walls after washing.

A dissolution method was seen as desirable as it provides an absolute measure of the quality of the unhydrated slag remaining in a sample. As slags are glassy materials, diffraction methods would seem unsuitable for examining their mineralogy. This wet chemical method offers an alternative which, although time consuming seems to be reliable.

2.3.4 Thermogravimetry

Thermal methods have been used in cement studies for a number of years and both the thermogravimetric and differential thermal methods are well established techniques. Thermogravimetry measures weight change in a sample

during heating (or cooling) providing a thermogram of weight vs temperature. This method is particularly suitable for cementitious materials as it allows the study of the following weight changes during heating:

1) Up to about 110°C (depending on heating rate); loss of adsorbed water from the sample surface. [* Taylor (144) suggests this is partially due to decomposition of the hydrates]

2) 130°- 200°C ; loss of loosely bound water from the CSH gel phase.

3) 450°- 500°C ; loss of structural water from calcium hydroxide

The method is particularly useful as a means of measuring the calcium hydroxide content of the cement with a high degree of accuracy (±2% wt.)

The instrument chosen is a British thermobalance supplied by Stanton - Redcroft of Wimbledon and is their model TG760. Its advantage over other instruments is the high sensitivity of the balance unit which permits measurements to be made on very small samples, ten milligrammes being typical. The small sample size allows rapid escape of evolved gasses and correspondingly sharp definition of thermal 'events' on the thermogram.

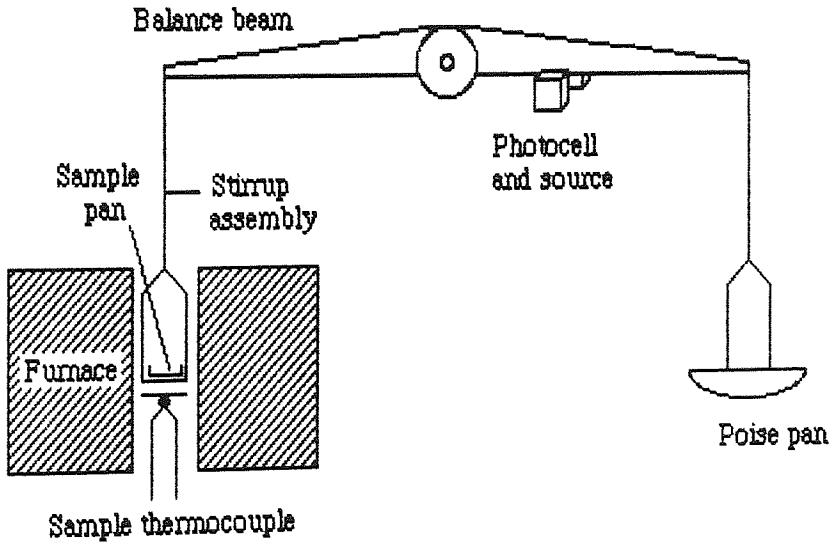

Figure 31 Apparatus for thermogravimetry - Schematic

The operation of the instrument is essentially very simple although poor design of the glass work makes setting up and calibration difficult and time consuming. The sample weight is counter - balanced by weights in the poise pan before the start of each run. Light falling on to a photoelectric cell is partially obscured by the balance beam and the signal from the cell is fed to a bridge circuit, causing it to go out of balance when a change of sample mass occurs. An amplified signal, proportional to the bridge imbalance, is then fed to an electromagnetic restoring couple which is positioned around the pivot of the balance beam. The force exerted by this couple exactly opposes the change in weight of the sample, thus the system is returned to its initial equilibrium position. The recorded signal is proportional to the current in this feedback circuit and is processed to provide an output to a chart recorder and a digital signal (which can be recorded as an absolute weight or as a percentage of the original mass).

Of particular interest in slag hydration studies is the calcium hydroxide content of the system. Previous workers have suggested that the mineral portlandite precipitates during Portland cement hydration and is subsequently consumed during slag hydration.

The thermogravimetric method was proposed as a suitable method for calcium hydroxide determination, by using powdered, calcined slag cement pastes which had been 'spiked' with varying percentages of calcium hydroxide as an internal standard. An old (c.18 months old) paste sample, assumed to be very low in calcium hydroxide, was powdered and sieved before calcining at 750°c in a platinum crucible for three hours to thermally decompose any calcium hydroxide. The sample was then reground and examined by T.G. for the presence of calcium hydroxide (none was detected). This powdered sample was then intimately mixed with a known percentage by mass of calcium hydroxide and again examined by T.G. By varying the proportion of the internal standard

in the sample it was possible to construct a calibration curve of apparent *vs* actual calcium hydroxide content .

2.3.2.3 Differential thermal methods

These closely related methods all measure the heat content change of a material which is subjected to progressive changes in temperature. Soon after Le Chatallier developed the thermocouple as an accurate temperature measuring instrument (1887), his application of it to measuring changes of temperature in minerals heated in a furnace, marked the initial stages of thermal analysis. Roberts-Austin (1899) applied the method we now know as differential thermal analysis to problems in metallurgy and by the middle of this century the method was a well established technique.

For differential thermal analysis, the instrument comprises of a mullite furnace tube, concentric about about a vertical silica stem, supporting a sample holder. The sample holder contains two holes, into which, fit a pair of platinum-rhodium crucibles. The instrument used (Stanton-Redcroft DTA 760) has a significant improvement over previous designs in that the base of each crucible has a depression allowing it to fit over a thermocouple bead (see figure 32) The temperature of the sample and standard may then be sensed without the great inaccuracy of introducing the thermocouple bead into the powdered material.

The powdered sample is loaded into one crucible and an inert reference material is loaded into the other. Theoretically, the reference material should not undergo any anomalous enthalpy change in the range of temperatures investigated, and should have the same heat capacity , thermal conductivity and coefficient of expansion as the sample. Thus, as the furnace temperature increases, the sample and standard will remain at the same temperature unless the heat content of the sample is varied by a chemical

reaction. In practice, these conditions are rarely achieved as few materials have identical thermal properties and the method is very sensitive to variations in packing and grain size (145, 146). None the less, acceptable results have been obtained by using calcined alumina as the reference material and it was this which was chosen for use here. It consists of roughly spherical γ - alumina particles of 500 - 600 mesh size which is supplied as a commercial product, intended for use in chromatography columns.

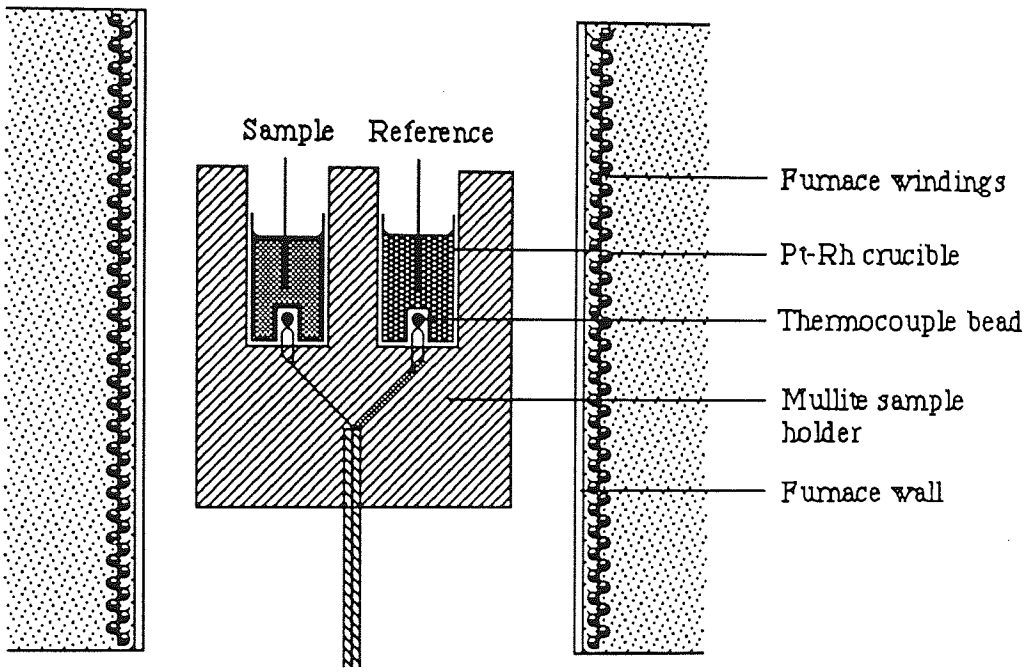

Figure 32 *Sectional view of differential thermal analyser*

There is no sample preparation required for this method - approximately 0.2g of sieved material was loaded into the sample crucible and the sample weight noted. The alumina was treated similarly and the two crucibles transferred to the sample holder. A heating rate of 20°c per minute yielded symmetrical peaks on the thermograms which are described in chapter 5.2. It is important to note the existence of reversible and non - reversible thermal reactions and that during some runs the furnace was allowed to to cool thus

permitting their identification.

Differential scanning calorimetry is essentially a development of differential thermal analysis, in which two crucibles (one containing the sample and one empty) are heated in a modified furnace. The furnace is capable of heating each side (and hence each crucible) independently, thus to maintain thermal equilibrium between the two as the furnace temperature rises, if the sample undergoes an endothermic reaction it will be heated in preference to the empty crucible. Similarly, if an exothermic reaction occurs, the heating current to the sample side of the furnace will be reduced to maintain it at the same temperature as the reference crucible. The heating current to the sample is therefore proportional to the enthalpy of the reaction and is measured to provide a voltage output to a chart recorder. The purpose of the empty crucible is to compensate for the heat content of the sample crucible and because no reference material is used, the results are not dependent on how closely its thermal properties reflect those of the sample.

Initial experiments using the DTA method (chapter 5.3) showed a pronounced, broad exotherm centred around 950°C which is thought to be associated with the devitrification of unhydrated slag glass. If this peak is proportional to the enthalpy of this reaction, it may follow that the peak area is proportional to the absolute quantity of unhydrated slag in the paste. Experiments to investigate this relationship were performed by DTA, as described above, but were of limited value for two principal reasons: First, the DTA furnace is only capable of operating upto 1000°C, so at the maximum temperature, the reaction had not gone to completion. Secondly, changes in the mechanical and thermal properties of the sample resulted in pronounced base-line shift.

Differential scanning calorimetry seemed to offer a more promising approach as it is capable of operating up to 1600°C and is much less susceptible to base line shifts. The instrument employed was also a Stanton-Redcroft device

which uses a refactory metal wound tube furnace of similar design to that of the DTA. The operation is also essentially very similar except that the thermogram is calibrated before each period of use. The calibration standard is loaded in place of the sample and a characteristic transformation is carefully measured. Traditionally, the heat of fusion of sodium benzoate is quoted, thus allowing comparison of results between different workers. As the recrystallization event produces a broad peak at a relatively high temperature, a fairly rapid heating rate (20°C per minute) could be employed. The results obtained were plotted as apparent enthalpy vs temperature and are discussed fully in chapter 5.

2.3.2.4 Nuclear magnetic resonance spectroscopy

The nuclei of certain isotopes posses an intrinsic spinning motion about their axes. The spinning of these charged particles or their circulation, generates a magnetic moment along the axis of spin (see figure 30). If the nuclei are subjected to an external magnetic field, their magnetic moment can align with or against the field. The individual nucleus spins around its axis and precesses about the force line of the applied magnetic field. These precessions are circular motions and are restricted to a distinct number of angles between the field line and axis. The field aligns the spinning nucleus against the disordering tendencies of thermal processes. The nuclei however, do not align perfectly parallel (or anti-parallel) to the imposed magnetic field. Instead, their spin axes are inclined to the field and precess about the field direction analogously to a gyroscope in a gravitational field. Each pole of the nuclear axis sweeps out a circular path in the x-y plane. Increasing the strength of the applied field only makes the nuclei precess faster. The frequency of precession, ν_0, is known as the Larmor frequency.

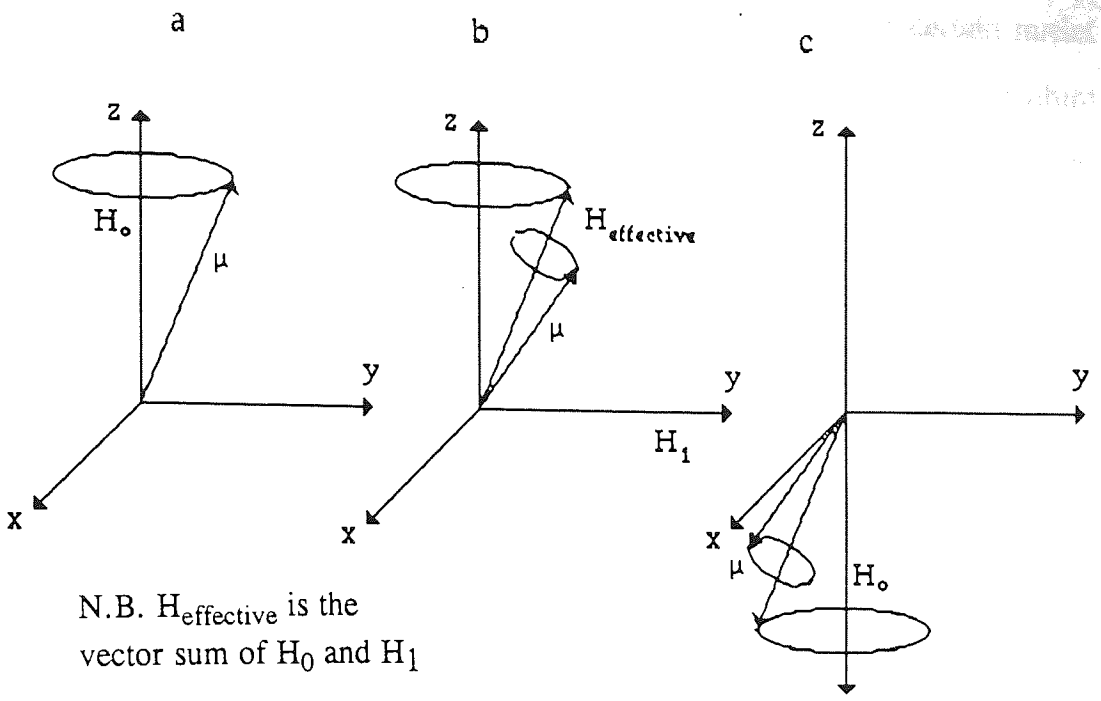

N.B. $H_{effective}$ is the vector sum of H_0 and H_1

Figure 32 Precession of magnetic moment μ, on application of an external magnetic field H.

a) On application of a steady magnetic field H_o

b) On application of H_o and r.f. field along the y-axis (H_1)

c) At resonance, precession flips to anti-parallel orientation w.r.t. H_o

For a nucleus to be magnetic it must possess a spin angular momentum whose magnitude is [h/ 2π √ I(I+1)] where I is the spin quantum number and h is Planck's constant. Nuclei with I=0 are non magnetic but several nuclei of relavence to cement studies have spin quantum numbers greater than zero: ^{29}Si, ^{27}Al, ^{43}Ca, ^{25}Mg, ^{57}Fe, ^{55}Mn, ^{23}Na, ^{39}K, ^{33}S and ^{47}Ti. In addition to these considerable interest has been shown in ^{1}H, ^{13}C, ^{19}F, ^{31}P, ^{14}N, and ^{11}B in other branches of structural chemistry.

Given the relative abundance of these isotopes and their elements in cementitious materials, the three isotopes of potential study are ^{1}H, ^{27}Al and ^{29}Si and it is the last of these which is used as an example below:

If a nucleus is placed in a magnetic field, it can align in certain directions

only. These orientations correspond to different energy levels for certain nuclei. The number of possible orientations is represented by the nuclear spin quantum number 'I'. In the simplest case (ie ^{29}Si or ^{1}H), I= 1/2. This represents two possible orientations and generally the number of orientations is 2I+1.

In addition to I, we must consider the magnetic moment 'μ', which governs the energy of the interactions of a particular nucleus and the magnetic field. If 'B' is the magnetic flux density, then for I= 1/2, the energy of the two possible orientations is -μB and +μB, so that the energy difference between the states is 2μB. It is this amount of energy which is required to change the nucleus from one orientation to the other. The basis of NMR spectroscopy is to supply exactly this quantum of energy and to measure its absorption by the nuclei.

For nuclei in the lower level, the condition for absorption of energy of frequency 'ν' is fulfilled when:

$$h\nu = 2\mu B = \Delta E$$

(Where h = Planck's constant)

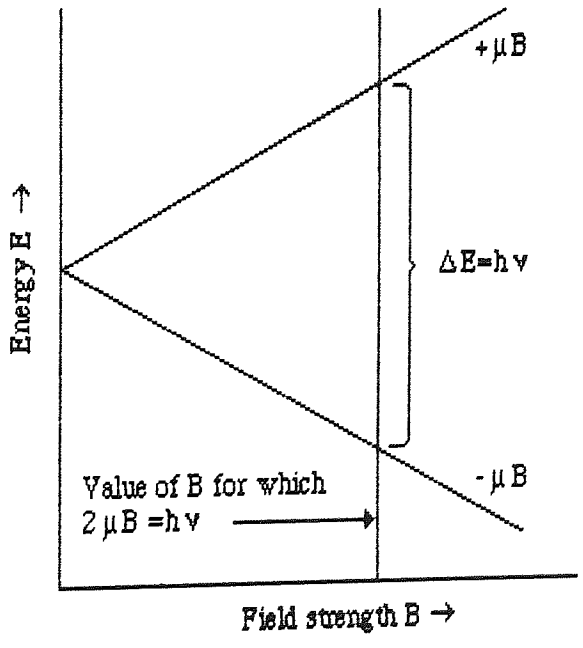

Figure 33 *Keeping 'ν' constant and varying magnitude of field strength*

These experimental conditions are essentially those achieved independendently in1946 by Bloch (149) and Purcell (150) and the fundamentals of NMR spectrometers have changed little since then:

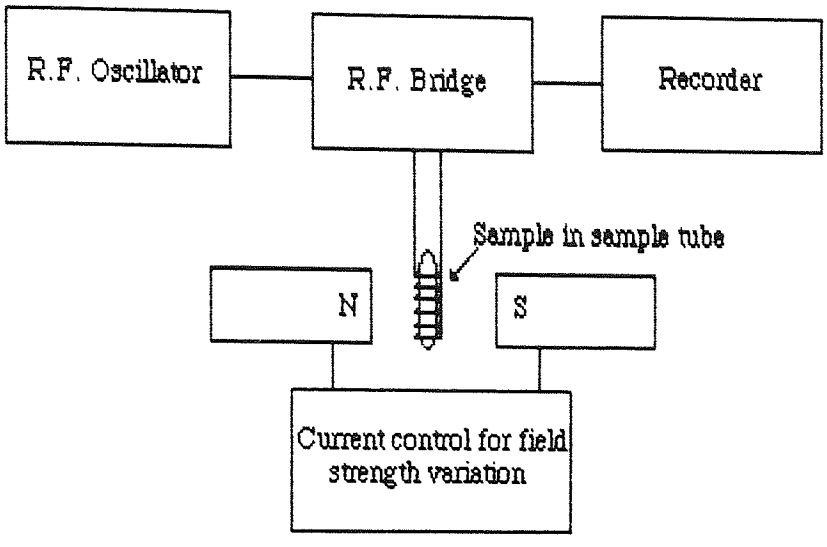

Figure 34 Schematic diagram of NMR spectrometer

Of significant importance however, is the development of the technique to permit the use of the multi-pulse method. This has become widespread with the development of the computer technology necessary to deal with the much more complex data collected in experiments of this kind. Instead of applying a continuous field to the sample as implied by figure 32, a radio-frequency pulse of varying frequency aligns all the nuclei and the spectrometer measures the field both during and after the application of the field. The data collected is then processed by Fourier-transform analysis to produce a spectrum in the frequency domain, similar to that obtained by the continuous wave method. The great advantage of this technique is that it permits the summation of spectra obtained from repeated scans and improves the signal to noise ratio considerably by addition of essentially random background signals. The energized system

requires a finite time to return to its un-magnetized state, which is known as the decay time. The pulses must therefore be applied at a frequency which permits the nuclei to return to an essentially random orientation before the next pulse is applied to the sample. In the results presented here, a period of five seconds was allowed for the relaxation of the silicon nuclei between the application of adjacent pulses.

Not all the nuclei occupy a particular energy level, such that the nuclei in each are given by the Boltzman distribution:

$$\frac{N_U}{N_L} = e^{\frac{-\Delta E}{kT}} = e^{\frac{-2\mu B}{kT}}$$

where N_U = number in upper and N_L = number of nuclei in lower energy state.

In practice the population in the lower energy state is slightly larger and since the transition from one level to the other is stimulated by energy input to the system, there are more upward than downward transitions and hence a net absorption of energy. This would quickly lead to equal populations but relaxation processes maintain a small excess in the lower level so continuous absorption is possible. The excess in the lower population increases as the field strength increases, hence spectrometers tend to use as high a field as practical, in order to achieve maximum sensitivity. The upper limit of sensitivity is instrumental as instability in the field becomes limiting. Practical maximum fields are currently 350 Teslas, with instruments of 1.4T at 60MHz relatively commonplace.

So far, we have only considered a situation of a single absorption peak on the energy vs field strength diagram. High resolution NMR shows that many molecules have several, slightly different resonances depending on the structure of the molecule and the chemical environment of the resonating

nuclei. As all nuclei are surrounded by electron fields in the electronic orbitals, when the instrumental field is applied, these electrons circulate around the lines of force and hence produce their own magnetic fields which oppose the applied field. This effect is known as shielding or screening. As different nuclei experience different electronic densities, so too, they require different magnetic field strengths to bring them into resonance. It is this high resolution data, the 'chemical shift', which makes NMR an attractive technique in structural chemistry. The chemical shift is usually reported in terms of parts per million of the resonance of a reference material.

For silicon-29 studies, the common reference material is tetramethylsilane which shows a single resonance and is available in states of high purity. Modern instruments, however, only use the chemical standards for initial calibration and rely on their internal processors to show the position of the standard with respect to the sample spectrum.

In the liquid state, dipolar molecules are free to rotate in the applied magnetic field in such a way that their own dipole - dipole interactions are minimized. In the solid state however, this is not the case, as the sample structure is a confining lattice, which prevents such relaxations from taking place. In mobile fluids, the rapid, isotropic motions of the nuclei average the anisotropic interactions between these nuclei and the applied field, effectively removing them from the spectrum. The resolved spectrum is thus narrow and yields important structural information. In the solid state, there is often insufficient motion of the sample nuclei to permit a high degree of isotropic averaging. The consequence of this is magnetic perturbations in the resultant field, which ultimately result in line broadening, (often of a similar order of magnitude as the chemical shift which is being investigated). This can, to some extent, be minimized by careful experimental technique. In order to reduce the perturbations in the magnetic field, spectroscopists attempted to emulate

Nature by imposing motion on the solid sample, through 'rapid sample spinning'. The mathematics describing the interaction of spinning dipoles in an applied field is described by a Hamiltonian expression containing a $(3 \cos^2 \theta - 1)$ term, where θ is the angle between the axis of rotation and the Zeeman field ('H_0' in figure 30). It therefore follows that for a particular inclination of the rotational axis, this term has a minimum value and that the magnitude of the dipolar line broadening then tends to zero. For silicon-29, this so - called 'magic' angle has a value of 54.73° and the method is known as 'Magic Angle Sample Spinning' or more commonly 'MAS' NMR.

The instrument used for these studies is a 'Bruker AC 300' series Fourier transform spectrometer capable of maintaining 7.2 Teslas. The sample was loaded into a PTFE sample holder and lowered into the core of the instrument. No sample pretreatment was done initially which lead to poor resolution, high background noise and instrumental problems. This was due to an iron-rich phase derived from the slag (see section 2.1) which was removed for subsequent samples by magnetic separation.

The interpretation of chemical shift data is discussed more fully in chapter 5 and the spectra reported have been collected over several hours and are the accumulation of over ten thousand pulses, analysed by Fourier transform and added to form single spectra.

2.3.3 Examination of the liquid phase - Pore solution chemistry

2.3.3.1 Pore fluid extraction and sample treatment

Studies on the extraction and analysis of pore fluids in cements have been made since the early part of this century and their application has been reviewed in the last chapter.

The extraction of pore solution from a wide range of solids has been discussed by several authors (151, 152) in recent years. In pore fluid extraction by means of a piston in cylinder type of press, several factors must be considered

if meaningful results are to be obtained. First, some dissolved ions will be attracted by the surface charge (ζ-potential) of the solid phase and these ions will be the last to be removed by pore squeezing. Naturally, ions with a high electrostatic charge and small ionic radius will be most strongly adsorbed and consequently fractionated species. Fractionation of ions during pore fluid expression is very pronounced in ion exchange media (152) such as resins, clays and zeolites but fortunately the ion exchange capacity of cements is relatively low. Ultrafiltration of larger species (especially hydrophobic ions and organics) is also responsible for fractionation but in the system considered here, the largest ion is thiosulphate so the effect is considered to be minor. These effects of species fractionation are dependent also on the pore size distribution and overall strength of the material and are shown as a change in concentration with both load and rate of loading. Some work has been done on these phenomena (132) which show fractionation of cement pore fluids to be measurable but significantly less than those of other materials.

The effect of temperature is also important. Diurnal and seasonal variations in laboratory temperature are sufficient to cause a measurable change in pore fluid composition. This, and the heat associated with loading, were seen as uncertainties which have not been addressed in the literature yet could be simply overcome by careful experimental design. These criticisms of the method aside, useful results can be obtained by employing a fixed loading rate to a maximum load and maintaining the temperature of the apparatus constant.

The equipment used for pore fluid extraction is a modification of that describedby Longuet (111), itself derived from pre - existing designs. The cell (figures 35-37) will accommodate samples of approximately 250g which are cast (section 2.2) to fit inside the cylinder bore. A water-tight seal is maintained between the piston and the bore by a PTFE disk which fits on top of the sample. The extracted pore fluids are collected from the drain tube under suction from a

plastic syringe, which is sealed with a push-on cap at the end of the experiment to minimize absorption of carbon dioxide and oxygen. The body of the cell is surrounded by a metal jacket containing a coiled tube through which water is circulated from a water bath. This allows the cell to be maintained at constant temperature during the extraction (figures 36 & 37).

For these experiments, extractions were performed at the curing temperatures (25°, 50° & 70°c) and the cell temperature was monitored during equilibration by inserting a sheathed thermocouple up the outlet tube so that it was in contact with the lower surface of the sample. Heat losses into the plattens of the press were minimized by fiber board insulators between the cell and the press. A pre load of c.1kN was applied to the cell and the unit was left to equilibrate to the desired temperature. In practice, heat losses required the water bath to be set about 5°c higher than the temperature required in the cell.

Loading was done at a steady rate (c. 100kN min^{-1}) to a maximum load of 5.9 tonnes (590kN) which corresponds to an internal pressure of approximately 300 MPa. By using a constant loading rate and maintaining the maximum load for a fixed period of time (10 minutes) it was assumed that errors due to fractionation were minimized as far as was experimentally possible.

The collected pore fluid was filtered from the syringe using a demountable filter and dispensed into a clean polycarbonate bottle. This solution was then diluted in several ways according to the analyses described below.

2.3.3.1 Hydroxyl ion titration

Immediately after extraction however (within approximately twenty minutes) the undiluted pore solution was titrated against nitric acid in order to determine the pH. 0.1ml of pore solution was diluted with 1ml of boiled-out water and titrated against 0.01M nitric acid using bromothymol blue as an indicator. As this is a strong acid - strong base titration, the middle tint green

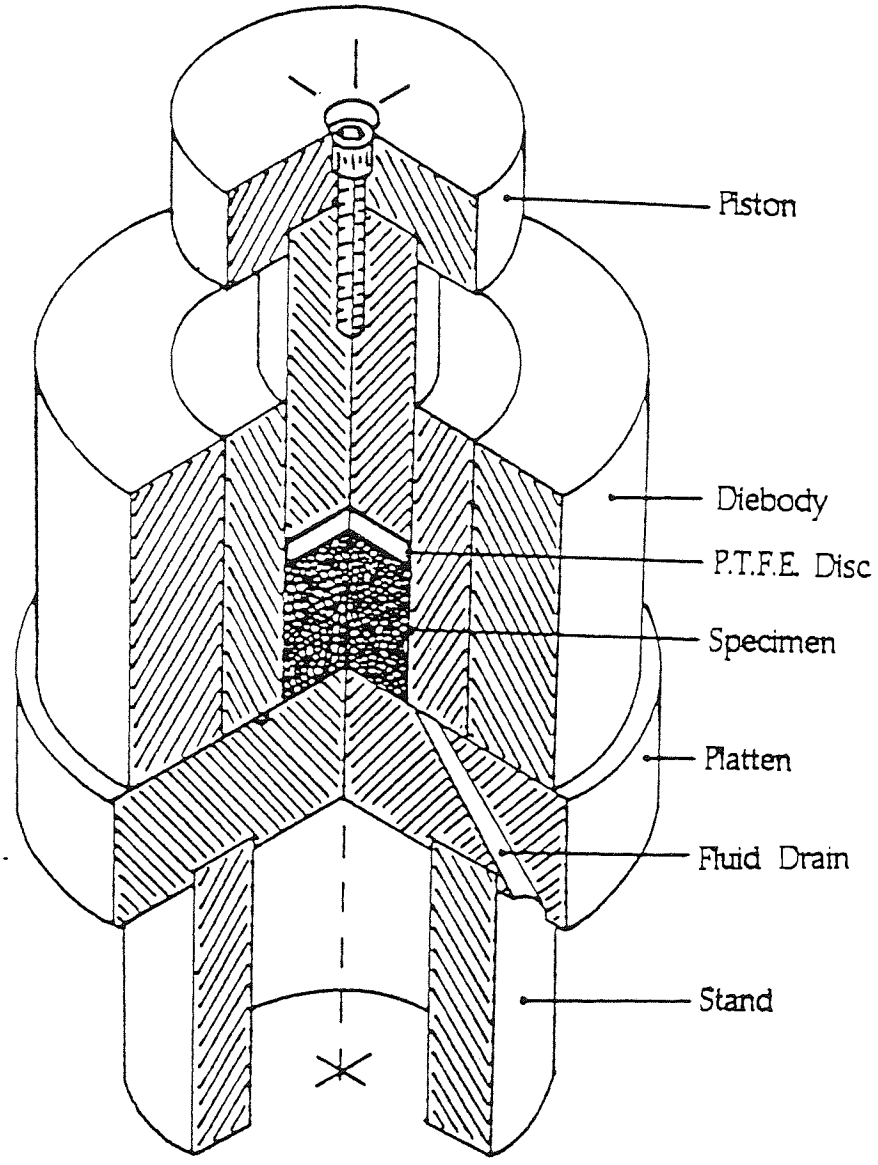

Figure 35 Isometric partial section of pore fluid extraction press

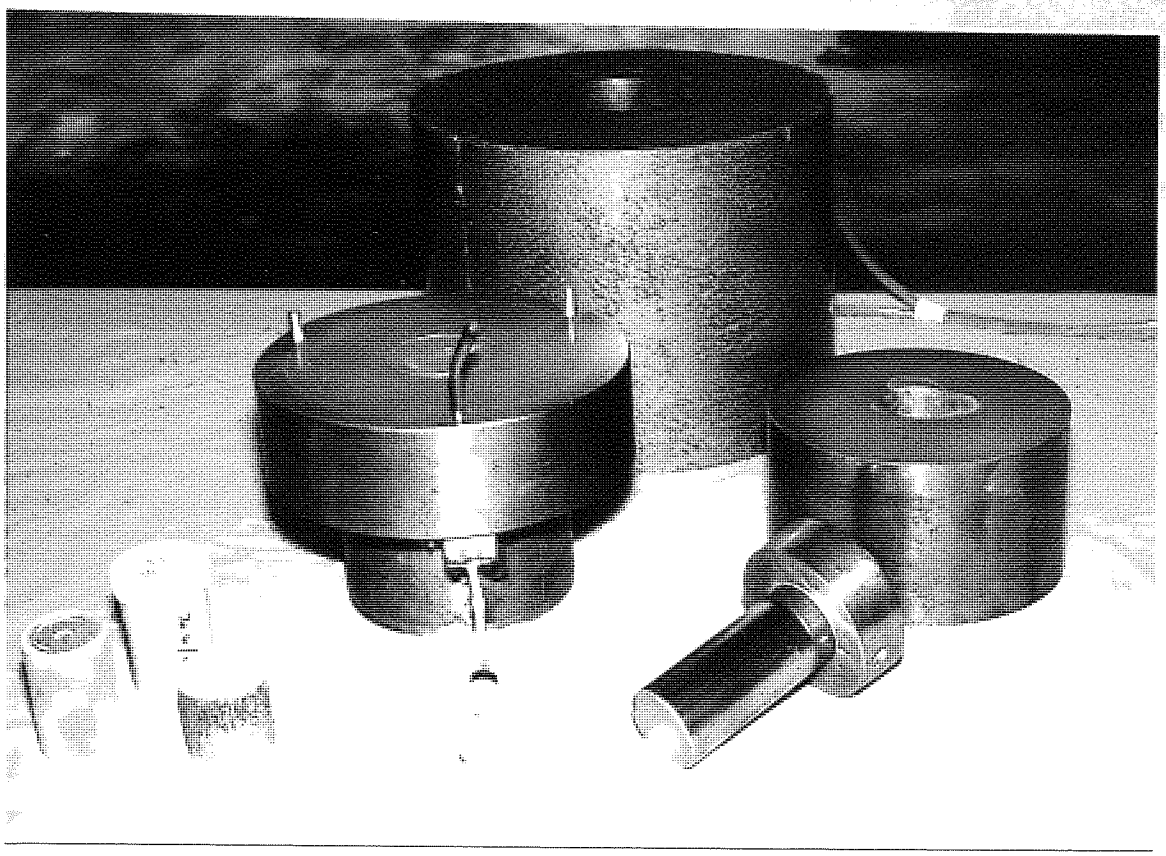

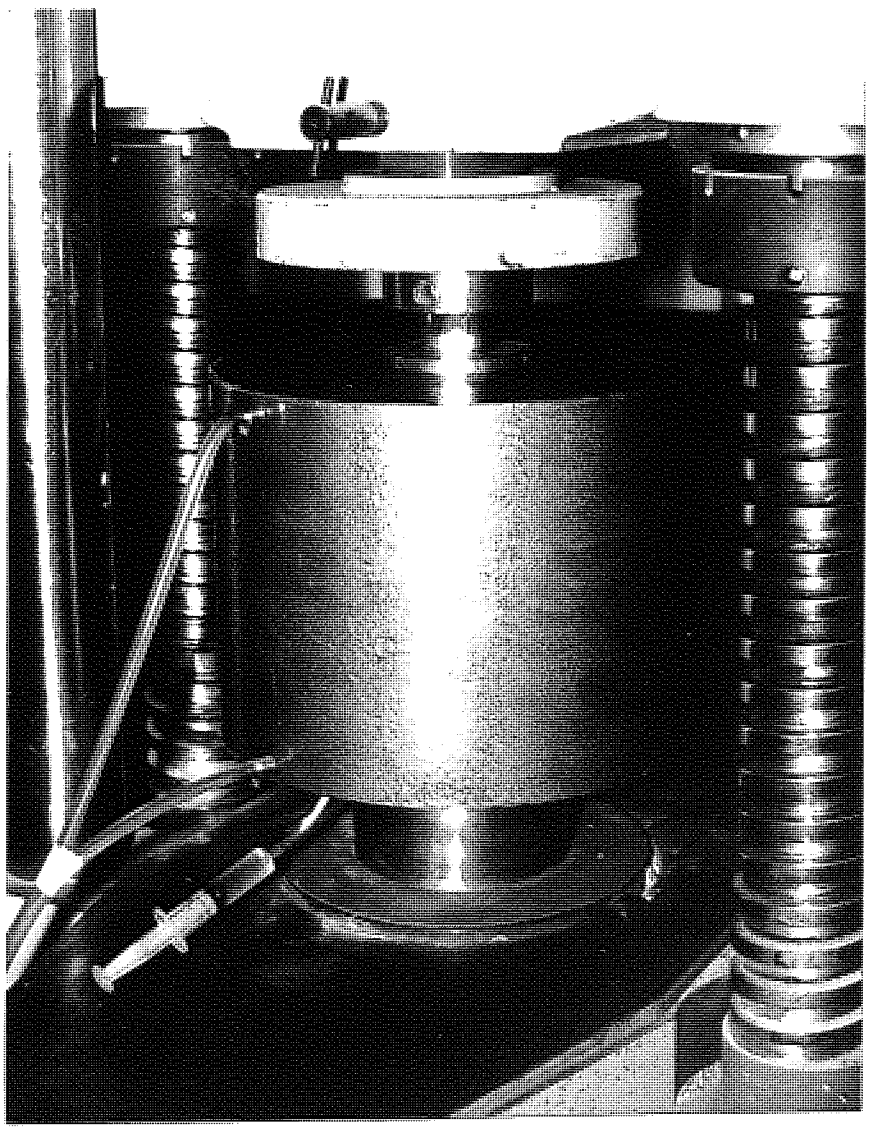

Figure 36 *(Above) Components of pore press. Note the cement paste cylinders (lower left)*

Figure 37 *(Left) Pore press in use. The water jacket covers the cell body to maintain working temperature*

(pH 6.9) of the indicator was used as the end point. The choice of indicator was a subject of some discussion in the laboratory and it is worthy of note that the same pH values were obtained with this indicator as with phenolphthalein. This check was performed independently by three workers showing that the point of inflexion on the titration curve is indeed very sharp. The acid was titratrated against carbonate free (Sorensen's oily lye method) sodium hydroxide, itself standardized against the primary acid standard potassium hydrogen phthalate (K-H- benzene 1,2 dicarboxylate)

K-H-phthalate is a weak acid so the equivalence point must be higher than pH 7 if titrated with a strong base (sodium hydroxide). This is determined by:

$$pH\,(eq) = 1/2\,pKw + 1/2\,pKa - 1/2\,pC$$

where: pKw = dissociation constant of water (14)

pKa = dissociation constant of acid (6.715)

pC = concentration of acid (0.1M)

The equivalence point is therefore pH 9.857, so phenolphthalein was used as an indicator.

2.3.3.3 Sulphide ion analysis

A second portion of the pore solution was dispensed at the time of titration to be analysed for sulphide. A minimum of 0.2 ml was mixed with an equal volume of a sulphide antioxidant buffer to be used for analyte addition (see below) The buffer solution contains a high concentration of d-ascorbic acid to minimize aerial oxidation of the sample. The analytical method for sulphide employed a silver-silver sulphide ion specific electrode, which has a high specificity to only silver and sulphide ions in solution providing a measurement range of 10^{-6} to 10^{-1} M. A standard solution of sodium sulphide

was prepared and diluted as required with the buffer solution. This contained d-ascorbic acid as an antioxidant, sodium hydroxide to maintain a high pH and sodium salycilate to provide a high overall ionic strength.

Figure38 *Sulphide ion selective electrode in cell with reference electrode. The cell is shown on a magnetic stirrer to the right of the high impedence voltmeter*

The buffered standard solution was titrated against lead perchlorate using the electrode as the end point detector. The end point is sharply defined as a fall in potential of several tens of millivolts. This procedure was carried out in a tray containing 'Benchcoat' absorbent paper to minimize the toxic and explosion risk of the lead perchlorate. The compound itself was standardized against perchloric acid (analar) secondary standard, using the perchlorate ion detected by ion chromatography.

2.3.3.4 Ion chromatography

From the remaining sample, 0.5ml was diluted for the analysis of sulphate, sulphite and thiosulphate by ion chromatography. This method is becoming very popular for anion analysis as it allows the rapid determination of a wide range of anions without the risk of oxidation of the sample or interference of ions other than the analyte. The instrument is essentially a development of HPLC design employing an analytical pump to move an eluant through a separating column to a conductivity detector. The instrument used here is a 'Dionex 2000i/SP' which contains a guard and separating column packed with an extremely fine ion exchange resin. The carbonate/ bicarbonate eluant washes the injected sample over the columns where the ions become separated into zones depending on their affinity for the resin's exchange sites.

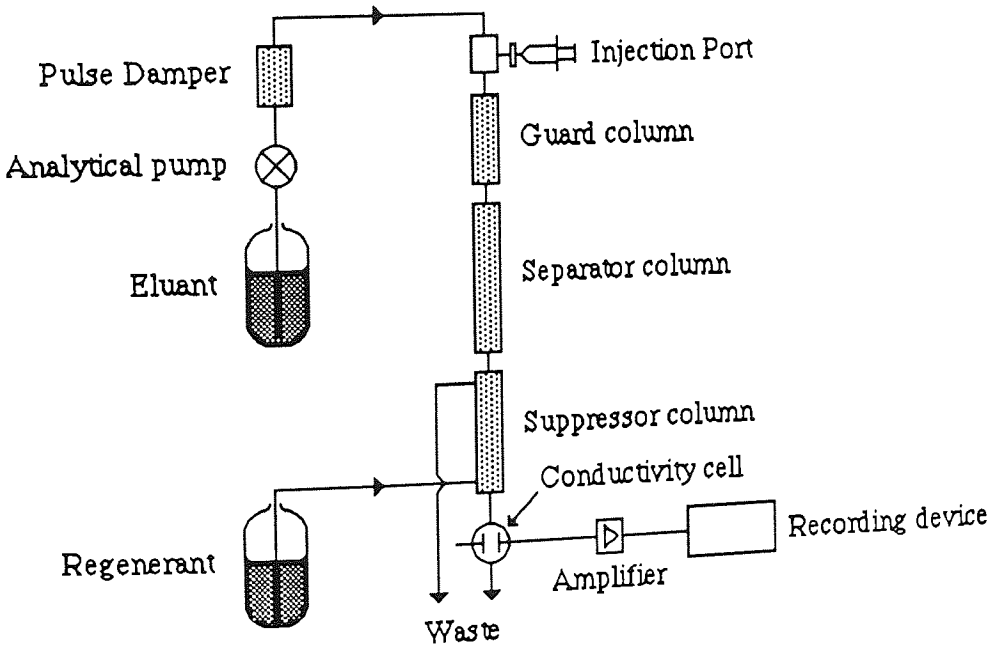

Figure 39 *Schematic diagram of ion chromatograph*

As the ions are eluted, they pass into a suppressor column which has the effect of reducing the effective conductivity of the eluant allowing a higher signal to be recorded from the conductivity cell. The suppression reaction,

shown diagrammatically in figure 41 is where, by permitting sodium and hydrogen ions to diffuse across the suppressor membrane, the eluant is effectively replace by poorly dissociated H_2CO_3. This contributes little to the conductivity of the system, thus the major charge carriers passing through the detector are the sample ions.

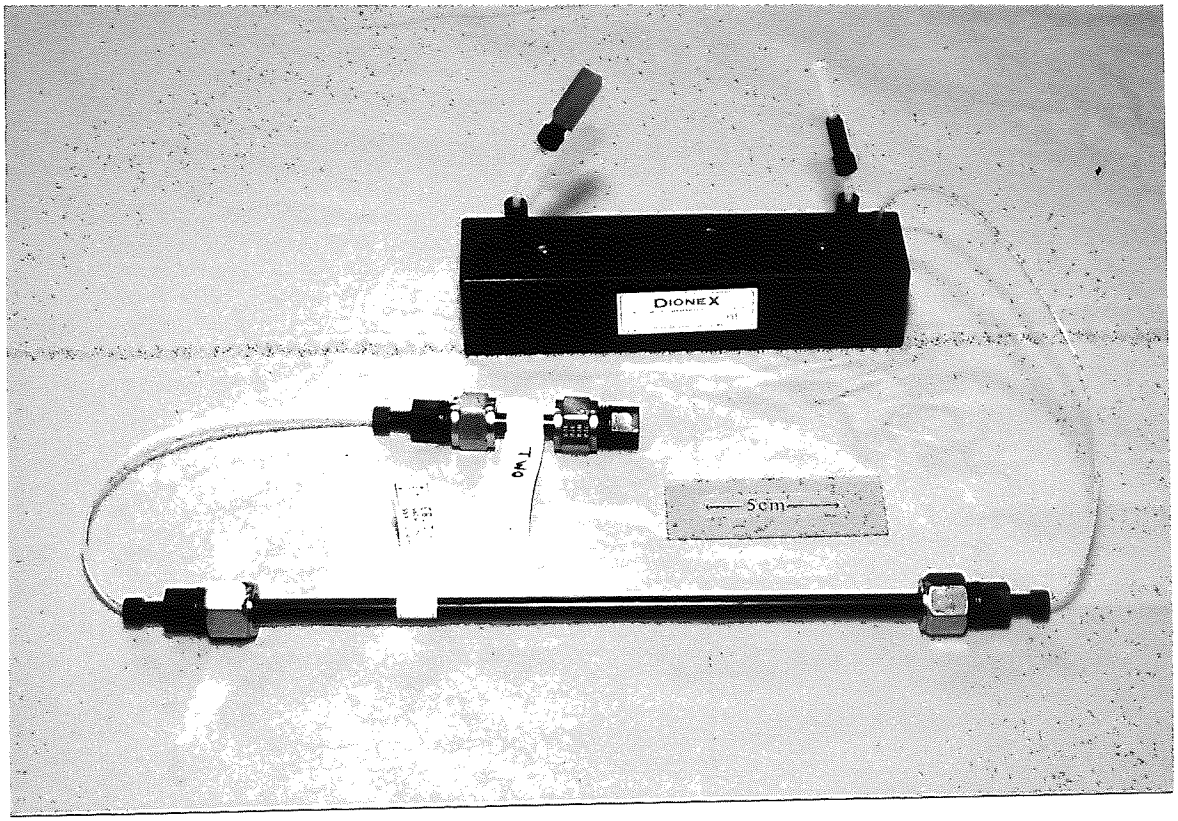

Figure 40 *Ion chromatography columns*

In the center is the guard column which is connected to the seperator column (below), whilst the micromembrane suppressor is shown above

As the ions of interest in slag cement pore solutions are present in similar concentrations (sulphate and thiosulphate: approximately hundreds of micromoles per liter) it was possible to analyse for them simultaneously and to check for the presence of sulphite (see discussion, Chapter 6).

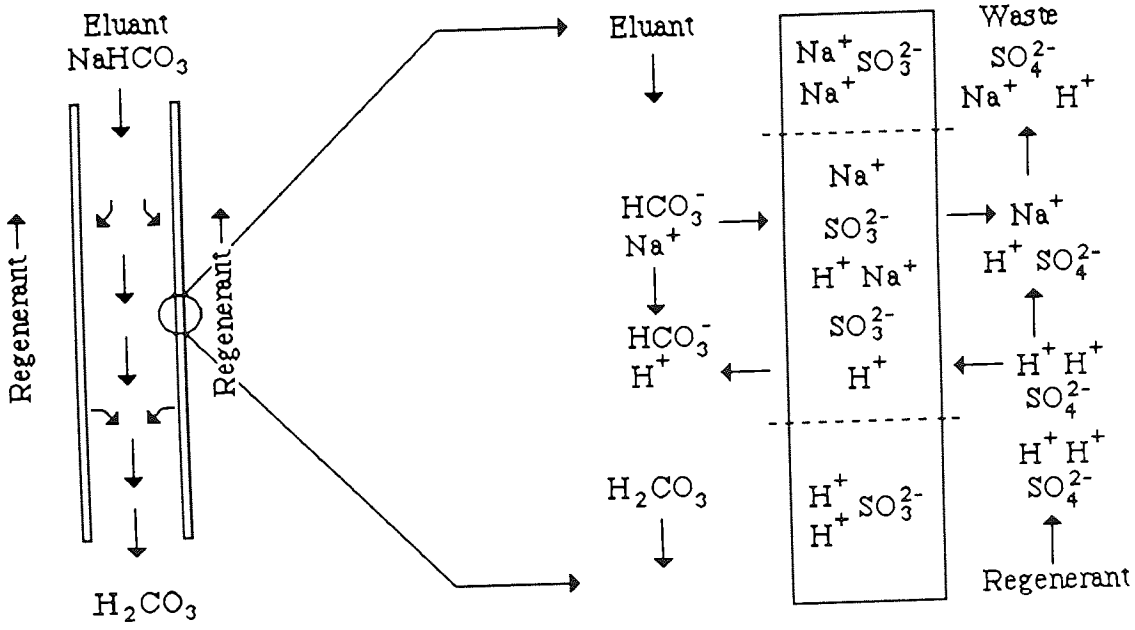

Figure 41 *Suppression reaction in ion chromatography*

The instrument has proven to be very reliable and permits the rapid simultaneous analysis of sulphate and thiosulphate which would not be possible by classical techniques.

Ion chromatography was also used to analyse for the next most abundant cation and anion. Aluminate seems to be present at hundredths of a nanomolar concentration as do strontium and barium. These concentrations were so low they were not thought to be significant. A family of four peaks thought to be silicate species was seen at c. 1μM. Silicate dissociates into several species during ion exchange but no further work was attempted, both because of the low concentrations involved and the complexity of the silicate speciation after ion exchange.

2.3.3.5 Flame photometry

The cations, by comparison, were relatively simple to analyse. The method chosen was flame emission using a flame photometer produced by 'Jenway Ltd.'

as shown below:

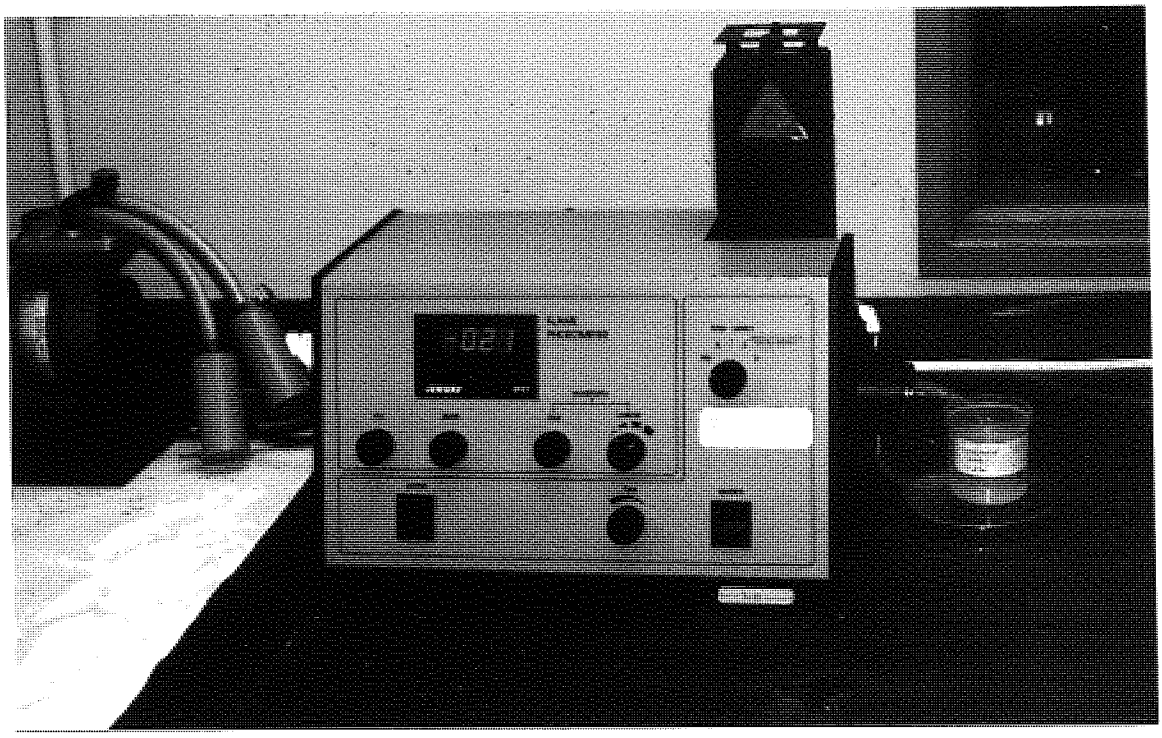

Figure 42 Flame photometer used for metals analysis

As the cations are dominated by sodium and potassium with minor calcium, they could be diluted in 0.01 M nitric acid (to retard bacterial growth and to ensure no precipitation occured) and stored in the refrigerator to be analysed at the end of the week. Dilution factors were as follows: Potassium 2000:1, Sodium 1000:1, Calcium 9:1, to bring the concentrations into a suitable range for analysis. Primary standards were prepared from the chlorides (1mM) and checked against their chloride concentration by ion chromatography. For each element, a calibration curve was plotted by serial dilution of the standards and the samples were diluted to fall in the linear portion of the response curve. Very little drift was experienced with this device and very reproducible results were obtained.

2.3.3.6 Redox potential measurement

Finally, Eh measurements were made on the residue by recording the

potential between a platinum and calomel electrode. This was done in a simple glass cell containing a platinum electrode in the base (figure 43) into which the calomel electrode closely fitted. The measured potential took approximately ten to fifteen minutes to reach equilibrium although the voltage had generally fallen to within five percent of its minimum within the first three minutes. To accommodate this drift, the output of the voltmeter was monitored by a chart recorder.

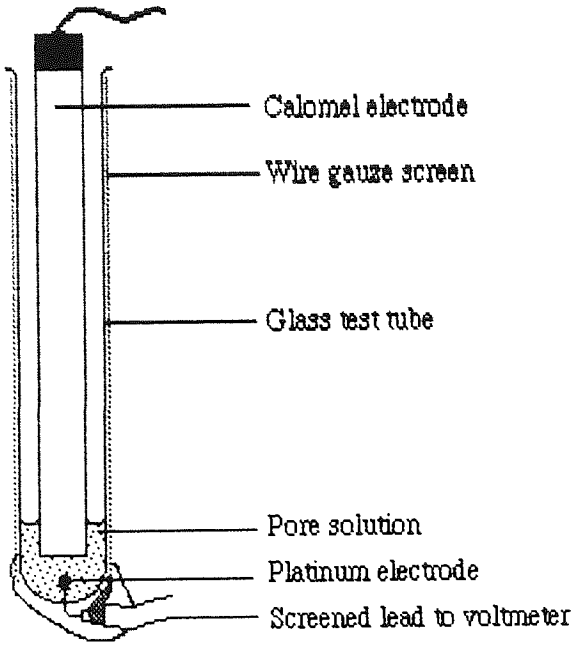

Figure 43 *Cell for redox potential measurements*

Finally, Eh measurements were made on the residue by recording the potential between a platinum and calomel electrode. This was done in a simple glass cell containing a platinum electrode in the base (figure 43) into which the calomel electrode closely fitted. The measured potential took approximately ten to fifteen minutes to reach equilibrium although the voltage had generally fallen to within five percent of its minimum within the first three minutes. To accommodate this drift, the output of the voltmeter was monitored by a chart

recorder.

Chapter 3
Conduction Calorimetry

3.1 Introduction

The principle of conduction calorimetry was introduced in the previous chapter hence only the details of the experimental tecnique and the interpretation of the results are considered here. The sample cell is shown in figure 44 and consists of a 'Perspex' cylinder closed at the base by an aluminium heat sink, through which the heat produced by the sample is conducted into the water bath. This method is an example of isothermal calorimetry and requires the sample cell to be immersed in a water bath which is maintained at a very stable temperature (± 0.05°C). The sensing elements are bismuth telluride n and p devices, faced with ceramic plates which allow them to be bonded onto the anodised aluminium heat sink through which heat out of (or into) the calorimeter is conducted. Two sets of three thermopiles are used, with the output of each set connected in opposition. The inner set supports the sample can, whilst the outer set support an aluminium compensating ring, which is designed to have the same thermal mass as the sample can and its contents. This compensating system accommodates inhomogeneities of the heat flow out of the cell and minimises external factors affecting the signal from the sensing elements.

The sample was tranferred immediately after mixing to a plastic bag in which it was weighed (30g ±0.02g), which was subsequently welded closed. Approximately 20 ml. of silicone "transformer" oil was poured into the sample can to provide good thermal contact between the sample and the can wall and the sample was then placed around the heating element as shown in figure 44. The cell was then assembled as shown in the diagram and placed in the water bath to equilibrate for temperature.

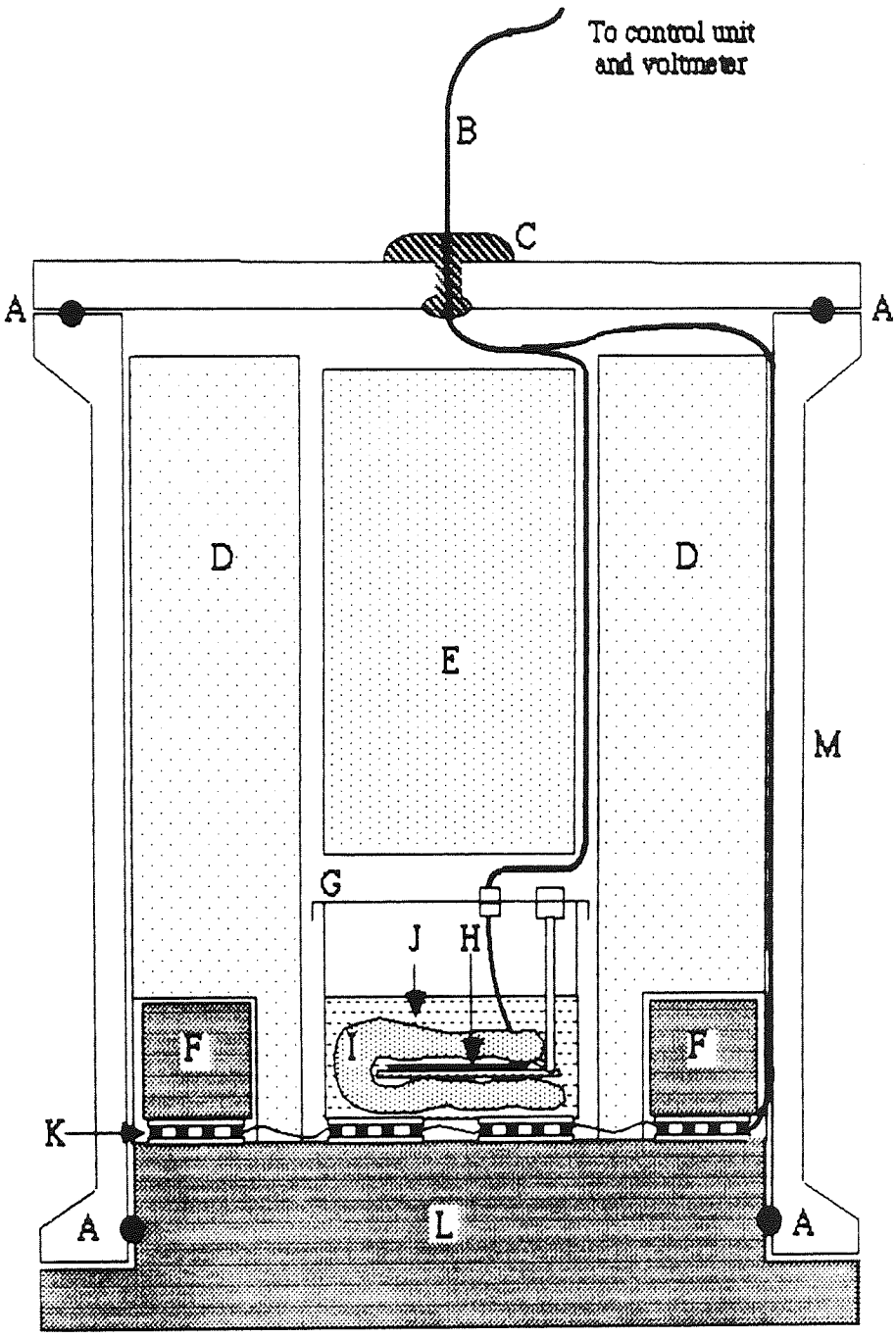

A 'O'-ring seal
B Electrical connexion to control unit
C Water-tight gland
D Polystyrene insulation
E Expanded Polyurethane
F Aluminium compensating ring
G Aluminium sample can
H Heater element
I Sample in plastic bag
J Conducting oil
K Thermopile unit
L Aluminium heat sink
M Perspex cell body

Figure 44 Section through calorimeter cell

In the case of elevated temperature experiments, the cell was partially immersed in the hot water before transfer of the sample, thus minimising the time required for the system to equilibrate at that temperature.

The sample pastes were mixed by a low-shear electric mixer as described earlier, and comprised the full range of compositions (50,70 & 90%BFS), at 0.3 and 0.4 water to solids ratio and examined at 25°, 50° & 70° Celcius. This gave eighteen possible permutaions of experimental compositions (although at 70°C the cell developed a slight leak and some experiments were stopped).

The time taken to transfer the sample from the mixer to the cell and upto obtaining the first reading was approximately ten minutes, thus the first readings were obtained after approximately thirty minutes hydration. In terms of the hydration reactions described in chapter one, this is during, or some time before the dormant period, depending on the curing temperature (see figure 16, Ch.1.). As a consequence of this, the bulk of the data represents the hydration of the silicate and ferrite phases, the reactions constituting the initial ('heat of wetting') were not recorded by this method.

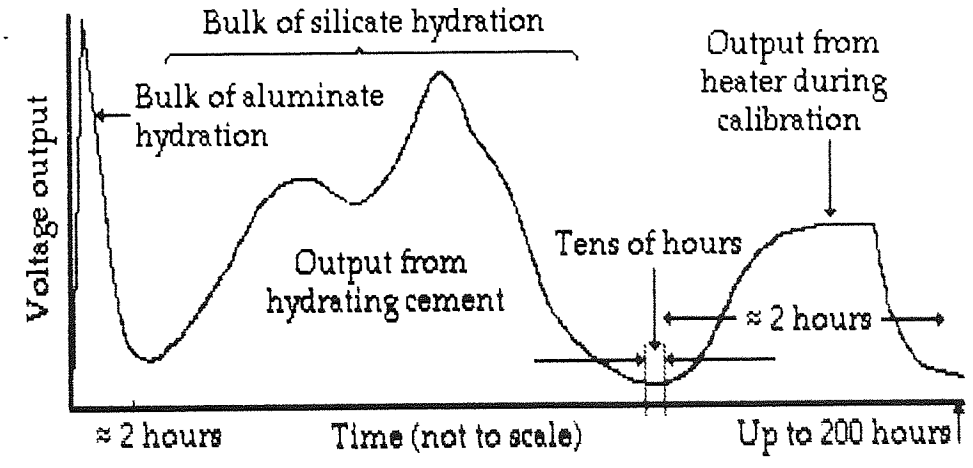

Figure 45 *Stylized output from calorimter during sample hydration*

At the end of the experiment (normally one week of hydration), the heat output from the calorimeter fell to a very low, almost constant value, at which time the system was calibrated by supplying a known ammount of heat to the sample can and thus calibrating the voltage - time graph to obtain results in terms of Watts per unit time as shown in figure 45 (above).

3.2 Theory of conduction calorimetry

In isothermal calorimetry, is assumed that the conditions in the calorimeter are stable and that the temperature of the heat sink can be maintained to within ±0.01°c during each experiment. Let the temperature of the sample can be T_1 and that of the heatsink be T_0. If a small quantity of heat dQ, is released by the sample in a short time dT, its effect is to raise the temperature of the sample can by an ammount T above that of the heat sink:

$T = T_1 - T_0$ (Assuming that the heat loss is by conduction only)

If the thermal capacity of the can and its contents is 'U', then the internal heating will absorb energy at the rate:

$$U \frac{dT}{dt}$$

The remainder of the heat leaks essentially by conduction rather than by convection or radiation therefore the rate of heat loss other than through the thermopiles is proportional to sample temperature T.

(or rate of heat loss = pT, where p is a constant).

The energy balance of the system is therefore the sum of the internal energy loss and the conducted heat, thus:

$$\frac{dQ}{dt} = pT + U \frac{dT}{dt}$$ (Where 'Q' represents heat energy)

i.e. rate at which heat is supplied = rate of heat loss + rate of heat absorption

The EMF produced by the thermopiles is directly proportional to the temperature difference T, ie: E= gT, where g is a constant. Substituing into the equations above, the following expression is derived:

$$\frac{dQ}{dt} = \frac{p}{g}E + \frac{U}{g}.\frac{dE}{dt}$$

This may be reduced into the Tian - Calvet equation as shown below:

$$\frac{dQ}{dt} = K_1 E + K_2 \frac{dE}{dt}$$

where: $K_1 = \frac{p}{g}$ and $K_2 = \frac{U}{g}$ (these being constants for the calorimeter)

After the output of the calorimeter has fallen to a low, almost constant level, a known amount of heat is supplied to the sample can from the internal heater. By measurement of the potential applied to the heater in comparison to that applied to a standard resistor, it is possible to determine the current through the heater and thus the rate of power dissipation into the sample can. The numerical value in Watts can be applied directly to the Tian - Calvet equation (where W= heater output in watts), thus:

$$W = K_1 E + K_2 \frac{dE}{dt}$$

Re-arranging this equation gives the following linear expression:

$$\frac{dE}{dt} = \frac{-K_1}{K_2} E + \frac{W}{K_2}$$

....such that a plot of dE/dt versus E produces an intercept at W/K_2 and a slope of $-K_1/K_2$ as shown below.

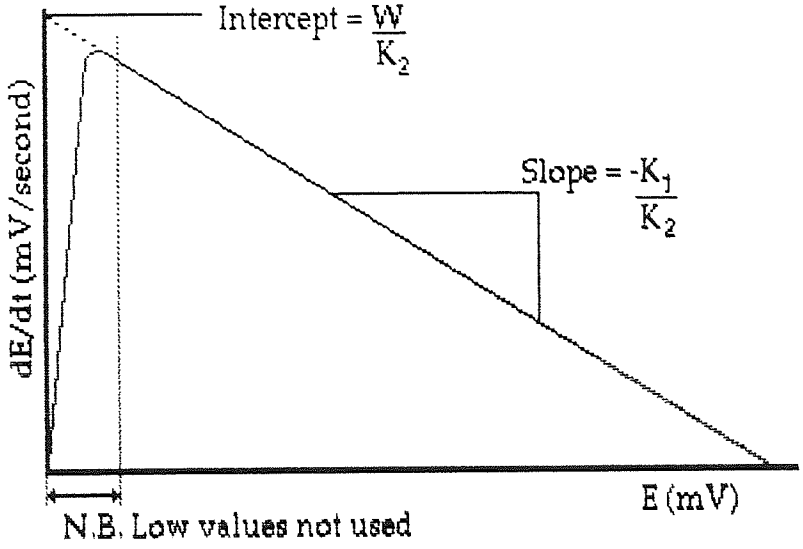

Figure 46 *Determination of calorimeter constants from thermopile outputs*

It is important to reject the data collected when the output voltage is low as they do not obey this linear relationship. Although it would be possible to adapt the mathematics to include additional terms accommodating these data, the potential increase in accuracy is very small and current practice (62,69) is to project the linear portion of the data in order to determine K_2.

Once the constants had been estimated, they were used to convert the initial data from mV to mW with respect to time. This was accomplished by using a ratio of finite differences such that at any point 'N', the rate of heat output 'W(N)' is given by:

$$W(N) = K_1 E(N) + K_2 \left[\frac{E(N+1) - E(N-1)}{T(N+1) - T(N-1)} \right]$$

In pratice the data file contained some noise spikes occurring as occasional

very high values, hence the data was treated in groups of five points, from which was calculated the mean and sample standard deviation. The datum furthest from the mean was rejected from each group and the mean recalculated before being transferred into a file of mean voltages and mean times. It was intended that any data set which contained values of more than two standard deviations from the (recalculated) mean would also be rejected as likely to contain erroneous data due to a sustained burst of noise. In practice this was not found to be the case as noise spikes were present as infrequent, short lived events occurring as discrete high value data only. The rejection of the datum furthest from the mean was therefore sufficient to trap the noise spikes recorded during these experiments. It was on the mean data files that the above conversion to Watts versus hours was finally made. These data were subsequently divided by the sample mass to produce values in terms of Watts per kilogramme of hydrating paste.

To obtain the cumulative enthalpy curve for each hydration experiment, a numerical integration was also performed on each data set. The area under the Watts versus time curve was calculated by summation to represent the heat of hydration up to any time 't', thus:

$$H_t = \int_0^t W \, dt$$

The results collected by the chart recorder (used in case of computer failure) were treated in a different way. Figure 45 (above) shows the shape of the voltage curve during calibration where it can be seen that the output reaches a plateau when the rate of change of heat output with repect to time tends to zero. Under these conditions, the K_2 term also tends to zero and the Tian - Calvet equation therefore reduces to:

$$W = K_1 E$$

Measurement of the output at this plateau (minus the background level) gives E and therefore K_1 may be calculated. To obtain the value of K_2 the time constant 'τ' is used, where 'τ' = K_2/K_1. Let the calibration voltage output be E_{cal} when the plateau condition is reached. Let also E = 0 when t = 0 and E = E_{cal} at t = ∞.

Given:

$$E = [\,1 - \exp(\frac{-t}{\tau})\,]\; E_{cal}$$

Then when $t = \tau$,

$$E = (\,1 - \frac{1}{e})\, E_{cal}$$ (where τ is the time constant)

$$\therefore E = 0.632\, E_{cal}$$

So from the chart recorder, the time constant 'τ' may be extrapolated as the time taken for the output voltage to reach 63.2% of its final (plateau) value. It is interesting to note that the K_2 term is only important when the rate of change of output with respect to time is rapid, otherwise the power output from the cell is linearly related to the voltage output of the cell.

3.3 Experimental results

The heat of hydration curves for OPC pastes are presented in figures 47 & 48 below. It can be seen that an increase in the temperature of the hydrating system greatly increases the rate of reation, such that the maximum rate of heat output occurs within the first three hours at 70°C. The effect of reducing the water : solids ratio is of minor significance and generally accelerates the early stages of hydration. Kondo (100) suggests that there is a corresponding rate of change of Ca^{2+} concentration which affects the length of the dormant period, but this is not fully understood.

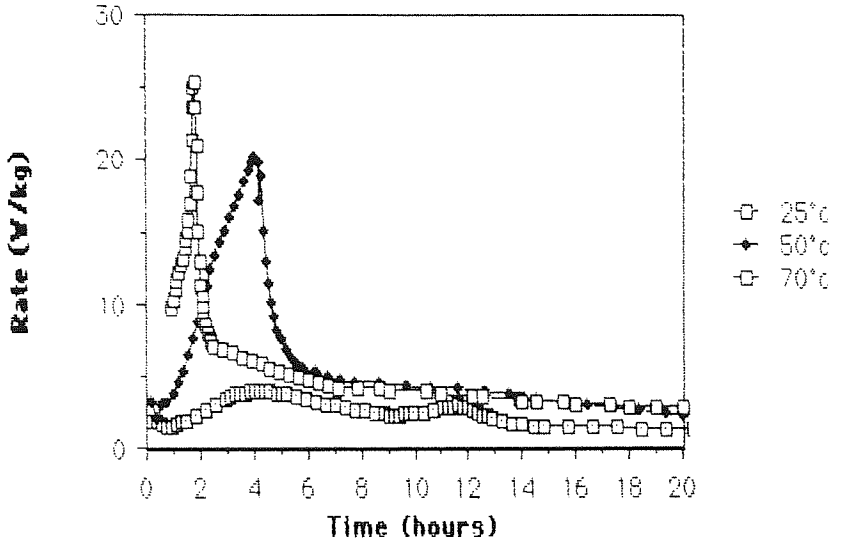

Figure 47 *Heat of hydration of OPC at 0.3 w/s ratio*

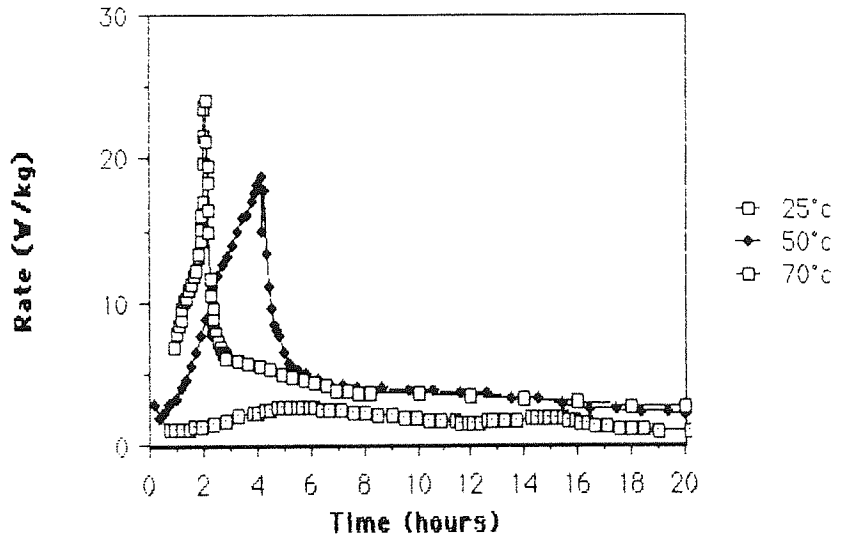

Figure 48 *Heat of hydration of OPC at 0.4 w/s ratio*

The relative position of the peaks remains the same for both water contents, with the second and third peaks well separated at 25°C. At higher temperatures, the two peaks merge such that at 70°C, the second peak occurs as a shoulder on the third. (N.B. the first peak shown on figure 45 is not recorded by this method). The accelerating effect of reducing the w:s ratio is most pronounced

at low temperatures when the time to the maximum for the third ('ettringite conversion peak'- see later) may be as long as fifteen hours. In addition to accelerating the hydration reactions, an increase in temperature results in a correspondingly large increase in the rate of heat output. The temperature interval from 25° to 70°C increases the rate of heat evolution by a factor of approximately five.

These results can be used to predict the degree of completion of the exothermic hydration reactions by adopting the approach proposed by Wu *et al* (65). They postulate that at any time 't', the heat liberated up to that time 'H_t', will be related to the total heat of reaction 'H_{max}' by the following expression:

$$H_t = H_{max} \frac{t - t_0}{(t - t_0) + t_{50}}$$

Where t_0 is the duration of the dormant period and t_{50} is the time at which $H=H_{max}/2$.

Re - arranging the above expression yields:

$$\frac{1}{H_t} = \frac{1}{H_{max}} \left[1 + \frac{t_{50}}{(t-t_0)}\right]$$

It can be shown therefore, that a plot of $1/H_t$ *versus* $1/(t-t_0)$ provides an estimate of both H_{max} and t_{50}, as H_{max} = 1/ intercept and t_{50} = H_{max} multiplied by the gradient. This approach has been used successfully by Lee (69) on blended cement systems which show a similar degree of linearity to that displayed by Portland cement.

As the hydration reaction is exothermic, the relative chemical potential energy of the system is lower for the hydration products than for the reactants. As shown in the previous chapter (figure 15) and demonstrated by Roy & Idorn (62), the hydration may be represented diagramatically as below. The calculations of H_{max} can be used to represent the net change of energy in the system, whilst the rôute by which the reaction proceeds, is governed by the apparent activation energy. Conduction calorimetry provides an estimation of this quantity by measuring the heat of reaction as a function of time over a range of temperatures.

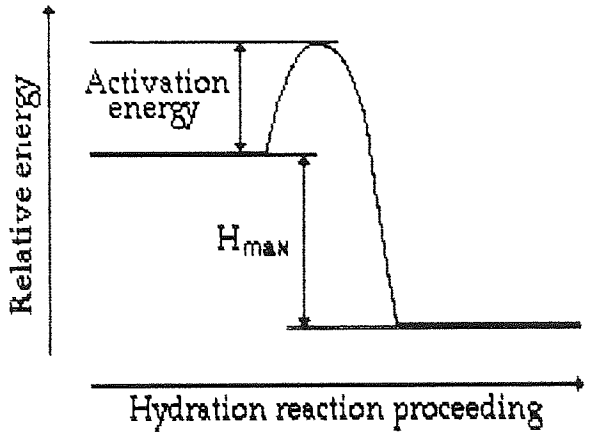

Figure 49 *Activation energy for hydrating system.*

The concept of activation energy is useful in explaining the the effect of temperature on the hydration of different cement compositions, even though the reactions concerned are not simple processes. The quantity of heat liberated can be used as a measure of the state of advancement of the hydration reactions and with certain limitations, it is possible to treat the reaction kinetics quantitively. The activation energy of a simple reaction can be determined by the Arrhenius relation:

$$k_T = A \exp\{-U/(RT)\}$$

Where k_T is the reaction rate constant at a given absolute temperature T, A is a

constant, U is the activation energy in J/mol and R is the universal gas constant taken as 8.314 J/mol/K.

The complex Nature of the reactants and their hydration mechanism prevent the direct measurement of the rate constants for this system. The ratio, however, of the rate constants can be determined, if it is assumed that the time taken to reach a given state of hydration is inversely proportinal to the rate constant.

Hence: $K_{T1} / K_{T2} = t_{T2} / t_{T1}$

Where T1 & T2 are the absolute temperatures.

Using this procedure, the activation energy for the OPC was calculated from the times taken for the system to reach 50% of its ultimate value (t_{50}).

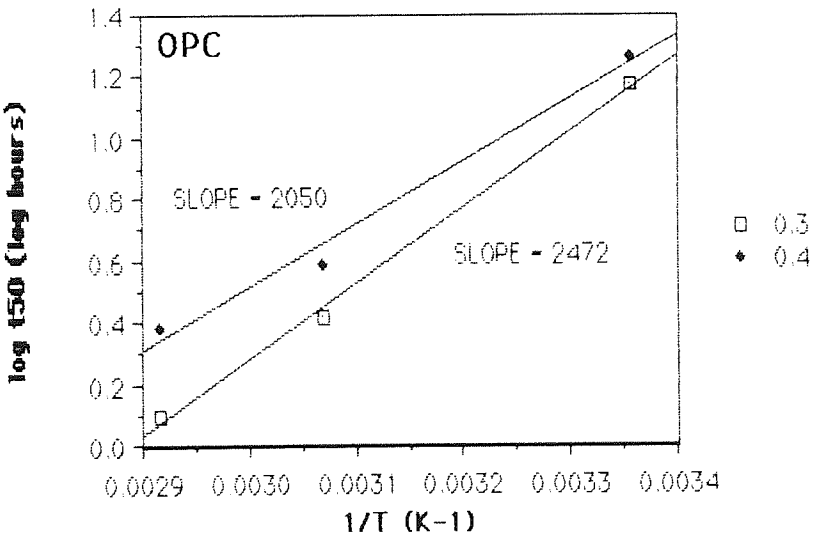

Figure 50 Arrhenius plot for Portland cement hydration

The slope of the above graph is proportional to the activation energy and yeilds numerical values of 47.33 and 39.253 kJ/mol for the 0.3 & 0.4 water : solids ratios respectively. Both these values are of the order expected, published values for this material being approximately 47 kJ/mol.

The results for the blended cements were treated in the same way to calculate t_{50}, H_{max} and hence the apparent activation energies. These results are essentially similar to those from the Portland cement, showing a marked acceleration with increasing temperature and a slight acceleration due to reduction of water : solids ratio.

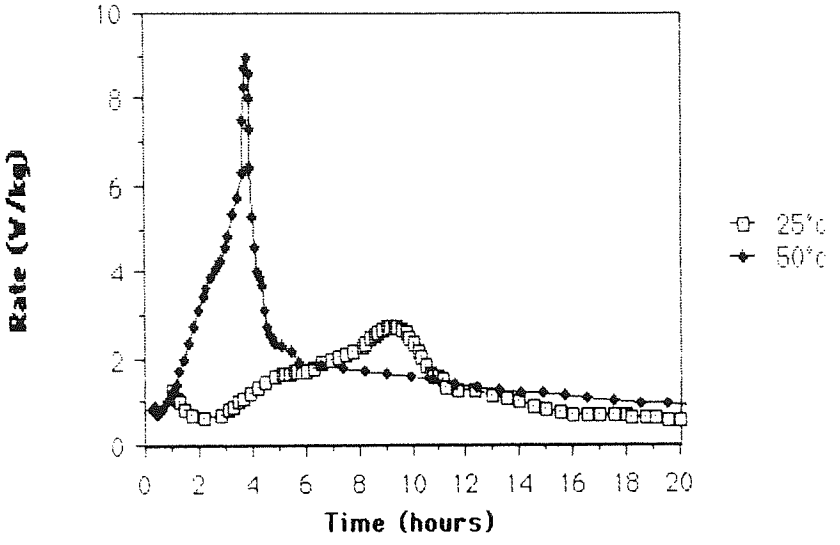

Figure 51 *Heat evolution during hydration of 50% BFS pastes at 0.4 w:s ratio*

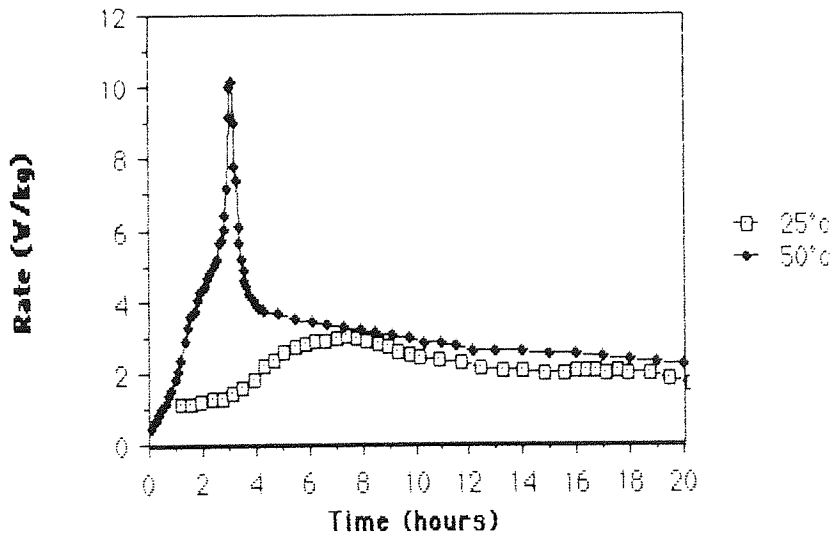

Figure 52 *Heat evolution during hydration of 50% BFS pastes at 0.3 w:s ratio*

At low temperatures, the second and third peaks are resolvable but, as found in the Portland cement, the peaks merge as the temperature of the experiment increased. The thermal activation is more marked in the blended cements than in OPC, this is to be expected from their higher reported activation energies.

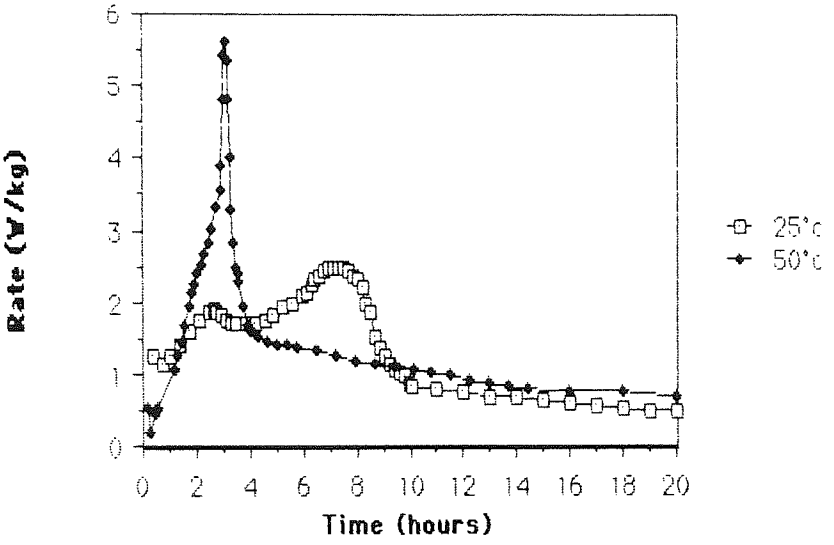

Figure 53 *Heat evolution during hydration of 70% BFS pastes at 0.4 w:s ratio*

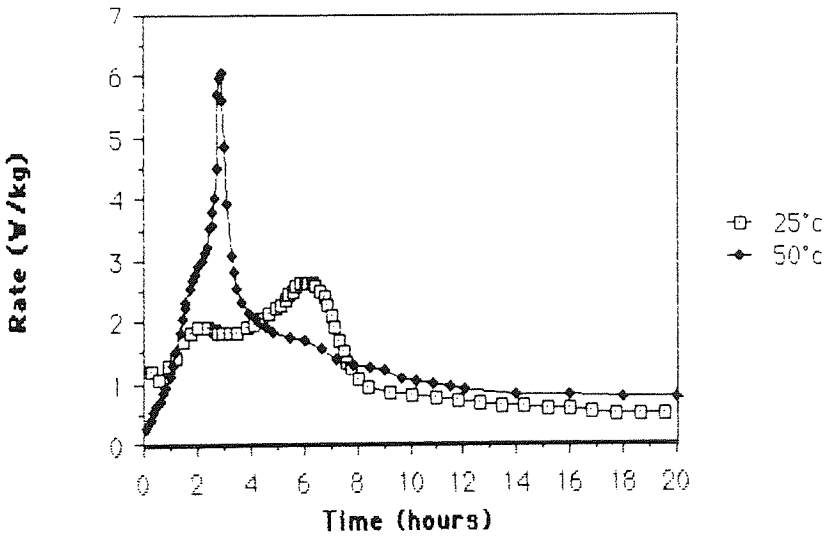

Figure 54 *Heat evolution during hydration of 70% BFS pastes at 0.3 w:s ratio*

The practical implication of this lower heat of hydration is that a

relatively large quantity of slag cement may be emplaced, yet remain workable where a similar quantity of Portland cement would set due to the self heating effect.

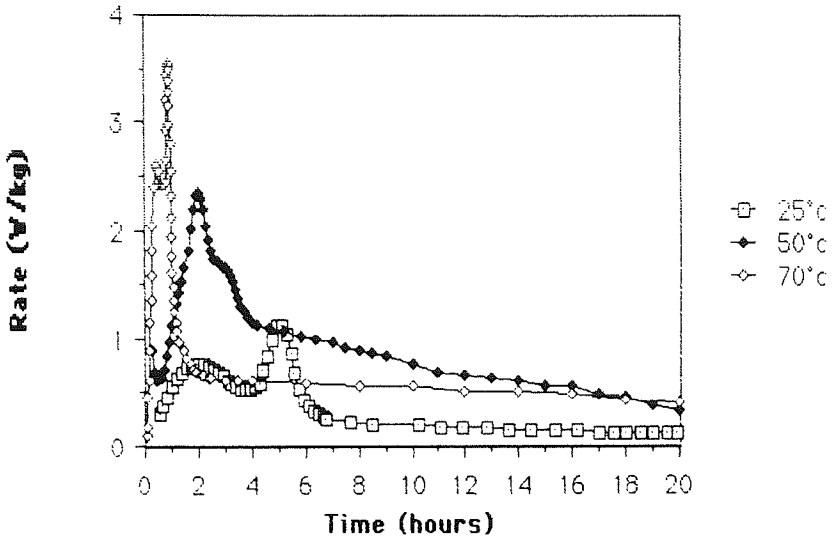

Figure 55 *Heat evolution during hydration of 90% BFS pastes at 0.4 w:s ratio*

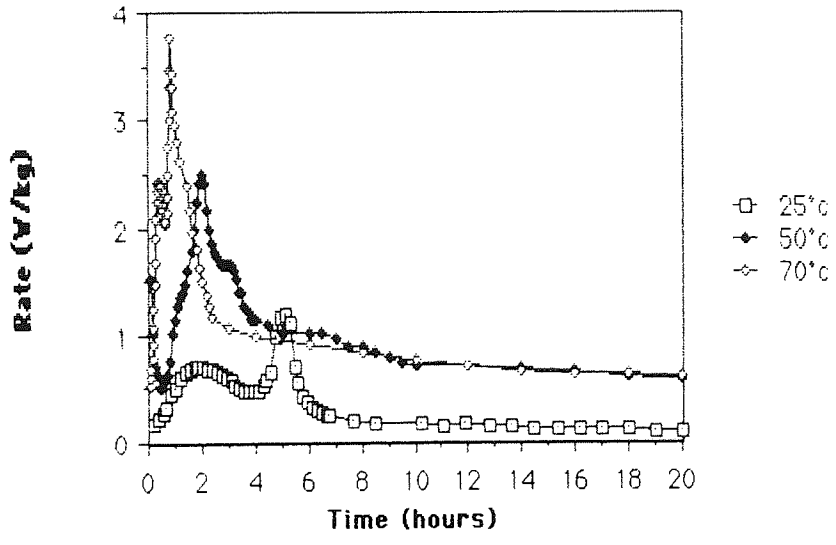

Figure 56 *Heat evolution during hydration of 90% BFS pastes at 0.3 w:s ratio*

No results were obtained at 70°C for the 50% or the 70% slag samples, as on each occasion the calorimeter cell leaked water and the experiment was

stopped. This temperature is evidently the practical limit for the instrument as the work on 90% BFS and pure Portland cement resulted in partial melting of the internal insulation and frequent aborted experiments due to leaking of the cell.

As expected, the rate of heat evolution at high levels of slag replacement is significantly reduced and at 90% BFS content, the maximum rate is less than twenty percent of that evolved by OPC. Figures 55 and 56 include results obtained at 70°c and show that even at this elevated temperature, the rate of heat output does not exceed 4 W/kg of paste.These results are in broad agreement with published work and show the essential features expected during blended cement hydration. After the initially rapid reaction and increase in Ca^{2+} (attributed variously to the heat of wetting of the cement, rapid hydration of the free lime and/or hemihydrate and formation of ettringite from C_3A), there is a dormant period of much reduced heat output. This lasts approximately one hour at room temperature and is thought to be due to the formation of surface hydrates surrounding the cement and slag grains. Midgely and Rosaman (152) have evidence that the calcium sulphoaluminate hydrate is in the ettringite ('high sulphate') form at this time, yet thermal analysis by Richardson et al (153) suggests that if this is so, it is in very low concentration. The possible mechanisms for the conclusion of this dormant period have been discussed in chapter one but it is reported by most workers to be accompanied by a gradual increase in Ca^{2+} in solution.

The second peak is normally attributed to the rapid hydration of alite as the surface hydrates are breached by the pore solution and this phase is retarded by the formation of calcium silicate hydrate on the grain surface. Barwick and Brown report that only about 10% of the available C_3S has hydrated at this stage.

The third and fourth peaks are a matter of some conjecture as they cannot confidently be atttributed to specific reactions. The third peak is commonly attributed to the conversion of ettringite to monosulphate although in blends

containing a large amount of BFS it has been correlated with the hydration of the slag fraction. A minor, fourth peak has been resolved by some workers which has been ascribed to the hydration of the ferrite phase (69) albeit with some caution.

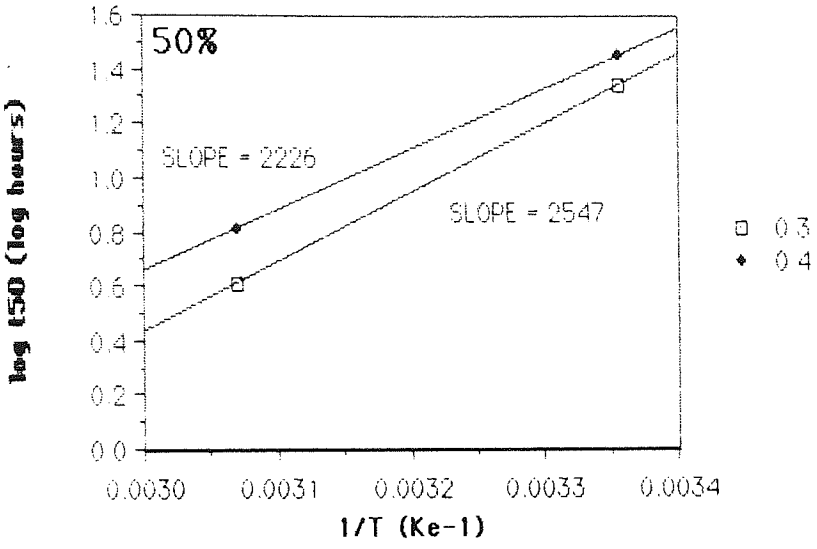

Figure 57 *Estimation of activation energy from data collected at 25 &50°C for 50% BFS pastes*

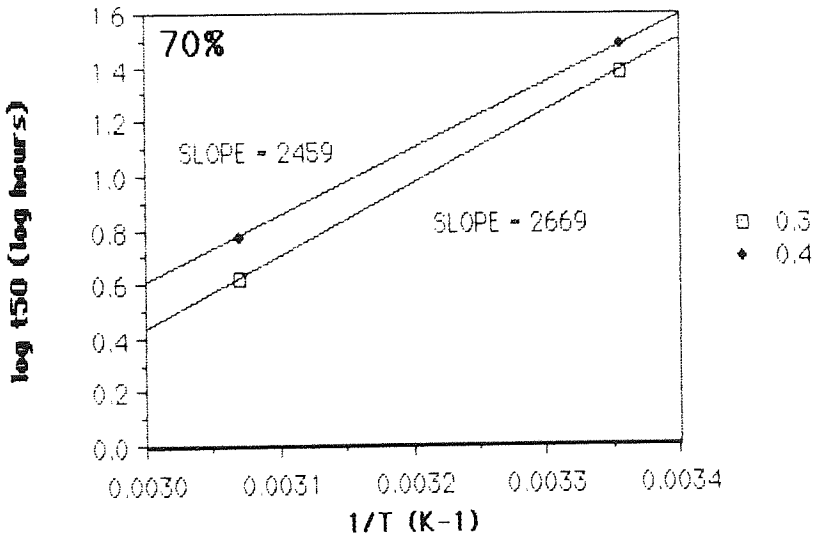

Figure 58 *Estimation of activation energy from data collected at 25 & 50°C for 70% BFS pastes*

The subsequent hydration is dominantly diffusion controlled and associated

with very low heats of reaction, and any significant changes are un-resolved by current calorimetric methods.

The overall form of the curves suggests that the underlying kinetics do not change over this range of compositions or temperatures but care must be exercised in making this assumption on such a complex system.

By using calculated values for t_{50} to determine the apparent activation energies in these experiments, homogeneous reaction kinetics are assumed. Some variations are shown in figures 57 to 59 but the estimates of the activation energies are to a first approximation, correct.

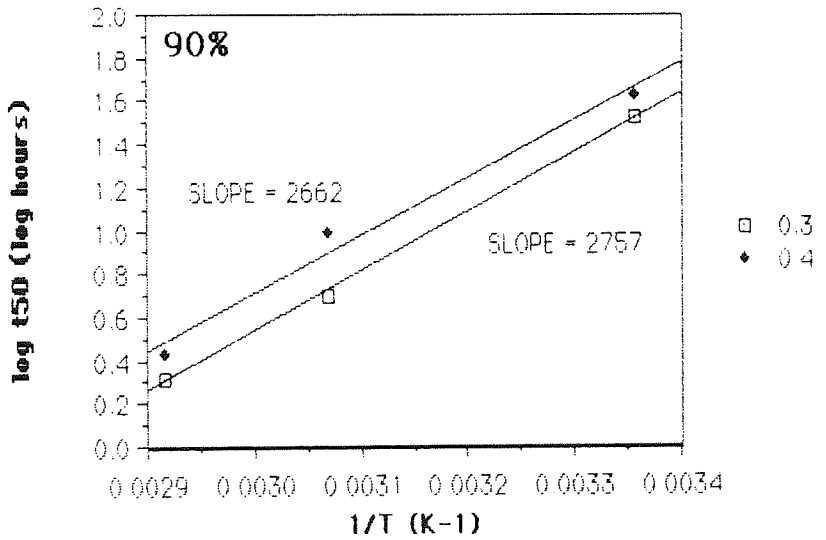

Figure 59 *Estimation of activation energy from data collected at 25,50 &70°C for 90% BFS pastes*

The data collected for the four compositions can be combined as shown in figure 60, overleaf, thus providing an estimation of the activation energies for each component.

The data show that the activation energy for these materials is approximately 42.6 and 52.5 kJ/mol for OPC and BFS respectively, which is close

to values published by other workers.

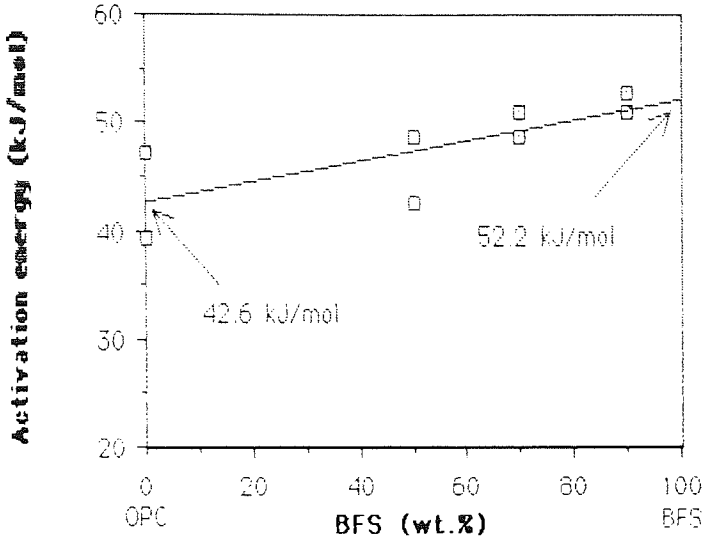

Figure 60 Variation of activation energy with composition of paste

3.4 Discussion

The significance of these results is threefold: First, the higher activation energy shown by the slag suggests that this material is most greatly affected by hydration at higher temperature. The rate curves would appear to confirm this finding, blast furnace slag being accelerated more rapidly than Portland cement over the same temperature interval. This is shown not least, by the time taken to reach 50% hydration:

Table 4 Time taken to reach 50% hydration (t_{50}) - Hours

%BFS ↓	25°	50°	70°C	25°	50°	70°C
0% 15	2.6	1.25	18.4	3.9	1.7	
50%	22.1	4.1	---	28.5	6.5	---
70%	24.5	4.2	---	30.5	5.3	---
90%	34	5.7	2.2	43	10.1	2.7

Secondly, the heat of hydration of blast furnace slag is appreciably lower than that of Portland cement, the maximum rate of heat evolution is similarly reduced with increasing slag content.

Lastly, the effect of changing the water/solids ratio between the limits 0.3 to 0.4 is of minor consequence to the heat evolution during the hydration reactions.

Chapter 4
Kinetics by Chemical Shrinkage

4.1 Theroretical treatment of chemical shrinkage

The chemical shrinkage method has successfully been applied by Geike *et al* (74 -80) to investigate the kinetics of Portland cement hydration and alkali - silica reaction. In the hydrating system, a volume change can be measured, which arises because the total volume of the hydration products plus unhydrated cement and water is less than than the volume of the initial, unreacted constituents. This volume, expressed as a fraction of the total, is a measure of chemical shrinkage, and is distinct from bulk or drying shrinkage.

Knudsen (145,146) has developed previous work, applying the dispersion model to Portland cement hydration by using the following equation:

$$\alpha = t_R^i / [t_R^i + (r_O / k)^i] \quad \text{.....(eqn. 1)}$$

Where α = the degree of hydration, t_R is the reaction time ($t-t_O$) such that t is the time of hydration and t_O is the duration of the dormant period. The term r_O is a constant related to grain size and k is a rate constant dependant on the sample temperature. The constant i, can assume values of 0.5 or unity and, in accordance with previous work, Knudsen refers to these conditions as parabolic and linear kinetics respectively. The relationship between hydration kinetics and grain size has been considered elsewhere by Larsen (147) who concludes that a direct relationship exists between grain size and the reaction time required to reach 50% hydration.

The dispersion model described by Knudsen (145,146) requires the calculation of the ultimate value of some property 'P' (in this case, chemical shrinkage) which corresponds to that attained after an infinate reaction time.

This value, P_{max} is estimated by re arranging the general equation for this model:

$$P = P_{max}(t-t_o)^i / [(t-t_o)^i + t_1^i] \quad \text{.....(eqn. 2)}$$

Where P is the property, t_o is the duration of the dormant period, and thus $t-t_o$ is the reaction time.

To estimate the ultimate value of the property equation 2 is re-arranged as a reciprocal expression:

$$1/P = 1/P\,max + (t_1^i / P\,max)[1/(t-t_o)^i] \quad \text{.....(eqn. 3)}$$

When $t >> t_o$, t_o can be neglected and hence the equation reduces to:

$$1/P = 1/P_{max} + (t_1^i / P_{max})(1/t^i) \quad \text{.....(eqn 4)}$$

Hence a plot of $1/P$ versus $1/t^i$ gives a straight line and as t tends to infinity $1/P \approx 1/P_{max}$:

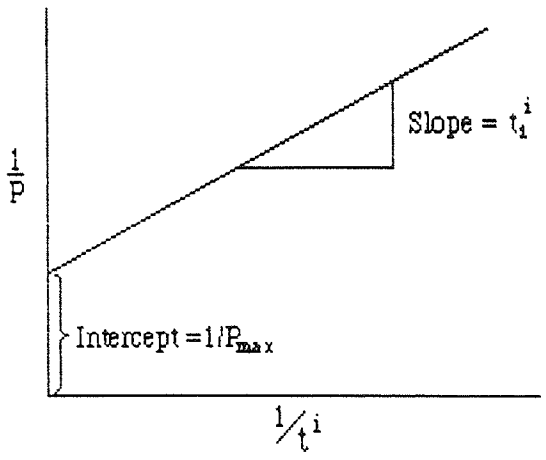

Figure 61 *Estimation of the value of* P_{max}

In the above, the constant i, is determined initially by trial and error, the appropriate value leading to a straight line relationship. Confirmation of this value can be obtained by applying equations 5 and 6 as shown in figure 62 below. In this equation the term α is introduced as an indicator of the degree of reaction, such that $\alpha = P / Pmax$.

$$\log [\alpha / (1-\alpha)] = i \log [(t-t_o) / t_1)] \quad \text{.....(eqn. 5)}$$

Simmilarly, when $t>>t_o$, t_o may be disregarded and equation 5 becomes:

$$\log [\alpha / (1-\alpha)] = i \log (t/t_1) \quad \text{.....(eqn. 6)}$$

Thus, plotting $\log [\alpha/(1-\alpha)]$ versus $\log t$, a straight line is obtained with a gradient of i:

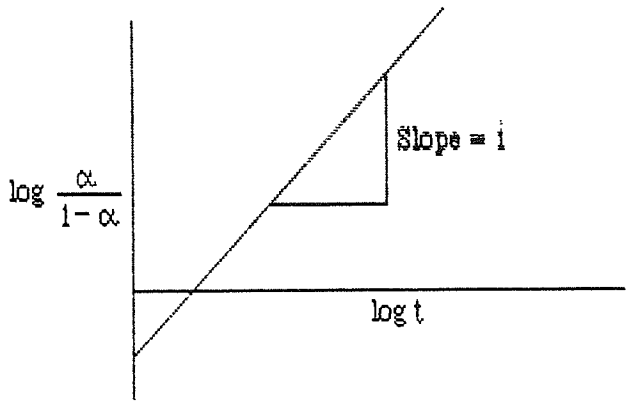

Figure 62 *Graphical estimation of the constant i*

The estimation of the duration of the dormant period is made from a rewriting of equation 5:

$$[\alpha / (1-\alpha)]^{1/i} = [(t-t_o) / t_1] \quad \text{.....(eqn.7)}$$

By plotting $[\alpha / (1-\alpha)]^{1/i}$ versus t, a straight line is obtained enabling the calulation of both the duration of the dormant period t_o, and the time taken to reach 50% hydration:

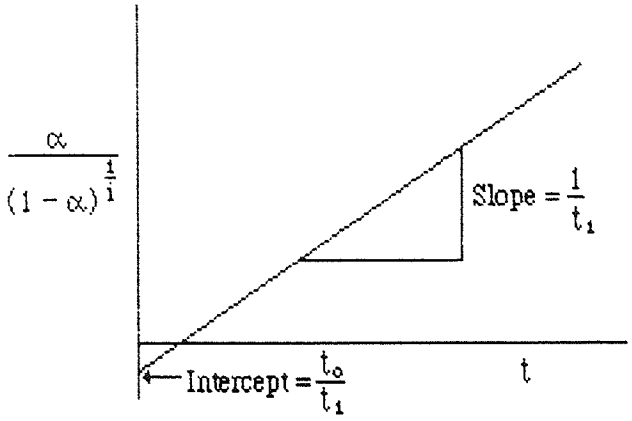

Figure 63 *Determination of t_1 and t_O*

It can be seen from the above that relatively simple measurements are capable of yielding useful kinetic data on the hydrating system. Geike (75) describes Knudsen's dispersion model in terms of the following equation which accommodates both linear (i=1) and parabolic (i=0.5) kinetics as applied to Portland cement:

$$t_1 \alpha / (1-\alpha) + t_2 [\alpha / (1-\alpha)]^2 = t - t_o \quad \text{.....(eqn. 8)}$$

or:

$$t_o + t_1 A + t_2 A^2 = t \quad \text{.....(eqn.9)}$$

Where A is known as the reaction ratio, $\alpha/(1-\alpha)$, and the ratio between t_1 and t_1+t_2 is named the degree of linearity 'DL'.

For dominantly linear kinetics, $t_1 >> t_2$

and For dominantly parabolic kinetics $t_2 >> t_1$

Where t_1 and t_2 are the reaction times at which α=0.5 for linear and parabolic kinetics respectively.

4.2 Experimental details

Geike (75) proposes two experimental methods of studying hydration kinetics; First, a method based on weight gain with respect to time and secondly the measurement of volume change with time. It is the latter of the two methods which has been adopted here. The technique is essentially very simple and uses the apparatus shown in figure 30 and below in figure 64.

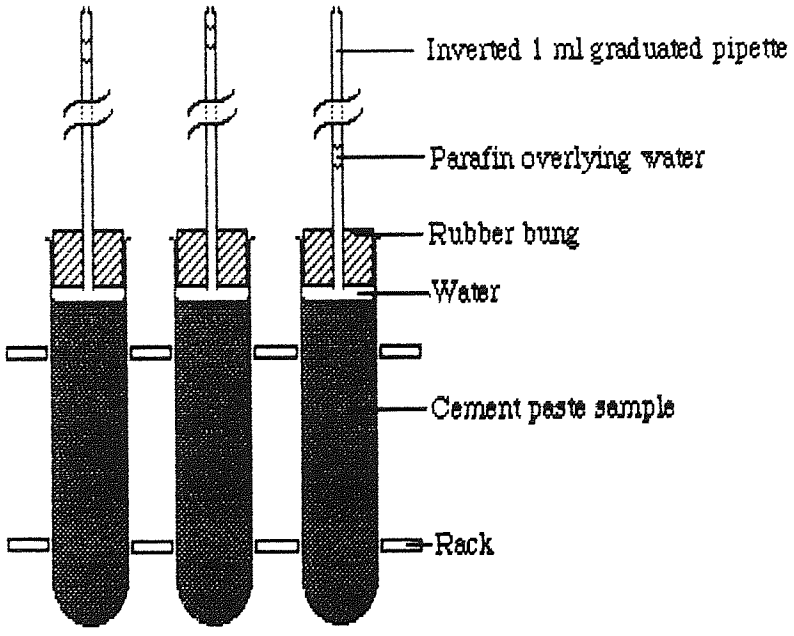

Figure 64 *Dilatometers for chemical shrinkage experiments*

A test tube, supported on a top -pan balance, was filled with freshly mixed cement paste by means of a plastic syringe, fitted with a short length of plastic tubing. The mass of cement paste used in each case was 30g ± 0.05g and the sample was injected carefully, in order to avoid air entrapment.

A small quantity of water was carefully poured onto the sample surface and the bung, containing the inverted pipette was fitted into the tube. A water - tight seal was effected by the use of 'Nescofilm', a commercially available elastomer sealing film, which was wound tightly around the joint. The tubes were supported in an aluminium test - tube rack and the whole assembly was placed in

a water bath to equilibrate for temperature.

Initial experiments included a pair of thermocouples in the sample, one cemented to the inner wall of the test tube, the other mounted in the centre of the sample. This allowed measurements of the variation in temperature through the sample to be made immediately after immersion of the dilatometer in the bath, (thus defining the time required for equilibration). As hydration proceeded, water from the pipette was drawn into the sample tube to accommodate the change in volume. By measuring this volume change with time, it was possible to obtain data on the kinetics of cement hydration.

Initially, the time for temperature equilibration was measured as the samples were immersed in the bath and a temperature - time graph of this data is presented in figure 65, (below). This confirmed that the sample core temperature had risen to the temperature of the bath before the first reading was taken, thus ensuring that the measured volume changes were due to chemical shrinkage and not to thermal expansion.

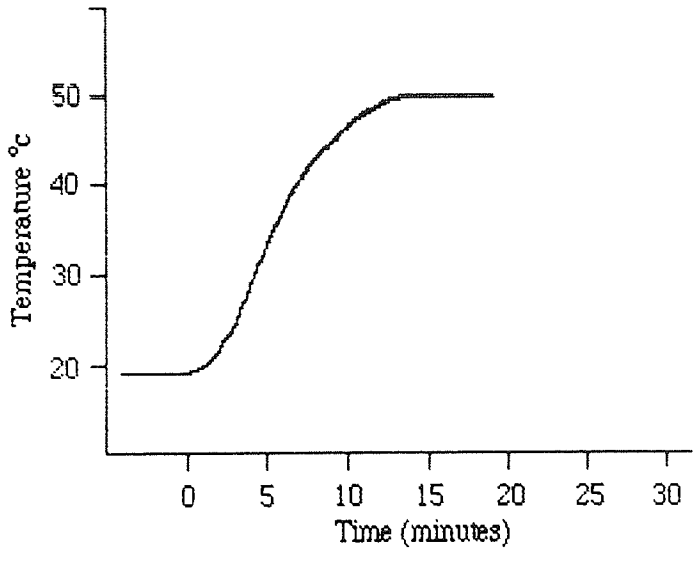

Figure 65 *Equilibration of dilatometers from ambient temperature to 50°C*

The pastes were mixed as described previously and the dilatometers were

filled and assembled such that each batch could be placed in the water bath after thirty minutes hydration. The samples were therefore placed in the bath thirty minutes before the initial reading was taken, hence thermocouples were considered unnecessary for subseqent experiments. The height of water in each dilatometer was set at zero by removing the slight excess with a hypodermic syringe fitted with a long needle. The surface was then covered with a small quantity of parafin to prevent evaporation of water from the dilatometer tube.

The sequence of experiments include ordinary Portland cement both as a reference with which to interpret the slag cements and as a comparison to those cements used by Geike. In addition to these, the majority of experiments were on blended OPC - BFS pastes as described in chapter two. The full range of proposed blends were examined at 25°, 50° and 70°C which gave a total of eighteen possible combinations of slag replacement, water : solids ratio and temperature and each combination was examined at least in triplicate.

4.3 Experimental results

4.3.1 Introduction

The data were collected over a period in excess of one thousand hours in order to ensure sufficient late-age information was obtained to apply the mathematical model described in section 4.1. All data processing was done with the 'Apple Macintosh' microcomputer, using the commercial statistics and graphics packages 'Cricket Graph' and 'Statworks' (Cricket Software Inc). As an example of the mathematical treatment employed, each stage of the processing is presented for one set of experimental data. The data set used is from a 50% slag replcement, at 0.4 water: solids ratio hydrated at 25°C. The chemical shrinkage is expressed as ml volume change per 100g of cement paste and the data represent six independant experiments labled S1 to S6 and plotted as a sigmoid curve in figure 66.

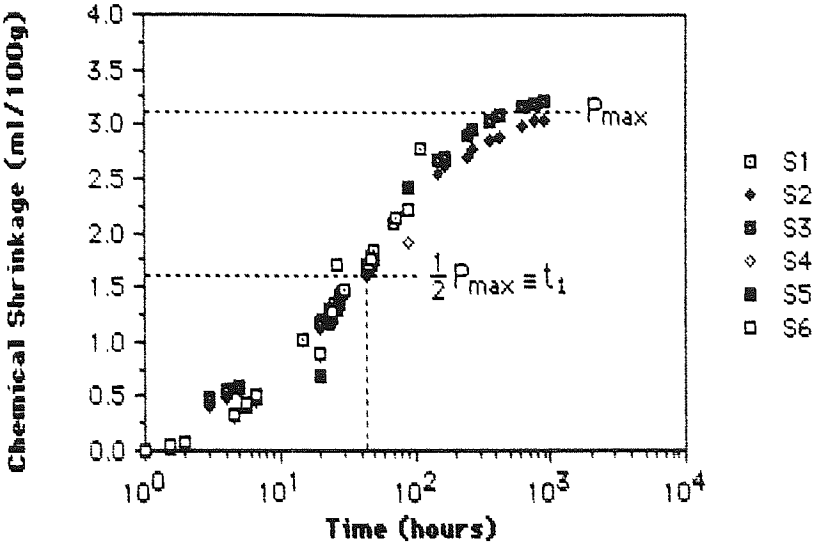

Figure 66 *Chemical shrinkage vs time (log scale) for 50%/0.4/25°C*

The individual data sets were combined to produce a scatter diagram (shown as "x" in figure 67 and the data were then subjected to minimal data reduction).

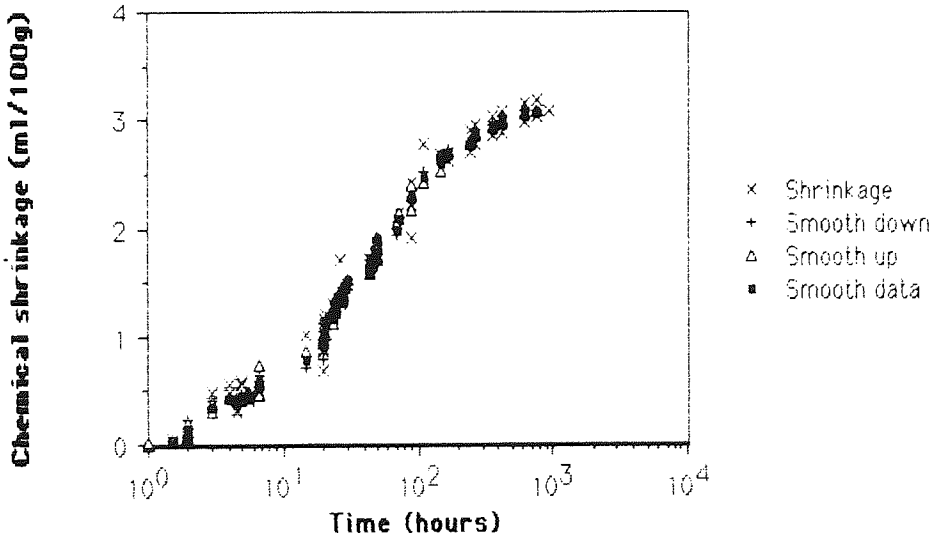

Figure 67 *Data reduction to reduce scatter of the raw data*

The data were arranged in ascending order of time and smoothed in groups of five points using a routine in the "Cricket Graph" software (shown as "+" legend in the figure). The data were then re-arranged in decending order of time

and treated in a similar way. The mean of the two data sets is represented by the solid legend and it is upon these smoothed data sets which further calculations were performed. The necessity for this treatment is apparent when considering the experimental variations found at high slag replacement (see appendix 1).

The smoothed data were re-plotted according to equation 4 assuming that the constant 'i' was both 0.5 (parabolic kinetics, figure 68) and 1 (linear kinetics, figure 69). From these figures it becomes evident that this system is governed by linear reaction kinetics (i=1). Using a linear regression fit on these data, the equation of the regression line is shown to be y = 11.4917x + 0.3161, (where y is the ordinate, 1/V and x is the abcissa, 1/t). The correlation coefficient (R) for this data set is 0.95. This results in a maximum value for the chemical shrinkage of 3.161ml per 100g of cement paste which is close to the experimental value obtained after a thousand hours hydration and this data has subsequently been super-imposed on figure 66.

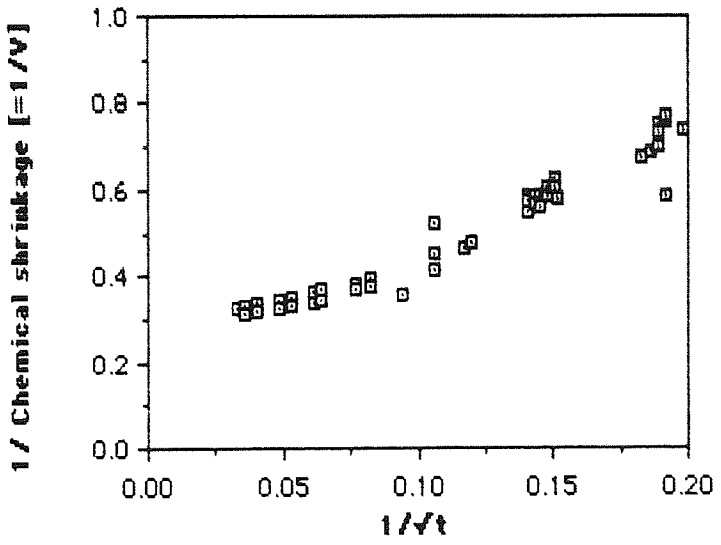

Figure 68 *Plot of 50%/0.4/25°c data assuming parabolic hydration kinetics*

The data were then re-plotted according to equation 7 in order to determine the duration of the dormant period (t_0) and the reaction time (t_1) required for the chemical shrinkage to reach 50% of its ultimate value.

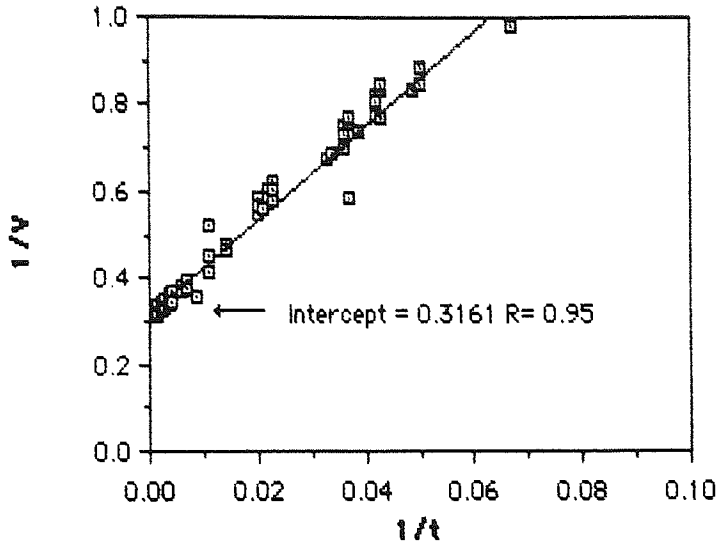

Figure 69 *Plot of 50%/0.4/25°c data assuming linear hydration kinetics*

Figure 70 shows the degree of scatter obtained from this treatment becomes un-acceptably high at later ages and for the data as a whole correlation coefficients as low as 0.8 are not uncommon.

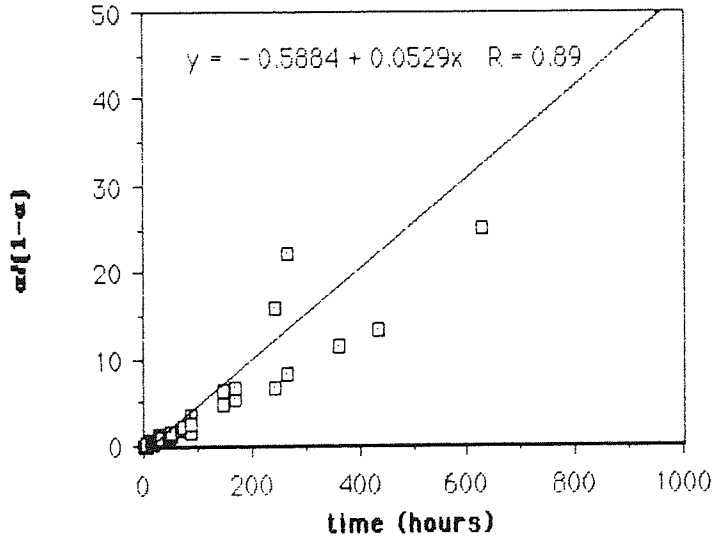

Figure 70 *Plot according to equation 7 where α = P/Pmax*

Whilst this poor correlation at late age should not cause a large variation in the slope (and hence the value of t_1) it does greatly effect the intercept which is very close to the origin. The numerical value of the intercept is theoretically equal to t_o/t_1 and therefore little confidence can be ascribed to the calculated values for the dormant period.

The calculated values of t_1 can be compared to the observed values for t_{50} (the time taken for α to reach 0.5) as $t_{50} = t_o + t_1$. This provides a ready means of establishing that the calculated value of t_1 is of approximately the correct magnitude as $t_1 \approx t_{50}$ and $t_o << t_{50}$. Although this equation offers a possible route to obtaining a numerical value for t_o, the measurement error in estimating t_{50} is of a similar magnitude to that obtained by calculation. The graphs shown in appendix 1 contain an additional plot of $\alpha/(1-\alpha)$ vs time, regarding only the early age data which display a higher degree of linearity than that of the whole set. In some experiments these yield values close to those obtained by conduction calorimetry, which suggests that these data do follow the linear kinetic model but are subject to a degree of experimental variation preventing the direct calculation of the dormant period.

Geike (74 pp17-18) cautions that:

" It must be pointed out that the estimated values of t_o and t_1 are strongly variant, the values depending on where the data sets have been truncated, this in contrast to $t_{50} = t_o + t_1$, which remains almost unaltered. It may be difficult to determine the kinetics of the reaction for hydration curves where t_o and t_1 are close in magnitude."

To surmount this arithmetic problem, the values of t_o from the previous chapter were used to fit the chemical shrinkage data to the dispersion model (145,146) and the final presentation of the data is as a double logarithmic plot of

V/(Vmax -V) vs the reaction time (t-to) as shown in figure 71 below:

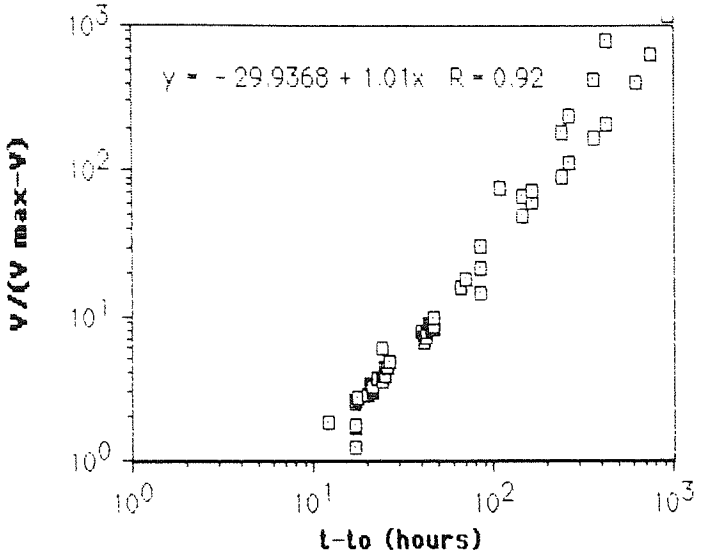

Figure 71 *Chemical Shrinkage for 50% BFS, 0.4 w/s ratio hydrated at 25°C*

For linear kinetics this plot will result in a line with a slope of unity whilst for parabolic kinetics the gradient of this line would be 0.5.

4.3.2 Portland cement hydration

The initial experiments were performed on 100% OPC to allow a comparison to be made with the results presented by Geike and to provide a reference with which to interpret the experiments on blended cements. Figures 72 and 73 show these results as raw and processed data for Portland cement with a water to solids ratio of 0.4 hydrated at 25°C. The general form of the data is similar to that reported by Geike although the ultimate value of chemical shrinkage is approximately 10% less in this case. This is probably due to differences between the compositions of the starting material, 'Westbury' OPC having a slightly higher alkali metal and aluminate content than the Danish cement. Figure 72 shows the estimation of 'P max' to be 3.4 ml/100g of cement paste which is close to the maximum value recorded in this experiment.

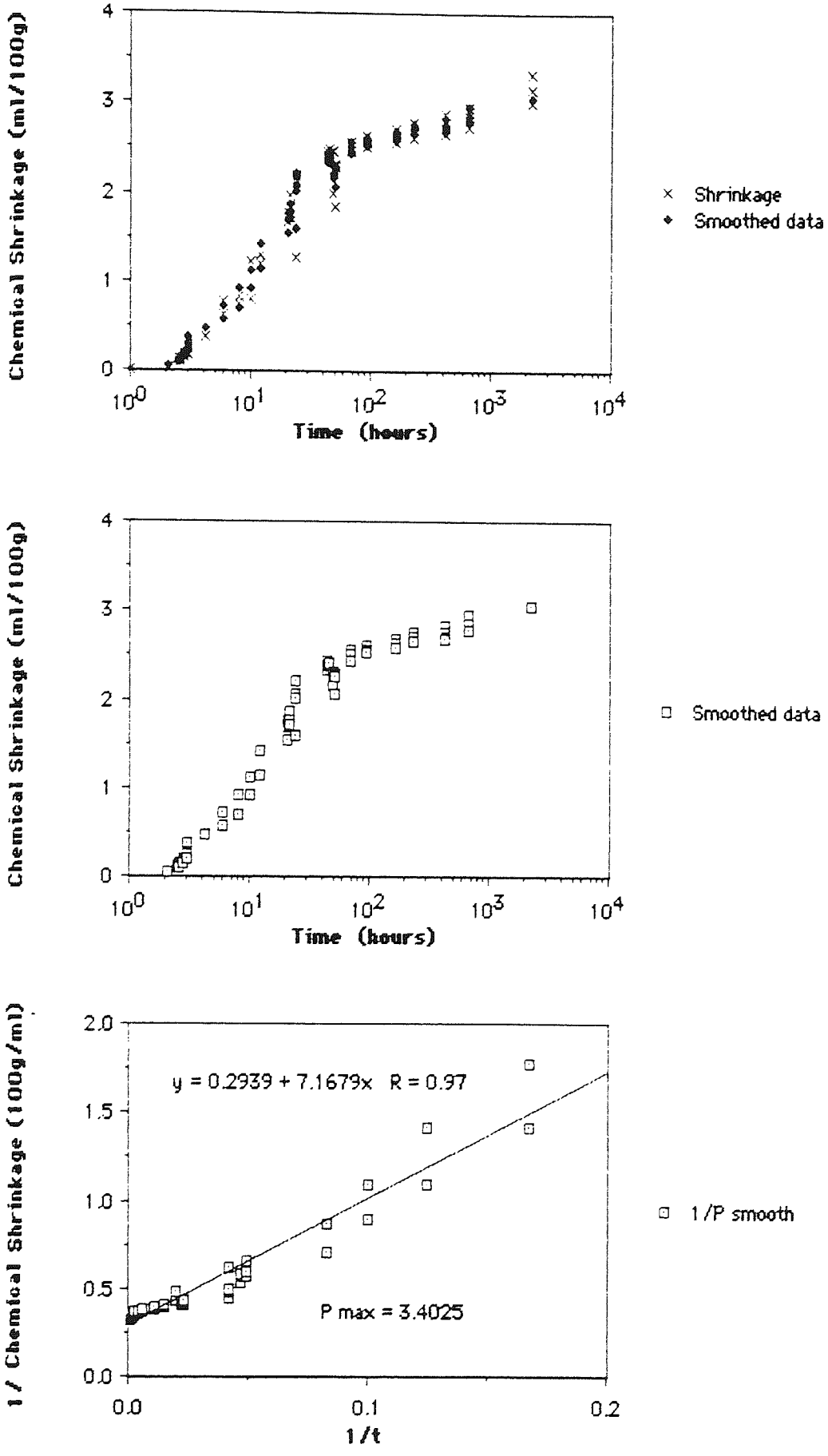

Figure 72 Data for Portland cement at 0.4 w/s ratio, hydrated at 25°C

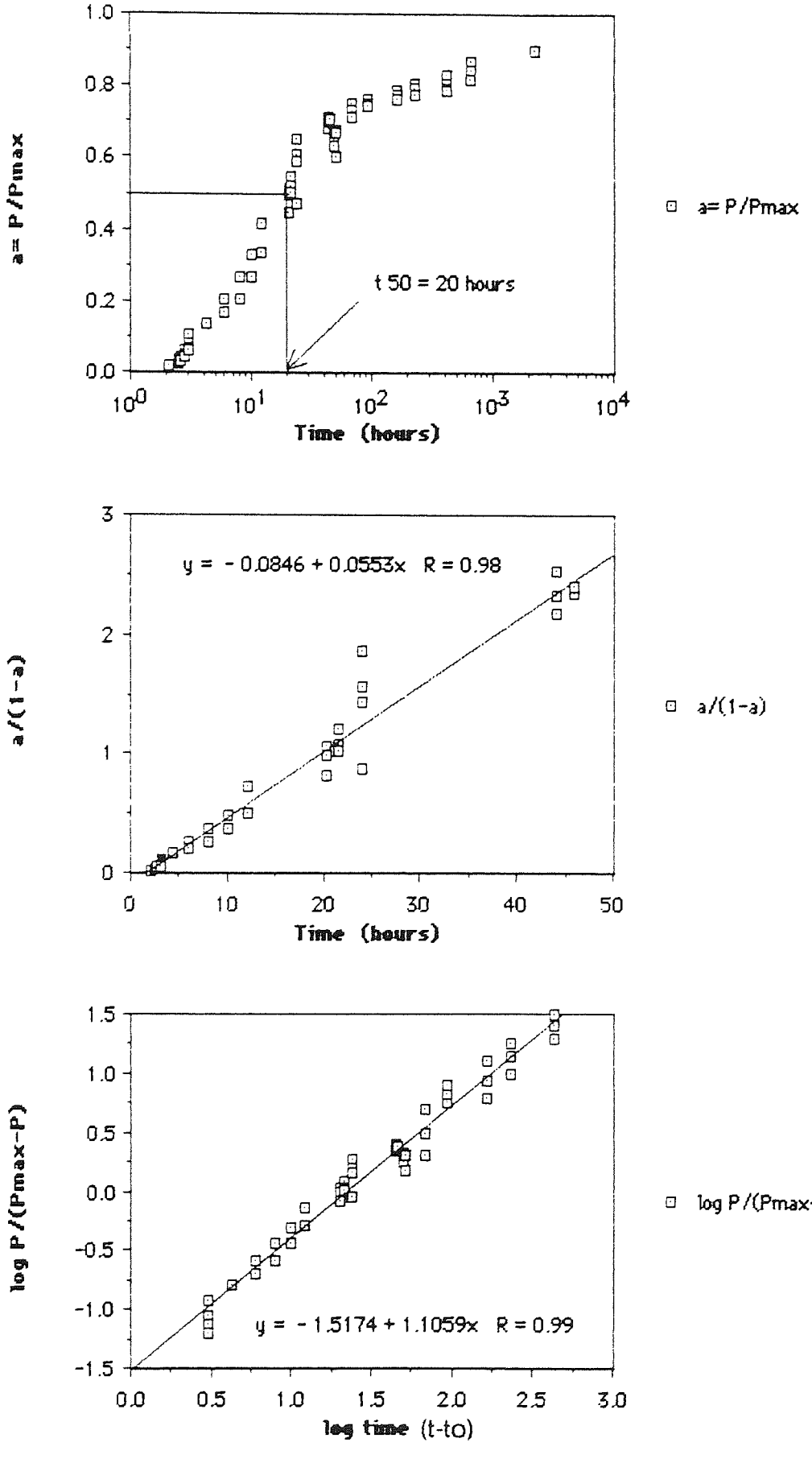

Figure 73 Portland cement data fitted to dispersion model hydrated at 25°c

Figure 73 shows that at 25°C, the system reaches 50% hydation after 20 hours (t_{50}) and the calculated values for t_0 and t_1 are 1.5 and 18 hours respectively. These values are of similar magnitude to those reported by Geike. Figure 49 also shows that the system hydrates according to linear reaction kinetics as demonstrated by the gradient of the final graph. It is pleasing to note that Geike's observation that $t_{50} = t_0 + t_1$ holds true for this data also.

4.3.3 Blended cement hydration

The graphs shown in figures 75 - 80 are the final plots according to equation 5 which results in a straight line plot of unity gradient corresponding to linear hydraion kinetics. Due to the high degree of scatter causing estimation of t_0 to be unreliable, these plots have incorporated the values of t_0 obtained from conduction calorimetry experiments described in the previous chapter.

In general, all samples show a close fit to the dispersion model when treated in this way. The only exceptions to these findings are both of the 50% BFS samples cured at 70°C which show a value for i of approximately two. This does not have any physical meaning in terms of the dispersion model and as the other parameters for these samples assume values which fit the sequence of the remaining data, no explaination of these irregular values can be made at this stage.

The effect of water to solids ratio variation is minimal between 0.3 and 0.4. The higher ratio results in an overall increase of the ultimate value of the chemical shrinkage and the rate of reaction is also correspondingly higher. This is in good agreement with previous work.

The slag content, by comparison, has the reverse effect. Increasing the percentage of blast furnace slag retards the reaction and greatly reduces the ultimate value of the chemical shrinkage. This is to be expected as the finer pore structure of hydrated slag cements is well documented. Figure 74 shows this variation for 50% BFS, 0.4 w/s, at 25°C.

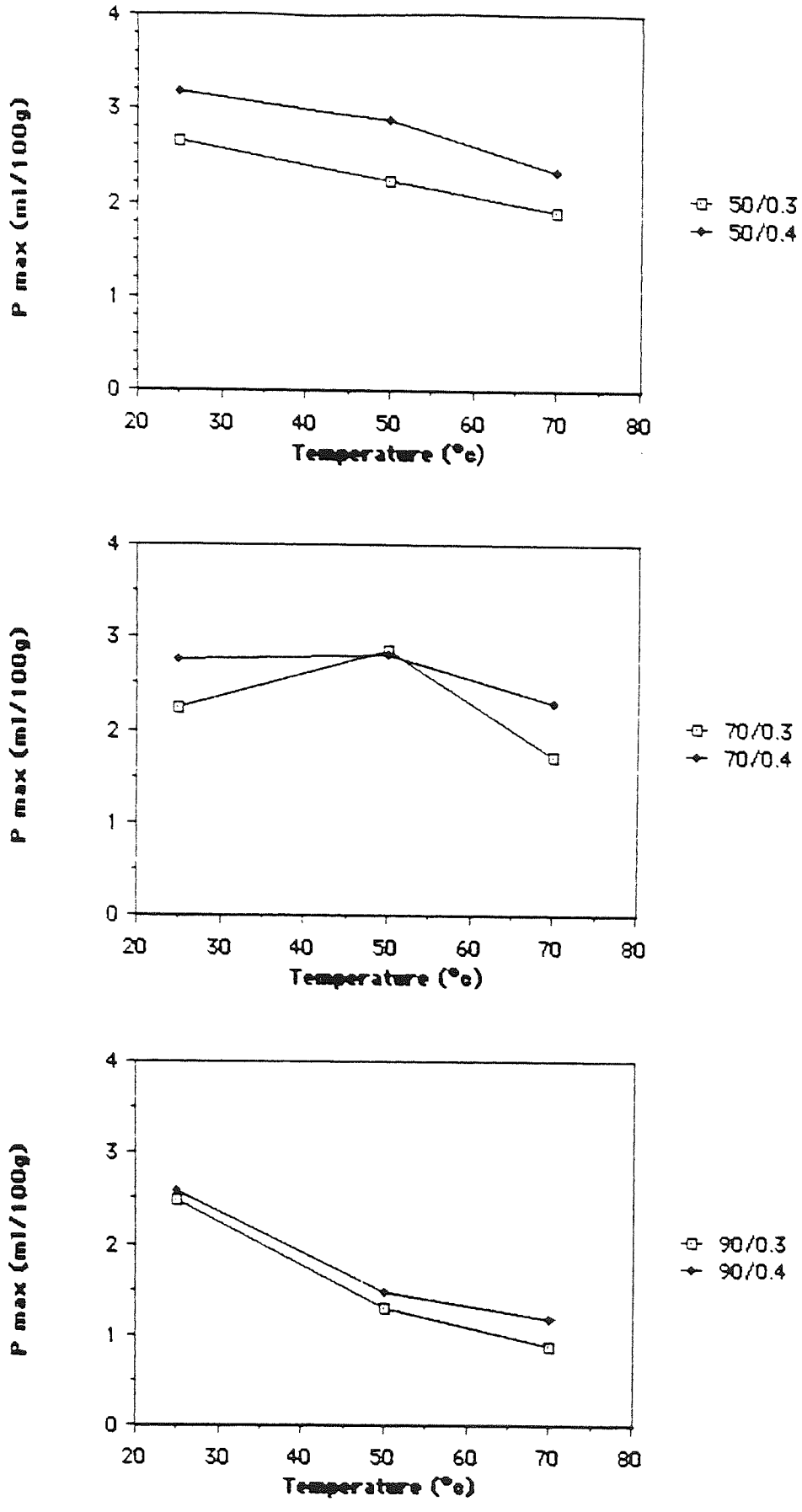

Figure 74 Variation of Pmax values for OPC - BFS blends with respect to temperature

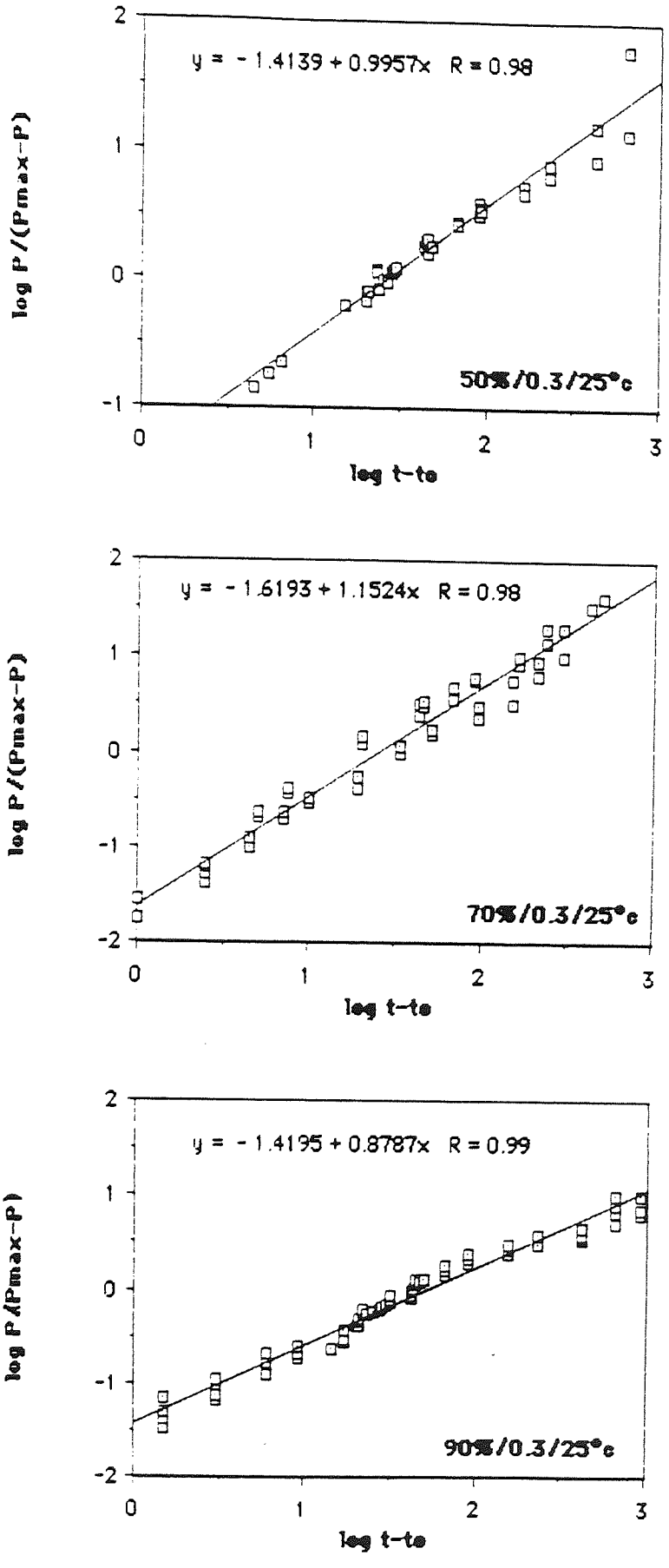

Figure 75 Chemical shrinkage for cement pastes at 25°c

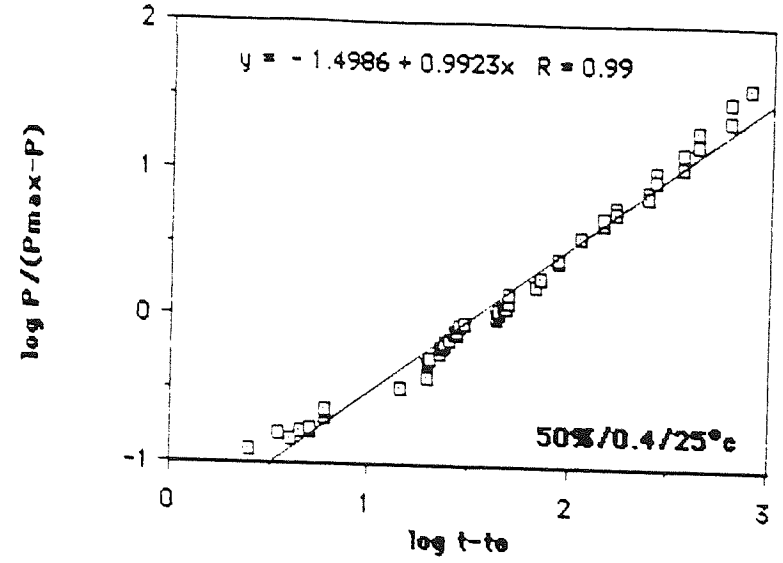

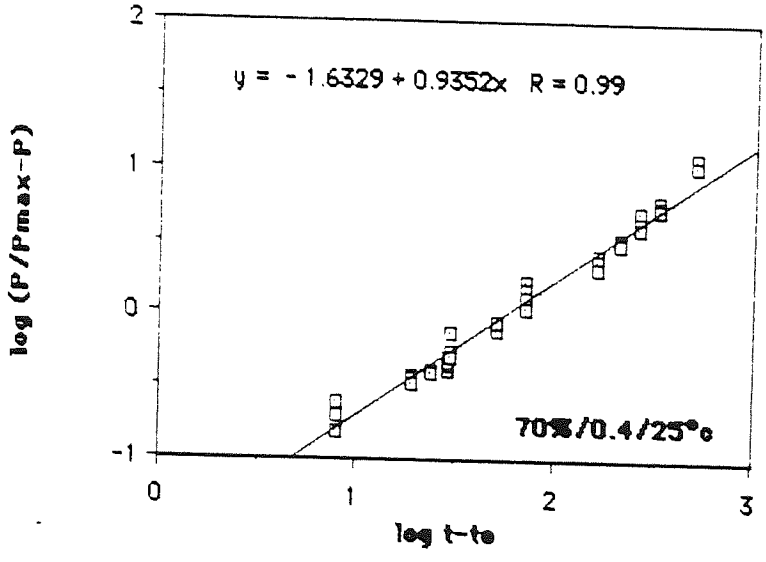

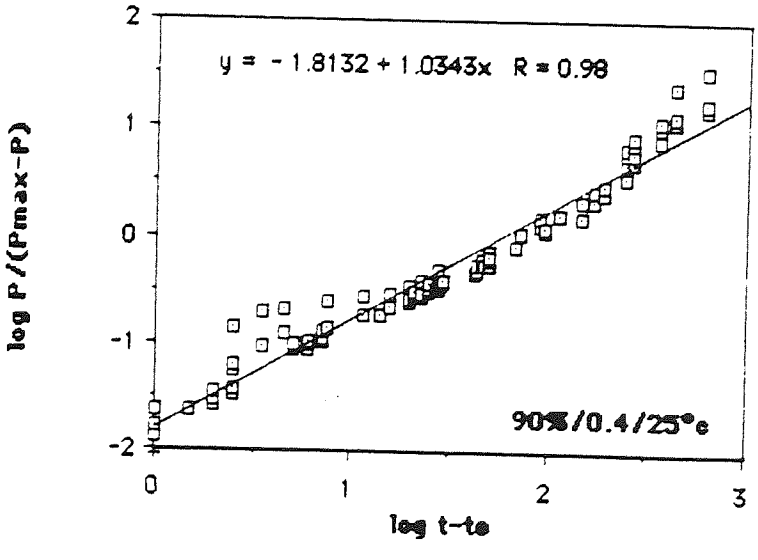

Figure 76 Chemical shrinkage for cement pastes at 25°c

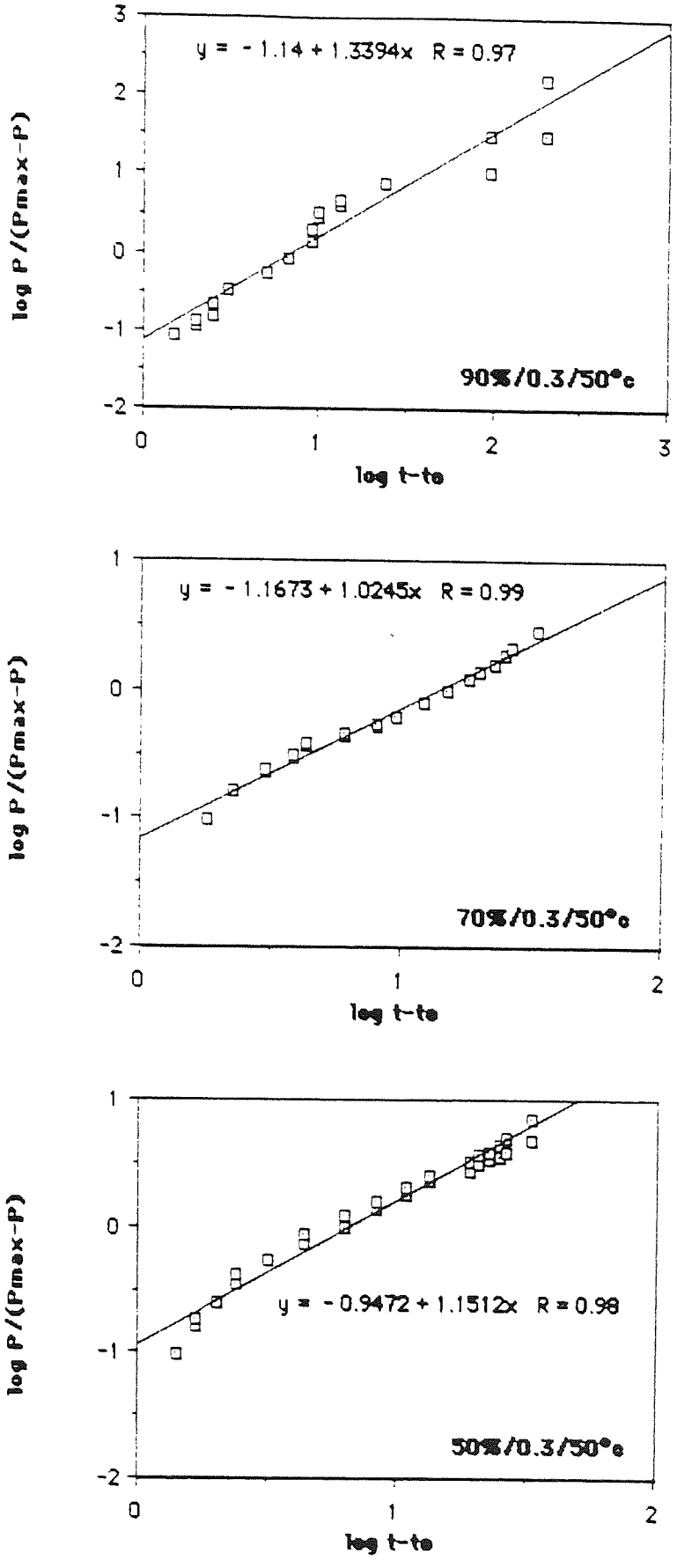

Figure 77 Chemical shrinkage for cement pastes at 50°c

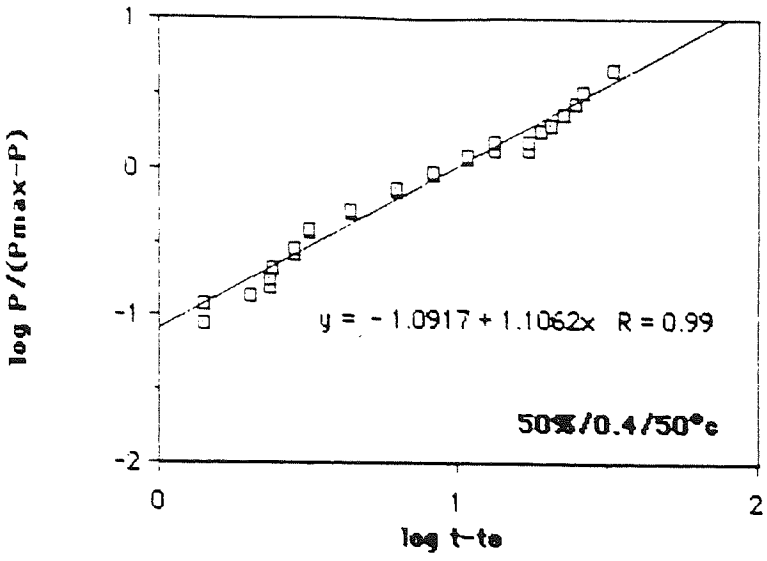

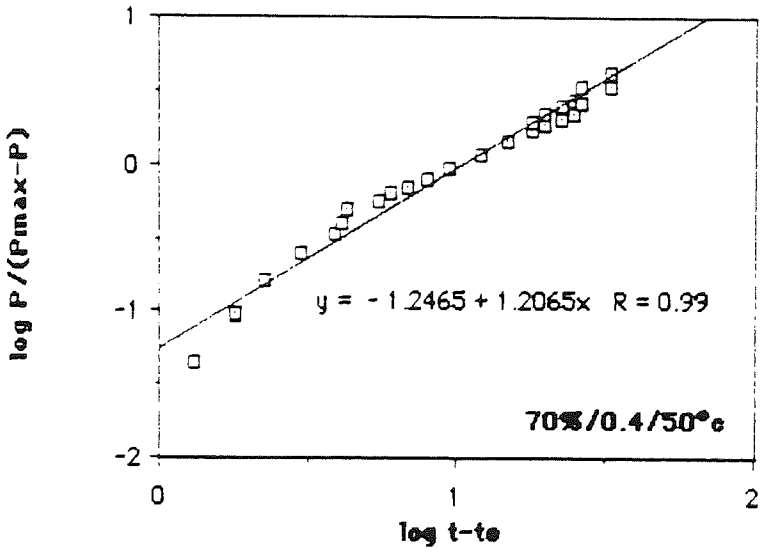

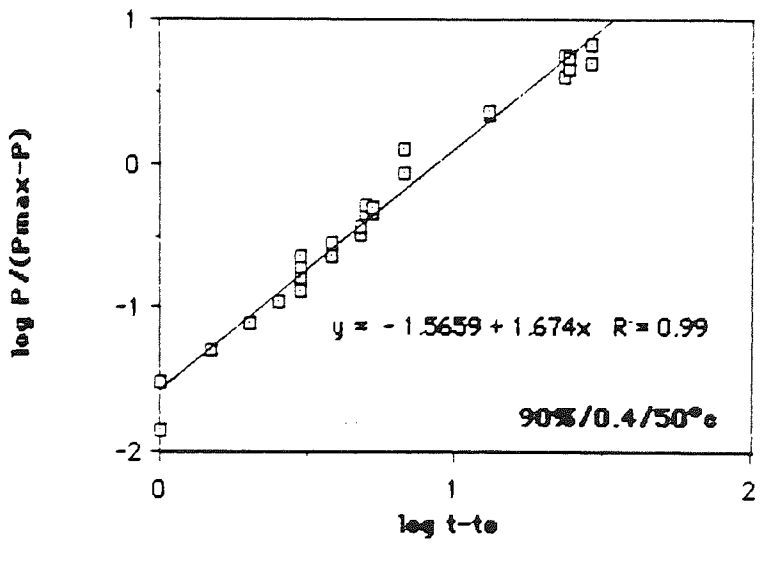

Figure 78 Chemical shrinkage for cement pastes at 50°c

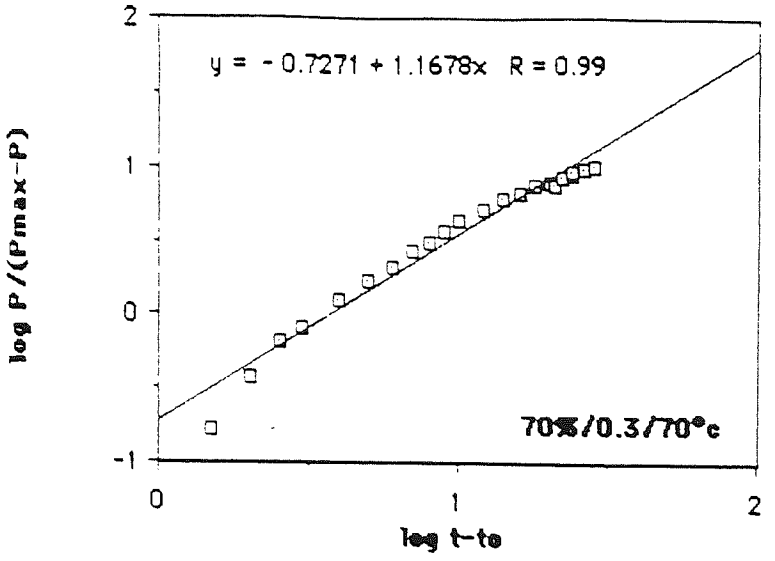

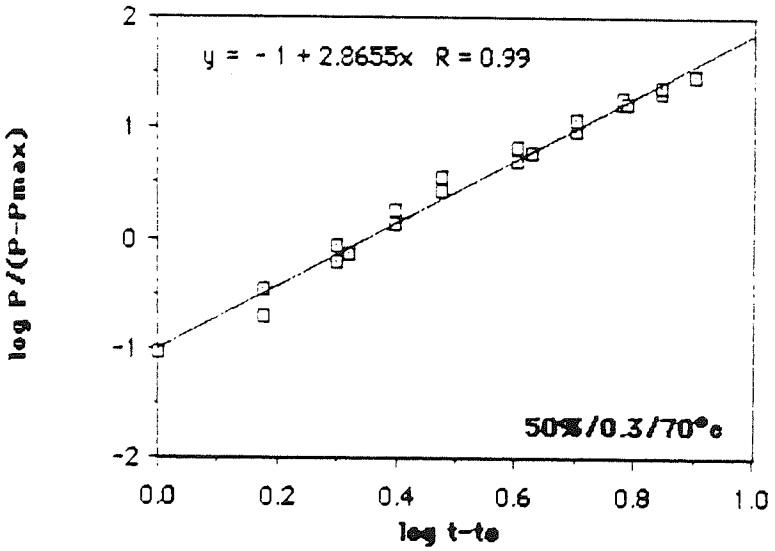

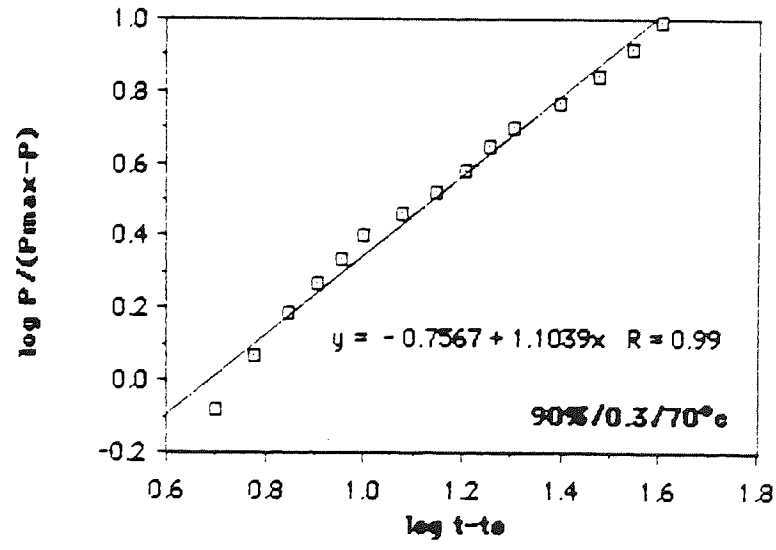

Figure 79 Chemical shrinkage for cement pastes at 70°c

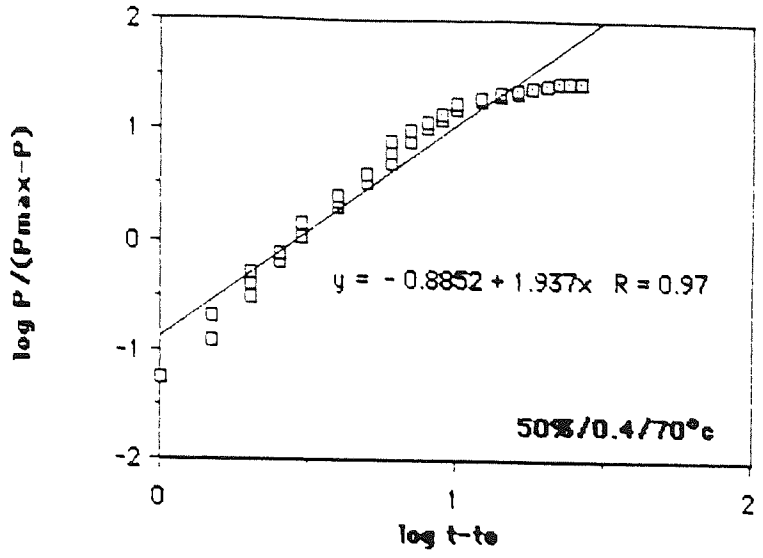

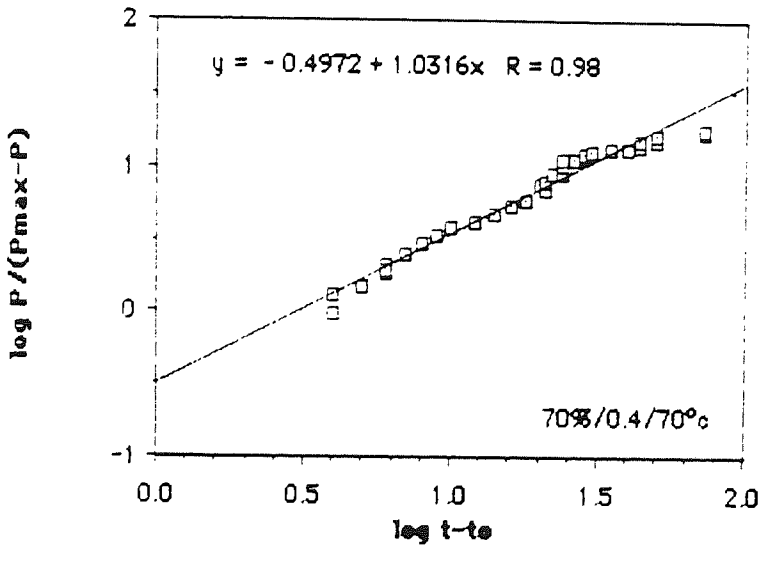

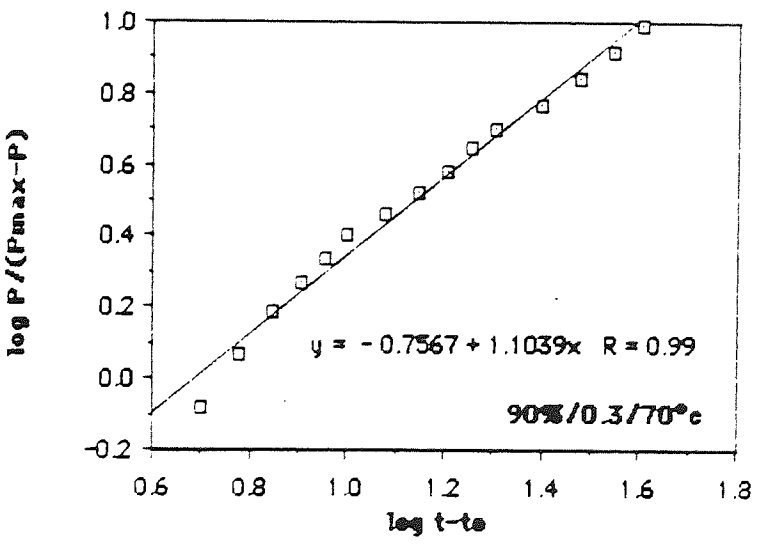

Figure80 Chemical shrinkage for cement pastes at 70°c

If the variation of 'Pmax' with slag content is considered to be broadly linear, it can be seen that a reduction of the ultimate value for the chemical shrinkage of over 30% is observed between OPC and BFS. Figure 74 also relates 'Pmax' with temperature and composition and is discussed more fully with other temperature effects. The most significant variation in the development of chemical shrinkage is shown as a function of temperature. As would be expected, an increase in temperature causes a corresponding increase in reaction rate. In addition to this, the ultimate value of chemical shrinkage is inversely related to temperature, but not in a simple way. The data presented in figure 74 show an obvious trend but variations in the data sets prevent a rigorous mathematical treatment. The erroneous value obtained for 70% BFS, 0.3w/s, at 50°C is probably due to loss of water from the dilatometer through a small leak rather than a function of hydration. The raw data for this sample shows an anomalously high rate of development of chemical shrinkage (see appendix) and results in an estimated value of 'Pmax' higher than either the 50% or 90% samples hydrated under similar conditions. The possibility that this is an effect of rapid hydration taking place before the first measurement is taken can be effectively discounted as the anomolous shrinkage occurs during the first hundred hours or so after the start of the experiment.

The reaction rates, as shown by the development of chemical shrinkage can be used to determine the energy of activation for the hydration of this system. Assuming homogeneous reaction kinetics dominate the hydration over the temperature range considered, it should be possible to determine an apparent activation energy for the hydration of each sample. From this it should also be possible to estimate the actvation energies for the constituent components. Geike (74), Lee (69) and Wu (65) independently postulate that the time t_1 is related directly to the rate constant for the hydration reaction. On empirical grounds, this would appear to be true although several authors caution the use of

homogeneous reaction kinetics on a complex, multi-phase system.

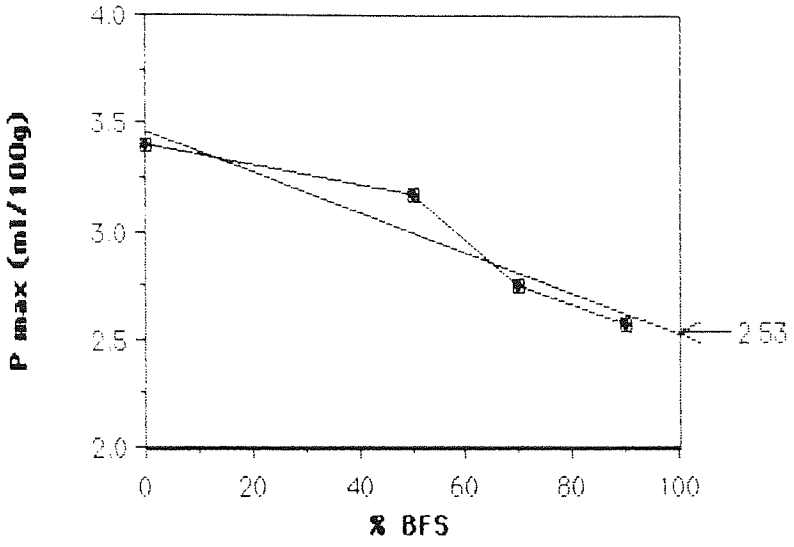

Figure 81 *Variation of the ultimate value of chemical shrinkage with BFS conetent*

The Arrhenius relationship permits the calculation of activation energies from obsevations made at different temperatures, such that:

$$V = A\exp\{-U/(RT)\} \quad \text{.....(eqn. 10)}$$

Where: V = Reaction rate constant

A = a constant over the range of conditions considered

U = the activation energy for the reaction

R = the universal gas constant

T = the thermodynamic temperature (K)

It is difficult to determine the absolute values of the rate constants due to the complexities of cement hydration. The ratio of the rate constants can,

however, be determined if it is assumed that the time, 't', to reach a given stage of reaction is inversely proportional to the rate constant:

$$V_{T1} / V_{T2} = t_{T2} / t_{T1}$$

Where T1 & T2 represent the temperatures.

A plot of the reciprocal of temperature versus the time $t_{\frac{1}{2}}$ will have a slope of U/2.303 R thus permitting the direct calculation of activation energy.

Figure 82 shows an Arrehnius plot for these data, the activation energies being used to produce figure 83. This suggests that for the system hydrated at 0.4 w/s ratio, the activation energy of the slag is 60±15 kJ/mol. This value is acceptably close to the energies reported elsewhere of 53 kJ/mol. The high degree of scatter reflects the variations in the calculated values of $t_{\frac{1}{2}}$ and it is this effect which is responsible for the disappointing results obtained for the same compositions hydrated at 0.3 w/s ratio.

In order to obtain a more acceptable value of activation energy, simmilar plots were made using the interpolated values of t_{50} instead of $t_{\frac{1}{2}}$. If it is assumed that t_0 is small in relation to $t_{\frac{1}{2}}$, then it must hold true that $t_{\frac{1}{2}}$ will approximate to t_{50}. The experimental variations and measurement errors inherent in $t_{\frac{1}{2}}$ are thus limmited as the value of t_{50} is determined directly and not subjected to an arithmetic increase during calculation. Figures 84 and 85 are determinations of activation energy using this method and yield values of 56 & 33 kJ/mol for BFS and 48 & 50 kJ/mol for OPC (for the 0.4 and 0.3 w/s ratios respectively). These are much closer to the activation energies reported by other workers (OPC has an activation energy of 47kJ/mol.

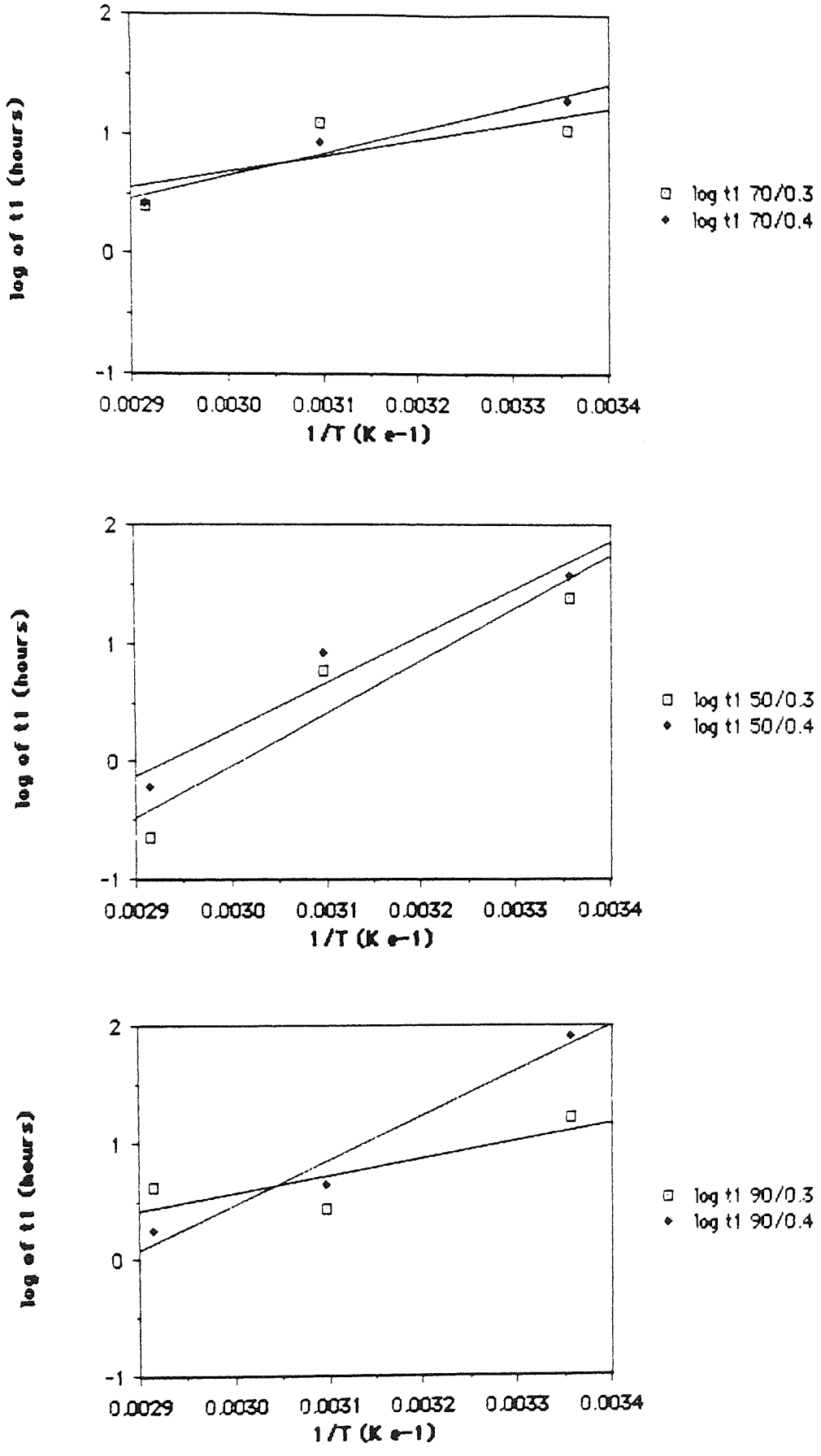

Figure82 Arrhenius plots for blended cements using t_1 as an indicator of rate constant

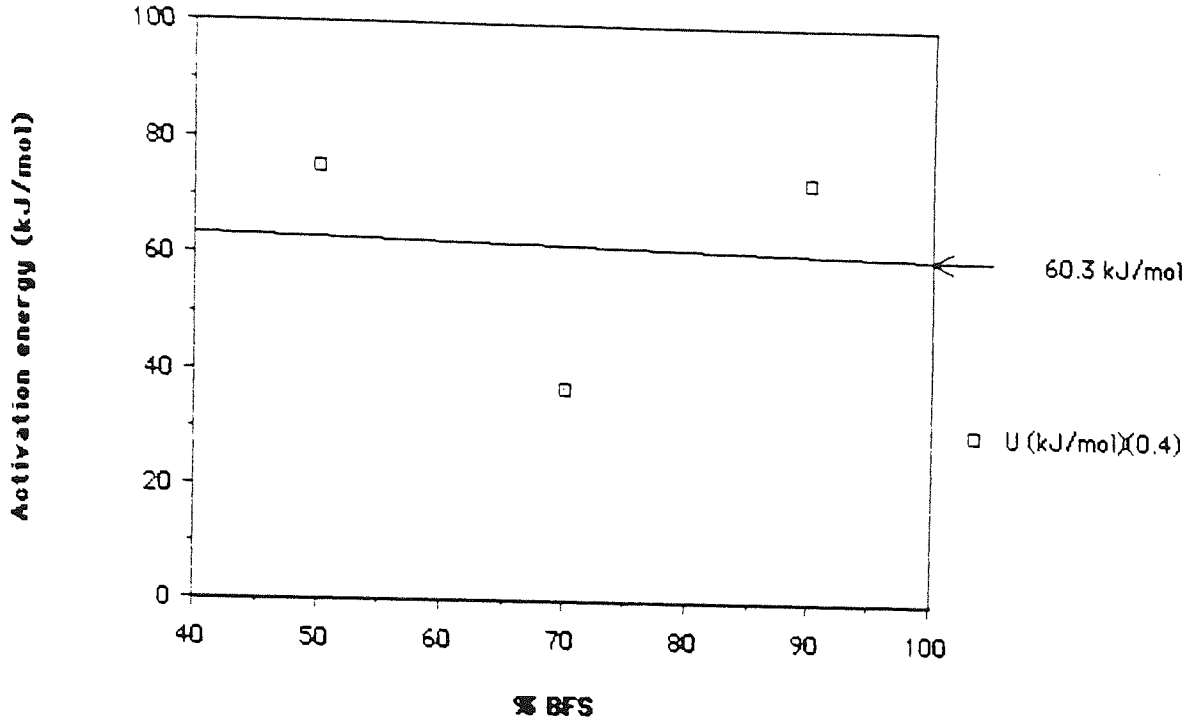

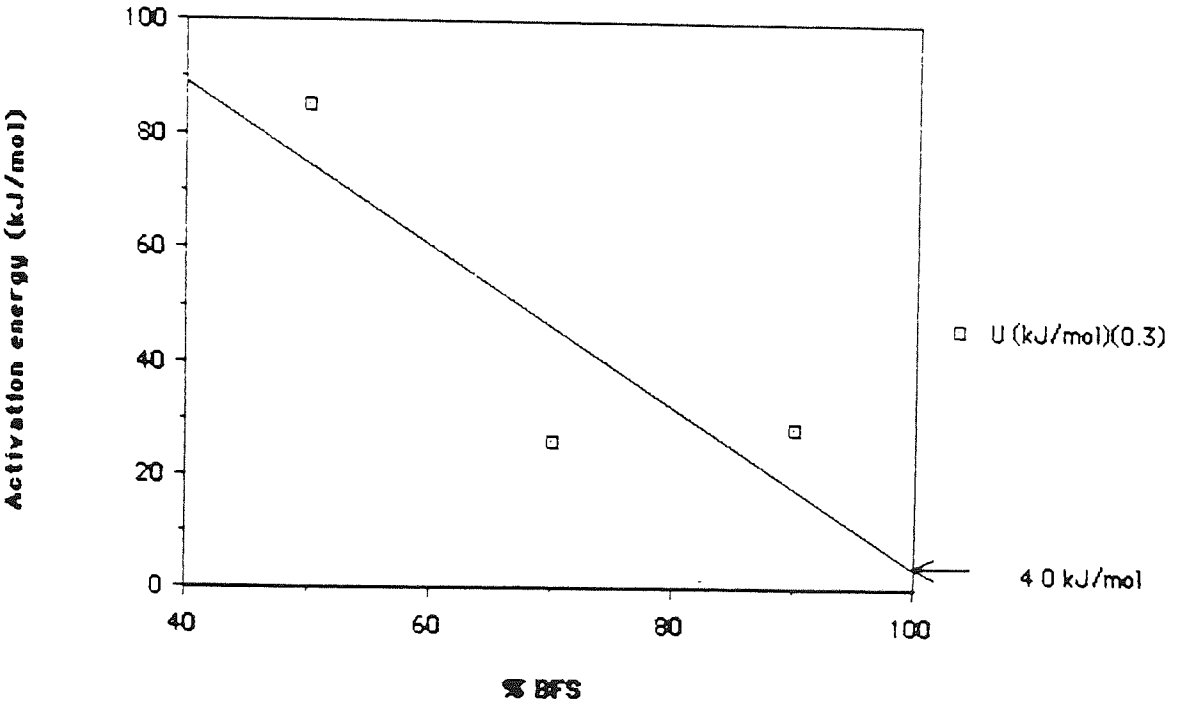

Figure 83 Variation of activation energy with slag content

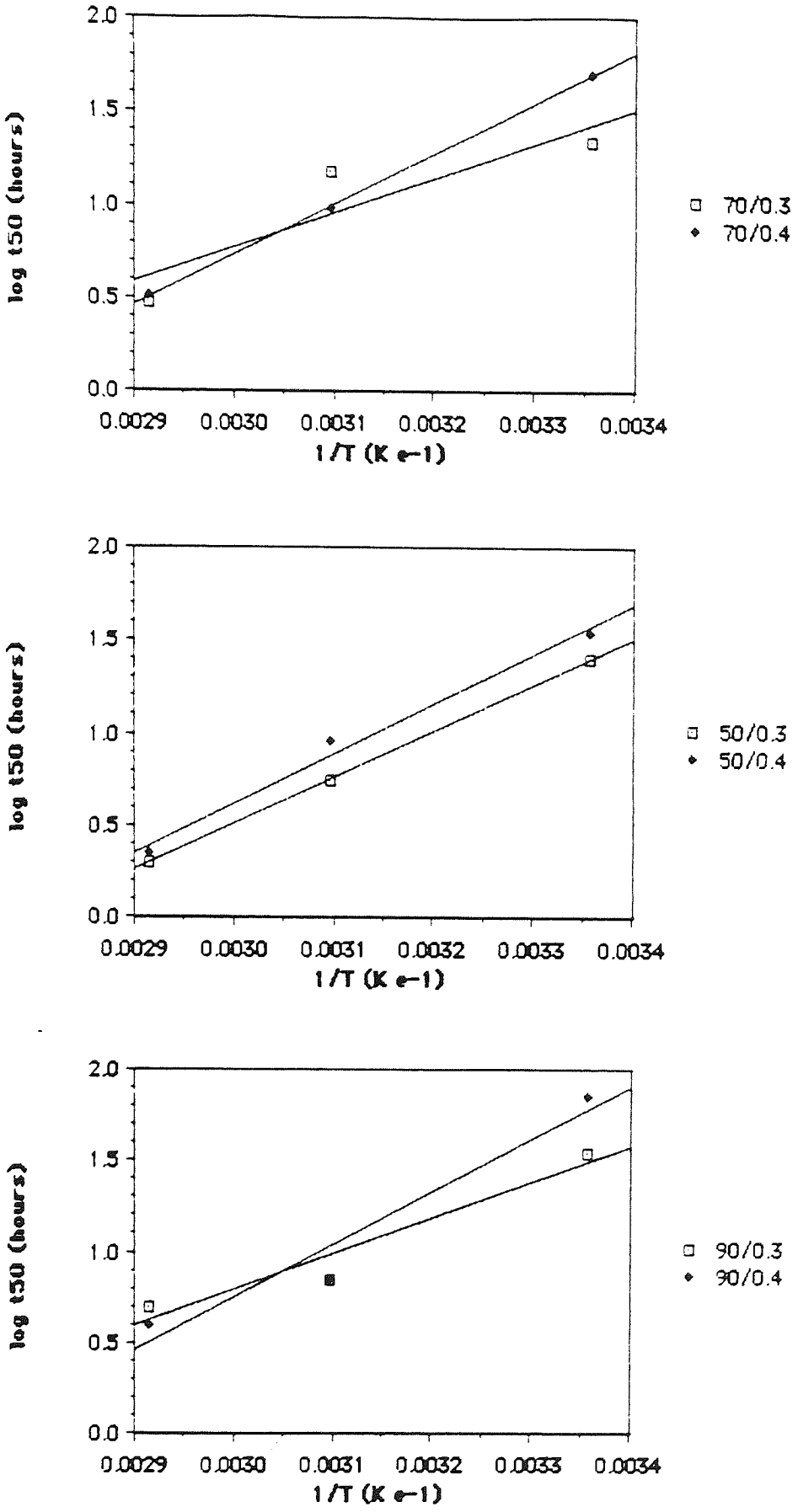

Figure 84 Arrhenius plots for blended cements using t_{50} as an indicator of rate constant

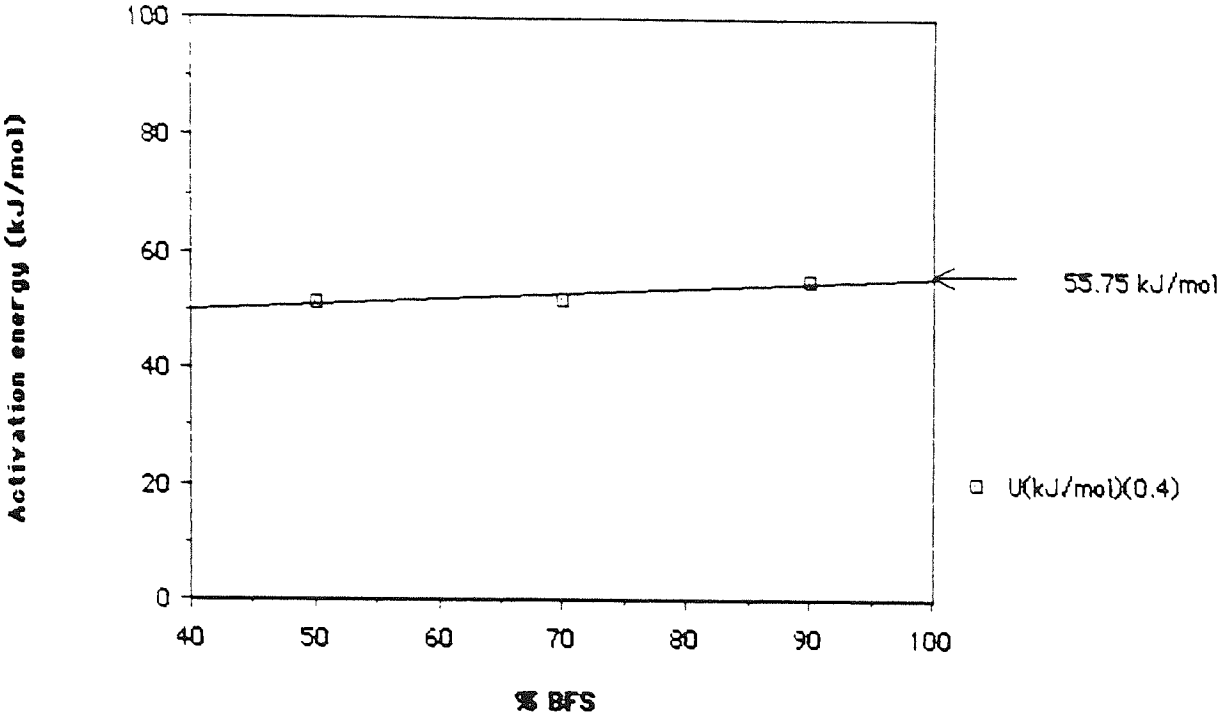

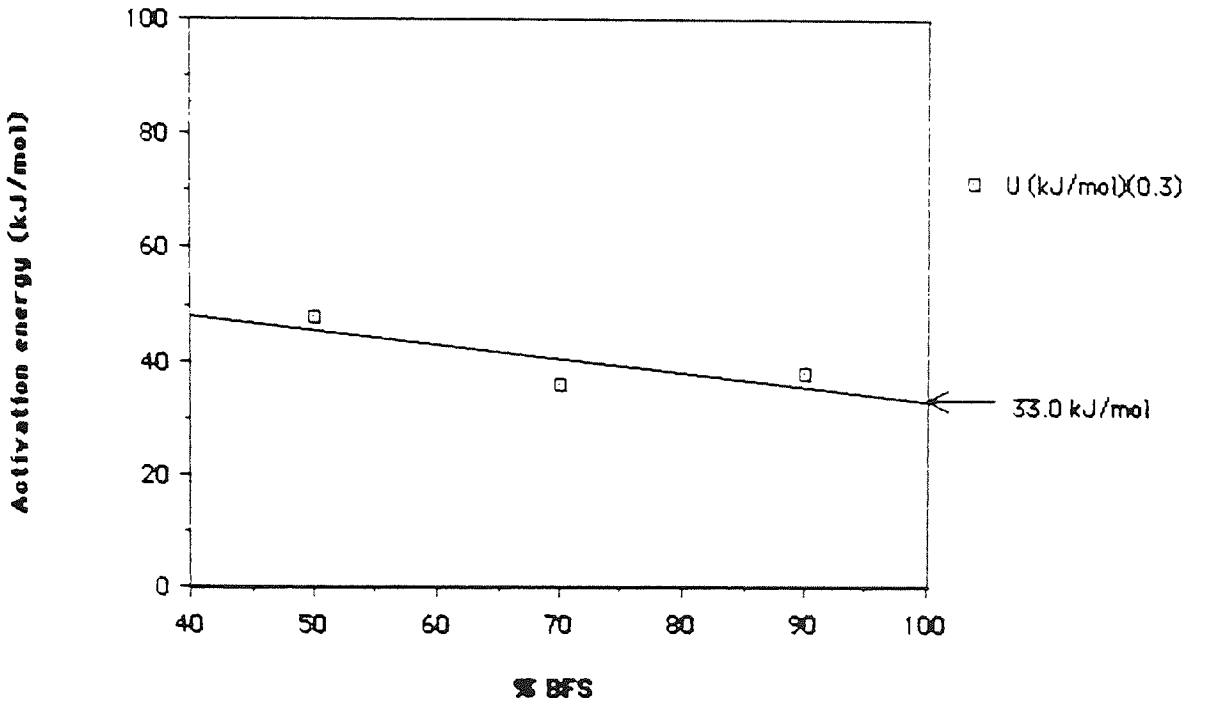

Figure 85 Variation of activation energy with slag content

4.4 Discussion.

The mechanisms of hydration described in chapter 1 give rise to numerous mathematical expressions which to a greater or lesser extent describe the hydration kinetics of cementitious materials. The "through solution" model assumes that the hydrated ions formed on the surface of a grain diffuse away and react to form tobermorite-like gel molecules. These eventually nucleate and grow, precipitate from solution and ultimately flocculate. The rate determining step in this process is nucleation and growth. By comparison the "topochemical" reaction is active at the surface of the grain where dissolution of calcium ions leaves a skeletal layer depleated in this ion, which becomes overgrown with the precipitating hydrate. In this case the rate of hydration is governed by diffusion of water through the hydrate layers and its subsequent reaction with the unhydrated core. Developments of this mechanism may be grouped together as "shrinking core" models. Whilst these models are of undoubted value in providing a mathematical description of the underlying mechanisms controlling the hydration kinetics, these mechanisms are obscured from direct observation.

Knudsen (145) showed that the detailed form of the underlying kinetics governing the reaction of a single particle, is of minor importance in a polysized material. Comparing the dominant reaction kinetics for polysized materials he found that the degree of hydration,α, was related to the rate constant,k, time of hydration,t, and the median grain size, r, in one of two ways: a function of the degree of hydration was shown to be equal to $(kt)/r$ or to $(kt)/r^2$. In keeping with previous workers he described these conditions as linear and parabolic kinetics respectively. He showed that although it was not possible to establish which of the many mechanisms was dominant in the hydration, it was a relatively simple task to determine whether the hydration curve corresponds to either of these groups. In addition to this, Knudsen noticed that the hydration curve for Portland cement closely resembled its cumulative particle size distribution curve.

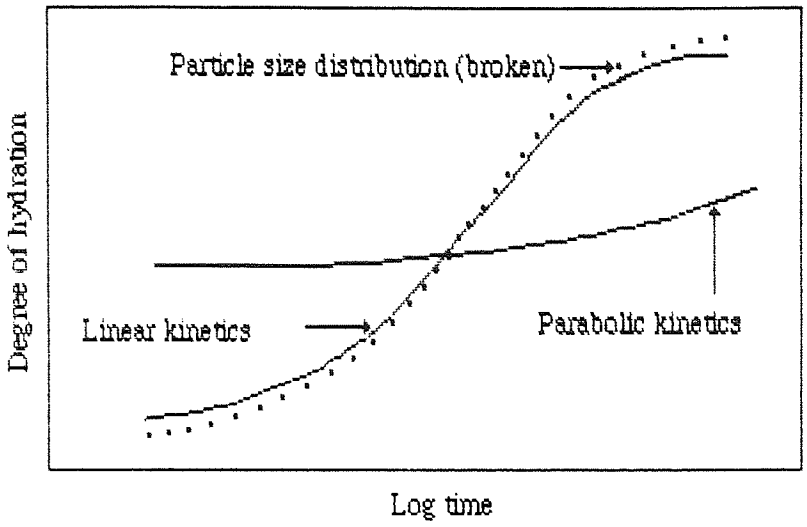

Figure 86 *Relationship between particle size distributon and kinetic mechanisms*

The agreement between these properties is good but the curves do diverge at late ages. Fitting experimental data such as compressive strength, chemical shrinkage or heat of hydration Knudsen saw a discrepancy between the predicted values expected from the particle size curve and the experimental data such that the data were lower than expected. This was identified as a second order effect of the underlying kinetics. He proposed the following equation where 'k' is the rate constant, t is the time and 'r' the median grain size.

$$-1 / \ln \alpha = kt / r \text{ (for linear kinetics)} \quad \text{.....(eqn 11)}$$

This expression yielded good agreement between theory and experimental data following the particle size distribution closely upto $\alpha = 0.7$ then taking on an apptopriately slower rate. Equation 11 does not describe an underlying mechanism but is an empirical relationship between observed and predicted values. It does however provide a useful basis for a predictive tool.

The development of these ideas into the dispersion model require

knowledge of the particle size distribution. This can be determined for a tube milled product by applying a simplified version of Rosin and Rammlers law:

$$W(r) = 1/r_0 \exp(-r/r_0) \quad \text{.....(eqn 12)}$$

or $$C(r) = 1 - \exp(-r/r_0)$$

Where 'r' is the grain size, r_0 is a constant, and C(r) is the cumulative weight distribution, which is the integrated form of W(r). This expression holds true for Portland cement down to $r \approx 1$ μm.

Assuming that the single particle kinetics obey equation 11 and that the particle size distribution can be described by equation 12, Knudsen developed the dispersion model as described by equation 1.

The application of this model to slag hydration assumes that the grain size distribution curve is of comparable shape to that of Portland cement. The model describes slag hydration as following linear kinetics with a similar hydration curve to that shown by Portland cement. The lower values of chemical shrinkage found at high levels of slag replacement are thought to be a function of the lower porosity of slag cements than that of OPC. The method has enabled an estimation to be made of the activation energies governing this system and has proved to be within acceptable levels of accuracy.

In conclusion, it would seem that given a sufficiently large number of samples to ensure variations between them are minimised, the chemical shrinkage method and dispersion model provide a useful method of predicting the degree of advancement of Portland-blastfurnace slag cement hydration.

Chapter 5
Solid Phase Analysis

5.1 Nuclear Magnetic Resonance Spectrometry

5.1.1 Introduction

The theory of the ^{29}Si 'MAS NMR' method has been discussed in chapter two and hence needs little elaboration here. Although NMR spectroscopy has been developed over some forty years (149 & 150) it is only with recent advances in instrumental design and experimental technique that solid state ^{29}Si investigations have yielded high resolution spectra. Correspondingly, a rapid expansion in the literature has followed in recent years and a number of publications now exist which review current developments. Of particular relevance are the Royal Society of Chemistry (annual) specialist periodical reports on NMR which publish a chapter on ^{29}Si spectrometry. The publishers 'Springer-Verlag' produce a book series "NMR: Basic Principles and Progress", occasional volumes of which (154 & 155) concentrate on ^{29}Si studies. Physical aspects of the technique are covered thoroughly by the journals "Progress in Nuclear Magnetic Resonance Spectroscopy" and the "Journal of Magnetic Resonance".

The bulk of the literature concerning specific applications is distributed throughout the scientific press. As a result of one particularly important paper, however, it is relatively easy to locate work in related fields from the citations index. Lippmaa *et. al.* (156) published pioneering work in 1980 examining synthetic minerals and excellent natural specimens from the Tallin University collection. This one publication was cited by over 150 authors in the subsequent five years. The work concentrated on the characterization of the spectra of the ^{29}Si resonance from minerals of high purity and known crystallography. This resulted in the terminology used subsequently to describe the degree of polymerization of silicon atoms according to the number of bridging oxygens to which they are

bonded(*c.f.* figure 4, Regourd (26,27) and Dron (29)):

Table5 *Speciation of silicon as resolved by NMR*

			Chemical Shift 'σ' (ppm wrt TMS)
Q_0	Single tetrahedra	Tektosilicates	-66.0 → -73.5
Q_1	Chain end group	Inosilicates (end)	-77.9 → -82.6
Q_2	Chain middle group	Inosilicates (mid)	-86.3 → -87.5
Q_3	Branching site		-90.4 → -99.3
Q_4	Cross-linking group		-107.4 → -109.9

Thus, Qn ($0 \leq n \leq 4$) Where n is the number of bridging oxygen atoms.

This work has been developed by Magi *et al* (157) in the DDR using mineral specimens of exceptional purity from the collection of the Humbolt University, Berlin. Due to the recent development of the method, there are relatively few text books devoted exclusively to this method. Shaw (158) has published a thorough volume on Fourrier transform NMR theory and applications, whilst McWhinnie's contribution to Berry and Vaughn's book (159) gives a rigorous account of NMR (&ESR) to chemical bonding in mineral chemistry. The current definitive text on "Solid State NMR for Chemists" (Fyfe,160) covers both theory and applications and has a section covering ^{29}Si spectrometry. Richards has edited a Royal Society publication (161) on aspects of NMR theory to which many of the leaders in the field have contributed.

The NMR method is very sensitive to the local electronic environment surrounding non-zero spin nuclei (162). ^{29}Si NMR has proven particularly useful in investigations of aqueous (163), crystalline (164), glassy (165) and molten silicate structures. Because both silicate speciation and geometric factors (such as Si - O - Si bond angles (167) and Si-O bond lengths (168)) influence ^{29}Si chemical shifts, NMR is particularly useful in characterizing local aspects of silicate structure.

A number of authors have concentrated on glass structure and the effects of network modifying cations. Generally, glass spectra are less well resolved than those of crystalline systems due to the slight variations in bond angles occurring in the glassy state. Regourd (26,27) reviews the structural chemistry of slag glasses (see chapter two) and her conclusions about the rôle of specific cations as network modifiers are confirmed by work on other glass systems. Schneider (165) reports the presence of two distinct silicate species in alkaline earth silicate glasses suggesting that even in the glassy state the number of bridging oxygen atoms between silicate tetrahedra does vary.

Silicate mineralogy work with NMR has covered a wide range of species but of particular interest are studies on tobermorite as an analogue of calcium silicate hydrate structure. Work at the Pennsylvania State University has resulted in a number of recent publications using both ^{29}Si and ^{27}Al spectra (166 &167) confirming the tetrahedral co-ordinations of aluminium. This is a renewal of interest in tobermorites due to their irreversible cation exchange capacity for Co^{2+} and Ni^{2+} (in place of Ca^{2+}). Cement mineralogy has also received some attention (168-171) and the polymorphism of dicalcium silicate has been successfully investigated by Grimmer *et al* (172).

5.1.2 Experimental work

Studies of slag hydration using NMR were incorporated in this work as no published material reports the use of the NMR technique on these materials. Lippmaa (173), Barnes (174) and Clayden (175-177) followed the hydration of tricalcium silicate by ^{29}Si MASNMR and it was decided that an initial study would involve characterizing the raw materials and following this relatively simple system (C_3S) in the light of previous work.

Figure 87 shows the typical spectrum obtained from a relatively short observation of the resonance from unhydrated slag. The doublet centred around

-72ppm (Q_0) is probably a statistical phenomenon, as the obsevation time for this spectrum was low (1262 scans) which resulted in a noisy signal. The constructions drawn on figure 87 show how the estimation of peak height (both from the measurement datum and above the level of background noise) have been made, in order to calculate the band-width (full width at half maximum; "FWHM") and signal to noise ratio. Note also in this figure the two smaller resonances above and below the Q_0 peak at approximately -10 and -140 ppm. These are the spin side bands (harmonics) of the Q_0 peak and are not of any practical value in interpretation of the sample structure.

Subsequent examinations of both BFS and OPC were made using greatly increased observation times in order to improve the signal to noise ratio of the spectra and these results are shown in figure 88. As expected, the unhydrated BFS shows a broader spectrum than that of OPC and is otherwise a symmetrical peak approximating to a Gaussian distribution. The OPC, by comparison, shows a well defined, sharp peak centered on -72.5 ppm displaying a well defined doublet at -71.7 ppm and -73.4ppm. This is probably the result of differing degrees of shielding experienced by silicon nuclei associated with C_3S and C_2S. The interesting feature of this figure is the difference in band-width between the OPC and BFS spectra. The Portland cement Q_0 resonance has a FWHM of only 6 ppm whilst the corresponding bandwidth for blast furnace slag is some 16 ppm. This is to be expected from the variation of bond angles displayed by a glassy medium and will obviously limit the interpretation of spectra from high slag replacement specimens.

The next set of experiments were on pure C_3S samples prepared by Lambert (178) and hydrated for one and twenty four hours. The 0.5 w:s ratio paste was mixed by hand and hydrated at 25°C, the hydration being stopped by "quenching" in proan-2-ol. The dispersed product was then filtered and washed with alcohol before being vacuum dried and then passed through a 53µm sieve. Magnetic separation showed that no recoverable ferromagnetic material was present in

these samples hence no further sample preparation was deemed necessary.

Figure 89 shows the spectra obtained from this experiment demonstrating the diminution of the Q_0 tektosilicates in favor of the chain end (Q_1) and ultimately chain middle (Q_2) member inosilcate resonances. These findings are in good agreement with those of Clayden *et al* (174) and show the growth of silicate chain structures from isolated tetrahedra, as a function of hydration time.

As the decay time following each magnetic pulse is several seconds, a relaxation time of ten seconds is required between individual pulses. To maintain an acceptable signal to noise ratio, a large number of pulses are required for each sample (for example figure 88 represents 65868, 70200 and 150000 pulses or approximately two weeks of observation). The demand for machine time for ^{29}Si observations on slag glasses is therefore very high and hence further experiments had to be planned with great care. It was decided to limit samples to two compositions hydrated at the same temperature and water : solids ratio, one of high slag content, the other low. The samples were hydrated at 0.4 w:s ratio at 25°C and contained 50% and 90% BFS respectively.

Figures 90 to 93 show the progress of hydration with time for the 90% BFS samples. It can be seen that the spectra show essentially little change within the first four hours which correspond approximately to the duration of the dormant period. As hydration progresses, the presence of higher order polymeric species is detectedand at fourteen days (figure 92) the distribution of ^{29}Si is approximately equal between chain end (Q_1) and chain middle (Q_2) sites sites. After one year's hydration, the (Q_0) resonance has diminished to a minor peak and the inosilicates (Q_0 & Q_1) dominate the spectrum.

Figures 94 to 97 show the same sequence for the 50% samples . As with the 90% sample, the dormant period is marked by little modification of the unhydrated spectrum.

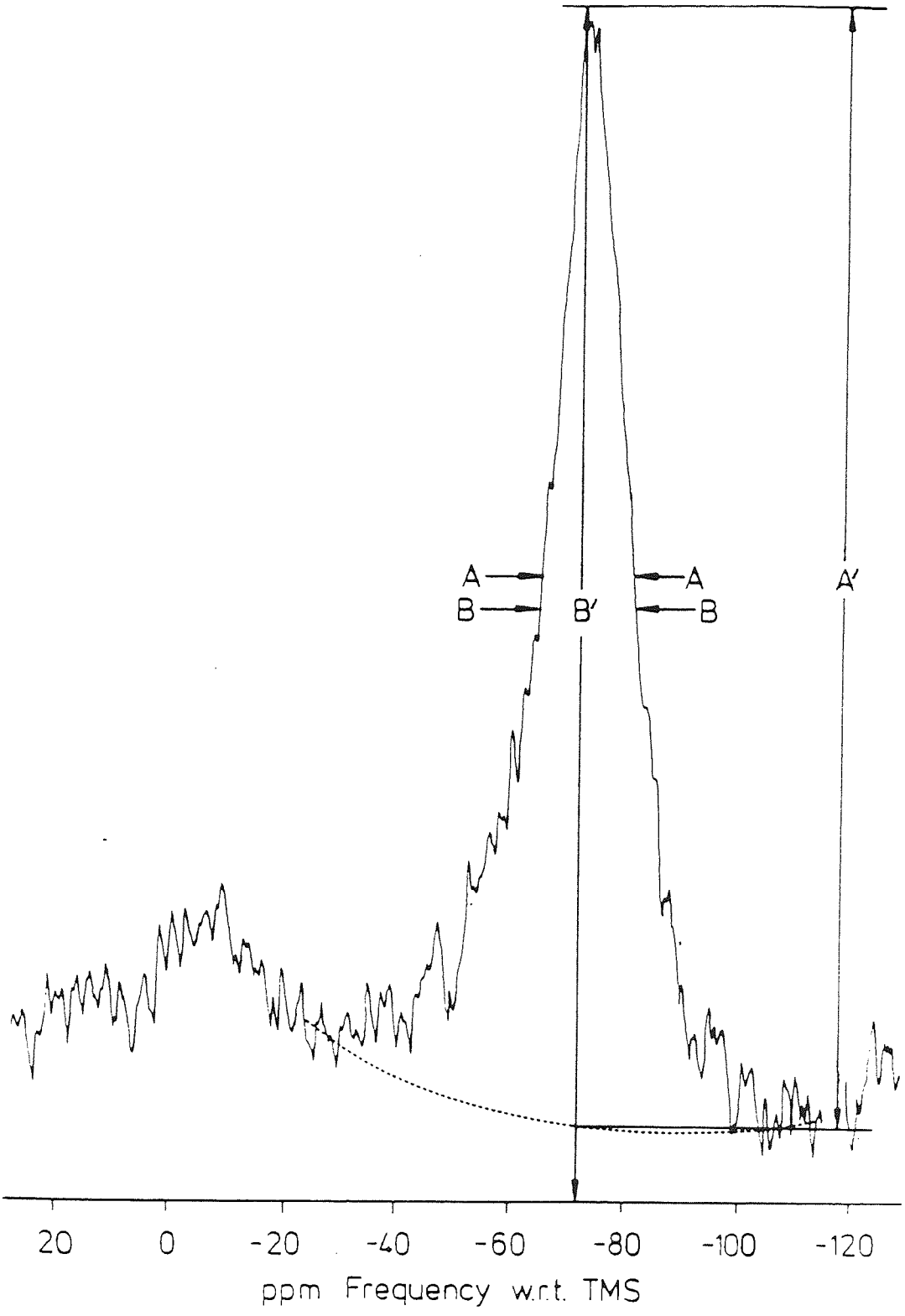

Figure87 ^{29}Si MASNMR spectrum of unhydrated blastfurnace slag

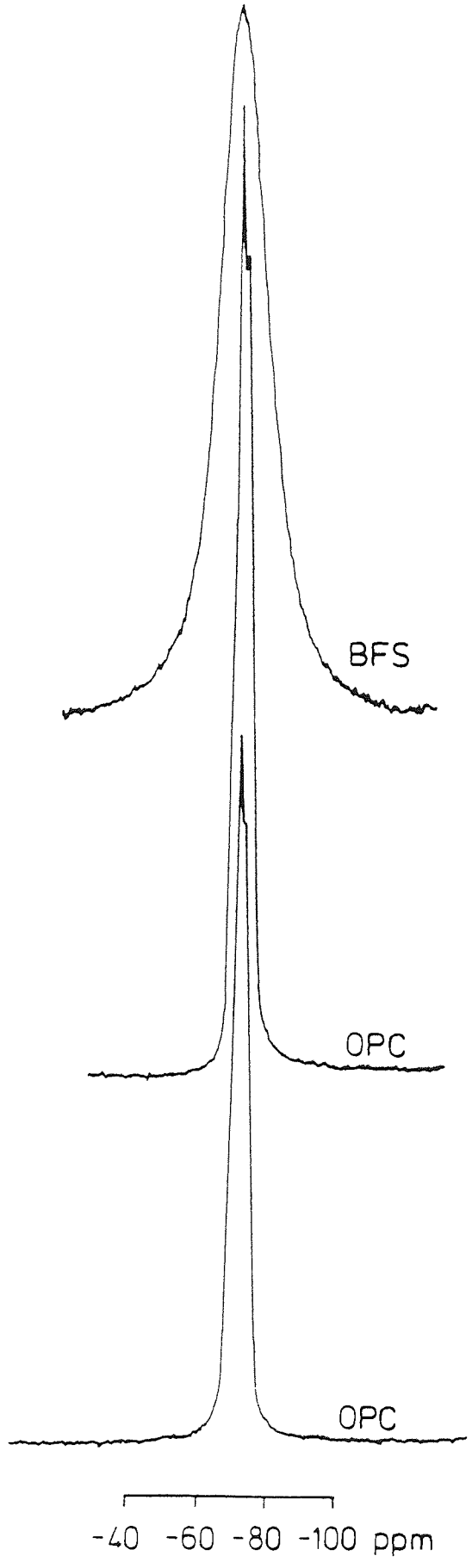

Figure88 Q_4 resonances for unhydrated materials

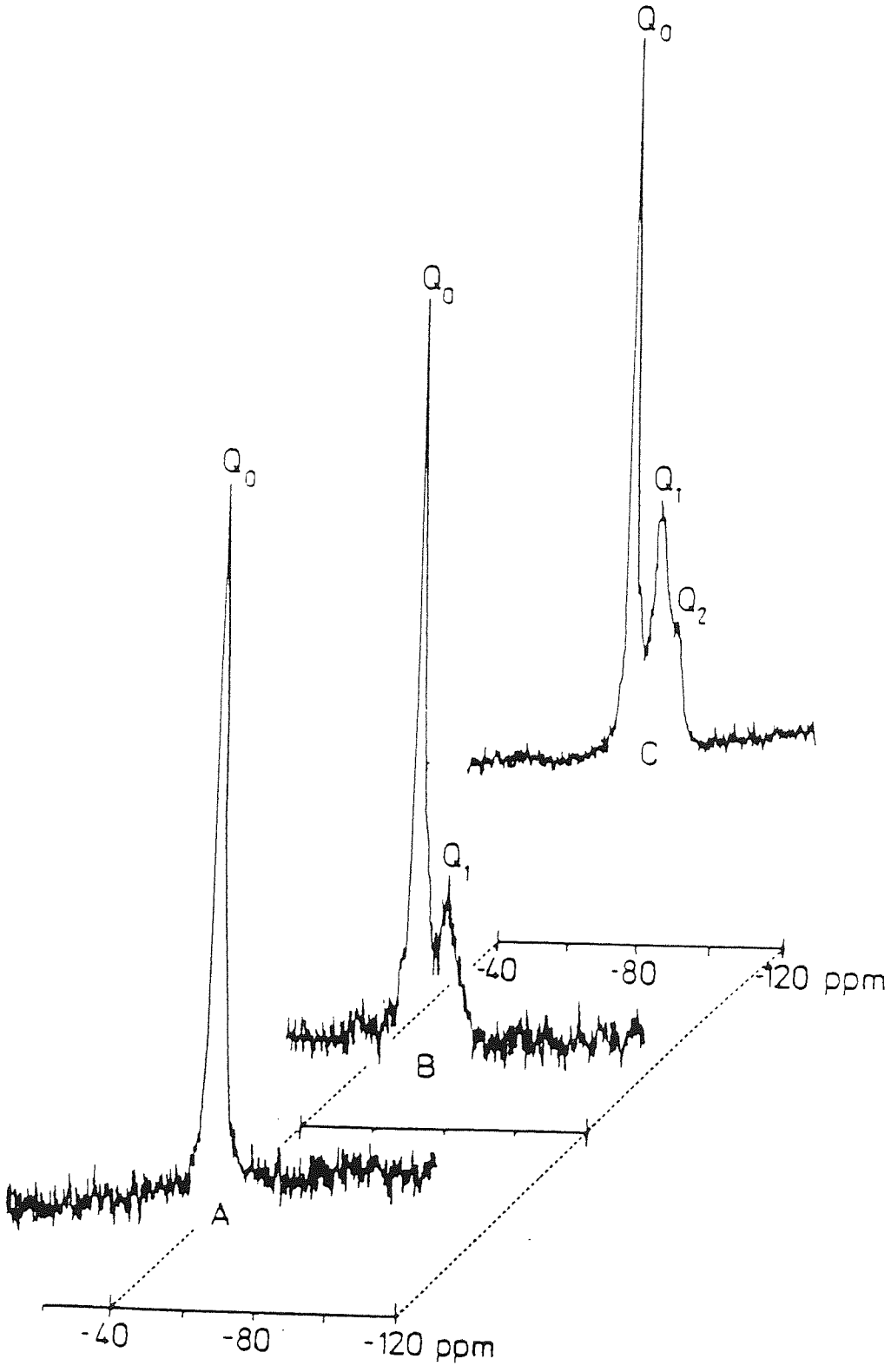

Figure89 Hydration of tricalcium silicate followed by ^{29}Si NMR

A = Unhydrated sample B = 1 hour hydration C = 24 hours hydration

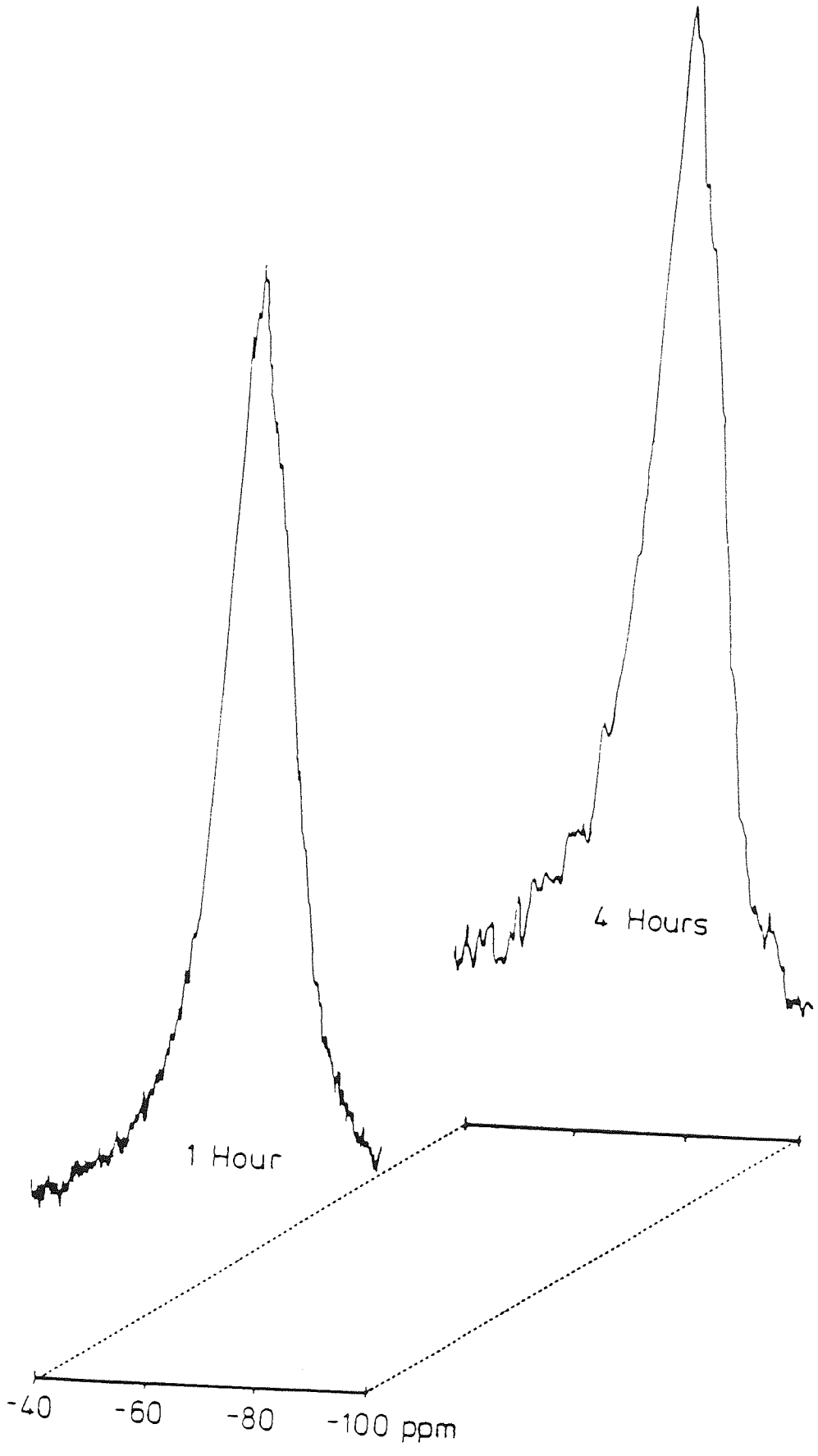

Figure 90 Early age hydration of 90% BFS / 10% OPC

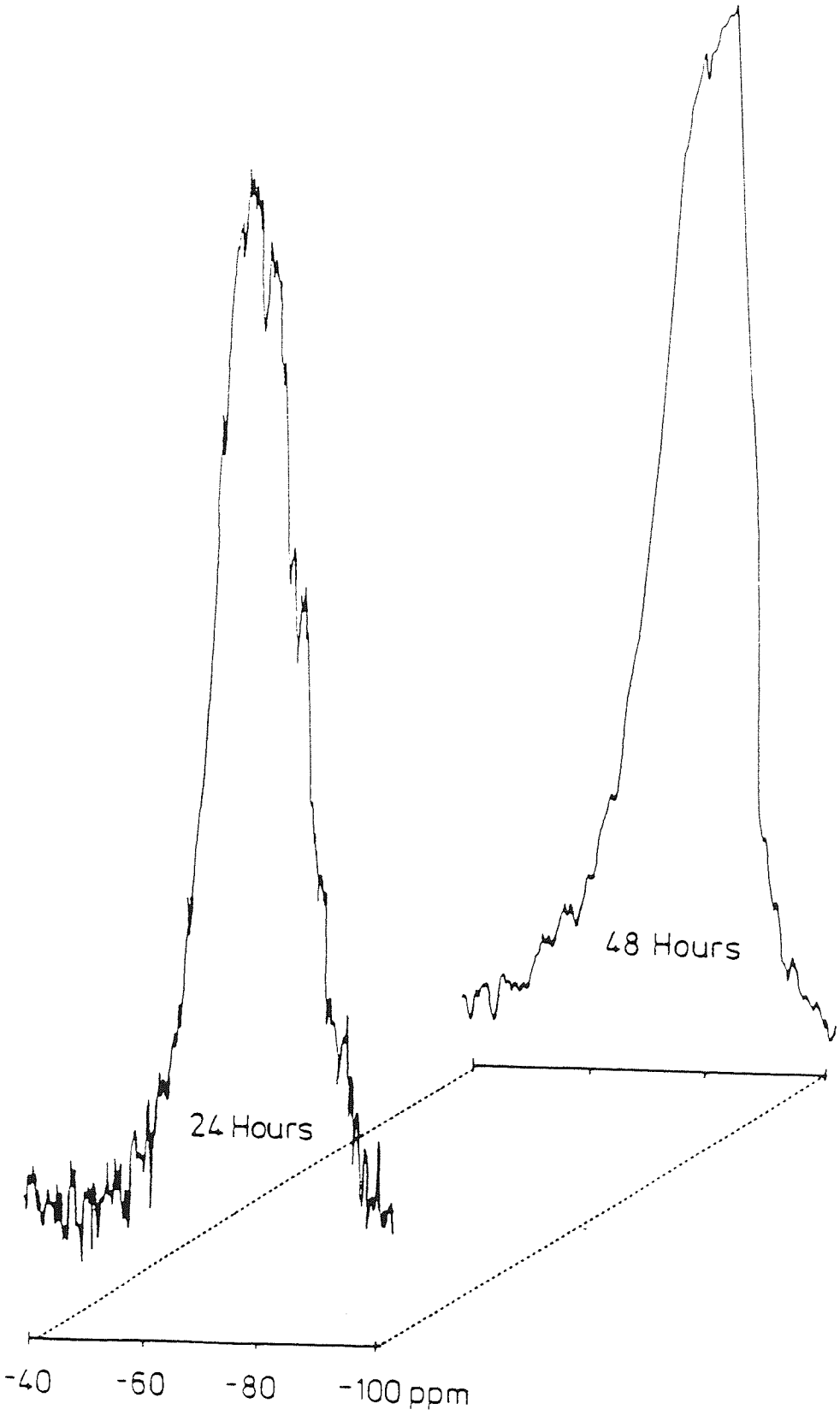

Figure91 Hydration of 90% BFS / 10% OPC pastes

Figure 92 Hydration of 90% BFS / 10% OPC pastes after 14 days

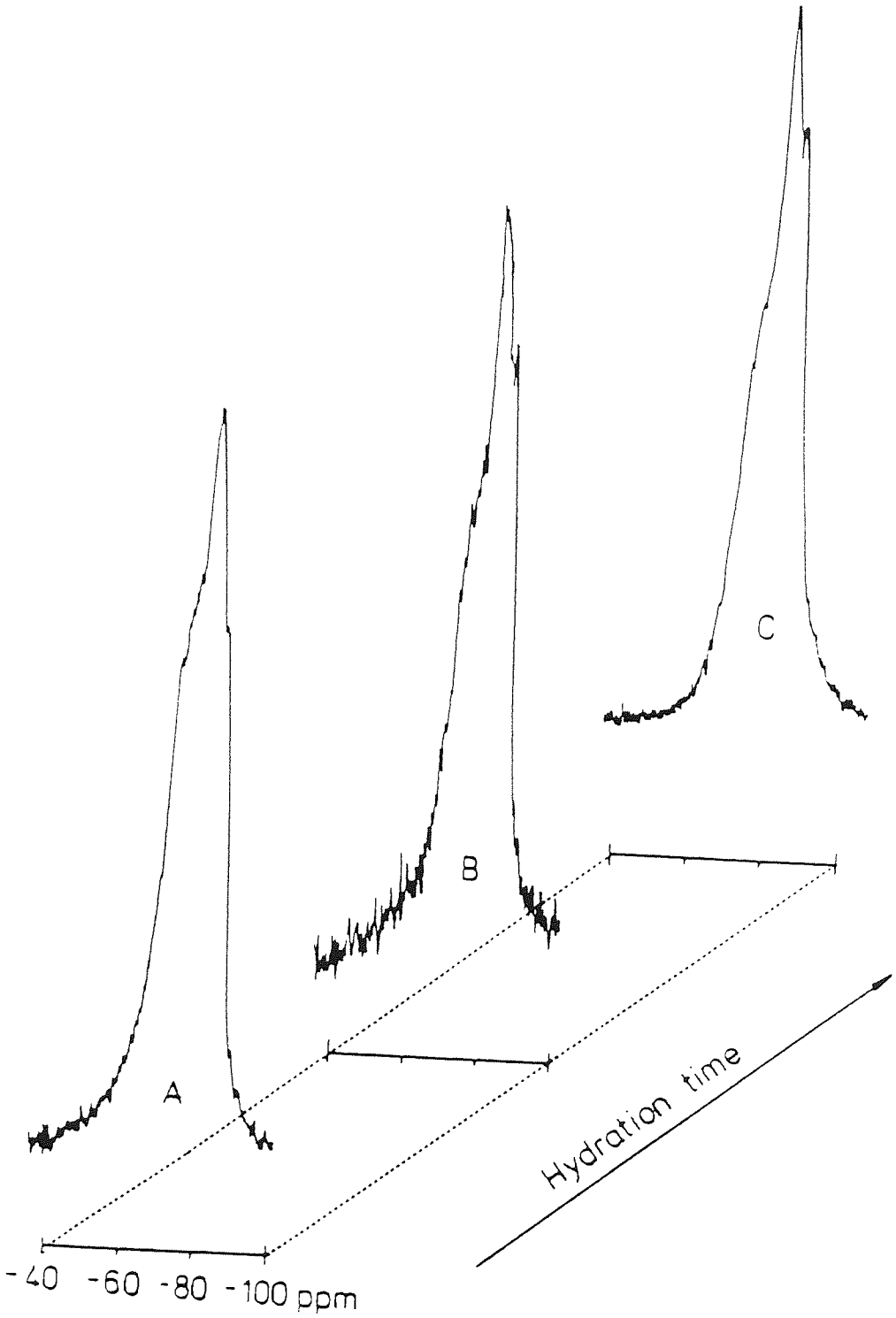

Figure 93 Late age hydration of 90% BFS / 10% OPC pastes

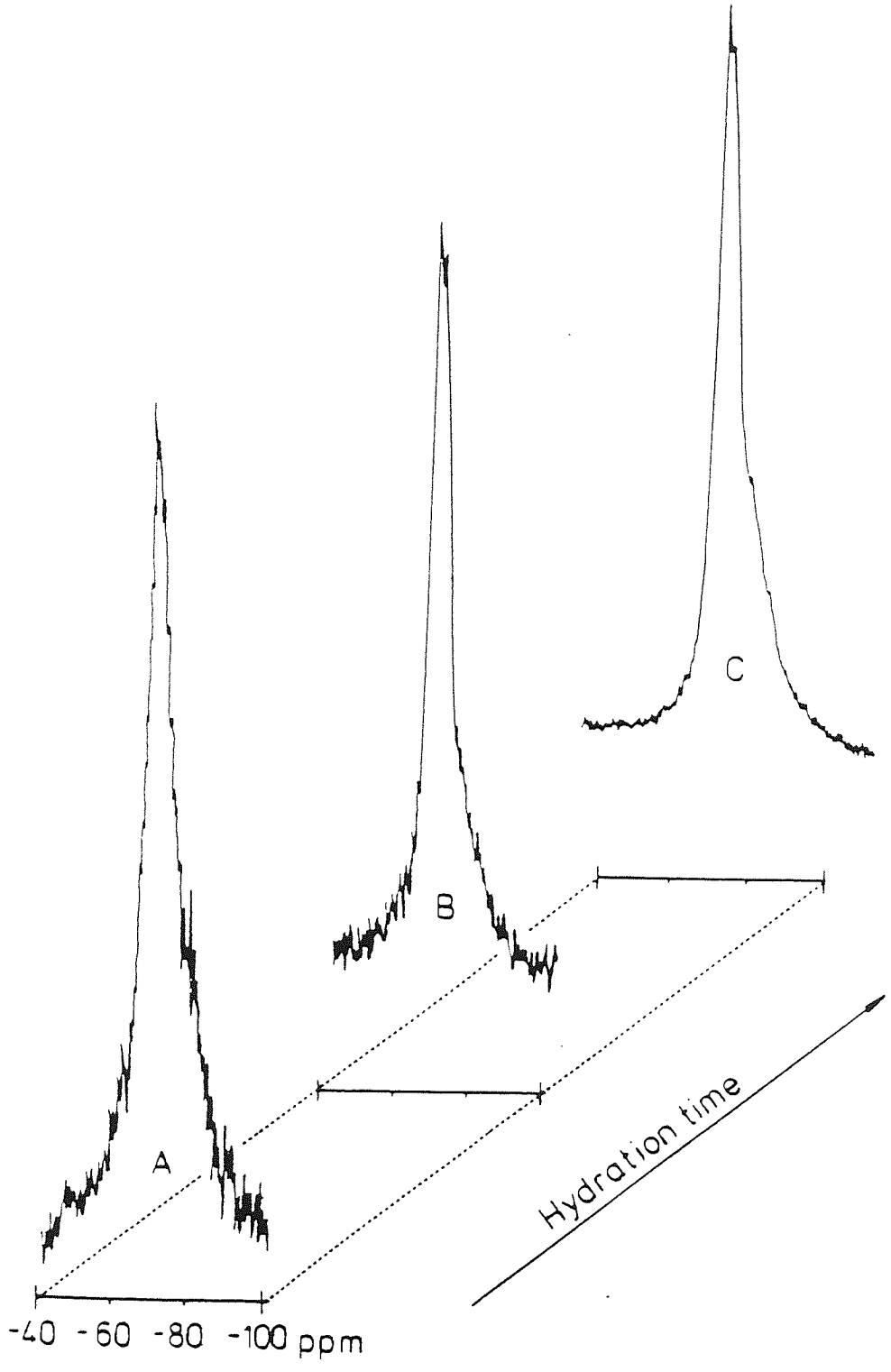

Figure 94 Early age hydration of 50% BFS / 50% OPC paste

A = 30 minutes B = 1 hour hydration C = 4 hours hydration

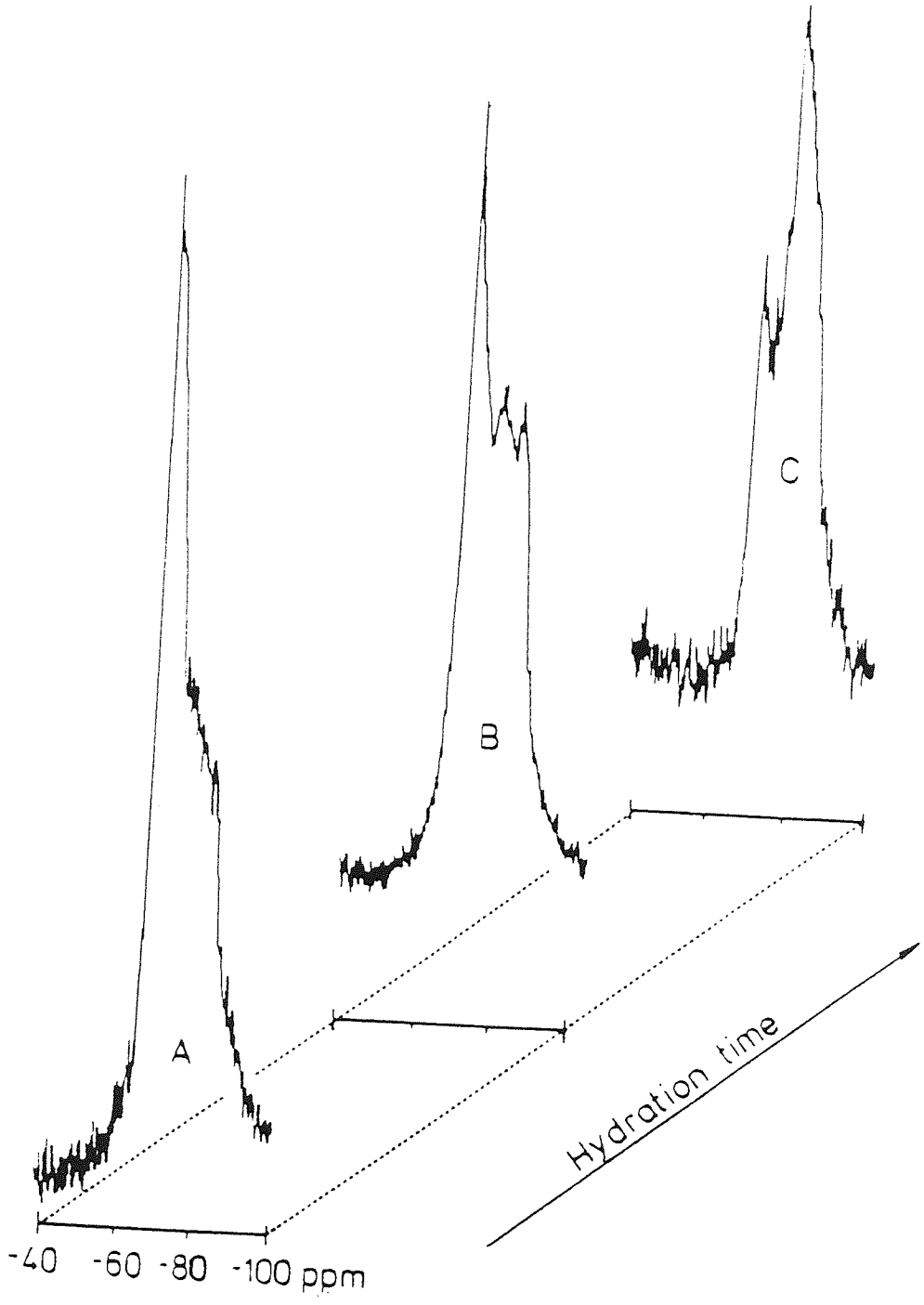

Figure 95 Hydration of 50% BFS / 50% OPC paste

A = 12 hours B = 52.5 hours hydration C = 7 days hydration

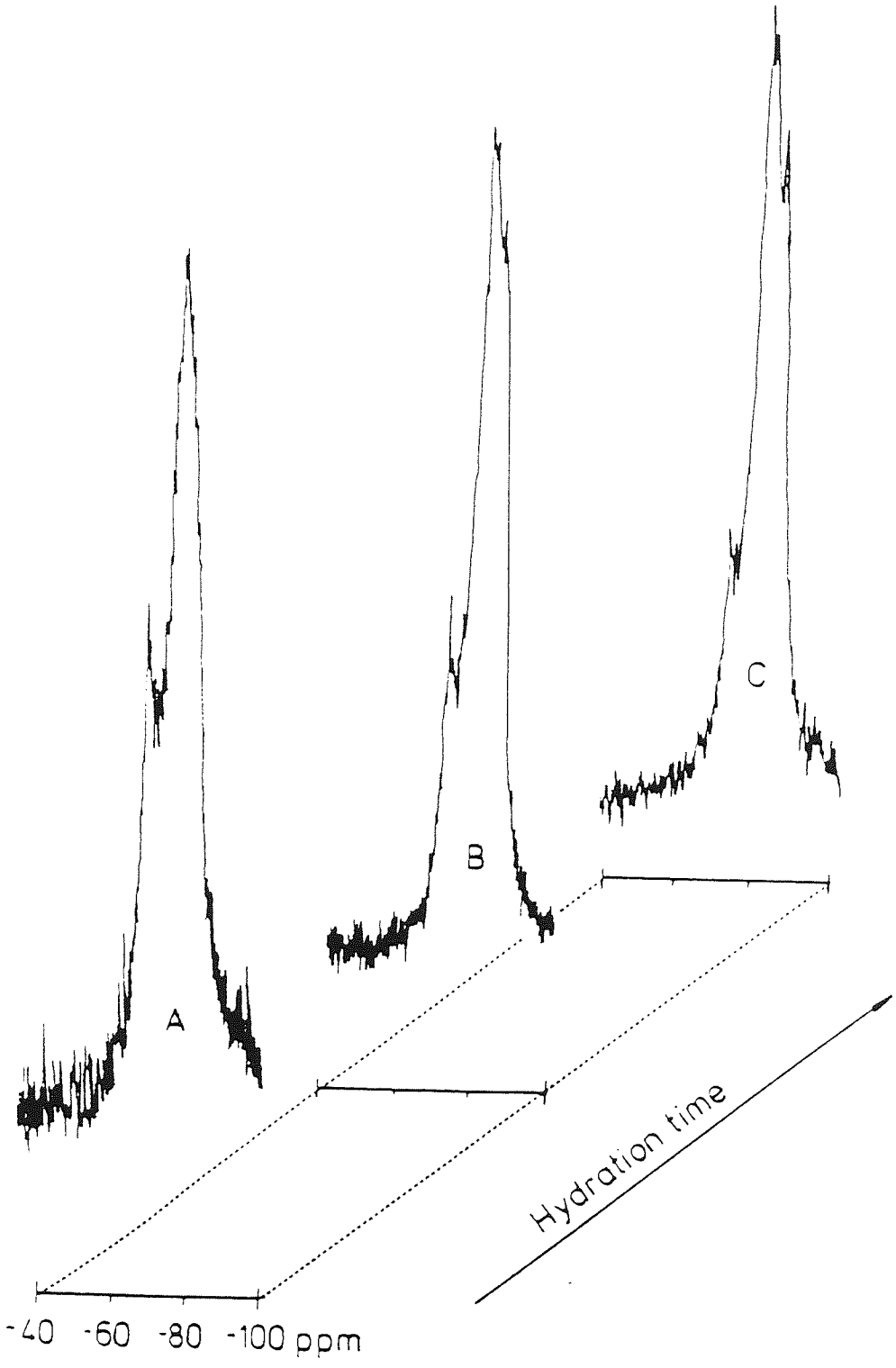

Figure 96 Hydration of 50% BFS / 50% OPC paste

A = 21 days B = 75 days hydration C = 6 months hydration

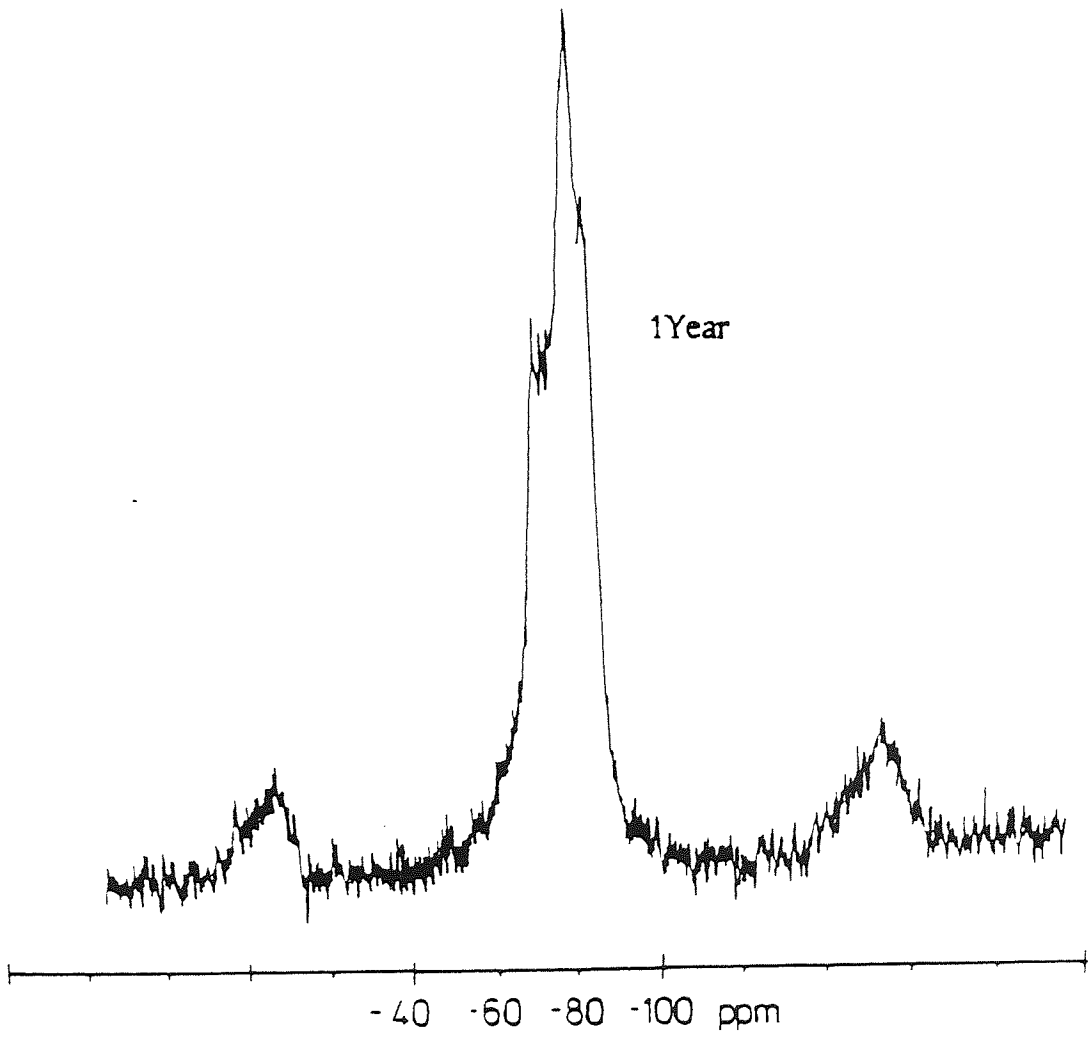

Figure 97 Hydration of 50% BFS / 50% OPC paste

Figure 95 clearly shows the three silicon resonances and figure 97 demonstrates that even after one year's hydration there remains a measurable fraction of unhydrated material in this sample. This is interpreted as the relict grains of OPC (dominantly C_2S), the cores of which may take many years to hydrate completely.

5.1.3 Quantitative interpretation of results

Initial studies comparing the normalized peak heights are shown in figures 98 and 99 below. Whilst these give a first approximation of the effects of hydration on this system, it is important to realize that little confidence can be ascribed to peak height measurements for the following reasons: First, the assumption that the distribution of counts about the mode is constant in all samples may be erroneous. As hydration progresses, bonding may occur between silicon and aluminium via an oxygen bridge which would result in a shift of resonant frequency, thus translating a peak along the chemical shift (σ) axis.

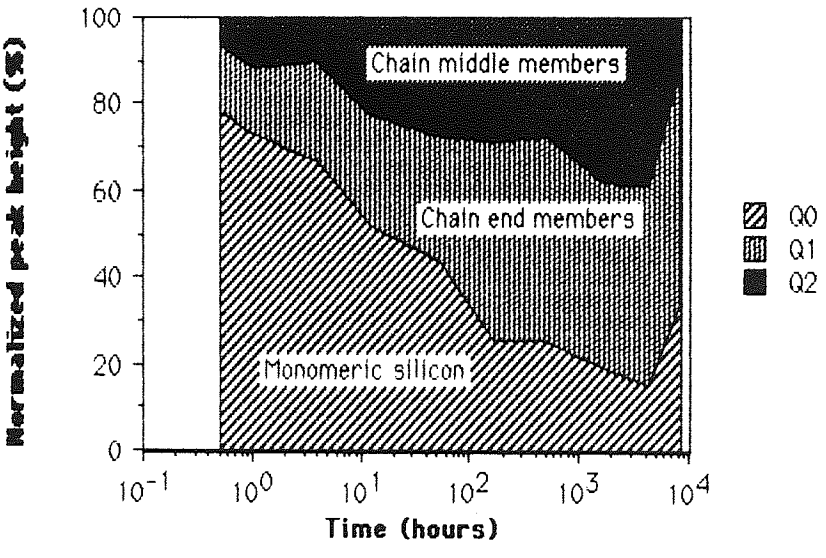

Figure 98 Distribution of silicon environments as a function of time (estimated by peak height measurement) for 50% BFS paste.

Secondly, a peak of small magnitude occurring as a shoulder on a larger resonance, may be disregarded amongst the noise signal. With appropriate caution however, these figures give an immediate visual impression of the distribution of the silicon nuclei between the possible environments.

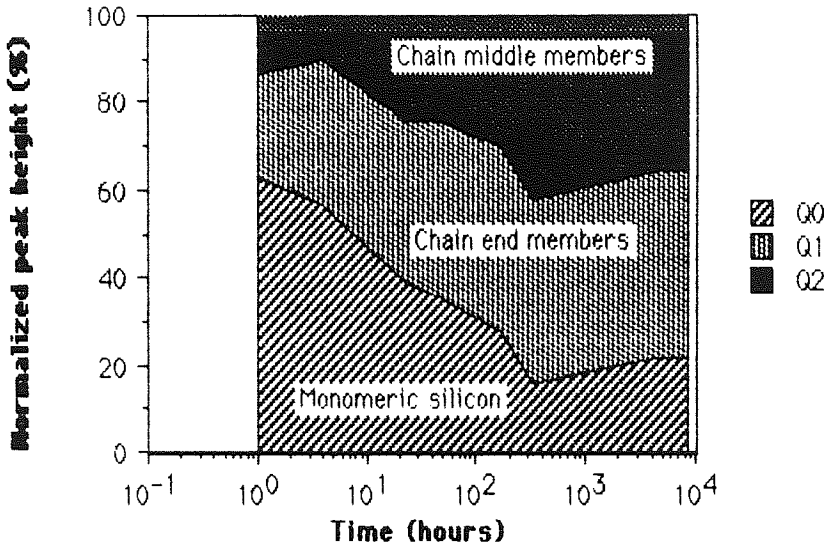

Figure 99 *Distribution of silicon environments as a function of time (estimated by peak height measurement) for 90% BFS paste.*

It must be stressed however, that the use of peak height measurement under estimates smaller peaks areas, thus a better method of distinguishing the individual resonances must be employed. If the assumptions are made that the peaks are symmetrical and the degree of overlap between them is limited, it is possible to estimate the peak areas as shown in figure 100 below. The peak area of the Q_0 resonance is assumed to be symmetrical about a vertical line (A-A) which bisectsthe line denoting the "full width at half maximum" . The estimated area (B) for the resonance Q_0, was then subtracted from the area bounded by the other two peaks. A similar method was then employed to subtract the Q_2 resonance from the remainder, thus estimating Q_1 by difference.

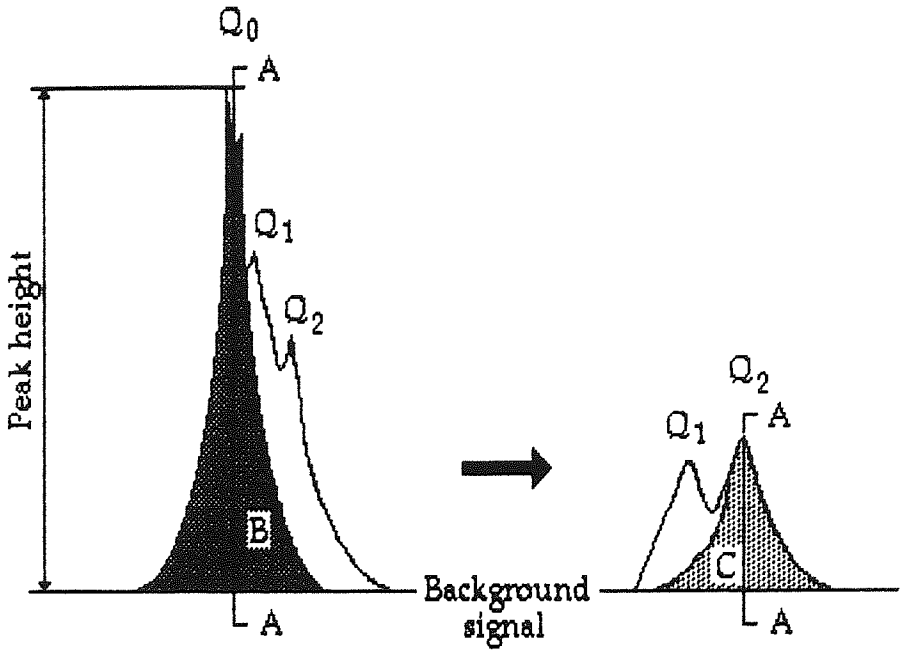

Figure 100 *Treatment of NMR spectra in order to resolve individual peak areas*

It is highly probable that the degree of overlap between the peaks is such that Q_1 is under estimated by this approach but conversely, the use of peak height measurements, leads to over-estimation of large peaks.

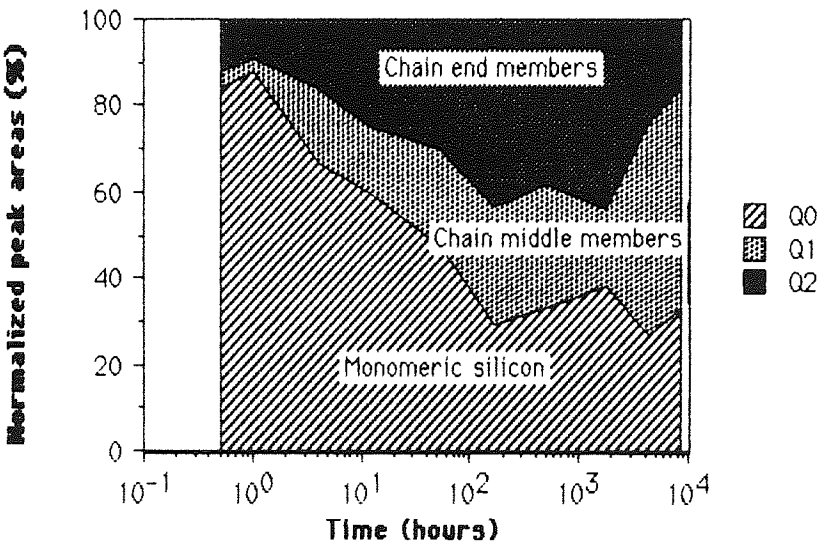

Figure 101 *Distribution of silicon atoms in 50% BFS samples as determined by peak area measurement*

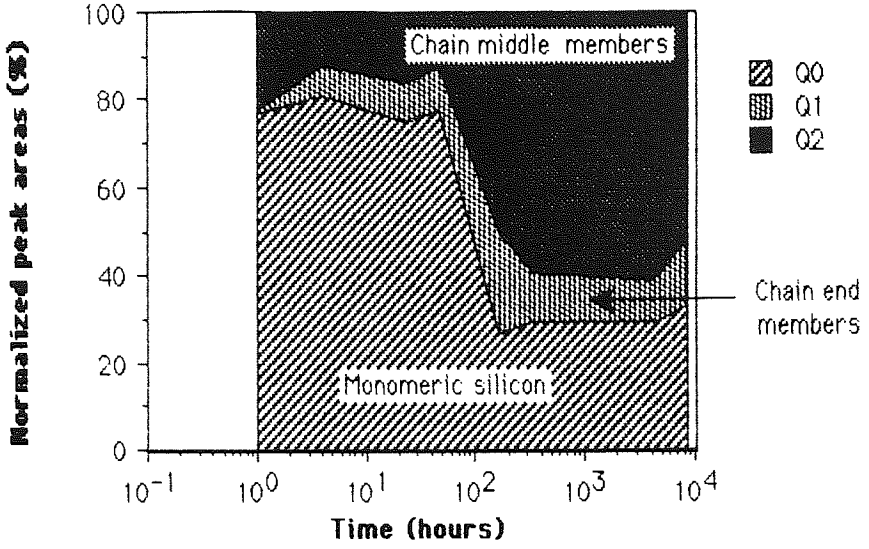

Figure 102 *Distribution of silicon atoms in 50% BFS samples as determined by peak area measurement*

As the Q_1 resonance is dominant after the first few days hydration, it is possible to assign upper and lower limits to the estimation of the relative populations of silicon atoms in the three chemical environments. Figures 101 & 102 are essentially similar diagrams to figures 98 & 99 and show the changing distribution of silicon atoms during hydration as determined by peak area measurements. These under-estimations of the Q_1 populations emphasize the rapid hydration experienced by the system during the first few days hydration.

Justnes (179) has produced two empirical relationships for the degree of hydration and average chain length of silicate polymers in the Portland cement system. The degree of hydration expression is strictly applicable to C_2S + C_3S in OPC, but in applying them to this system we must assume that the hydration of BFS and OPC are similar processes and that the system is dominated by the silicate - water reaction. That the former is true, is suggested by the kinetic analysis presented in the previous chapters but the validity of the latter can only

be estimated stoichiometrically. In terms of oxide weight percent composition the two samples are compared below:

90% BFS =	35.01% SiO_2	+	9.77% Al_2O_3	$SiO_2 : Al_2O_3 = 3.58$
10% BFS =	28.25% SiO_2	+	8.45% Al_2O_3	$SiO_2 : Al_2O_3 = 3.34$

It can be seen that in both compositions there is a similar excess of silica and consequently, although the degree of Al - O - Si bonding is unknown, we may assume that even in fully hydrated samples, the degree of this type of bonding will not vary by more than ± 5% between the two compositions. It is reasonable to assume that this effect is small as the spectra do not show a Q_4 (chain crossing) resonance.

In the light of the above discussion the expressions are:

$$\text{Degree of hydration } (\%) = 1 - \frac{I_{(Q_0)}}{I^0_{(Q_0)}} \cdot 100\% \qquad \text{.....(equation 13)}$$

and

$$\text{Average chain length} = \frac{I_{(Q_1)} + I_{(Q_2)}}{I_{(Q_1)} / 2} \qquad \text{.....(equation 14)}$$

Where: $I_{(Q_n)}$ = Intensity of peak corresponding to resonance '(Q_n)'

and $I^0_{(Q_0)}$ = original intensity of peak 'Q_0' at time t = 0

It is important to note that the estimation of chain length does not account for the occurrence of cyclical structures comprising exclusively Q_1 units. Cyclosilicates are found in Nature (beryl, tourmaline etc.) but no reference is apparent describing under what conditions the structures in this system would "chase their tails".

Figures 103 and 104 show the variation of degree of hydration with time for the two compositions. It is interesting to note that although the apparent rates of hydration are somewhat different, both systems contain approximately 20% of unreacted silicon after one year's hydration. This cannot be readily ascribed to relict grains of OPC as the cement content of the two systems is so very different. Evidently, a similar amount of silicon hydration occurs over this time-scale irrespective of the starting composition. At one years hydration, it is reasonable to expect that little free water would be available in either system. This limited availability of water (the principal source of hydroxyl ions and hence bridging oxygen atoms) may account for the low rate of hydration at these ages but does not satisfactorily explain the absolute amounts of monomeric silicon remaining. It would appear that after a long (>6 months) period of hydration the amount of unreacted silicon in the system is determined by the original silicon content of the samples and not on the mineralogical source of the element. The two compositions are shown above to contain a similar amount of silicon (32±4% SiO_2) and appear to hydrate to approximately the same amount at late ages.

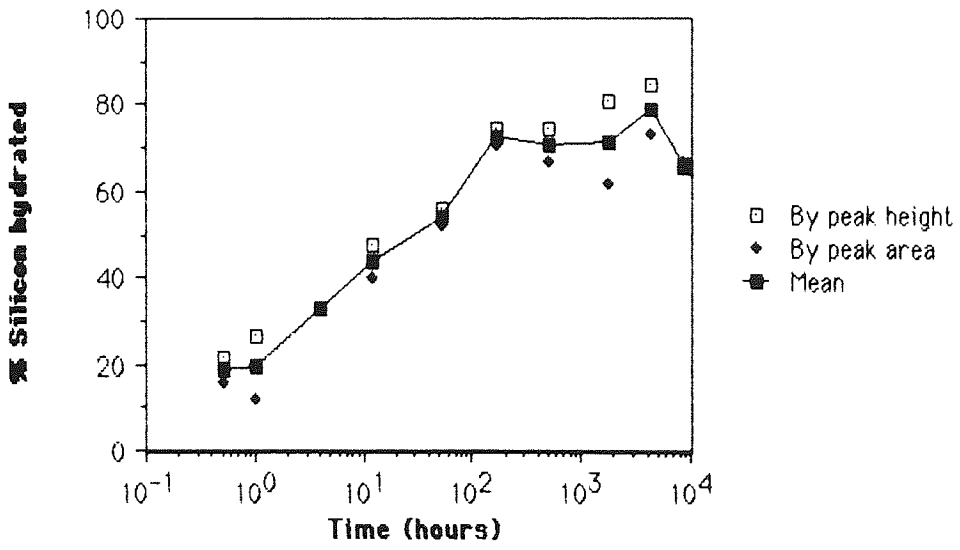

Figure 103 *Hydration of silicon in 50% BFS cement paste at 25°C*

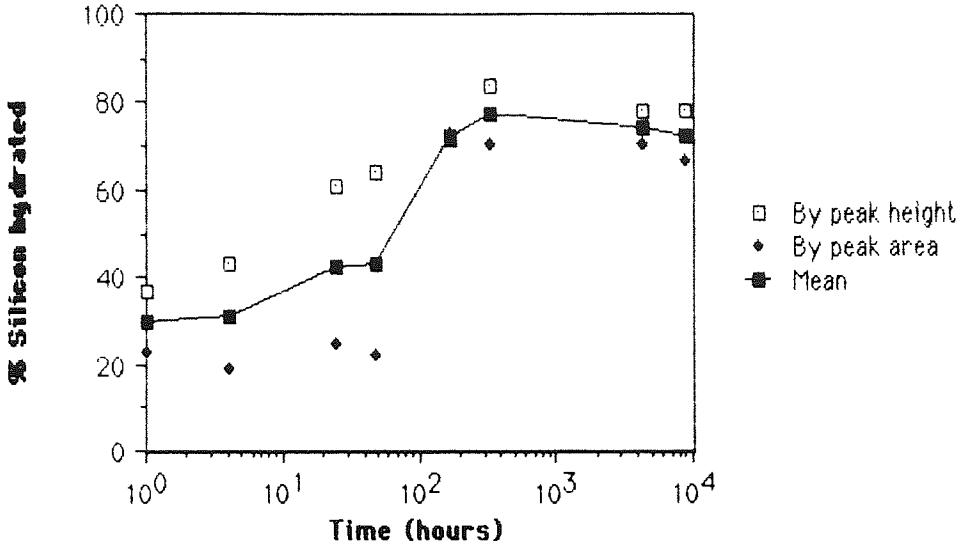

Figure 104 *Hydration of silicon in 90% BFS cement paste at 25°C*

Given the information concerning speciation of silicon atoms within the hydration products, it is possible to calculate the apparent chain lengths from equation 14. Figures 105 and 106 show the variation of chain length with reaction time for the two compositions studied. As expected from the overlapping spectra, the high slag replacement (90%) samples show the greatest variation of apparent chain length. This demonstrates the inadequacies of the two methods for estimating the population distributions. As shown in the figures below, values obtained from peak heights produce a maximum estimation of chain length, whilst those derived from peak area measurements provide the lower limit.

If the peaks are well defined, such as the 50% BFS samples or those spectra obtained at relatively late ages, the two estimations are of a similar magnitude (± 0.5 silicon units or better). At early ages however, significant variation between the two estimations is seen and little confidence can be ascribed to these values. The late age chain length of approximately 3 silicon atoms to each chain in the hydrates is in good agreement with the results obtained by workers studying Portland cement systems (178 & 179) where a chain length of 2.7 units is reported.

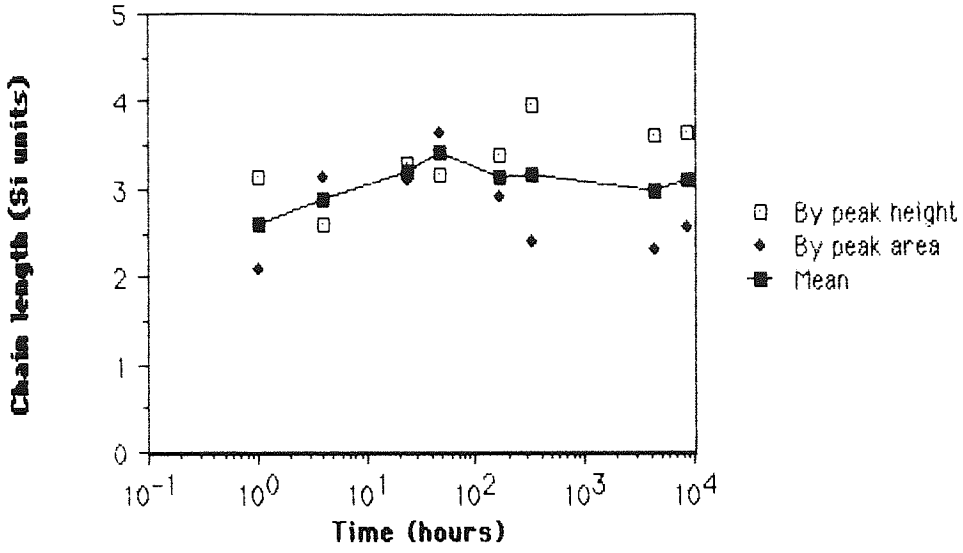

Figure 105 Variation of chain length with reaction time for the 50% BFS system

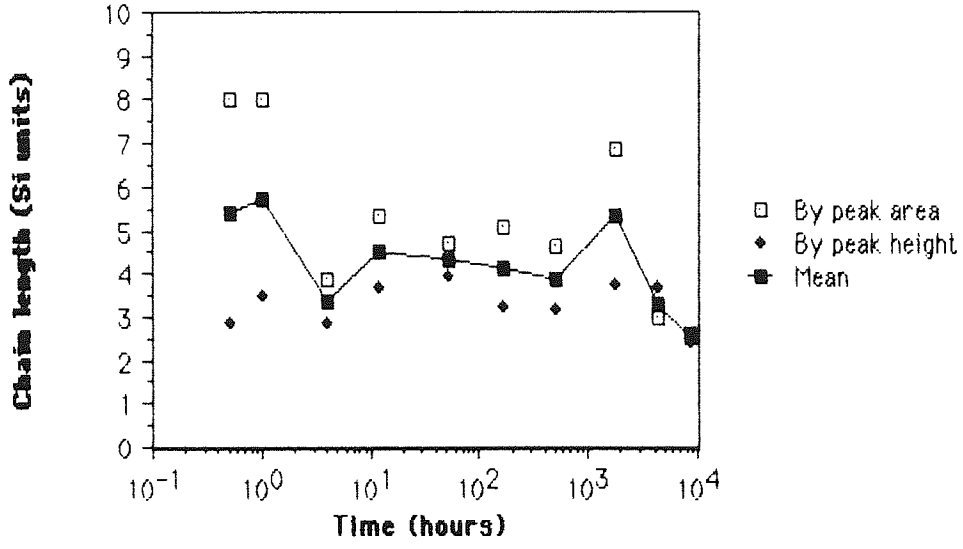

Figure 106 Variation of chain length with reaction time for the 90% BFS system

5.1.4 Conclusions

The NMR method has proved useful in estimating both the degree of hydration and average chain length in the hydrating system. It is evident that at high slag content, the degree of overlap of the peaks is also high, which

consequently limits the technique to investigations of late-age properties. In both the 50% and 90% slag replacement systems, 20% of the original silicon remains un-poylmerized after one year and that which has reacted forms chain structures approximately three units in length.

The incorporation of glassy materials into a cement system necessitates a large number of pulses to obtain useful data and consequently careful choice of late-age or lower slag content samples is seen as expedient. No evidence of chain branching or crossing was shown in these samples, but at very late ages this may occur.

5.2 Selective dissolution

A method which allows the measurement of the absolute rate of consumption of blastfurnace slag during cement hydration has been sought by numerous workers as reviewed by Luke and Glasser (103 & 104) and by Demoulian (102). The method used here is that reported by the former and is a controlled pH dissolution with EDTA (ethylene diamine tetra acetic acid) and triethanolamine of the unhydrated slag remaining in the dried, powdered and sieved (<53μm) pastes. The method is described by the authors thus:

"A stock solution was prepared containing 0.05M EDTA in 0.1M Na_2CO_3. 125ml of the stock solution was placed in a conical flask with 12.5 ml of a 1:1 triethanolamine : water mixture and 125 ml of distilled water. The pH was adjusted to 11.6 ± 0.1 with 1.0M NaOH. An accurately weighed sample of approximately 0.25g was added slowly with shaking to prevent formation of agglomerates"*"The solution was shaken for 30 minutes then filtered through a Gooch No.4 crucible with GF/A filter paper"*", dried at 105°C and tared beforehand. The residue was washed seven times with c.20ml methanol. After washing, the crucible with residue was dried to a constant weight."

*The slight variations from this method are as follows:

1) When adding the sample, the flask was stood in an ultrasonic bath to agitate the solids and prevent the formation of agglomerates.

2) A sintered crucible was used in place of a Gooch crucible with a disc of GF/A paper placed over the frit. The very fine grain size of this material requires careful filtering to recover the solids and glass fiber - asbestos media offer a very tightly packed filter structure which is chemically very robust.

5.2.1 Experimental results

The results below are presented in terms of percentage slag reacted at a given time and are thus 100% - the percentage remaining. Calculation of the results was made assuming that in pastes younger than 28 days, the amount of OPC recovered would be 6% of the original, those between 28 and 180 days would recover 5.5% OPC and the later age samples would recover 4.8% of the original OPC content. These are to within a percent or so, justifiable from control experiments on Portland cement, the results of which are listed below:

The following percentage of material was not dissolved by this method:

Unhydrated OPC	7.22%
OPC after 28 days hydration	5.94%
OPC after 180 days hydration	4.87%
(Mean	6.01%)

A similar correction must be made for dissolution of unhydrated slag removed by this method. Dissolution of GGBFS by this method allowed recovery of 94.94 % of the solids, therefore this correction was applied in proportion to the original slag content. Since these experiments were started, the original authors have published a modified method (104) which uses dimethylformamide (1% w/w) in the dissolution mixture which acts as a hold-back carrier for silicate. This prevents precipitation of silica which they observe increases the residual weight

in an unpredictable way. (They have reduced the sample standard deviation for the dissolution of OPC from 2.10 to 0.52 % wt.).

Figures 106 to 108 show the results from the dissolution of slag pastes at 25°C:

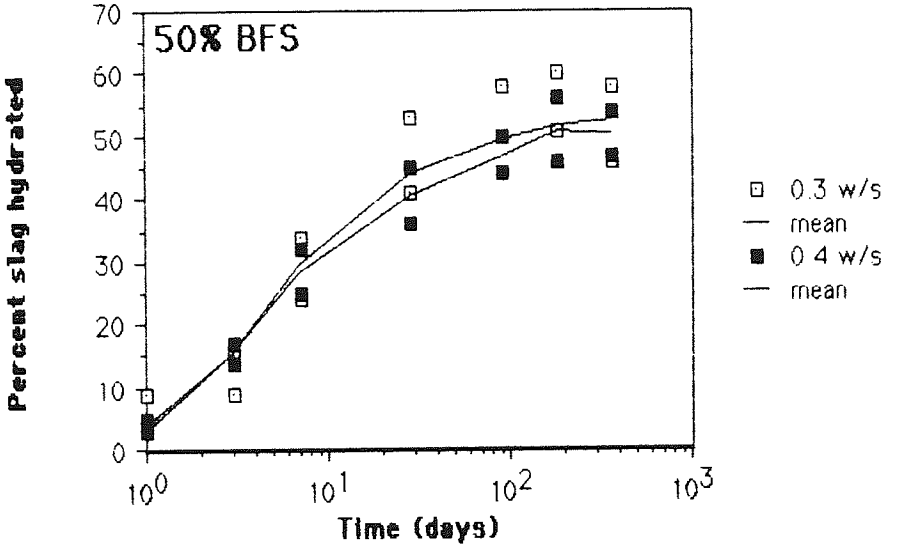

Figure106 Selective dissolution of 50% BFS pastes at 25°C

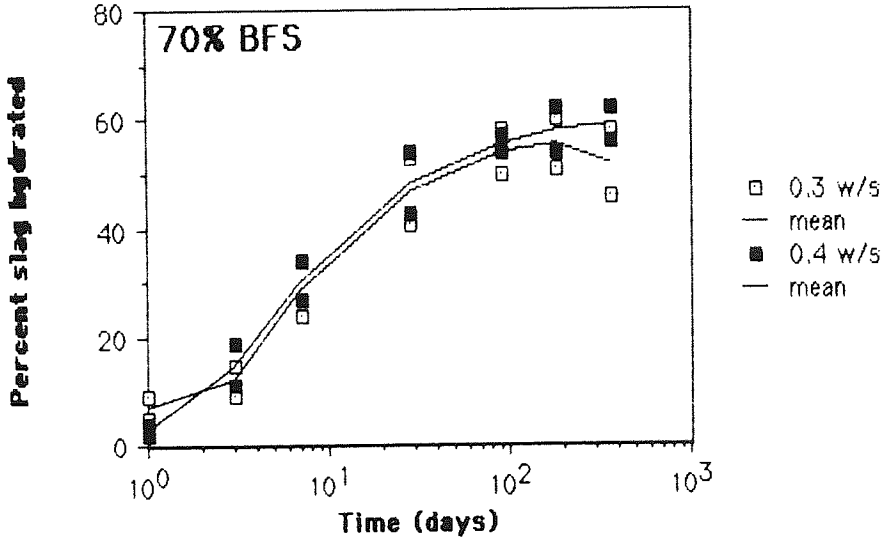

Figure107 Selective dissolution of 70% BFS pastes at 25°C

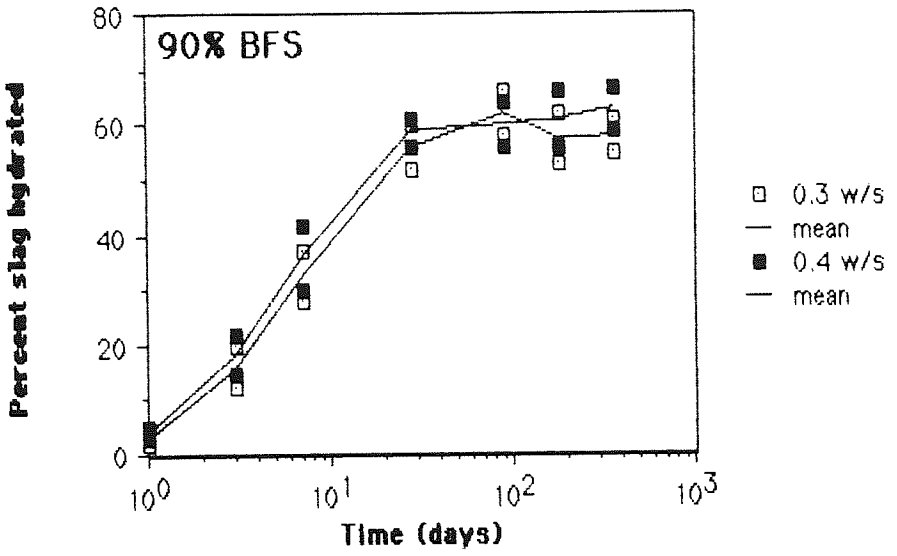

Figure108 *Selective dissolution of 90% BFS pastes at 25°C*

The figures show that the rate of dissolution is marginally higher for the 0.4 as compared with the 0.3 w/solids ratio, although there is a reasonable degree of overlap between the results. As can be seen from the figures, the variance of the data is approximately ±6% (which is greater than the difference between the two water/solids ratio samples). That the rate of reaction is greater for the higher water/solids ratio is in agreement with the results of earlier chapters although this finding has not been reported elsewhere using the selective dissolution method.

An increase in slag content increases the rate of slag consumption which is to be expected as the slag constitutes more of the hydrating system. It is important to see these results as the rate of slag consumption in pastes of varying slag content, and not as a measure of the overall hydration of the system. Whilst earlier experiments show the rate of hydration to decrease with slag content, the selective dissolution method shows that, within the limits examined, the higher slag content pastes, consume their slag at a greater rate. These two findings are not incompatible when considered in this way

The elevated temperature experiments were done on 0.4 w/s samples as the effect of water content on slag hydration has been shown to be slight.

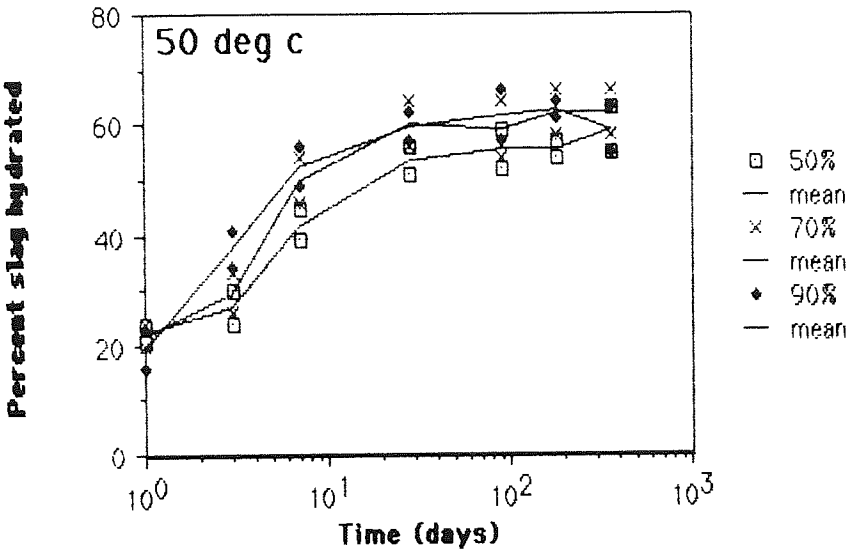

Figure 109 Selective dissolution of slag cements at 50°C

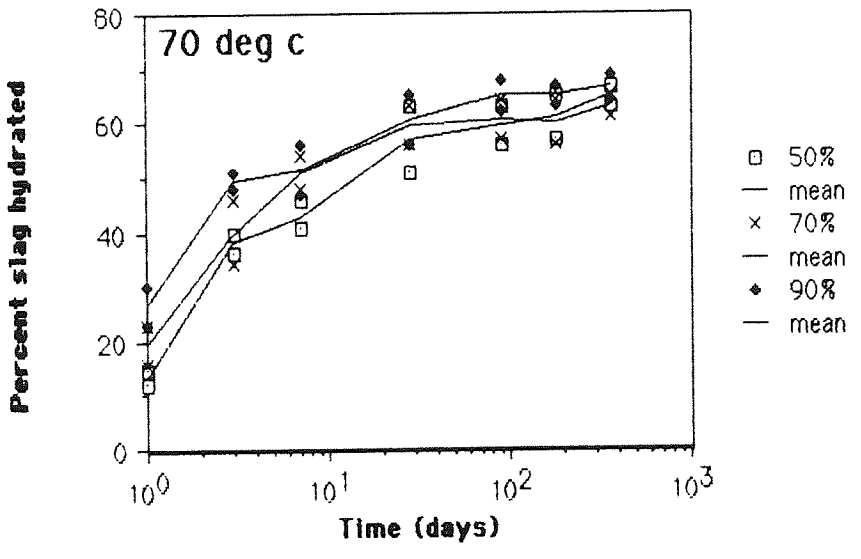

Figure 110 Selective dissolution of slag cements at 70°C

The effect of temperature is shown in figures 109 & 110 above. In comparison with those hydrated at 25°C, there are notable differences, principally shown at very early ages. At the lowest temperature, very little hydration had

occurred within the first twenty four hours. For all compositions at 50°C, this figure had risen to 20±4% and at 70°C, between 12 and 30% of the initial slag had hydrated.

5.2.2 Discussion.

The selective dissolution method allows a direct measurement of the amount of unreacted slag remaining in the cement paste. The rate of consumption appears to be related to the amount of slag present in the original paste such that the slag fraction in a high slag paste reacts proportionally faster than that in a paste of lower slag content. The effect of water to solids ratio is slight such that a change from 0.3 to 0.4 results in a change of rate of slag hydration which is less than the variations shown by the data. It can be seen however that the rate of slag consumption does increase with increasing water content.

The most significant finding of these results is that the plateau value for the total percentage of slag reacted is similar for all compositions and temperatures. This was surprising, as it may be reasonably expected that the hydration of the high temperature pastes would be in a much greater state of advancement than those at 25°C. Figure 111 shows the plateau value for the blended pastes which was calculated as the mean of the 90 to 360 day values. At 50% slag content this would appear to be the case but as the percentage of slag increases the maximum percentage hydration of the material converges at around 50%. It must be remembered that the variance of the data is around ±6% but taking this into account the effect is not insignificant.

Little published data is available on the rate of slag hydration but figure 112 combines that from the references cited above and that of Hinrichs and Odler (126) which employs thermal analysis to the same end. No attempt has been made to distinguish between compositions in this figure although the range is from 30 to 70% slag all at 0.5 w/s over a range of temperatures from 20 to 25°C.

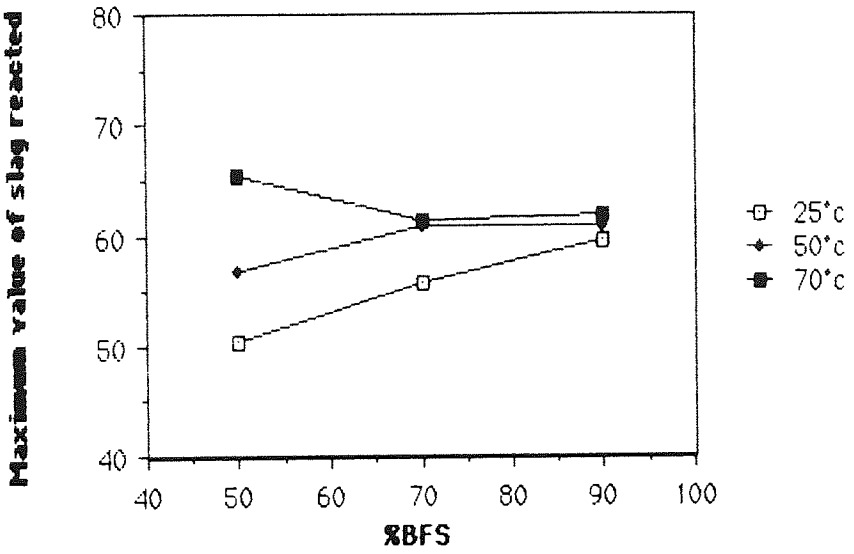

Figure111 *Maximum value of slag hydration*

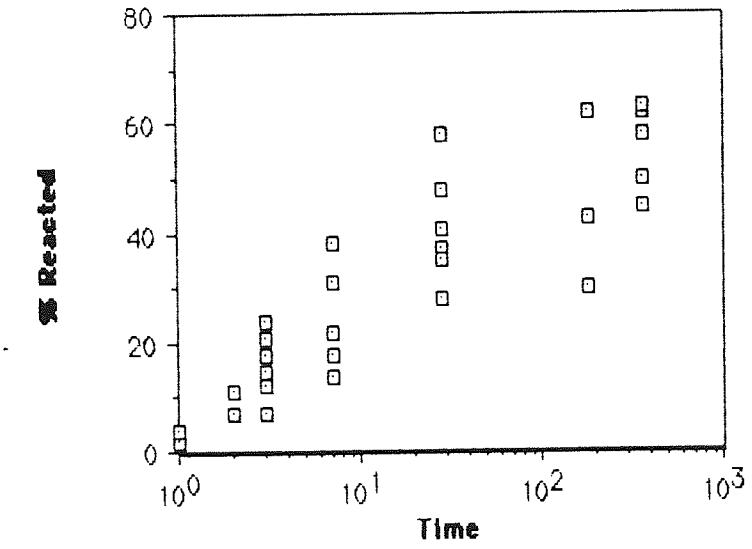

Figure 112 *Published results from workers cited in text*

The range of values reported above at 25°c tend towards the higher end of this range although they are in broad agreement with other workers. Two publications by Luke and Glasser (103 & 104) report an anomalous stage in slag hydration which has not been reported elsewhere (or seen in the results above).

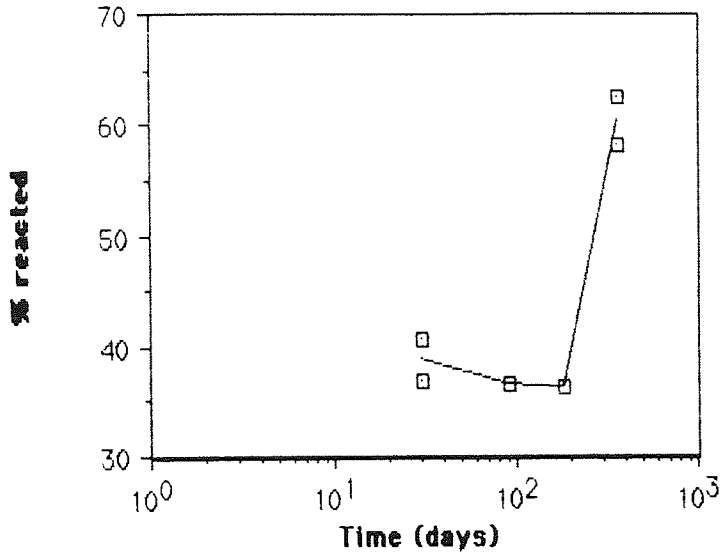

Figure113 *Anomalous hydration reaction reported by Luke & Glasser (103 &104)*

They observe that for a 30% slag at 20°c, approximately 40% of the slag had reacted after one month and that this condition was maintained for pastes up to six months old. Between six months and one year however, a further 20% of the slag was seen to hydrate in a renewed period of activity. They report:

"Eventually, however, some sequence of events, not yet elucidated, results in a renewed burst of hydration; it is suggested that the breakdown of a protective layer is responsible. This allows pore solution to reach unreacted slag, which initiates a further burst of hydration and a repetition of the cycle".

It is interesting to note that no other workers have reported this behaviour but Luke and Glasser have reported the phenomenon more than once.

In conclusion, this method permits a direct measurement of the rate of slag hydration and can evidently be improved upon by using the modified technique (104). The rate of slag hydration at one year is very slow and appreciable amounts of the material (c.40%) remain at this late age.

5.3. Thermal analysis

These techniques have been described in chapter two and therefore require little expansion here. The apparatus is shown in figure 114 below.

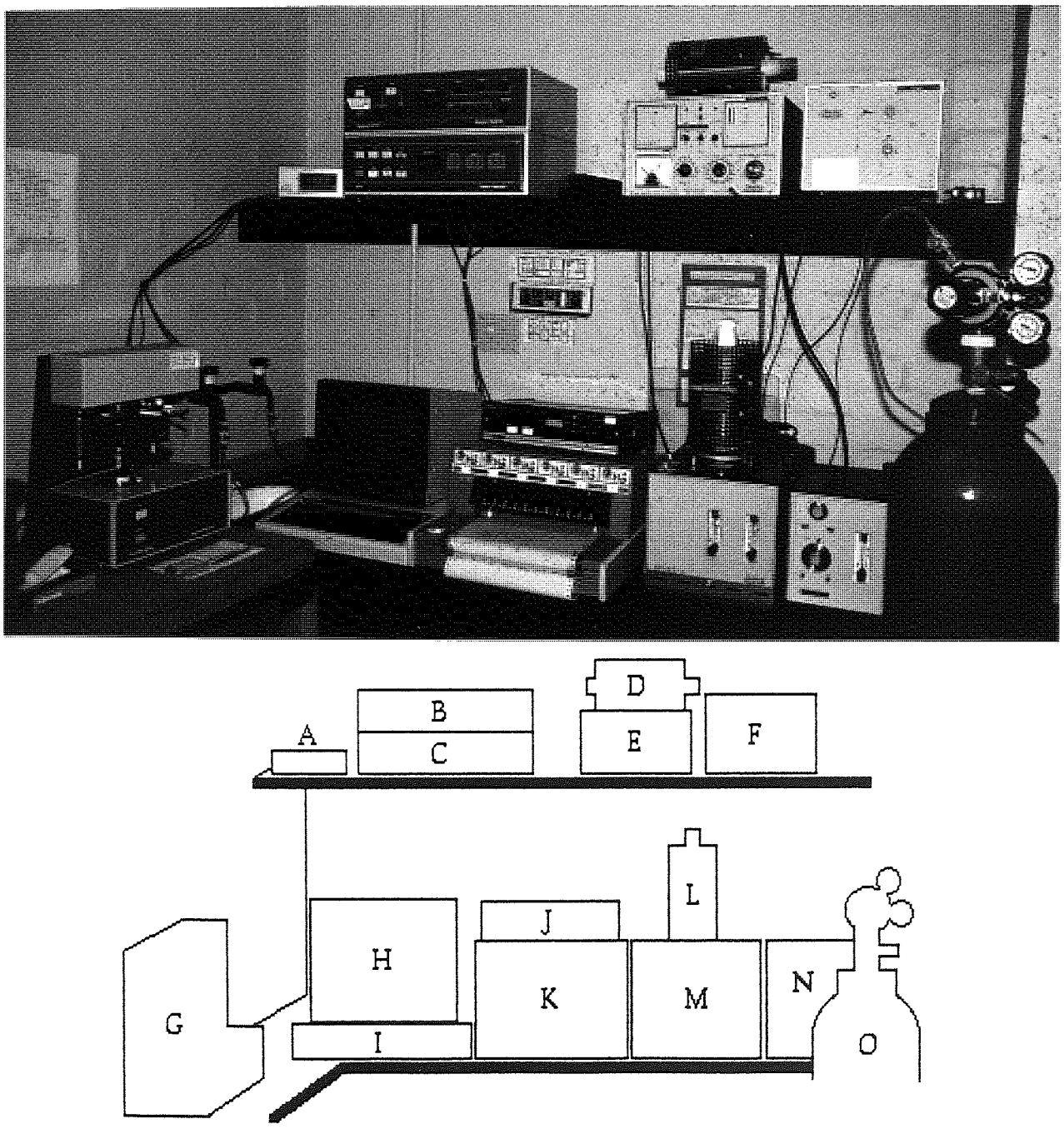

Key: A=Compensated cold junction (TG), B=Balance control, C=Temperature controller, D=Spare DTA furnace, E=DTA controller, F=DTA amplifier, G=Thermobalance, H=Monitor, I=Microcomputer, J=Voltmeter (calibration), K=6 pen recorder, L= DTA furnace, M=DTA base & gas control, N= Low temperature DTA, O=Gas supply

Figure114 *Thermal analysis apparatus*

5.3.1 Thermogravimetry

The thermogravimetric method allows a continuous measurement of sample mass with respect to temperature over a chosen range. The method was used here to determine the calcium hydroxide content of slag cement pastes as described in chapter 2. The instrument used was capable of recording percentage weight loss and the first derivative of weight loss which is useful in deliniating the begining and end of a gradual thermal event.

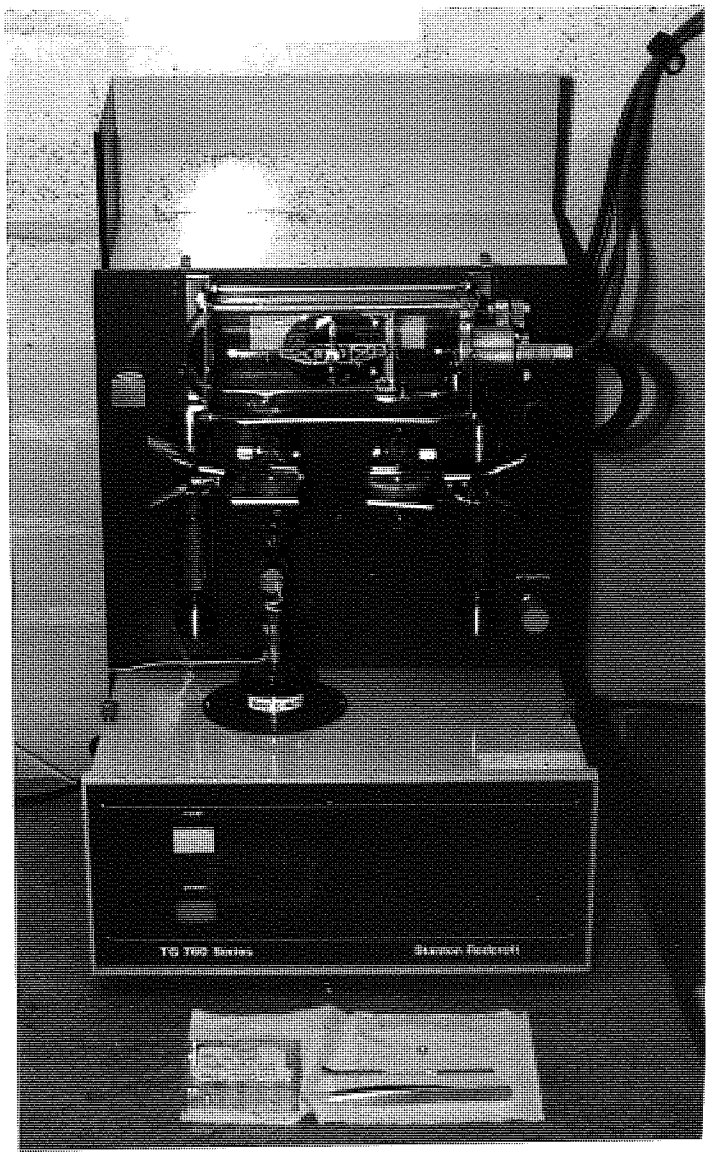

Figure115 *Stanton Redcroft TG760 Thermobalance*

Figure 116 shows typical output recorded by the device during the examination of slag cement pastes. Initially, loss of adsorbed moisture from the sample accounts for perhaps a 2% loss of mass up to 100°c (Taylor, 144 argues that this is partially due to decomposition of the hydrates). Between 100 & 200°c, water is lost from the CSH gel phase although part of this is the decomposition of Af_t at 105°c and Af_m at 145°c. A peak corresponding to loss of water from hydrogarnet may be resolved at 410°c followed by a distinct increase in the rate of weigh loss at 470°c. This corresponds to the loss of water from $Ca(OH)_2$ during its dehydroxylation to CaO. The rate of change is steeper than that either side and is delineated by the peak in the DTG trace. In these experiments, it is assumed that all the weight loss in this region is due to:

$$2\,Ca(OH)_2 \rightarrow 2\,CaO + 2\,H_2O$$

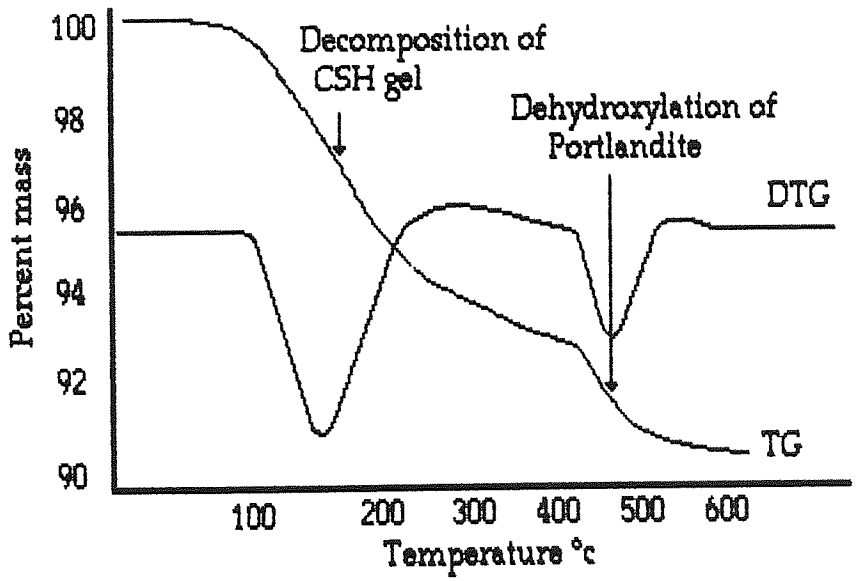

Figure116 *Thermogram from TG and DTG*

The mass loss permits direct calculation of the amount of portlandite present in the sample and hence it is possible to use the method to follow its precipitation and subsequent consumption.

Figures 117 & 118 show the $Ca(OH)_2$ content determined for pastes cured

at 25°C. It can be seen from these results that the precipitation reaction is initially rapid and that the subsequent consumption of the calcium hydroxide by the slag is substantially slower.

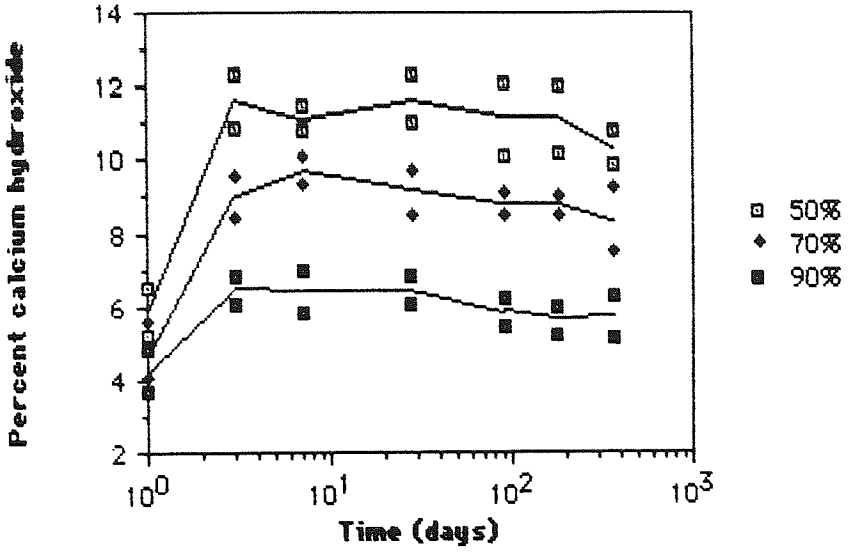

Figure 117 *Calcium hydroxide content of 0.3 pastes at 25°C*

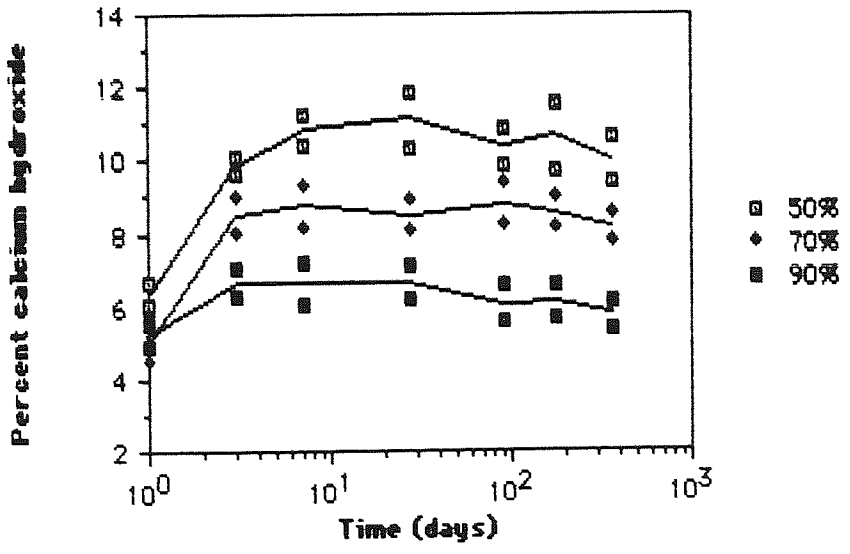

Figure 118 *Calcium hydroxide content of 0.4 pastes at 25°C*

Little difference can be seen between the 0.3 & 0.4 w/s ratio pastes, the calcium hydroxide content is similar for both water contents. The 0.3 paste reaches a maximum $Ca(OH)_2$ content after three days and the concentration falls

by around 1.5% of the total mass over the course of one year. By comparison the 0.4 w/s data show that the maximum value was not reached until about 28 days and the subsequent reduction of $Ca(OH)_2$ was approximately 1% of the total mass irrespective of initial slag content. It would seem unlikely that the increase in water : solids ratio would have such an effect, indeed previous experiments would suggest that the paste of higher water content would react the faster. Given that the spread of these data is 1% of the total sample mass, (c.16% of the fraction consumed by the slag after the maxima) it would be unwise to assign great significance to this finding.

The samples hydrated at elevated temperature were again the 0.4 w/s ratio pastes and their $Ca(OH)_2$ contents are shown in figures 119 & 120 below:

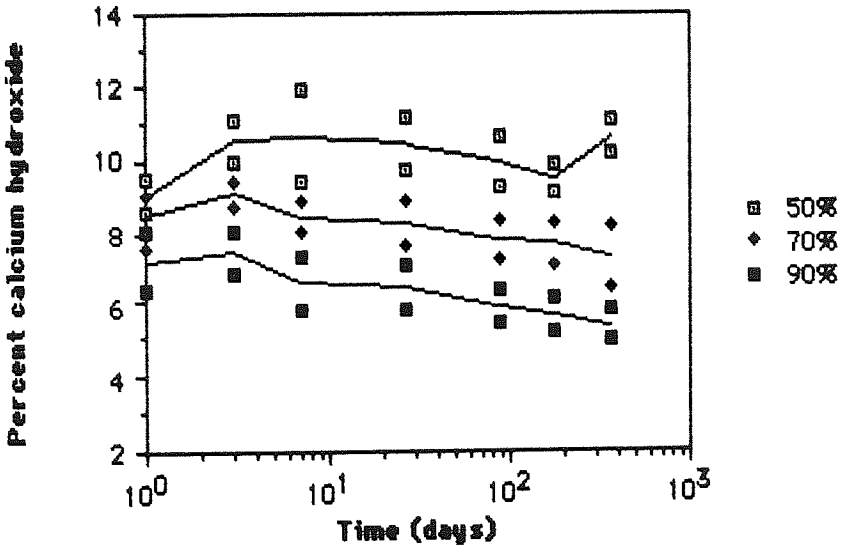

Figure 119 *Calcium hydroxide content of pastes at 50°C*

As may reasonably be expected, these samples demonstrate an increase in reaction rate with temperature. They both show increased $Ca(OH)_2$ contents at 1 day and both reach a maximum between the first and third day. The significant difference is in the subsequent rate of $Ca(OH)_2$ reduction compared with the low temperature samples. The 50°C pastes consume approximately 12% of the

available $Ca(OH)_2$ within the first year whilst for pastes cured at 70°C the figure is as high as 18%. As would be expected, pastes of high slag content consume $Ca(OH)_2$ at the highest rates.

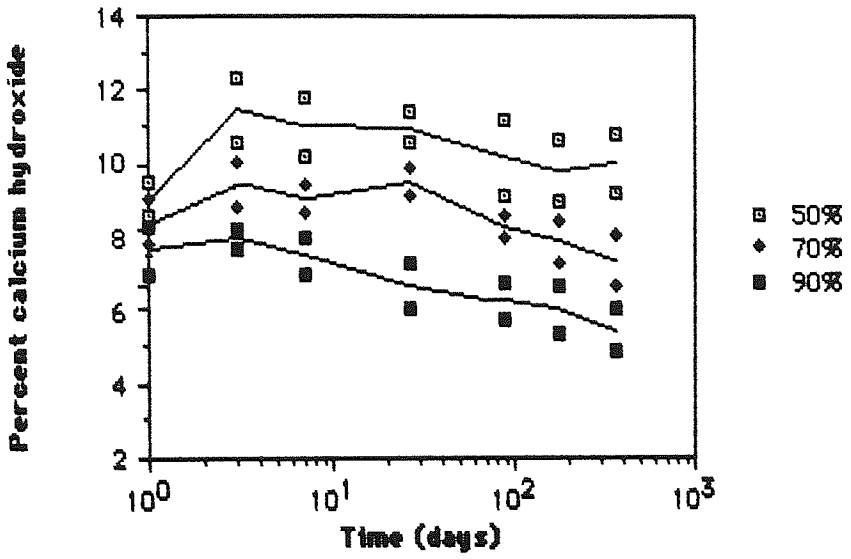

Figure 120 *Calcium hydroxide content for pastes at 70°C*

In conclusion, The precipitation of $Ca(OH)_2$ is rapid in comparison to its rate of consumption, this accounting for a maximum reaction over one year involving approximately 2% of the sample mass. When the dilution factor of the slag content is taken into account, the total $Ca(OH)_2$ is of the same order as is found in hydrated Portland cement, suggesting that the quantity consumed by the hydration of the slag is, over this time scale, quite small.

5.3.2 Differential Thermal Analysis

The DTA method records an enthalpy change associated with any thermal events which occur during the heating of the sample. The thermal reactions describedabove are detected along with others not associated with a change of mass. Typical of this latter type are recrystallization reactions and ultimately, changes of state.

Early in this project, a method was sought to determine the absolute rate of hydration of the slag. The hypothesis was proposed that this could be quantified by measuring the heat of fusion of the slag glass and thus the proportion of unhydrated material could be deduced. Given that the enthalpy change required to convert the slag from its glassy state to its constituent merwinite and melilite was detected by the DTA, it may be possible to use this method as a direct measure of the degree of hydration.

A typical DTA thermogram is shown in figure 122. Peaks A,B & C are the dehydration of the CSH gel, aluminate hydrates and calcium hydroxide discussed above. Peaks D,E,F & G are all associated with the recrystallization of the glass. The peak shown at D is probably an intake of heat prior to the re-ordering and is intimately associated with the peaks E & F (thought to represent the two end members of the melilite solid solution series, Gehlenite - C_2AS and Akermanite - C_2MS) The peak shown as G is almost certainly not merwinite which would be unlikely to recrystallize at such a low temperature.

Preliminary experiments consisted of peak area measurements of the combined peaks D,E,F & G for a limited range of high slag compositions. Typical results are shown in figure 123 which demonstrates an obvious trend of slag content decreasing with time. These are for a high slag replacement (90%) at 25°C and 0.4 w:s ratio. Unfortunately, the reproducibility of these quantitative results was very poor, peak areas for supposedly identical samples varying by as much as 25%. It was thought likely that the thermal reactions were not going to completion, even though the furnace was held at its maximum temperature (980°C) until the base line had stabilized. In addition to this, some samples showed a pronounced base-line shift in this region which introduced an additional element of uncertainty to the deliniation of the peaks.

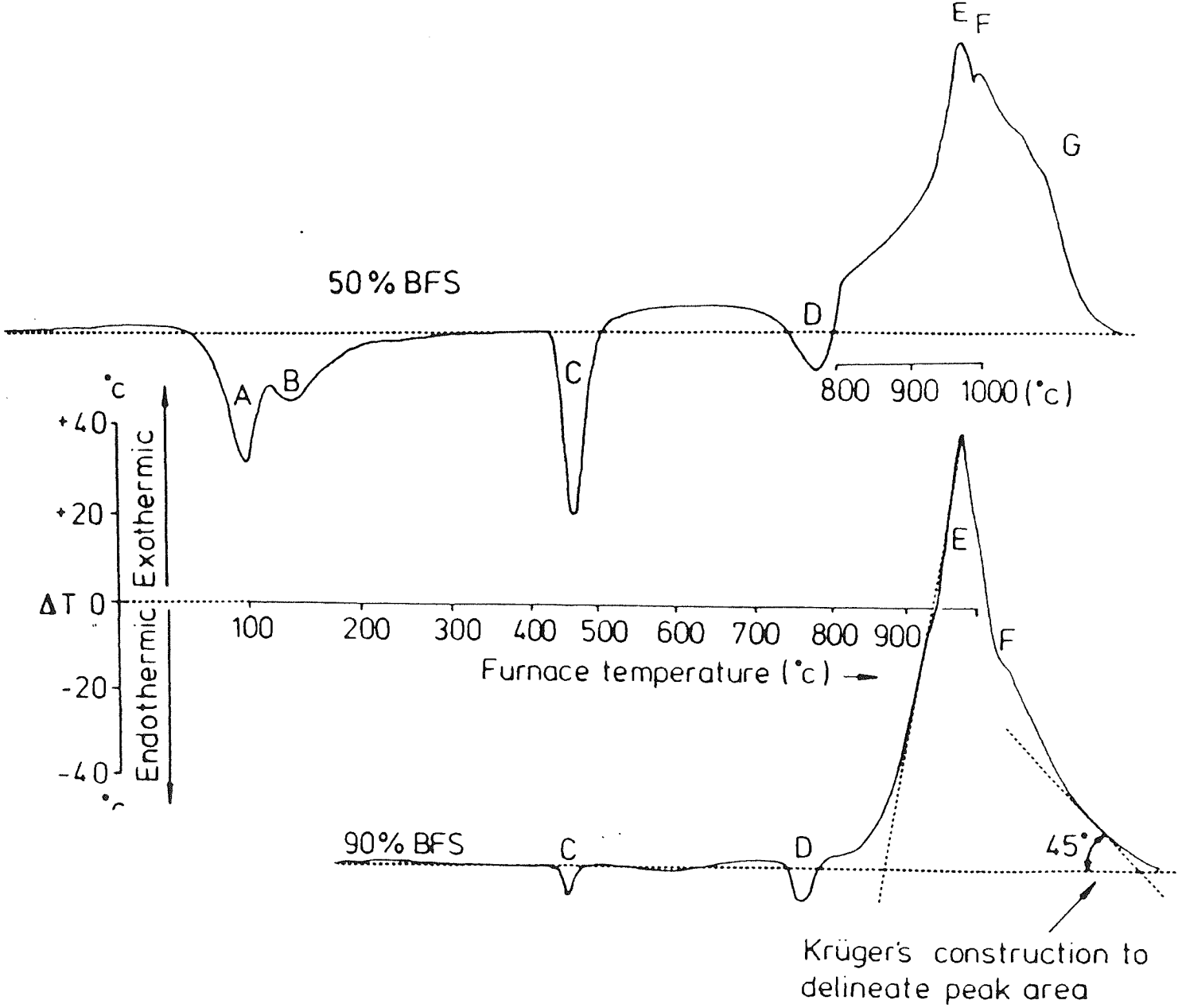

Figure 121 DTA thermograms of 0.4 w/s pastes after 12 hours hydration

Regourd (63) reports the crystallization of merwinite at 950°C in her thermal analysis and Hinrichs and Odler (126) have recently used the recrystallization exotherm to follow slag hydration. These workers make no mention however of the possibility of further recrystallization occuring at higher temperatures. Given the irreproducibility of the peak areas, no further quantitative DTA studies were made until a high temperature facility became available.

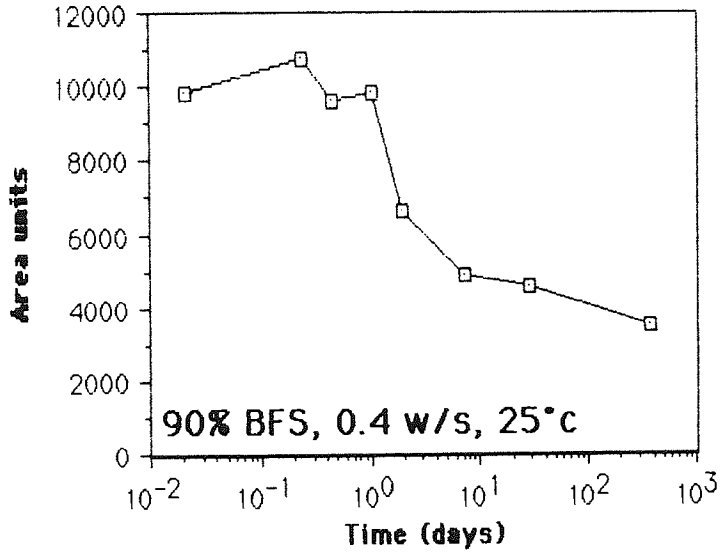

Figure 122 *Peak area vs hydration time for devitrification of BFS (90%,0.4)*

5.3.3 Differential Scanning Calorimetry

The method and results described here are strictly a variation of the DTA method although a number of manufacturers market high temperature equipment as DSC. The samples were run at UKAEA Winfrith using a Stanton-Redcroft STA1500 in conjunction with a 'Trace 2" data acquisition system. The thermogram shown in figure 123 is typical of the high slag pastes and shows, as suspected, a second exotherm corresponding to the devitrification of merwinite.

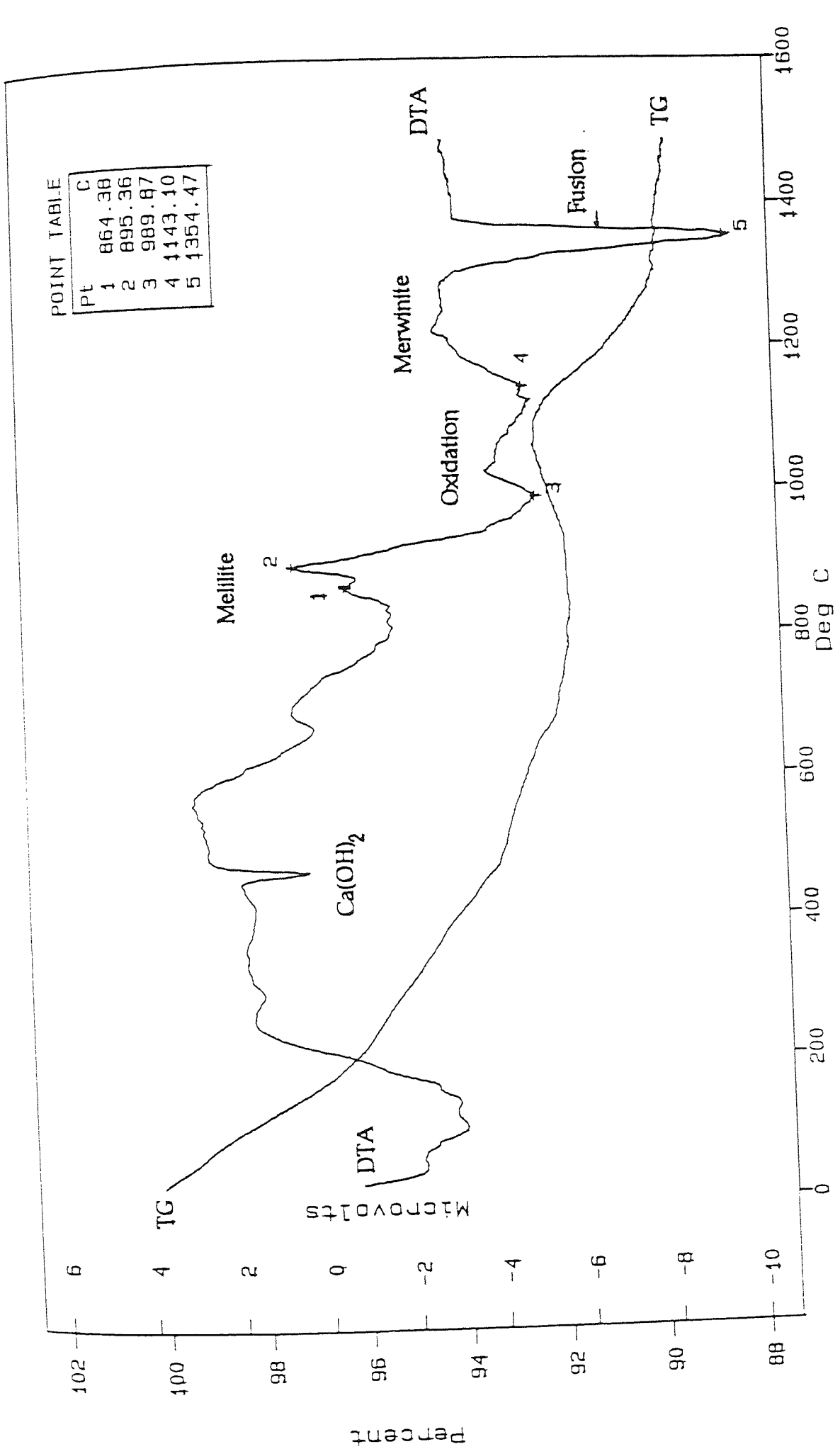

Figure123 High temperature thermal analysis for 90% BFS, 0.4 w/s 7days @ 25°c

Above this is a major thermal event (peak 5) centered at 1355°C which is undoubtedly the fusion of the fully crystalline slag. It is this heat of fusion which should be proportional to the concentration of the unhydrated slag and a number of samples hydrated for different times were examined in this way. Comparing peak areas, associated with both devitrification and fusion produces figure 124.

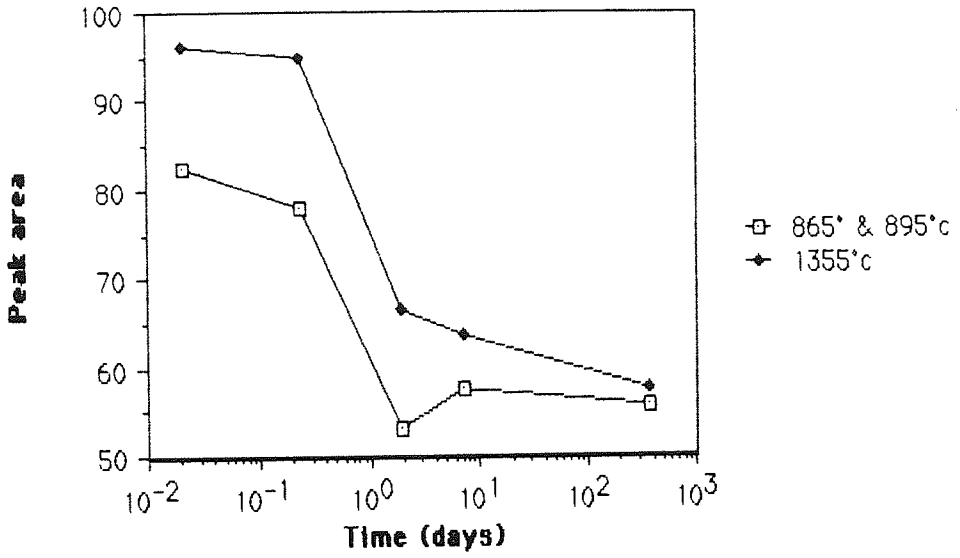

Figure124 *Peak area vs time for high temperature thermal reactions*

This shows clearly that the devitrification of melilite (865 & 895°C) peak area closely follows the total area for the fusion of the glass, from which we may infer that the glass is dominantly melilitic.

5.3.4 Discussion

These experiments demonstrate that the devitrification is not a simple process and in fact, occurs in six recognizable stages. Initially a pair of exotherms are recorded (865° & 895°C) associated with the gehlenite - akermanite recrystallization. Endotherms at 989°C and 1143°C (probably internal transitions) are separated by a minor exotherm at 1050°C which is associated with a weight

gain. This is most likely the oxidation of an interstitial phase (such as the iron particles reported in chapter 2) which have been liberated by the partial melting of the glass. At about 1200°c, the merwinite devitrification is marked by an exotherm which is followed finally, by the melting of the crystal mixture at 1354°C. Note the gradual onset of melting is due to this being a poly-phase crystalline system at this stage and, though diffuse, is much sharper than would be expected for a glass transition.

It is interesting to correlate the sum of the peak areas associated with the devitrification reactions measured by DTA, (peaks E,F & G in figure 121) with those recorded for the complete fusion of the glass (peak 5, Figure 123). This is shown in figure 125 below:

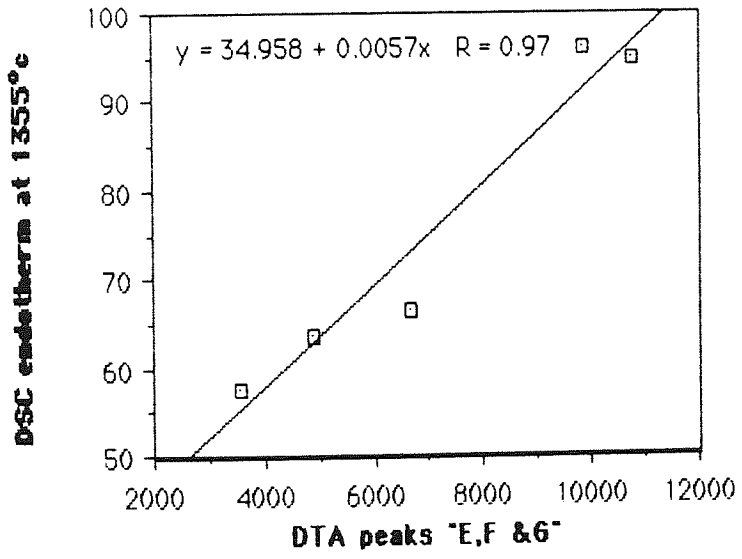

Figure125 *Correlation of results from low and high temperature thermal analysis. (Arbitrary area units, abscissa is sum of peaks E,F & G)*

This figure shows excellent agreement between the heat of fusion and the heat of devitrification which would be expected if only the slag undergoes all its thermal reactions within this temperature range. The results suggest that if the enthalpy of devitrification is to be used as an indicator of the amount of

unhydrated slag remaining in the system, then thermograms extending to 1370°C should be used. For this material, the merwinite contribution is relatively small but this need not be the case for slags from other sources.

Chapter 6
Pore Solution Chemistry

6.1 Introduction

The chemistry of expressed pore solutions provides a direct means of examining the chemical environment within the hydrating cement paste. As described in chapter 2, these liquids are recovered by means of a pore fluid extraction press, which loads the paste, driving the liquid phase into a plastic syringe. The press is shown in figures 35 - 37. Figure 35 shows an isometric partial section of the cell body, shown in component form in figure 36. The lower photograph (fig 37) shows the cell (covered by its water jacket) in use between the plattens of the hydraulic press.

The liquid samples contained some suspended solids released from the solid during compression and were therefore filtered before dilution and analysis.

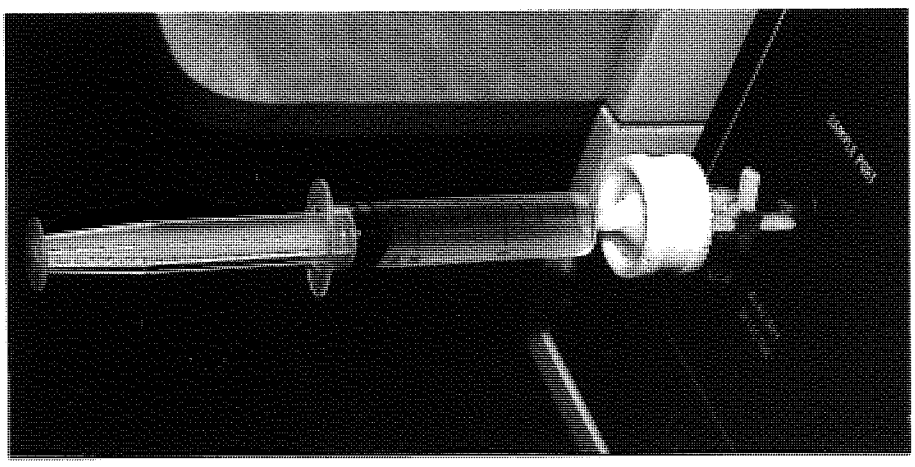

Figure 126 *Demountable syringe used both for filtration of sample after collection and before injection into ion chromatograph.*

The water jacket effectively maintained the required cell temperature at

within the pores as practically possible.

Because of deterioration of the samples during storage, certain analyses were performed immediately after recovery of the sample. The major anion (hydroxyl) was titrated against 0.01M nitric acid and the approximate redox potential of the solution was estimated within one hour of the extraction. Details of these methods are given in chapter 2. A sub-sample for sulphide determination was buffered against atmospheric oxidation and the remainder of the sample diluted for ion chromatography and metals analysis.

6.2 Hydroxyl ion chemistry

Figure 129 shows the variation of hydroxyl ions with time at 25°c for the full range of samples.

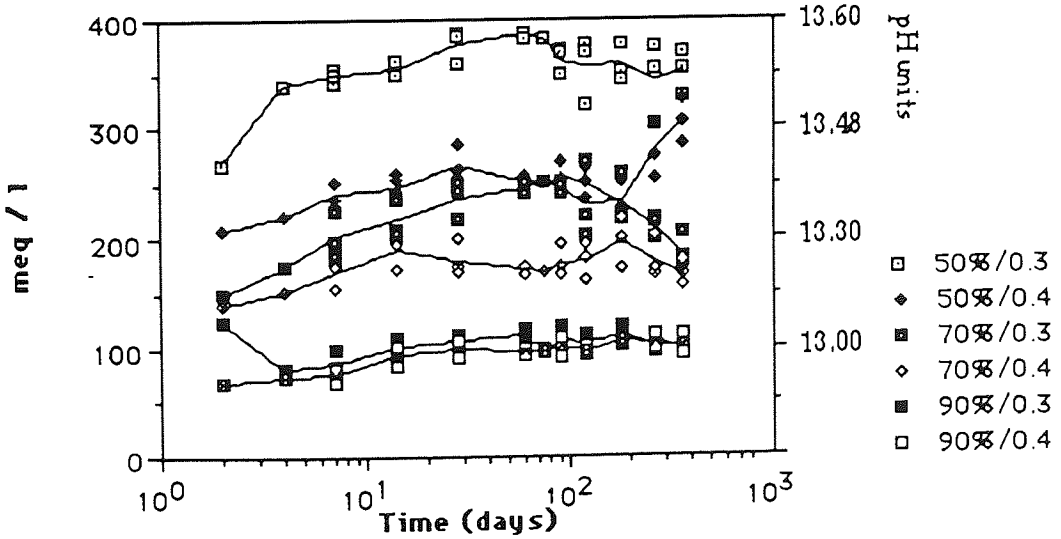

Figure129 *Hydroxyl ion concentrations at 25°c*

On wetting, the pH of the solution is moderately alkaline and the concentration of sulphate is relatively high. Within the first few hours of hydration however, the hydroxyl concentration rises rapidly to reach a meta-stable state after a few days at pH 13 to 13.5. This increase in hydroxyl concentration is at the expense of sulphate, such that when the hydroxyl

stable state after a few days at pH 13 to 13.5. This increase in hydroxyl concentration is at the expense of sulphate, such that when the hydroxyl concentration becomes generally stable it constitutes the bulk of the anions. The absolute pH of the solution is broadly related to the initial OPC content of the sample and to its water : solids ratio. Those with the highest proportions of OPC and lowest water contents yielding the most alkaline pore solutions. This is to be expected as the OPC readily liberates hydroxyl ions during its early hydration.

Although the general range of pH is in good agreement with previous work, it is interesting to note that there is a measurable difference between the hydroxyl concentrations in pastes of similar composition, which differ only by their original water contents. It would be expected that the solid phase would be in great excess and that the pH would be governed by the solubility of hydroxyl ions. Although the scatter of the data affords some degree of overlap at 70% and 90% slag content, no explanation of the apparently higher pH of the 50% BFS, 0.3 w/s paste is offered at this stage.

There is a trend towards a fall in pH with time, as long term hydration removes group one metals from the liquid phase (see below). This difference is within the range of experimental variation after one year's hydration.

6.3 Alkali metal chemistry

Sodium and potassium are the dominant counter ions, with the next most concentrated cation being calcium, some two or three orders of magnitude less concentrated. To a first approximation, sodium and potassium follow a similar trend to that shown in figure 129, the concentration of sodium being lower than that of potassium. Figure 130 shows the variation of sodium concentration with time. The important features are that after reaching a maximum concentration, sodium is gradually removed from solution, the rate of incorporation into the hydrates is obviously greater than the rate of supply from

Glasser (117) notes that unlike calcium, sodium and potassium are poorly buffered and he estimates that 25% of the available sodium is released into solution as is 70% of the available poassium.

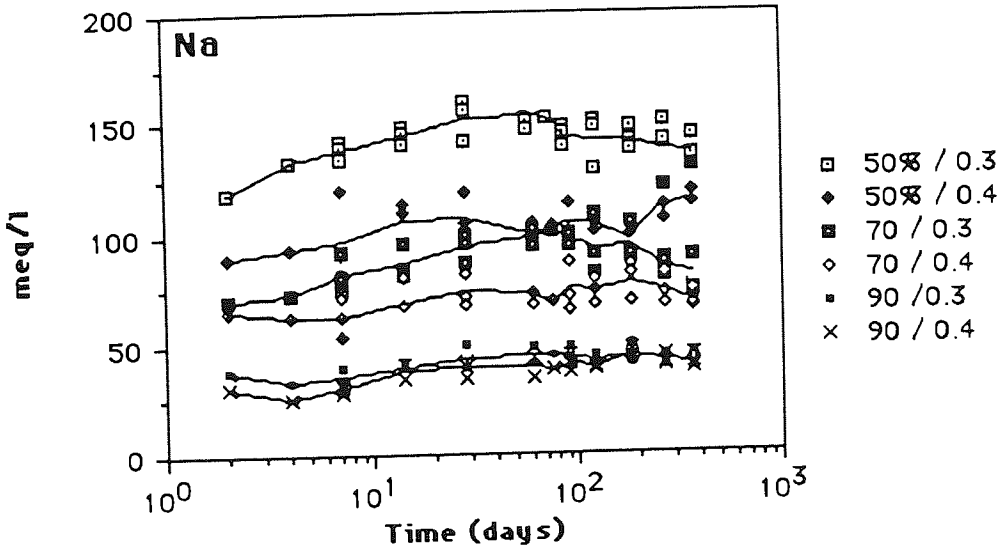

Figure130 Sodium ions in solution at 25°c

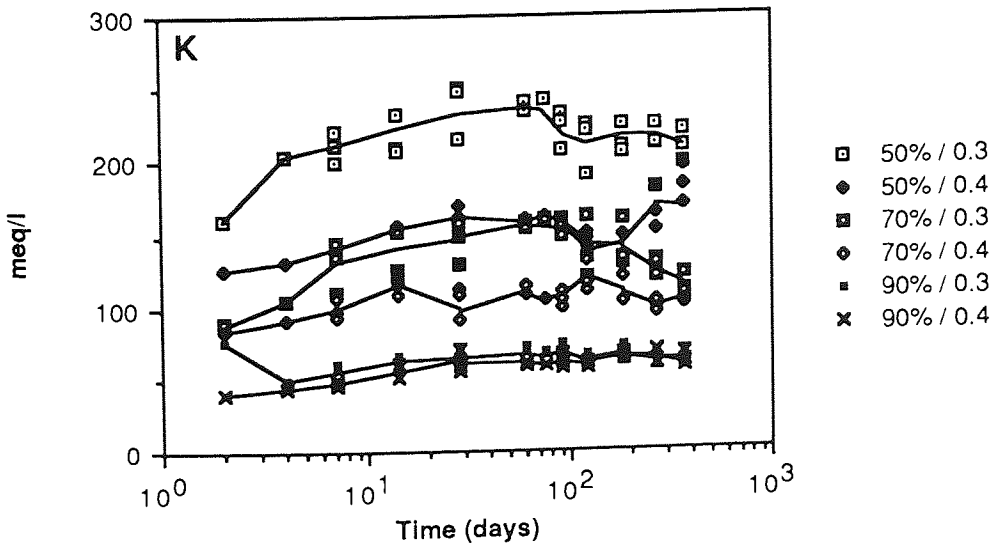

Figure131 Potassium ions in solution at 25°c

6.4 Calcium ions in solution

The behaviour of calcium is unlike that of sodium or potassium in as much as it is not irreplaceably removed from solution as the system hydrates. Figure 132 shows the concentrations of calcium are much less varied with respect to cement paste chemistry than are the alkali metals. This is an effect of the limited solubility of calcium ions at high pH. The solubility of $Ca(OH)_2$ at 18°C is quite low at 1.1g /l (117) and this value is, of course, reduced at 25°C. The majority of the concentrations recorded lie in the range 3 to 5 meq / l which is close to the limit of solubility at this temperature.

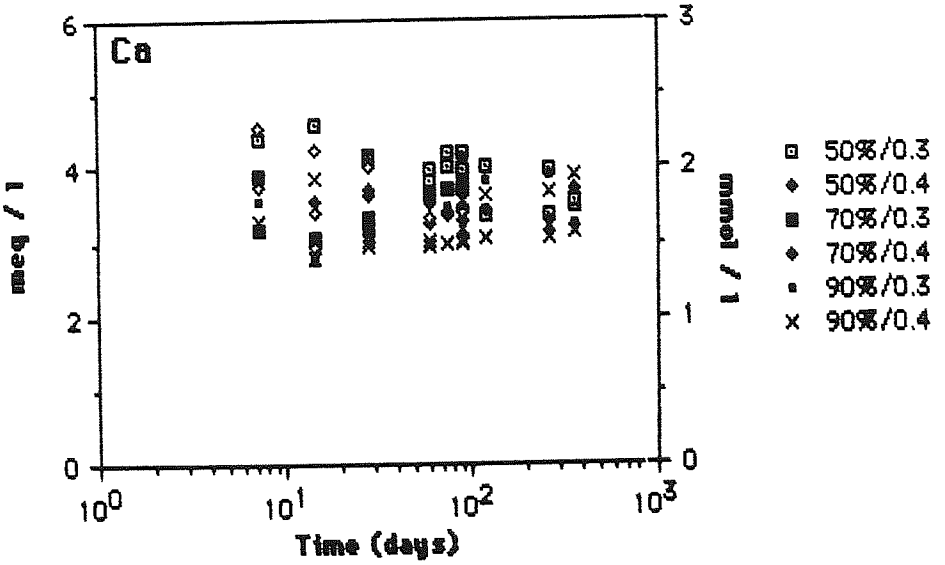

Figure 130 Calcium ions in solution at 25°C

The liberation of calcium ions into solution on wetting the paste is very rapid, (dissolution of gypsum) and is associated with initially high concentrations of sulphate. These species decrease in concentration in the early stages of hydration as the precipitation of sulpho-aluminate hydrates removes them from solution.

To demonstrate this effect, a single composition (90% BFS / 10% OPC, 0.5 w/s ratio) was mixed at room temperature and sampled by vacuum filtration through a Buchner funnel. The pore solution was effectively removed by using a

polythene membrane over the sample as a filtration dam, allowing the paste to be compressed against the filter paper.

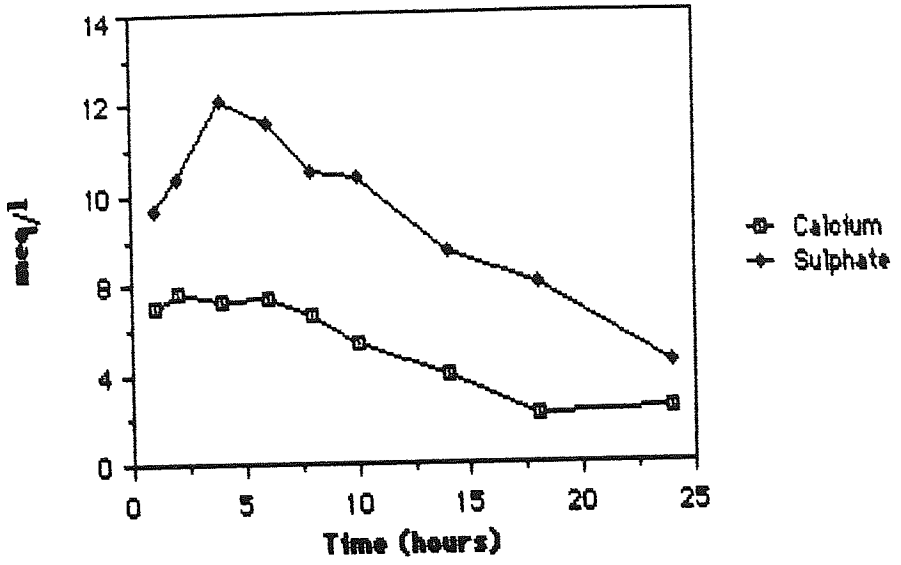

Figure 131 *Early age dissolution and precipitation of* Ca^{2+} *&* SO_4^{2-}

This effect is well documented and the reduction in calcium during the first few hours has been shown to be pH dependent; Roy and Idorn (68), amongst others, show solubility isotherms for $Ca(OH)_2$ as a function of alkalinity. The solubility falls rapidly with increasing pH and it is the rise in hydroxyl concentration which permits the precipitation of calcium in the form of sulphates.

For later ages it can be seen that little change occurs in the calcium concentrations as the system is both well buffered and saturated with respect to this ion. At alkalinities greater than c.pH 12.5, the species in solution is probably $CaOH^+$ (113), although for the purpose of mass balance calculations, Ca^{2+} is assumed.

6.5 Sulphur species in solution

In addition to the sulphate released from the dissolution of gypsum, there is an appreciable quantity of sulphur (2.2wt% as SO_3) incorporated in the slag

itself. As found by Glasser and co-workers (10,83,113,-121), speciation of the sulphur in solution depends both on the pH and E_H of the system. It was seen as a useful exercise to quantify the development of these changes as they had not yet been published in the open literature.

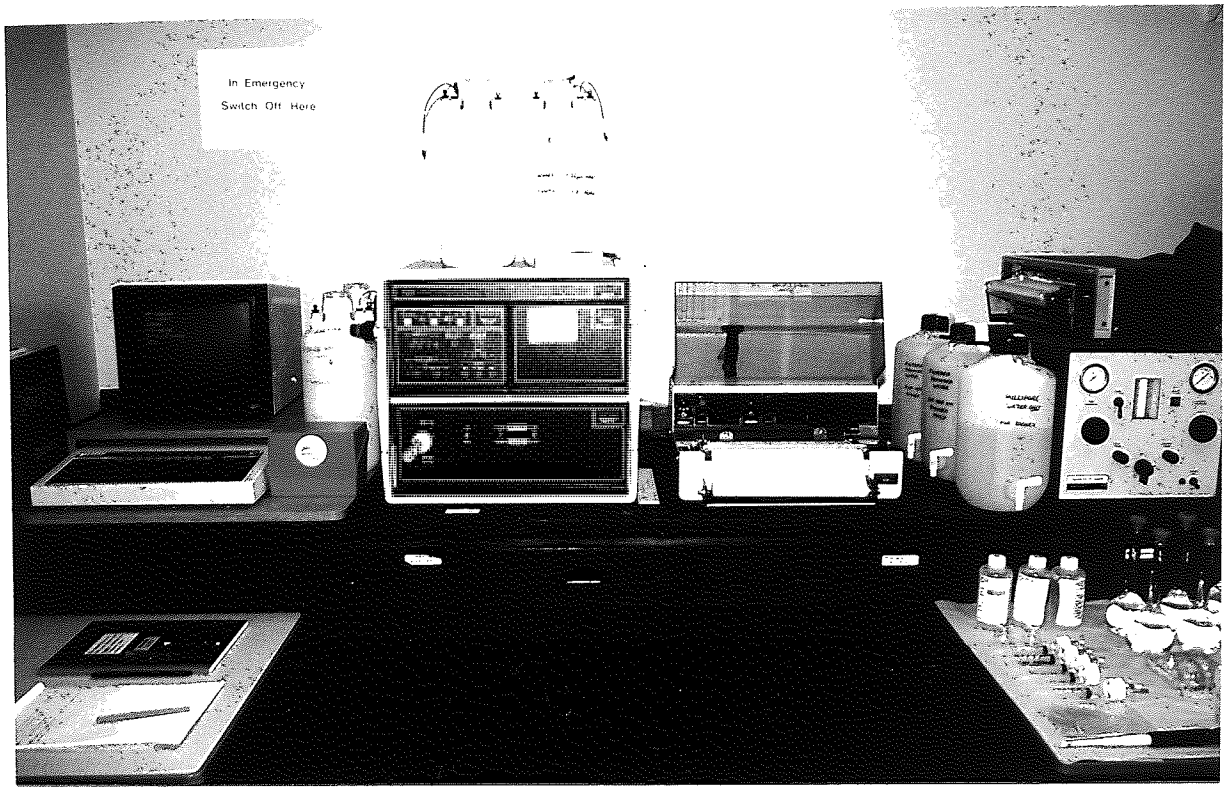

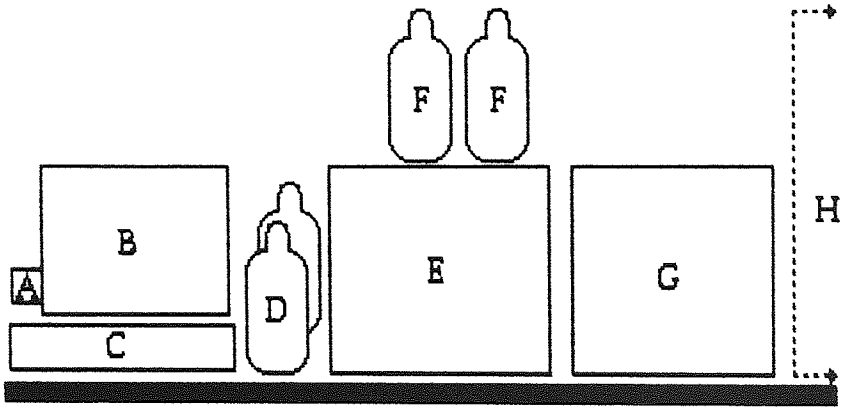

Key: A=Disc drive, B=Monitor, C=Computer, D=Regenerant bottles, E=Ion chromatograph containing pump, columns and detector. F=Eluant containers G=Chart recorder (H= gas supply for AAS; not part of this equipment)

Figure132 *Ion chromatograph (Dionex model 2000i/SP)*

Given that sulphate, sulphide(s), thiosulphate and possibly sulphite may co-exist in the pore solutions, this technique was considered desirable as it is essentially seperative and thus can detect analytes which may change from one species of interest to another. Thiosulphate and sulphite are meta-stable and may both be oxidized to sulphate or undergo the following reaction:

$$2S_2O_3^{2-} \rightarrow 2SO_3^{2-} + S_2\downarrow$$

This reaction is slow, but does occur if a thiosulphate solution is allowed to stand. Rapid analysis of the pore solutions and exclusion of air from the collecting syringe were seen as essential if meaningful results were to be obtained. The eluant used for these analyses was as follows:

2% v/v Propan-2-ol

5% v/v Acetonitrile

0.002M 4-Cyanophenol

0.0086M $NaHCO_3$

0.0068M $NaCO_3$

This is an empirical development of the manufacturers recommended eluant composition and provides more rapid elution of thiosulphate at the expense of some resolution. As the sulphate and thiosulphate concentrations are well within the working range of the instrument, this was seen as an acceptable compromise, the pore solution requiring a 50x dilution to bring it into the working range.

Figure 133 shows a typical chromatogram obtained by this method and in normal running, a calibration curve would be plotted each day to ensure stability of operating conditions (less than 4% standard deviation for the whole sequence). The normal method of operating employed an external combined standard of 5µM sulphate and 10µM thiosulphate in aqueous solution. This was injected between samples, allowing comparison of each sample to two adjacent standards on the chart. This showed a maximum drift of 2% response between adjacent

shown below. Within the first minute, there was a rapid, reversible drop in conductivity as the water present in the sample (without the dissolved ions it was carrying), moved through the detector. At 3.8 minutes, the sulphate was eluted as a near symmetrical peak with little adsorption tailing. This is followed by the thiosulphate at 9.6 minutes which was a much broader peak typical of a large, moderately well adsorbed, hydrophobic ion. For peaks of the same area, the full width at half maximum is approximately five times greater for thiosulphate than for sulphate.

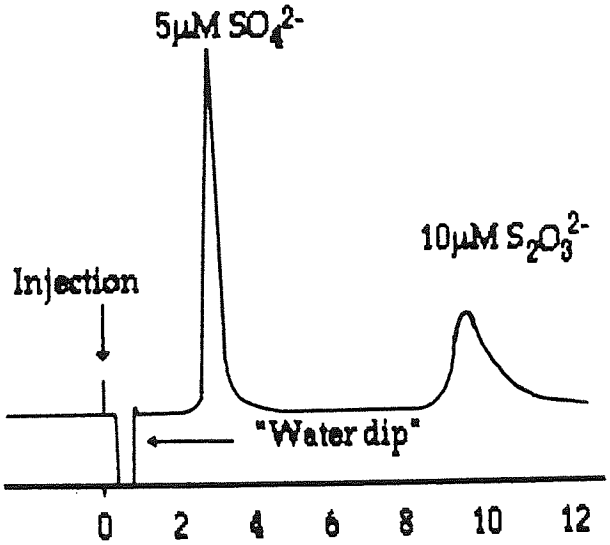

Figure133 *Chromatogram of species analysed by ion chromatography (Horizontal scale in minutes)*

Sulphate was detected in all the samples analysed and gradually increased its concentration over a period of one year by a factor of approximately ten. It is reasonable to associate this change with the continued, slow hydration of the slag releasing sulphur into solution. The initial dissolved form cannot of course be ascertained, but it is possible that the sulphate is an oxidation product of other sulphur species. This is addressed more fully later. The minimum value shown around the 7 day analyses, is likely to be dominated by the remnants of gypsum dissolution and precipitation of the sulphoaluminates. The concentration

increased with the continued hydration of the slag (as shown in figure 136) from approximately 0.5 mM to over 5 mM for the 90% pastes.

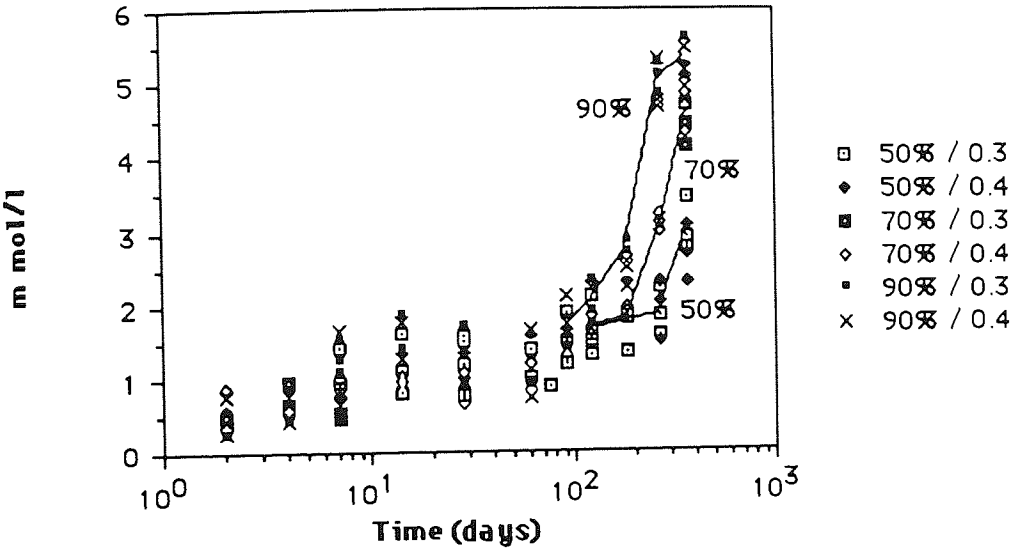

Figure136 *Sulphate ions in solution at 25°c*

Given that the concentration change is greatest for the high slag samples and that the concentration increase is most marked at later ages we may deduce that this phenomenon is governed by slag rather than OPC hydration. At less than 28 days, no trend is visible between the compositions, indeed they are of very similar magnitude.

By comparison, thiosulphate shows a different trend in that it rises gradually for all compositions over the course of the first year's hydration. Although the concentration of this species is not high (c.2.5 mM max) it is of significance as a redox indicator. Thiosulphate, although a metastable species, occupies a narrow domain between sulphate and the sulphides (see Pourbaix diagram, fig 19, page 53). In a system containing sulphate which is gradually becoming (electrochemically) reducing, the conditions prevail for the formation of thiosulphate. Because of the transitory nature of this ion, its absolute concentration is not of great significance in comparison to its rate of change of

concentration is not of great significance in comparison to its rate of change of concentration. In these experiments, thiosulphate ions are seen to increase with time and are a useful indicator of the prevailing redox conditions.

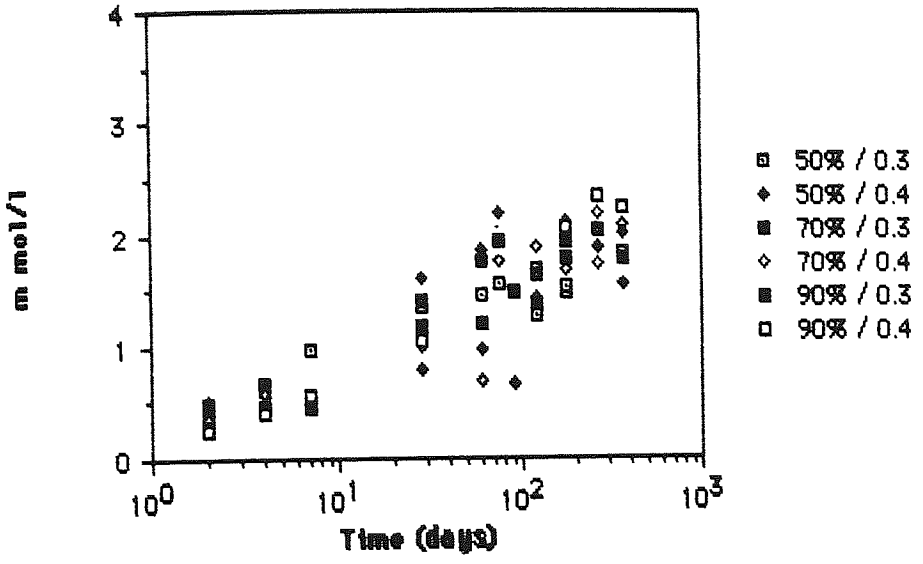

Figure 135 Thiosulphate ions in solution at 25°C

The sulphide concentrations proved to be less predictable and occupied a field of values from 19 to 171 µM.

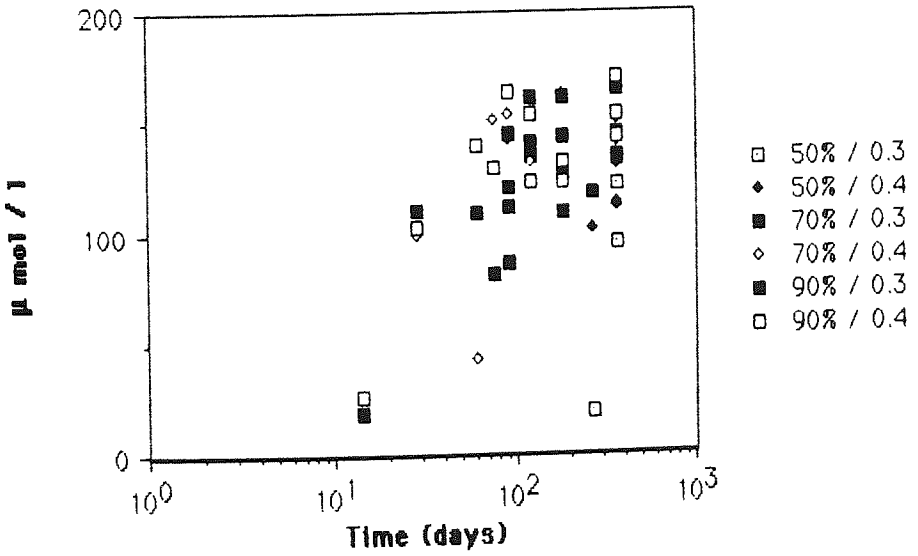

Figure136 Sulphide ions in solution at 25°C

As described in chapter 2, this ion was detected by an ion selective (Ag/AgS) electrode. As very little of the pore solution was available for each analysis, the analyte addition method was used, by which a known volume of the sample was added to a standard solution of the (buffered) ion and the concentration calculated from the change in potential recorded. The method is as follows:

$$\Delta E = S \log\left[\frac{C_s . V_0 \pm C_x . V_a}{(V_0 + V_a)\ C_s}\right]$$

(Cx is +ve for analyte addition)

Therefore:

$$C_x = \frac{C_s}{V_a}\left[10^{\Delta E/S}(V_0 + V_a) - V_0\right.$$

When Va << V0

$$C_x = \frac{C_s . V_0}{V_a}\left[10^{\Delta E/S} - 1\right]$$

Where: C_x = Concentraion of sensed ion in analyte

C_S = Concentration of sensed ion in standard

V_0 = Volume of standard solution

V_a = Volume of addition

ΔE = Initial potential - final potential

S = Slope of electrode response

Figure 138 shows that at seven days, sulphide was not detected in any sample (< 1μM) whilst at 14 days, only the high slag blends showed a measurable quantity. Subsequently, sulphide was found in all samples at approximately the same concentration (70 to 170 μM). with no obvious trend to the measured

values. Excepting measurement errors (the variations seem improbably high) this could be explained in two possible ways: First, inspite of the use of an antioxidant buffer for dilution of the sample, the sulphide detected was not representative of the sample due to oxidation. This possibility is addressed in the final chapter. Secondly, the system could be in a state of change, sulphide being incorporated in the solid phase (unlikely) or in the liquid phase as undetected polysulphides (more probable). The implications of sulphide being removed from, in addition to being supplied to the solution, is that we are observing a kinetic equilibrium which is maintaining the sulphide concentration at approximately the same level irrespective of the initial composition. To test this hypothesis, it would be useful to measure the redox potential of the solution in order to ascertain whether or not the system is becoming increasingly more reducing. If the former is the case, it would not be unreasonable to suggest that the sulphide concentration would continue to increase over time. If the redox potential is reasonably stable, the sulphide concentration would also be expected to reach a stable value.

6.6 Redox potential measurements.

The simple method of measuring the potential developed between a platinum and reference electrode has been described previously (fig 43). In this case, a saturated calomel electrode was used as a reference and hence the potentials recorded (E_{cal}) required correcting to the hydrogen scale (E_h). At 25°C the calomel electrode is 0.244 volts above the hydrogen electrode.

Figure 139 shows the redox cell in use, the platinum electrode in the base is in electrical contact with the screen, and the potential was measured with a high impedence ($10^{13}\ \Omega$) voltmeter. Between samples, the cell was washed with molar nitric acid (to dissolve any precipitated salts) and then repeatedly with deionised water before drying.

The results are shown in figure 138 and follow a similar trend to those reported elsewhere (83). The redox environment in all young pastes is similar,

with positive Eh values indicating an oxidizing matrix. The change from oxidizing to reducing conditions is more or less rapid, and is associated with the changes in sulphur chemistry noted in the previous section.

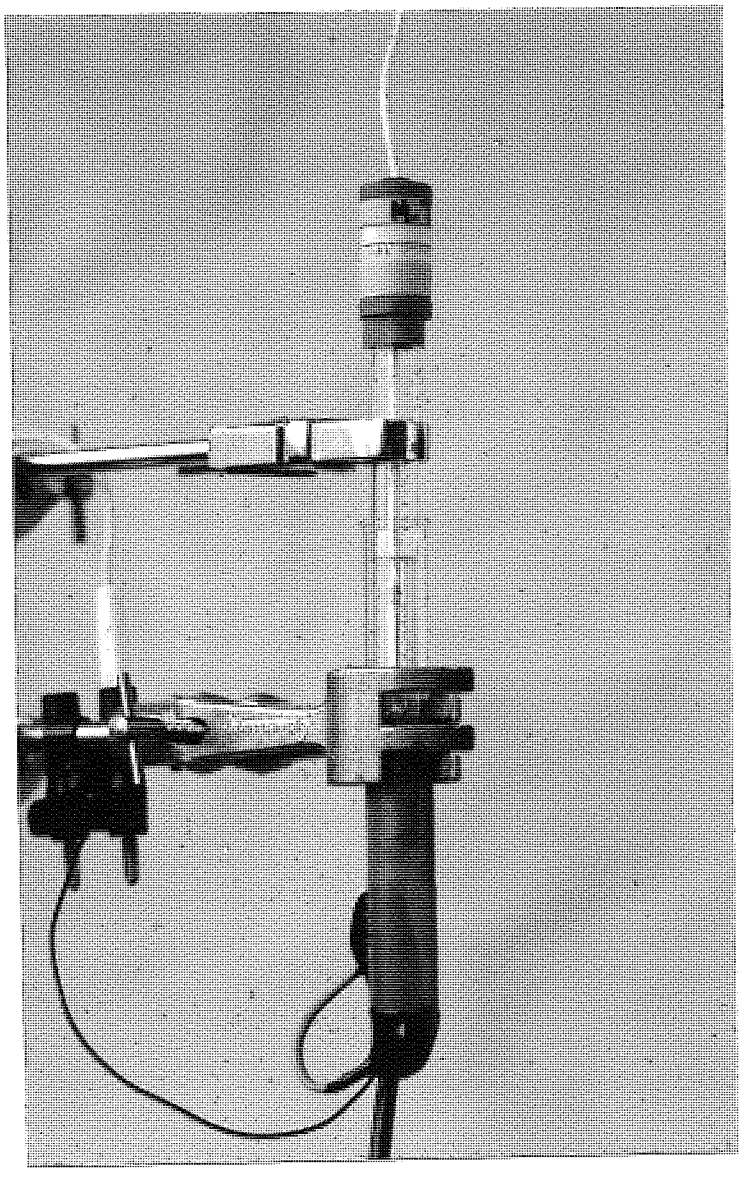

Figure 137 *Redox potential cell*

These data suggest that the redox potential is more or less stable after the onset of reducing conditions has occurred. This is in agreement with previous work and can be related to the sulphur speciation data. After mixing, the

cement dominate the redox chemistry, maintaining a redox potential of approximately 100mV (Eh). The hydrating paste has an oxidized component which is evidently fixed at the mixing stage and a tendancy to become reduced during hydration. The initial redox potential is limited by the dissolved oxygen in the system and probably to a small extent by the Portland cement minerals.

During hydration, the slag appears to scavenge oxygen from the pore solution until this reserve is exhausted. At this point, a rapid conversion from an oxidizing to a reducing environment is seen as the redox potential of the cell falls rapidly as shown in figure 140. Comparison with figure 138 shows that the switch between oxidising and reducing conditions is associated with the appearance of sulphide ions in solution.

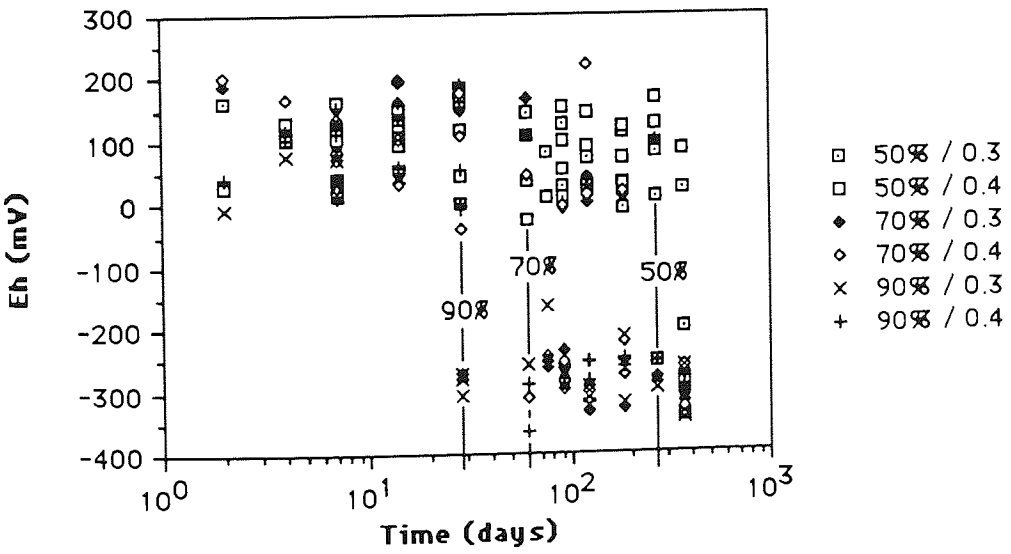

Figure140 Redox potential of pore solutions at 25°c

Before proposing an explanation for this mechanism, the following observations must be considered:

1) The sample was in a sealed container, hence it was isolated from atmospheric oxygen in addition to which, we may assume that the deionized

1) The sample was in a sealed container, hence it was isolated from atmospheric oxygen in addition to which, we may assume that the deionized water used in mixing was, in each case close to 100% saturated with oxygen. A fixed amount of oxygen was therefore incorporated in each sample on mixing.

2) A small amount of oxygen in solution will maintain a high redox potential, even though it does not strongly poise the system towards oxidizing conditions. (*cf.* pH titrations).

3) The time taken to the onset of reducing conditions is an inverse function of slag content.

4) The appearance of the sulphide ion in solution occurs at approximately the same time as the change from oxidizing to reducing conditions.

It is likely that the hydration of the slag consumes the dissolved oxygen to the point when the system can undergo a rapid fall in redox potential. Up to this time, the oxygen is removed from the aqueous phase and incorporated as oxide ions in the hydrates (and to some extent oxides of the iron-rich phase). After the system becomes depleted in oxygen, the hydrating slag acts as an electron donor which reduces the the oxidized ions in solution.

If this was a complete explanation of the redox chemistry, it would be reasonable to expect the aqueous sulphate concentration to fall rapidly after the switch to reducing conditions as it reacted to form sulphide and thiosulphate. Figures 135 to 138 shows that this is not the case, but that while the reduced sulphur species appear under reducing conditions, the sulphate concentration continues to rise during hydration. It can be seen that the sulphate concentration approximately doubles between three months and one year, the most pronounced change being associated with the higher slag compositions.

It is interesting to compare these results with figure 113, (page 187) which is based on Luke and Glasser's selective dissolution results (103,104). They propose a "renewed burst of hydration" at approximately this time. There is not

sufficient evidence to ascribe these results to an increase in the slag hydration rate *perse* . It is the case however, that the major portion of the sulphur which is not either in solution or incorporated in the hydrates, is present in the remaining slag. It would be reasonable to propose therefore, that the increase in total dissolved sulphur which occurs between three and twelve month's hydration, is associated with reactions of this slag.

The reduced Nature of the ions derrived from the slag raises another problem in interpretation. If sulphur is released during slag hydration, it would be expected to dissolve as sulphide or thiosulphate ions (fig 19 page 53). Two possible explanations exist for this incongruity: First, there may be a portion of the sulphur present in late-age samples as (undetetected) polysulphides, which dissociate and oxidize before analysis. Secondly, in later age pastes, both the connective porosity and the absolute amount of the remaining aqueous phase are low. The consequence of this is that to obtain enough pore solution to analyse, the paste was subjected to high pressures (c.300MPa) for a number of hours. During this time, the liberated solution would be undergoing re-equilibration at this higher pressure, with a solid phase of high surface area. As the extractions continue, the first portion of the pore fluids to be released may have time to re-equilibrate at atmospheric pressure and absorb atmospheric oxygen from the interior of the cell and fluid collection system (thus oxidizing to sulphate) .

Of the two explanations discussed, the latter mechanism seems most likely. Dissolution under increased pressure, possibly followed by oxidation to sulphate, may account for the changes in concentration shown by these results.

6.7 The effect of temperature.

The pore solution experiments were performed up to two months hydration and over the same range of compositions and temperatures as those described in other chapters. This is in excess of the time at which a large waste drum (200l) may experience a self - heating effect due to the hydration reactions of

its contents.

Figure 139 shows the change of hydroxyl ion concentration with respect to time for pastes hydrated at elevated temperatures.

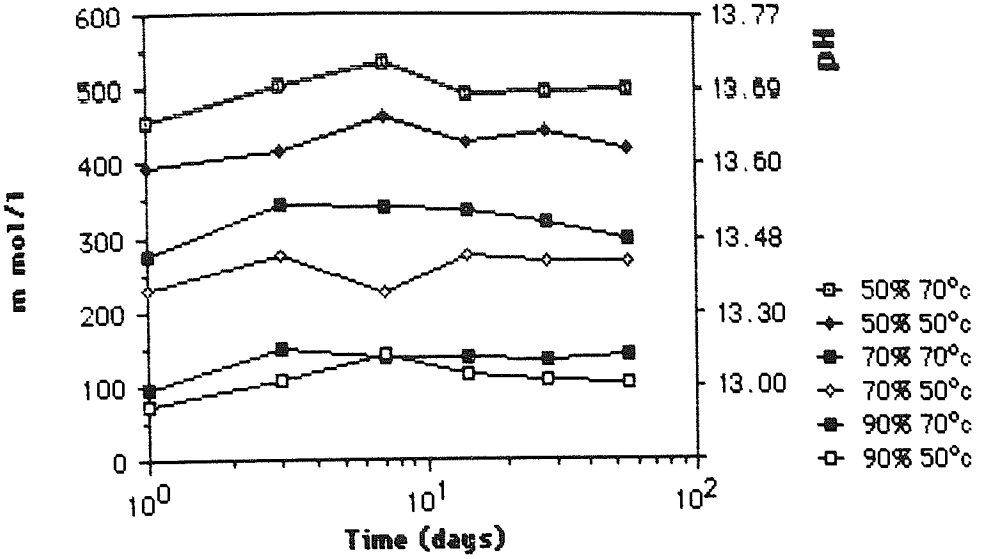

Figure 139 *Hydroxyl ion chemistry at elevated temperatures*

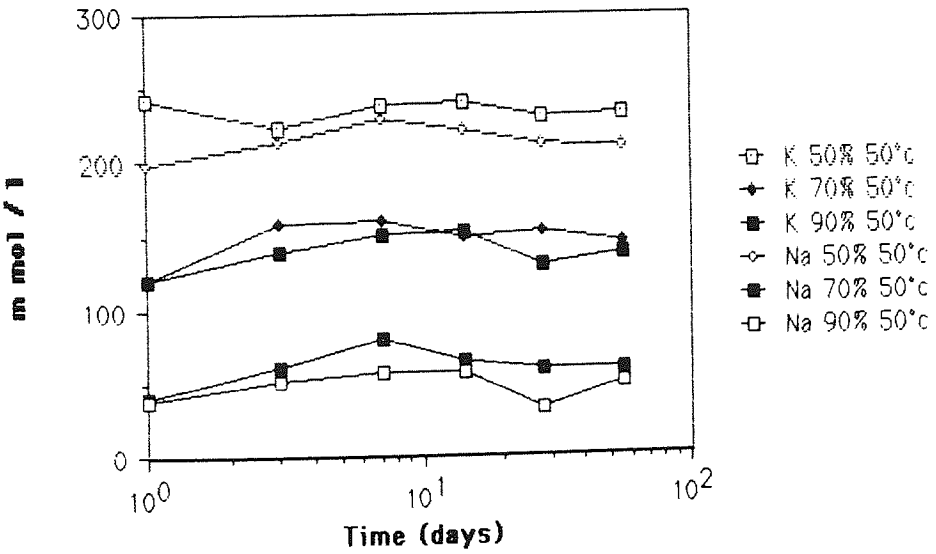

Figure140 *Alkali metal chemistry at 50°C*

The pore solution compositions are dominated by alkali metal hydroxides but as can be seen from the figures (139-141) there is an overall increase in

concentration in comparison with that reported at 25°C. This is to be expected simply from the increase in temperature causing a corresponding increase in the solubility of sodium and potassium hydroxides.

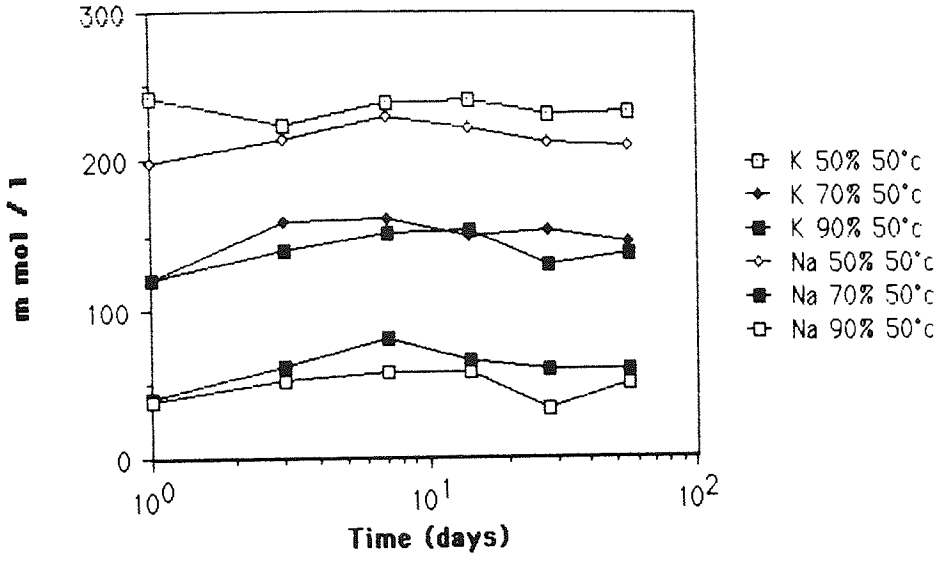

Figure 141 *Alkali metal chemistry at 50°C*

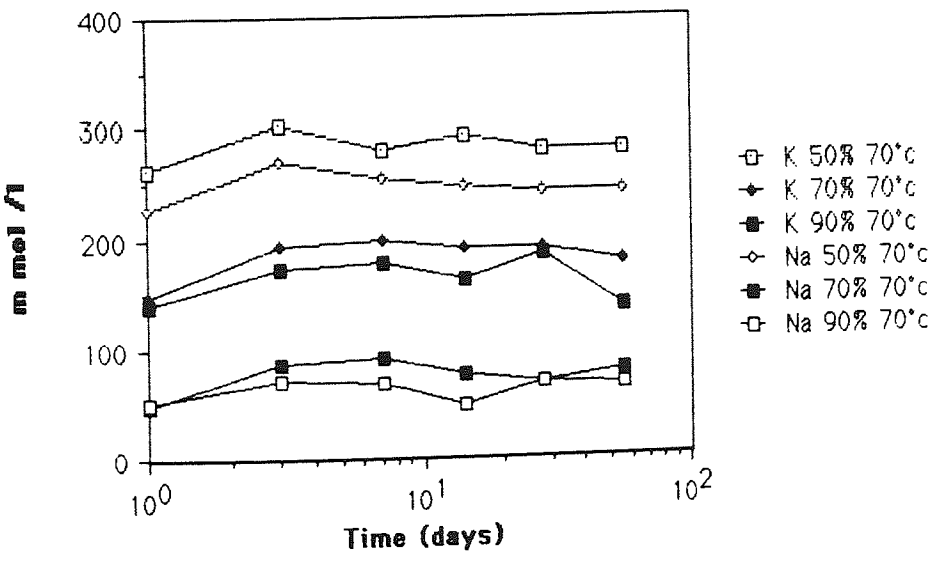

Figure 142 *Alkali metal chemistry at 70°C*

These results show two essential features: First, the overall increase in

dissolved solids, (which can be attributed to a rise in temperature) causing a corresponding rise in pH which, at maximum, is approximately 0.1 unit. The second change is that at elevated temperature, the sodium concentration is approaching that of the potassium. By comparison, at 25°C, the dissolved potassium is roughly twice as concentrated as the sodium (*c.f.* fig 130-131). The thermodynamic studies of C-S-H gel dissolution (10) do not yet allow prediction of dissolution coefficients at a range of temperatures, but the effect can be explained to some extent by the relative solubilities of sodium and potassium hydroxides. As temperature increases, the solubility of sodium hydroxide rises much more rapidly than that of potassium, such that at 50°C, the masses dissolved in water are similar and above this temperature sodium hydroxide is significantly the more soluble.

The relative increase in sodium concentration over potassium seen here is rather less pronounced than that of the simple system described above but this may go some way to explaining these data.

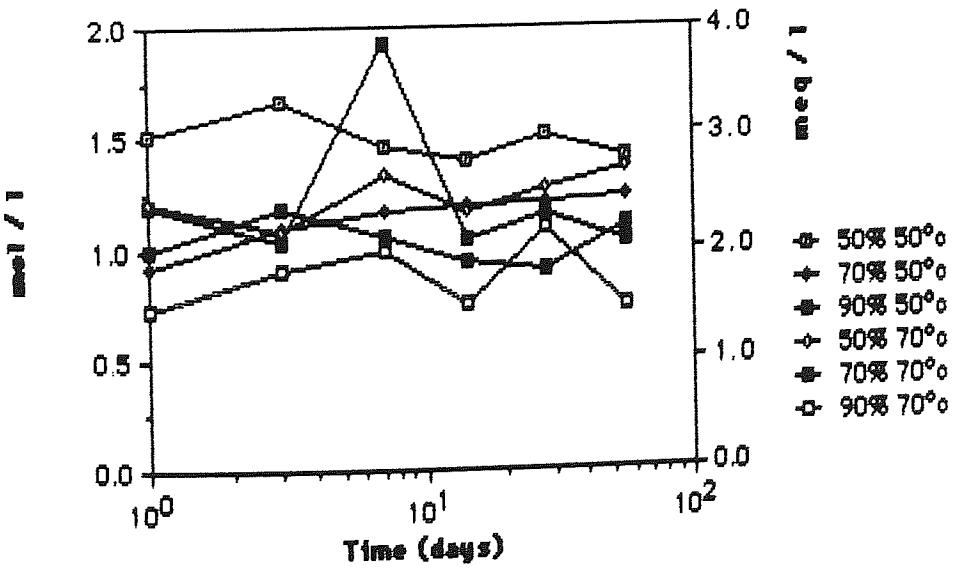

Figure143 *Calcium in solution at elevated temperatures*

As can be seen above, the concentration of calcium falls with increasing

temperature, which is to be expected from the solubility of its hydroxide. The system is still well buffered with respect to calcium at these temperatures although the saturation concentration is suppressed. As with the 25°C samples, no significant changes occur with respect to time.

The sulphur chemistry shows a general increase in solubility of all species and a corresponding decrease in the time to the appearance of the reduced conditions. Figure 145 shows a general increase in the sulphate concentration with time, rising at a similar rate for each composition. The total amount of sulphate in solution is increased with respect to that at 25°c and on this time scale no abrupt changes in composition are seen.

Figures 144-146 show the development of redox potential change at elevated temperature and those ions in solution which are affected by this change. Thiosulphate is present at about 2 mmol/l after one day in the 90% samples and in the 70% sample cured at 70°C. The appearence of this ion occurs more quickly in the high slag or high temperature samples and continues to rise to at least 9.3 mmol/l as shown by the 90% sample cured at 70°C.

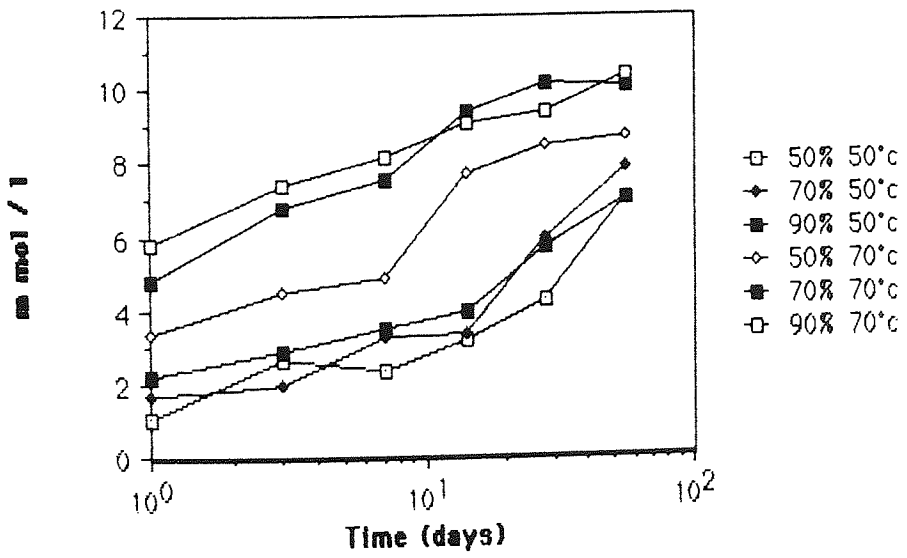

Figure144 *Sulphate ions in solution at elevated temperature*

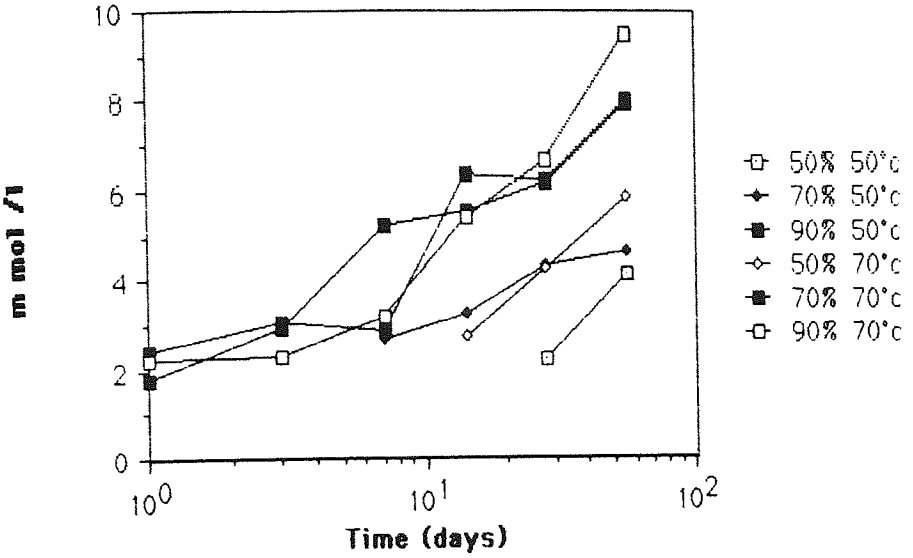

Figure145 *Thiosulphate ions in solution at elevated temperatures*

Comparing figures 143 & 144, the appearence of thiosulphate does not seem to be at the expense of dissolved sulphate ions. This suggests that sulphur containing ions are released by the hydrating material (presumably slag) and that although the hydration reaction has undoubtebly been speeded up by the elevated temperatures, the dissolution of these ions is still occuring after two months.

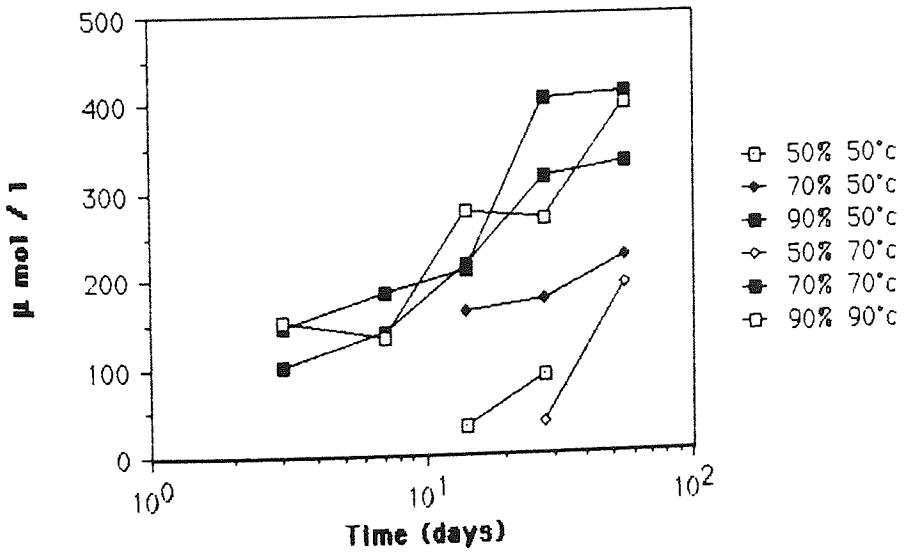

Figure146 *Sulphide ions in solution at elevated temperatures*

The sulphide ions take longer to appear that do the thiosulphate, but are recorded after three days hydration in the high slag blends, taking between four and ten times longer in the lower slag pastes. The concentration range is approximately double that shown at 25°C otherwise the sulphide chemistry shows similar trends at all temperatures. Comparing sulphide and thiosulphate to redox potential reveals that sulphide ions appear at the onset of reducing conditions.

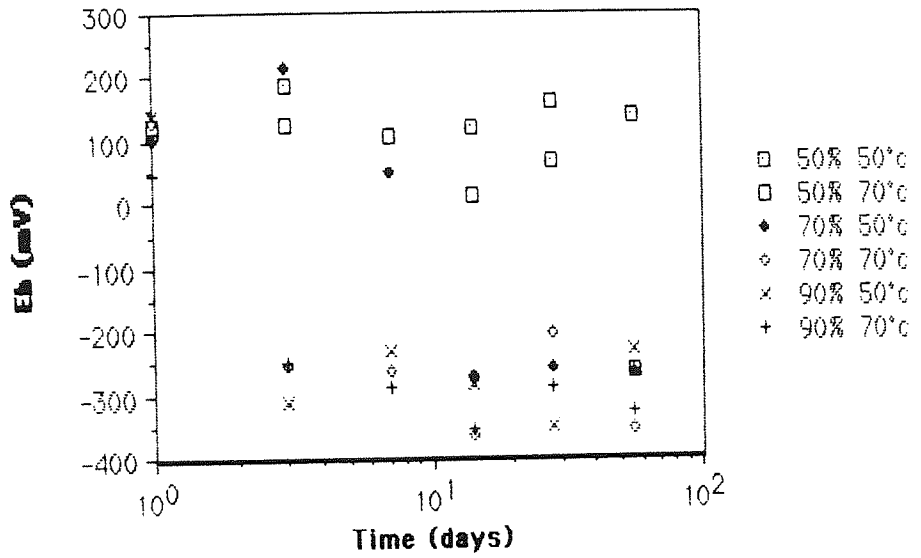

Figure147 *Redox potential measurements at elevated temperatures*

The redox chemistry is similar to that seen at lower temperature in as much as two regions of stable potential occur although the time taken to develop reducing contitions increases with temperature. The potential associated with oxidising conditions ranges from 16 to 214 mV whilst that seen under reducing conditions is between -206 and -365 mV. At one day's hydration the measured potentials are very similar (c100-150 mV) after which, the system develops reducing conditions more rapidly than at 25°C. The 90% pastes show a fall in potential at three days which appears to then be stable. By comparison, the 50%

pastesstay close to their initial potential with the sole exception of the 70°C sample which shows a low potential after 56 days. The 70% samples show behaviour between these two limits, falling after seven and fourteen days for the 50°C and 70°C pastes respectively. As with earlier experiments these changes are reflected by those seen in the sulphur chemistry.

It would appear that as with the samples hydrated at 25°C, there is an overall increase in total dissolved sulphur with time. It cannot be ascertained from these data whether the sulphate ions dissolve as such, or are oxidation products of thiosulphate and/or sulphide. As the changes in sulphur chemistry are more pronounced in pastes containing high proportions of slag, it would seem reasonable to propose that the source of these ions is the slag itself.

Chapter 7

Discussion and recommendations for further work

7.1 General discussion

7.1.1 Kinetics

Chapters 3 & 4 describe two techniques, one novel and one well established, for determining the kinetic parameters of the hydrating system. Both methods have been used to determine apparent activation energies for the hydration of the starting materials and these results are shown below:

Table5 Activation energies for hydration of OPC & BFS

	0%	50%	70%	90%	100%	
Conduction calorimetry	[47.33]	48.76	51.10	52.78	[52.20]	(0.3w/s)
	[39.25]	42.62	47.08	50.9	[ave↑]	(0.4w/s)
Chemical shrinkage	[57.84]	47.68	35.78	37.21	[33.00]	(0.3w/s)
	[46.36]	51.57	51.92	55.33	[55.75]	(0.4w/s)

(All values in kJ/mol) (N.B. Square brackets indicate interpolated data)

Combining these data allows a final estimation of the activation energies by using the whole of table 5 as shown below in figure 147. This gives values of 43 kJ/mol for OPC and 48 kJ/mol for BFS respectively. Figures 148 and 149 show these data replotted with respect to method and water content. The diagrams show that the closest approximations are obtained by calorimetry although the difference between the methods is not great.

Cross-correlating the results as shown in figure 148 reveals a poor correlation (r=0.4) with negative slope as shown by the smaller line "a-a". If the

points shown in the box "c" are disregarded as erroneous, the data replot to give the line "b-b".

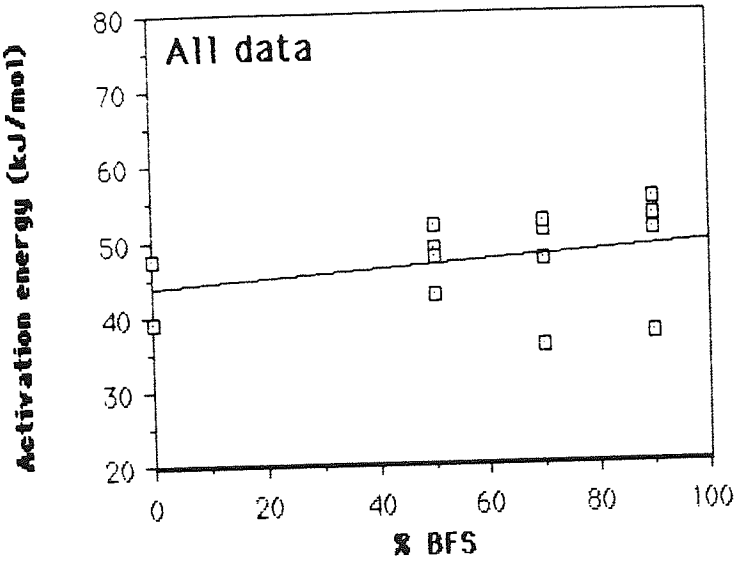

Figure 148 *Estimation of activation energies*

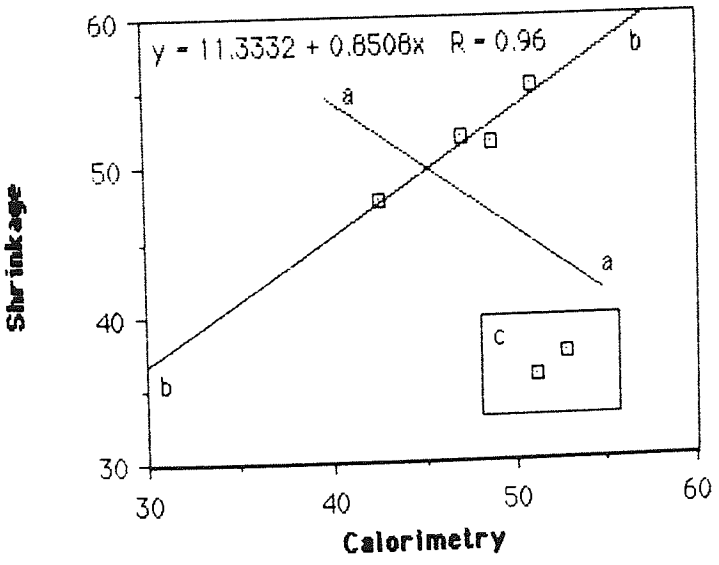

Figure 149 *Correlation of methods to determine activation energies (kJ/mol)*

This approach shows a much higher correlation between the data (r=0.96)

although it is obvious from the gradient that the estimations made by calorimetry are higher than those by chemical shrinkage by a factor of approximately 1.17.

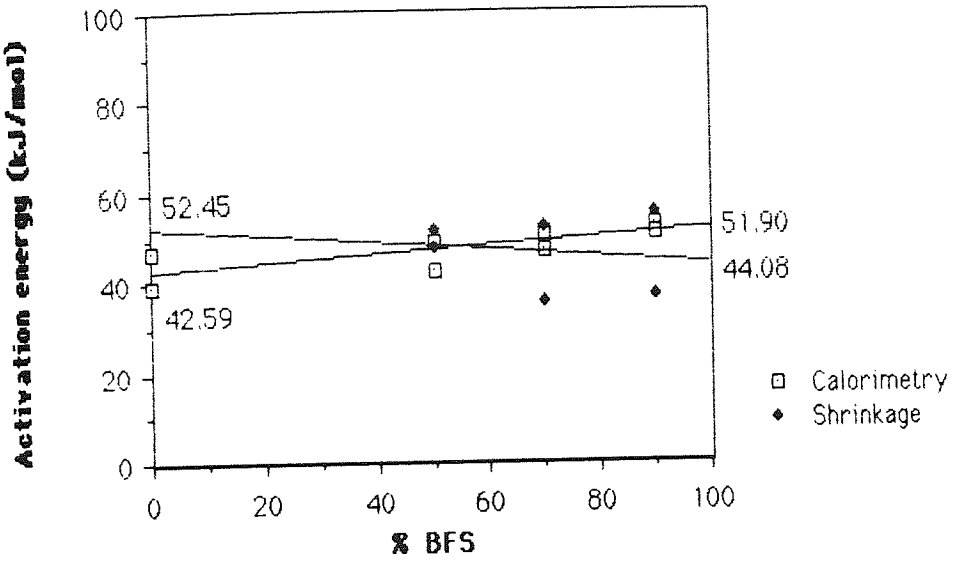

Figure150 *Estimation of activation energies with respect to method*

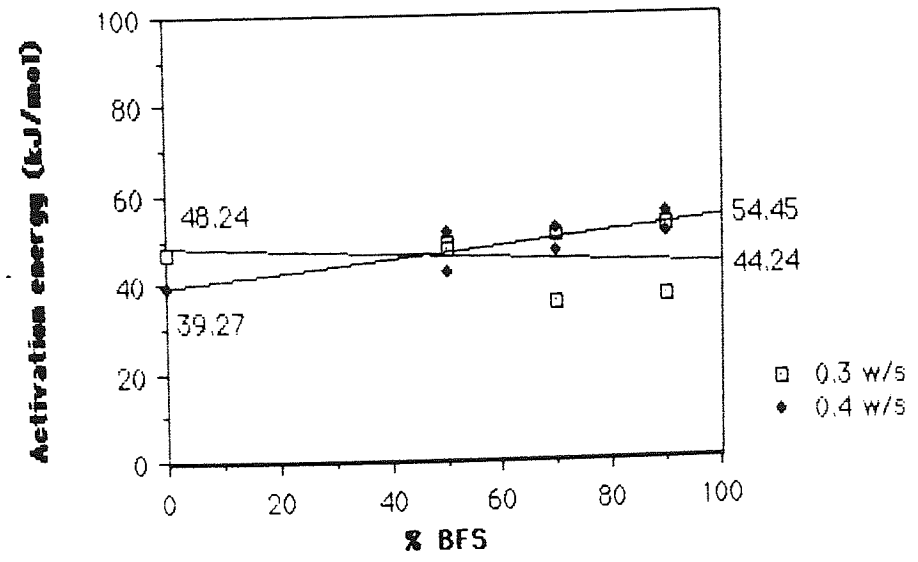

Figure151 *Estimation of activation energies with respect to water content*

Conduction calorimetry is a well established and reliable technique although the instrument used in these experiments would benefit from better data collection facilities. Slight improvements could be made to the system to ensure that the cell has water-tight seals which remain so at elevated

temperatures. A dedicated data collection program capable of performing the numerical calculus required would speed up the data processing enormously. It is absolutely essential that any such program should be able to write data files capable of being read by, or imported to, a proprietry graph plotting package.

Other than the comments above, the method has produced reliable results and yielded credible estimations of activation energy.

The chemical shrinkage method can be criticised for allowing highly alkaline pore solutions to be in contact with the glass for long periods. Dissolution of the soft glass test tubes undoubtably occurs but no published data is yet available which quantifies the significance of this effect. The surface of the glass is very small in comparison with the available surface area of the sample. (Even at very late ages the areas will be different by factors of thousands). Nontheless, after the experiment, the inner surface of the tube appeared frosted and has obviously undergone some dissolution.

In order to quantify this effect, sections were cut through the tubes and then examined by reflected light microscopy. Figure 151 shows a typical section through the glass/paste interface at 150 diameters magnification.

Given that the maximum thickness of the interface was measured at 140μm and that the volume of the paste and average dimensions of the tube are known, it is possible to estimate the volume occupied by the interface.

This represents a maximum volume of 5.08% which, although small, may not be insignificant. In the worst case this would lead to an under-estimation of "Pmax" by c.5% but the additional available volume will, to some extent, be filled with precipitataing hydrates. Geike (74) has found a slight difference in the results when using polycarbonate ware in place of glass, however it must be remembered that the dimensional changes with respect to temperature will also be different. In addition to this, more silicate species will go into solution from the glass (and consequently compete with the hydrating slag for available

hydroxyl ions, thus possibly reducing its reaction rate).

It would be interesting to quantify these changes using Knudsen's automated dilatometers (76), although as shown here and suggested in published work, a large number of experiments would be needed to yield useful results.

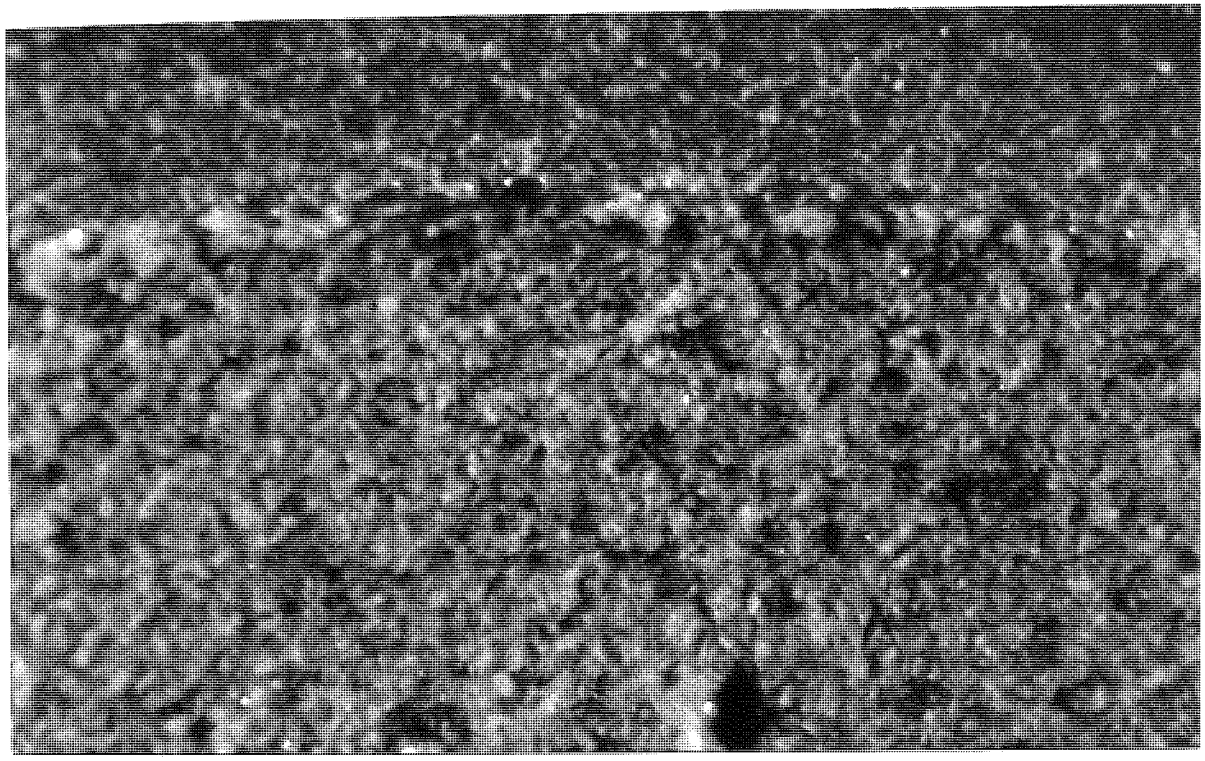

Figure 152 *Horizontal section through paste filled dilatometer tube after end of experiment. Reflected light, oblique illumination from top right, x150 dia.*

In conclusion, these methods provide complementary data and the chemical shrinkage data suggests that the underlying hydration kinetics of the blended system is linear and thus similar to Portland cement hydration. Both methods provide useful estimations of activation energy for the hydrating materials which are close to those reported elsewhere.

7.1.2 Solid phase analysis

The NMR experiments have proved useful in determining the degree of hydration and average chain length of the silicates incorporated in the solid

phase. For the 50% slag replacement, a plateau around 70% hydration was reached after approximately 200 hours. The 90% slag samples take rather longer to reach a stable (and very low) rate of reaction at around 300 hours after which 80% of the slag had hydrated. At these times, the average chain length of the oligomers is close to three silicate units for the 50% samples and four units for those containing 90% slag. The varience of the data is approximately one unit so no great significance is assigned to this difference. These experiments provide a novel insight into the hydration at a molecular level, of a very complex system.

Future experiments should make full use of the data processing facilities now available, which negate the use of the graphical methods to evaluate peak areas as described in chapter five.

Selective dissolution has proved to be a useful tool in directly quantifying the rate of slag hydration. A recent publication (104) suggests that the standard deviation of the data can be reduced by a factor of four over the method employed here and future experiments should adopt this modified method.

The conclusions drawn from these experiments are that both the absolute rate of slag hydration (as measured by the time taken to reach 50% of the apparent maximum) and the ultimate value of this slag hydration increases with the initial slag content. Although the overall hydration is slower in blended cements than that of Portland cement alone, the relative rate of slag hydration depends on the starting composition, such that the BFS fraction in a high slag paste, is consumed more rapidly than that in a lower slag paste. It would seem reasonable tosuggest that when the OPC content far exceeds the BFS content, that a similar increase in slag hydration rate may be observed. Experiments with pastes at low levels of slag replacement are outside the scope of this work but may form the basis of future studies to demonstrate the variation of relative slag hydration rates in pastes of differing composition. It is proposed that a minimum relative rate of slag hydration would be found at a composition containing less than 50% slag.

In addition to these results, the maximum value of the slag hydration is some positive function of the initial slag content (as shown in figure 111, page 186) although this effect is not shown by the 50% samples cured at 70°c. This is probably an erroneous result. As slag content increases, the maxima converge towards approximately 63% hydration for an (albeit hypothetical) paste composed of pure slag. It is interesting to note that a large portion (over one third) of the slag had not hydrated after one year and that increasing the temperature of the system did not appreciably increase the maximum proportion of slag reacted.

The thermal analysis results can be discussed according to the methods employed: First, thermogravimetry shows that calcium hydroxide precipitation occurs rapidly, comprising between four and seven percent of the dry mass after one day's hydration. The maximum concentration is reached within a few (typically 2 to 3) days and its subsequent consumption is a relatively slow reaction. The absolute amount of $Ca(OH)_2$ is dependent on the Portland cement content of the original paste such that high levels of slag replacement yield pastes of lower $Ca(OH)_2$ content. As would be expected, increasing the temperature of the sample correspondingly increases the rate of both the precipitation and dissolution reactions. The continued consumption of $Ca(OH)_2$ at high temperatures, suggests that the slag fraction continues to react at later ages, although this effect has been shown to be small by the selective dissolution experiments.

Secondly, the differential thermal methods show that the unreacted slag fraction can be detected as either the sum of the enthalpies of devitrification, or as the latent heat of fusion and that these quantities are directly proportional to each other (see figure 127, page 199). It is obvious that this could form the basis of a method to determine the relative slag content of a paste, or with calibration against the selective dissolution method, a rapid and reliable method of determining the absolute slag content. To effectively follow slag hydration by this method, it is essential that equipment capable of maintaining a temperature of

1400°C is employed. Work at low temperatures, such as that published by Heinrich and Odler (126), makes the assumption that the slag is exclusively a merwinite glass. To require that all samples are either examined by polarized light microscopy (not an easy task given the small grain size of the sample), or by X-ray diffraction to confirm this, negates any possible time advantage that the thermal method offers over that of selective dissolution. The attraction of differential thermal methods is, in this case, their relative rapidity (typically one and a half hours, of which fifteen minutes is operator time). For the remainder of the run, the equipment may operate un-attended. An instrument capable of high temperature work will reveal both the devitrification peaks (allowing an estimation of the relative mineralogy of the slag to be made) and that associated with the fusion of the glass. Figure 152 below, shows a correlation of the selective dissolution and high temperature thermal analysis results.

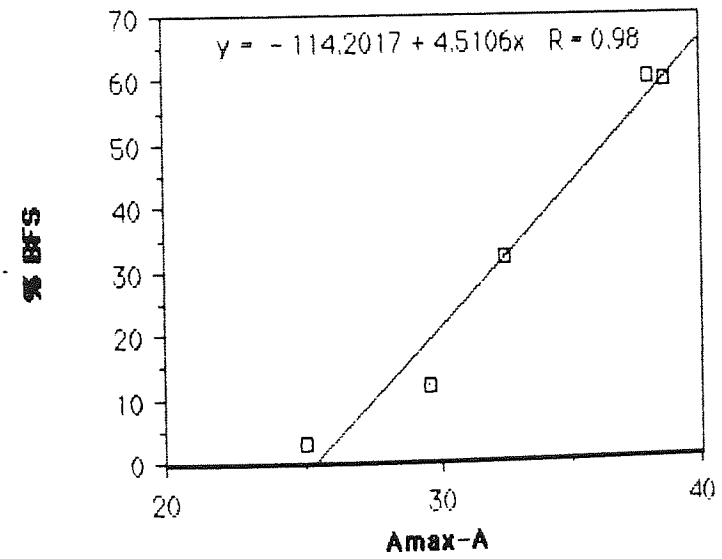

Figure153 *Correlation of heat of fusion and selective dissolution data for 90% BFS pastes cured at 25°c & 0.4 w/s ratio. (Units are those of peak area)*

The vertical axis represents the absolute amount of slag remaining after selective dissolution of the OPC and hydrates, whilst the horizontal shows the

normalized area bounded by the enthalpy of fusion curve found by DSC (plotted as 100% - area). It can be seen that an excellent correlation is found between the two data sets and that in this case 1% slag by weight is represented by 4.5 area units. In practice, this may be converted to joules per kilogramme by measuring the heat of fusion of a non - volatile compound known to melt at approximately this temperature. The heat of fusion of benzoic acid (m.p. 122.13°C) is commonly used, but is inappropriately low for these experiments. A more suitable compound is natural wollastonite, which undergoes a β–γ inversion at 1200.6°C and would therefore provide an enthalpy reference at around the required temperature without the aggressive ions liberated from a molten salt. Degradation of the platinum crucible surface by dissolution in molten salts gives rise to both confusing results and expensive repair bills.

In summary, thermal analyses provide several measurements which are of direct application to hydration studies showing the mineralogical changes in the system with respect to time. Their obvious advantge over classical "wet" techniques is one of time and this may be further optimised by employing modern equipment which combine calorimetric and gravimetric functions in one instrument.

There is a strong correlation between the glass content estimated by thermal and by dissolution methods suggesting that DSC is a suitable technique for the measurement of degree of hydration.

7.1.3 Liquid phase analysis

The pore solution chemistry is in all cases dominated by sodium and potassium hydroxides with calcium as the next most abundant ion. On wetting calcium and sulphate are rapidly released into solution to prevent flash setting of the OPC by the hydration of the aluminate. The solution at this stage is only moderately alkaline but over the first few hours of hydration, the calcium and sulphate are replaced by sodium and potassium hydroxides. The major ion

chemistry is then metastable at around pH 13-13.5 although the continued hydration does gradually incorporate sodium and potassium in the precipitating gel phase. At 25°C, the potassium concentration is to a first approximation, twice that of the sodium. Hydration at elevated temperature relatively increases the solubility of sodium such that its contribution to the metal chemistry is of a similar order to that of potassium.

Calcium in solution reaches a low, stable level of a few milimoles per liter once the sulphate concentration has diminished and will potentially stay at this reduced level of saturation for a very long period as the ion is very well buffered. This ion shows an inverse relationship between solubility and temperature such that its concentration at 70°C falls to approximately 25% of that shown at 25°C.

The sulphur species, by comparison, are all concentrated by raising the temperature of the hydrating system although their behaviour is seen to be more complex. Sulphate is present in all solutions and rises steadily from around 0.5 to 2 mmol/l over the first hundred days or so of hydration. The concentration was then seen to rise progressively to around 5 mmol/l towards the end of the first year. This change remains unaccounted for and does not appear to coincide with any other features of the hydration. As mentioned in chapters 5 & 6 however, Luke & Glasser (103,104) report a renewed burst of activity at around this time. Whatever the cause of this phenomenon, it would seem reasonable to suggest that it is associated with slag hydration as the effect is greatest in the high slag blends and occurs earliest in these samples.

Thiosulphate is absent from many early-age samples as the onset of reducing conditions has not yet prevailed. It appears at approximately 0.5 mmol/l after two days in the high slag blends but may take as long as two weeks to appear in 50% pastes. In all cases the concentration of this ion rises gradually over the course of the first year and the rate of concentration increase diminishes during the latter half of the year. At elevated temperatures, the ion appears

rapidly and its concentration is raised by a factor of approximately four over that seen at 25°C.

The sulphide ion is present in low concentrations, mainly between 50 and 150 µmol/l at 25°C. Its sampling and measurement are limited by the small amounts of liquid available and the use of the analyte addition method in an antioxidant buffer is less than ideal. It is no surprise therefore, not to see a relationship between this ion and the original slag content although the range of values seen are indicative of the likely concentrations in the matrix. The appearance of the ion more or less coincides with the change of redox potential of the system and this can be shown by compiling the data from all compositions and temperatures into a composite diagram as shown below:

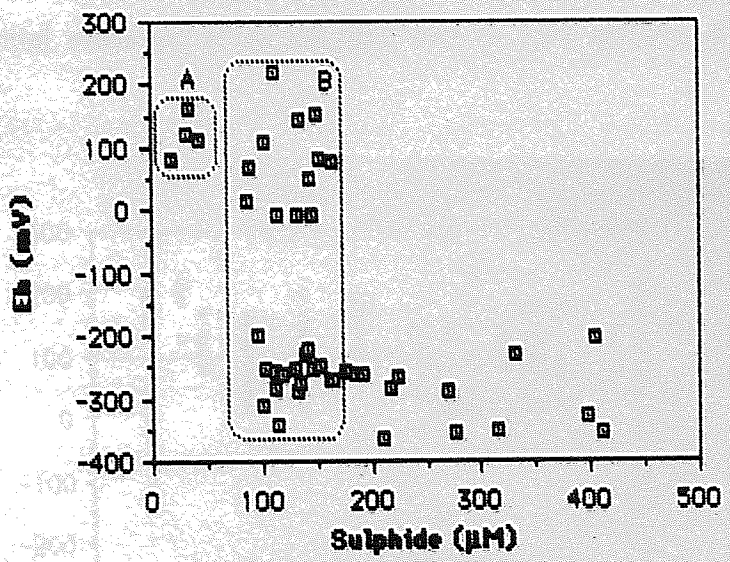

Figure154 *Correlation of sulphide concentration with redox potential measurements*

The majority of sulphide samples are coincident with low redox potential measurements and these are dominantly associated with the high slag content, late-age samples. Some samples do show low sulphide concentrations even under oxidising conditions and these are marked in the figure. Those in box 'A' are of such low concentration as to be disregarded as spurious data, possibly due

to electrode drift or contamination. The box marked 'B' indicates those samples in which sulphide ions have been detected in both oxidising and reducing pore solutions. The probable explaination of this is that as the Eh and sulphide measurements are made independently, the sulphide ion is satisfactorily protected by its antioxidant buffer whilst the poorly poised pore solution reacts with atmospheric oxygen to re-establish a high redox potential. If this was the case, it would be reasonable to expect to record some redox potentials indicating pore solutions undergoing this transition. The twelve samples in which sulphide was detected inspite of there being a high redox potential, do not show any values outside the expected range. Considering the redox potential measurements for the whole data set, it can be shown that there are well defined voltage ranges for the oxidized and reduced conditions. This shows that all the redox potential measurements fall into one of two groups, either oxidized or reduced.

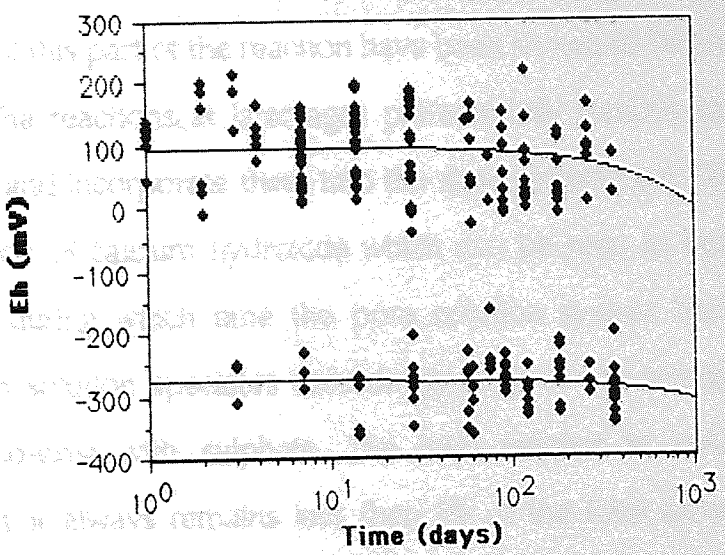

Figure155 *Redox potential with respect to time for all samples*

7.2 Conclusions

The general conclusions from this work are that the Portland cement - blastfurnace slag - water system is one of great complexity where the starting

material compositions are free to vary between limits. The general chemistry of hydration displays rapid dissolution of gypsum followed immediately by the precipitation of aluminate hydrates and the dissolution of alkali metal hydroxides into solution. This initial exothermic phase is followed by a relatively inactive 'dormant' period during which the alkalinity of the solution rises to a plateau value around pH 13 - 13.5. A exothermic period of hydration is associated with the setting of the pastes after which further reactions fall increasingly under diffusion control. In general, the rate of reaction is governed by the starting composition, such that the time to set is inversely related to the slag content. The degree of hydration of the silicates rises steadily at this stage from 20% hydration after one hour (the onset of the dormant period) to a plateau of 60% after around 100 hours. Within this time scale the length of the silicate oligomers is around three units with the proportion of slag hydrated also reaching a plateau of between 45 and 65%. Calcium hydroxide is precipitated along side the gel hydrates and comprises between 6 and 12% by mass after the first hundred hours. The kinetics of this part of the reaction have been shown to be linear.

The reactions at later ages preferentially remove the alkali metals from solution and incorporate them into the slow growing gel. There is also a gradual dissolution of calcium hydroxide which can be seen to occur over a period of months during which time the pore solution system becomes reducing. The sulpur in solution speciates accordingly to produce sulphide and thiosulphate which co-exist with sulphate. The total sulphur in solution rises gradually although it always remains less than 1% of the total anion composition. After some six months hydration there is a rise in sulphate concentration which is so far unexplained.

7.3 Recommendations for further work

An interesting development of the kinetic work would be to combine

results of the absolute rate of slag hydration such as those reported from selective dissolution and/or thermal analysis with analogous work on Portland cement such as may be obtained from x-ray diffraction studies. This would allow the kinetic model to be refined to incorporate results from the individual cement minerals and to examine their reaction with different slag compositions. Early-age data should be obtained by quenching the reaction in a solvent or possibly by rapid freezing.

If such a study was to incorporate dilatometry experiments, then much attention should be given to the possibility of an automated experimental system. This would allow a large number of samples to run in such a way that data collection and subsequent processing was relatively simple and thus allow for statistically excellent data reduction.

The experimental programme would benefit from calorimetric data collected during the early stages of hydration. The existing apparatus can be readily modified to provide such results and correlation of these data with x-ray diffraction studies should yield kinetic information on the hydration of the components of the mixture.

Work on surface analysis of hydrating slag grains is surprisingly sparse. A simple set of experiments comparing the effect of various drying methods on surface morphology of grains hydrated in suspension with an 'artificial' pore solution should determine the least aggressive technique. Once this has been proved, auger and x-ray photoelectron spectroscopy may be used to determine the ultimate fate of the alkali metals located in the hydrates such as that reported by Regourd (85)

Spectroscopic methods such as Fourier transform infra-red and laser Raman techniques offer two tantalising areas which have not been fully explored: In the first instance, FTIR could be used to examine the developing Nature of bonding during hydration for the individual components and their

mixtures. This would be useful in a non-crystalline system and would therefore support NMR studies. The results could be used to compare the hydration of slag grains both in a Portland cement mixture and an artificial pore solution. The second application is that of laser Raman microscopy. Individual grains, or grain clusters may be removed from suspension and scanned to determine inhomogeneities in their structure. The method is currently being evaluated in the USA on unhydrated material and extending this work to include slag hydrates would be a valuable complement.

The nuclear magnetic resonance experiments promise a great deal of structural information on the hydrating system. The next set of experiments should include Aluminium-27 spectra with proton spin-decoupling to produce pseudo three dimensional spectra. This would show which of the structural units in the aluminate (and/or silicate) chains are associated with protons. The significance of this is that the site of the hydration reaction can be located with respect to the growing polymer. A similar '2D' plot could be obtained for decoupled ^{29}Si and ^{27}Al spectra in order to investigate the degree of branching with respect to time. Reference to the 'chain crossing element' of figure 4, page 27, shows that the metallic nature of aluminium leads to its rôle as a site of chain crossing (Dron, 29). A ^{29}Si - ^{27}Al 2D plot would show which silicate units were closely associated with which aluminate units and in what proportion. This information could be used to estimate the degree of chain branching with respect to the degree of hydration.

The method may be developed along these lines to incorporate the group I and II metals but the sensitivity will be low due to the low concentrations in the sample and the low isotopic abundance of suitable nucei.

Further experiments in pore solution chemistry could be directed towards a quantitative accounting for the rôle of sulphur in hydration. The presence of polysulphides in aqueous solution has not been satisfactorily confirmed or

denied. The adoption of an NMR method may provide a simple answer to this question. If sufficiently large quantities of pore solution were recovered, ^{33}S NMR may detect the presence of polysulphide chains.

The origin of the sulphur species could be determined by hydrating a system in which some of the sulphur had been isotopically labled. The easiest rôute would be to use pure cement minerals interground with $Ca^{36}SO_4$ inplace of natural gypsum. The sulphur-36 would be detected by mass spectroscopy of the ionic fractions separated on an ion exchange column. An alternative method would be to radio-label the sulphate with sulphur-35 ($t_{1/2}$ = 87d) which is a low energy β-emitter and could thus be detected by liquid scintillation counting. Either technique would show whether the source of any of the sulphur anions was the gypsum in the cement or, by implication, the slag. An attraction of the radiochemical method is the possible use of auto- radiolysis on the solid phase as part of the same experiment. By coating a fracture surface of the dried solid with a photographic emulsion, it may be possible to locate preferential sites of ^{35}S precipitation. It would be reasonable to expect that the aluminate and alumino-hydrate phases would scavenge sulphate from solution early in their hydration. This approach may prove that the gypsum is the source of the ion as the slag had had insufficient time to contribute any sulphate. A study of the morphologies and distribution of any radioactive phases would be an essential part of such a study.

Any future pore solution work would benefit from an anoxic sample squeezing and handling system. The purging of the pore-press with (say) nitrogen before applying the load, will undoubtedly require modifications to the structural metal work. This in turn could cause problems due to either failure of the components or by contamination from poor cleaning of inaccesible gas ports or valves. A modification of this type therefore, requires the most careful design. Subsequent sample handling and analysis must similarly be done with the exclusion of atmospheric oxygen and carbondioxide, which would be extremely

time consuming. The results would however, show very quickly whether the data varied significantly from those obtained under a normal atmosphere. It is suggested that overall ionic balance could be improved by reducing the carbonation of the pore solution during handling and titration. It would also be interesting to know if the sulphur speciation is changed by the exclusion of atmospheric oxygen. It was suggested in chapter 6 that the variations seen in sulphide concentrations are due to the uptake of oxygen by the sample. Performing similar experiments under a controlled atmosphere would give some idea of the magnitude of this effect.

Finally, future studies need to be of a much longer duration. The application of these materials to the encapsulation of radioactive materials cannot be addressed by laboratory studies alone because of the extensive half-lives of some actinide species. Long term laboratory studies must run in conjunction with the development of predictive models of the behaviour of blended cement systems. The hydration reactions comprise only one area of study during modelling of the source term and near field. The developing microstructures, available water, corrosion reactions of components within the matrix and of the matrix containers, radiolytic oxidation, radiolysis of water and hydrogen liberation, diffusion of mobile species and many other factors are of immediate concern just within the waste drum.

The possible factors to be modelled in the planning of a working repository are legion and one strength of a developing model must be its flexibility. If nuclear waste management is to be based on the results of predictive modelling, then the ability of the models to expand and adapt to new data and new questions cannot be understated.

References

In the list which follows, certain of the major conference proceedings have been abreviated as shown below:

Proceedings of the 7th. International Congress on the Chemistry of Cements, Paris, 1980. (Publ. Editions Septima. Paris)

Becomes: Proc. 7th. ICCC., Paris, 1980.

Proceedings of the 8th International conference on the Chemistry of Cements, Rio de Janeiro, 1986.

Becomes: Proc . 8th. ICCC., Rio, 1986.

Proceedings of the First CANMET/ACI International Conference on Fly Ash, Silica Fume, Slag and Natural Pozzolans in Concrete., Montebello, 1983. (Publ. ACI/CANMET ref: SP79/51).

Becomes: Proc. 1st. CANMET/ACI conference, Montebello, 1983

Proceedings of the Second CANMET/ACI International Conference on Fly Ash, Silica Fume, Slag and Natural Pozzolans in Concrete., Madrid, 1986. (Publ. ACI/CANMET ref: SP91).

Becomes: Proc. 2nd. CANMET/ACI conference, Madrid, 1986

Proceedings of the Third CANMET/ACI International Conference on Fly Ash, Silica Fume, Slag and Natural Pozzolans in Concrete., Trondheim, 1989. (Publ. ACI/CANMET ref: SP114/61).

Becomes: Proc. 3rd. CANMET/ACI conference, Trondheim, 1989.

The book series "Scientific Basis for Nuclear Waste Management", Published in the USA by "The Materials Research Society" is abbreviated to: SBNWM followed by the volume number and year of publication.

List of references cited in text

(1) Frodingham Cement Company (Product information brochure) "Cemsave" 1986.

(2) Thomas., G.H. "Dry Granulation". Presentation No.3 at "Workshop on Blastfurnace Slag Cements", York, 14-17 October 1985 (Proceedings not published).

(3) Haynes., D.J. "Aspects of blast furnace burdening and constraints on chemical composition". Presentation No.1 at "Workshop on Blastfurnace Slag Cements, York, 14-17 October 1985 (Proceedings not published).

(4) Frigione., G. "Manufacture and characteristics of Portland Blast-Furnace slag cements" in: "Blended cements" ASTM STP 897 (Ed. Frohnsdorff., G) Philadelphia 1986 pp 15-28.

(5) Lea F.M., "The Chemistry of cement" London. Arnold. 1970. pp 454-489.

(6) Czernin., W. "Cement Chemistry for Civil Engineers". London Crosby Lockwood & Son. 1962. pp 105-112.

(7) Daube., J. & Bakker., R. "Portland Blast Furnace Slag Cement: A Review" in: "Blended cements" ASTM STP 897 (Ed. Frohnsdorff., G) Philadelphia 1986 pp 5-14.

(8) Cannon., R.P. "Ground Granulated Blastfurnace Slag - Its supply, Properties and Trends in the UK" (Document prepared for: Philip Owens & Partners" Presentation No.8 at "Workshop on Blastfurnace Slag Cements", York,

14-17 October 1985 (Proceedings not published).

(9) Reeves., C.M. "How to make today's concrete durable for tomorrow" (Seminar offprint) The institution of Civil Engineers, 8th May 1985, London.

(10) Glasser., F.P. et.al. "Immobilization of radioactive waste in cement-based matrices" Report to The Department of The Environment, Commission of The European Communities DOE/RW/85.189. 20th November 1985

(11) Smolczyk,H.G. "Slag structure and identification of slags" 7th ICCC, Paris, 1980. III - 1 pp. 3 - 17

(12) Prince., A.T. "Liquidus relationships on 10% MgO plane of the system Lime - Magnesia - Alumina - Silica" J. Am. Ceram. Soc. 1954 37 (9) pp 406 - 408

(13) Czernin., W. "Cement Chemistry for Civil Engineers". London Crosby Lockwood & Son. 1962. pp 107.

(14) Hooton., R.D. & Emery.,J.J. "Glass content determination and strength development predictions for vitrified blast furnace slag" Proc 1st CANMET/ACI conference, Montebello, 1983. pp.943-962

(15) Frearson J.P.H. & Uren J.M. "Investigations of a ground granulated blast-furnace slag containing merwinitic crystallisation" Presentation No.6 at "Workshop on Blastfurnace Slag Cements, York, 14-17 October 1985 (Proceedings not published).

(16) Frearson J.P.H.; Sims.,I & Uren J.M. "Development of test procedures to determine the glass content of ground granulated blast furnace slag" Proc. 2nd.

CANMET/ACI conference, Madrid, 1986. pp.1401-1421

(17) Van Roode.,M., Douglas.,E. & Hemmings.,R.T. "X-ray diffraction measurement of glass content in fly ashes and slags" Cem. Concr. Res. 1987 17 p.183-197

(18) Van Loo "Glass content and hydraulicity in Blastfurnace slag" Seminar CEMBUREAU University of Technology 1977 Eindhoven. Unpublished

(19) Porai - Koshits., E.A. (1959) "On the structure of silicate glasses" Glasstech Ber. 32 pp.450 - 456

(20) Sersale., R. "Aspects of the chemistry of additions" pp. 537 - 568 in "Advances in cement technology" ed. Ghosh., S.N. publ. Pergamon, Oxford, 1983. 751pp.

(21) Dron.,R. "Structure et réactivité des laitiers vitreux" PhD Thesis. Paris VI. Janvier 1984.

(22) Scott., P.W. et. al. "Microstructure and phase relations of some granulated and pelletised blastfurnace slags" Presentation No.5 at "Workshop on Blastfurnace Slag Cements, York, 14-17 October 1985 (Proceedings not published). and- Mineralogical Magazine (in prep)

(23) Frearson J.P.H.; Sims.,I & Uren J.M. "Development of test procedures to determine the glass content of ground granulated blast furnace slag" Proc. 2nd. CANMET/ACI conference, Madrid, 1986. pp.1401-1421

(24) Sersale., R. and Frigione., G. "Microstructure and properties of hydrated

cements with different slag content" 7th ICCC, Paris, 1980. II - 3/63-68

(25) Satarin., V.I. "Slag-Portland Cements" 6th ICCC, Moscow, 1974. 1. pp 1-51

(26) Regourd., M. "Structure and behaviour of slag Portland cement hydrates" 7th ICCC, Paris, 1980. III - 2/10-26

(27) Regourd.,M "Ciments speciaux et ciments avec additions" 8th ICCC, Rio, 1986. 3.1 pp.190-229

(28) Roiak., S.M. & Chkolnik., J.Ch. "Influence des particularités physiques et chemiques des laitiers de haut fourneau sur leur activité hydraulique" 7th ICCC, Paris, 1980. III pp. 74 - 77

(29) Regourd., M. "Slags and slag cements" EMMSE module, Paris 1980 pp 1-23

(30) Dron., R. "Strucure et réactivité des laitiers vitreux" 1984 Ph.D thesis, Paris IV

(31) Scheetz., B.E. "Applications of laser Raman microscopy to cement studies" Proc. 2nd. CANMET/ACI conference, Madrid, 1986 Supplimentary

(32) Hemmings., R.T. & Berry., E.E. - Preliminary report of selective dissolution experiments Proc. 2nd. CANMET/ACI conference, Madrid, 1986 Supplimentary

(33) Bogue., R.H. "The chemistry of cements" (1955) Reinhold Publishing. New York. 351pp.

(34) Ghosh., S.N. (ed) Advances in cement technology, Pergamon Press, Oxford, 1983, 751pp.

(35) Bye., "Portland cement" Pergamon Press, Oxford, 1983, 145pp.

(36) Czernin., W. "Cement Chemistry for Civil Engineers". London Crosby Lockwood & Son. 1962. 139pp.

(37) Gribenshikov., R. Uzbek Khime Zh. SSSR 14 35 1970 (Reviewed by Ghosh, ref. 34)

(38) Regourd,. M. "Crystal chemistry of Portland cement phases" pp. 109-138 in Barnes., P. (ed.) "Structure and properties of cement" Elsevier, Amsterdam, 1983, 291pp.

(39) Regourd., M & Guinier., A. "The crystal chemistry of the constituents of Portland cement clinker" Proc. 6th. ICCC., Moscow 1974.

(40) Tarte., P. 1968. "Structure and composition of tricalcium silicate"Silic. Ind. 33 pp. 333

(41) Sakurai,.T & Sato.,T. "Minor constituents of the ferrite phase in Portland cements" Proc. 5th. ICCC.,Tokyo 1969. v1. pp.61

(42) Regourd., M. "Microstructure and properties of cements, mortars and concretes". Cim. Beton. Platres. Chaux. 734 pp. 41 -48

(43) Forest., J. "Structure and composition in dicalcium silicate" Silic. Ind. 32 1967 pp.373

(44) Boikova., A.I. "Cement minerals of complicated composition" Proc. 7th ICCC, Paris, 1980. II pp. 6 - 11

(45) Tamas., F. et. al. "Polycondensation of Si-O anions in the hardening of cement pastes from alite and β-belite" Tsement 3 1988 pp. 18 - 19

(46) Jennings., H. M. & Pratt., P. L. "On the reactions leading to calcium silicate hydrate, calcium hydroxide and ettringite during the hydration of cemnt" Proc. 7th ICCC, Paris, 1980. II pp. 141 - 146

(47) Double., D.D. & Hellawell., A. "An osmotic mechanism for cement hydration" Nature 1976 261 pp.486

(48) Powers., T.C. "Mechanisms of Portland cement hydration" J. Portland Cement Association Research & Development Laboratories 1961 3 pp. 47

(49) Double., D.D et. al. "The hydration of Portland cement. Evidence for an osmotic model" Proc. 7th ICCC, Paris, 1980. II pp. 256 - 260

(50) Birchall., J.D. et. al. "Some general considerations of a membrane/osmosis model for Portland cement hydration" Cem. Concr. Res. 10 1980 pp. 145 - 155

(51) Double., D.D "New developments in understanding the chemistry of cement hydartion" Phil. Trans. Roy. Soc. Lond. A 310 1983 pp. 53 - 66

(52) Barnes., P. et. al. "Cement tubules, another look" Cem. Concr. Res. 10 1980 pp. 639 - 645

(53) Skalny., J. & Young., J.F. "Mechanisms of Portland cement hydration" Proc. 7th ICCC, Paris, 1980. I pp. 1 - 45

(54) Stein., H.N. & Stevels., J.M. "Mechanisms of Portland cement hydration" J. Appl. Chemistry (London)1964. 14 pp 338

(55) Taylor., H.F.W. "Physical chemistry of hydration process; Influence of minor components and admixtures." Proc. 8th ICCC, Rio, 1986. I pp. 82 - 112

(56) Skalny., J. : Jawed., I. & Taylor., H.F.W. World Cement Technology 9 1978 pp. 183. [Reviewed by Jawed., I. : Skalny., J and Young., J.F. - Chapter 6 (pp. 237 - 311) in Barnes., P., "Structure & properties of cement" 1983 Applied Science Publishers. London. 488pp.]

(57) Breval., E. "C3A Hydration" Cem. Concr. Res. 6 1976 pp. 129 - 138

(58) Copeland., L.E. et. al. "Chemistry of hydration of Portland cement" Proc. 4th ICCC, Washington, 1960. I pp. 429 - 465

(59) Rogers., D.E. & Aldridge., L.P. "Hydration reactions of dicalcium ferrite" Cem. Concr. Res. 7 1977 pp. 399 - 404

(60) Regourd., M. et. al. "Hydration of C3A in synthetic mixtures and in industrial Portland cements" Proc. 7th ICCC, Paris, 1980. IV seminar A

(61) Roy., D. M. & Parker., K.M. "Microstructure and properties of granulated slag - Portland cement blends at normal and elevated temperatures. Proc. 1st. CANMET/ACI conference, Montebello, 1983 pp.397 -413

(62) Roy., D.M. & Idorn., G.M. "Hydration, strucure and properties of blast furnace slag cements, mortars and concrete." Am. Concr. Inst. J. 11/12 1982 pp.444-457.

(63) Regourd., M. et.al. "Caractérisation et activation thermique des ciments au laitier" Proc. 7th ICCC, Paris, 1980. III pp.105-11.

(64) Roy., D.M. & Parker., K.M. "Microstructure and propoerties of granulated slag-Portland cement blends at normal and elevated temperatures" Proc. 1st. CANMET/ACI conference, Montebello, 1983 pp. 397-414.

(65) Wu., X.; Roy., D.M. & Lanton., C.A. "Early stage hydration of slag cement" Cem. Concr. Res. 13 (2) 1983 pp.277-286

(66) Totani., Y. et.al. "The hydration of blast furnace slag cement" Proc. 7th ICCC, Paris, 1980. III pp.95-98.

(67) Courtault., B. & Briand., J.P. "Etude de gaz des laitiers granulés de haut forneau" Ciments, Betons, Platres, Chaux, (Paris) 717 1979 pp.87-98

(68) Roy., D.M. & Idorn., G.M. "Development of structure and properties of blast furnace slag cements" International conference on slag and blended cements, Birmingham Alabama Feb 18-19 1982. Proc. pp. 1-39

(69) Lee., D.J. & Palmer., J.D. "Studies on the hydration of slag cements at high replacement levels" Presentation No.11 at "Workshop on Blastfurnace Slag Cements, York, 14-17 October 1985 (Proceedings not published).

(70) Totani., Y. et.al. "The hydration of blast furnace slag cement" Proc. 7th.

ICCC., Paris, 1980. III pp. 95-98.

(71) Douglas., E. et. al. "Charaterization, conduction calorimetry , micro-structure and properties of ground granulated blastfurnace slags and fly ashes" Proc. 3rd. CANMET/ACI conference, Trondheim, 1989. pp. 618-641

(72) Kokubu., K. et. al. "Effect of curing temperature on the hydration and adiabatic temperature characteristics of Portland cement - blast furnace slag concrete" Proc. 3rd. CANMET/ACI conference, Trondheim, 1989. pp. 1361 - 1376

(73) Skalny., J & Brophy., J. E. "Hydration of Portland and blended cements" International conference on slag and blended cements, Birmingham Alabama Feb 18-19 1982. Proc. pp. 1-16.

(74) Setter., N. & Roy., D.N. "Mecanical features of chemical shrinkage of cement paste" Cem. Concr. Res. 8 1978 pp. 623 - 634

(75) Geiker., M. & Knudsen., T. "Chemical shrinkage of Portland cement pastes" Cem. Concr. Res. 12 1982 pp. 603 - 610

(76) Geiker., M. "Studies of Portland cement hydration, measurements of chemical shrinkage and systematic evaluation of hydration curves by means of the dispersion model " 1983 Licenciat afhandling, Institutet for mineralindustri, Danmarks Tekniske Højskole [Ph.D. Thesis, Danish Technical University, Lyngby DK-2800]

(77) Knudsen., T. et. al. "Metode til prøvning af reaktivt tilslag" Dansk Beton 3 1985 pp. 15 - 19.

(78) Geike., M & Knudsen., T "Chemical shrinkage" Presentation to "The Engineering conferences, Henniker, USA, Aug 1985. (Unpublished)

(79) Knudsen., T. "On the possibility of following the hydration of fly ash, microsilica and fine aggregates by means of chemical shrinkage". Internal report, 1986 Technical University of Denmark. 3pp.

(80) Knudsen., T & Geiker., M. "Chemical shrinkage as an indicator of the stage of hardening" in prep. - pre print.

(81) Knudsen., T. "A continuous method for the characterisation of the alkali-silica reactivity of aggregates" Proc. 7th International Congress on Alkali-Silica Reactions, 18th - 23rd August 1986, Ottowa, Canada. pp.77-81

(82) Malhotra., V.P. et. al. "Plaster of Paris activated supersulphated slag cement" Cem. Concr. Res. 12 1982. pp. 463 - 473

(83) Atkins., M. et. al. "Chemical modelling in blended cement systems" Proc. 3rd. CANMET/ACI conference, Trondheim, 1989. pp. 73-95

(84) Teoreanu., I "Hydrated phases in slag - water - activator systems Proc. 7th. ICCC, Paris, 1980. III pp. 99 - 104.

(85) Regourd., M. "Structure and behaviour of slag - Portland cement hydrates". Proc. 7th. ICCC, Paris, 1980. III pp. 10 - 26.

(86) Regourd., M. "Blast furnace slag hydration - surface analysis" Cem. Concr. Res. 1983 13 (4) pp. 549 -556

(87) Regourd., M. et. al. "Study of the early hydration of Ca_3SiO_5 by x-ray photoelectron spectrometry". Cem. Concr. Res. 1980 10 (2) pp. 223 - 230

(88) Regourd., M. et. al. "X-ray photoelectron spectrometry investigation of the early stages of C_3S hydration - The role of NaF admixture. Proc. 7th. ICCC., Paris, 1980. III pp. 123 - 128

(89) Regourd., M. "Microanalytical studies (x-ray photoelectron spectrometry) of surface hydration reactions of cement compounds". Phil. Trans. R. Soc. Lond. A 310. 1983 pp. 85-92.

(90) Dron., R. & Brivot., F. "Approche du probleme de la réactivité du laitier granulé". Proc. 7th. ICCC., Paris, 1980. III pp. 134 - 139

(91) Tanaka., H. et. al. "Structure of hydrated glassy blastfurnace slag in concrete" Proc. 1st. CANMET/ACI conference, Montebello, 1983 pp. 963 - 977

(92) Ludwig., U. "Slag cements - hydration and durability" Presentation No.13 at "Workshop on Blastfurnace Slag Cements", York, 14-17 October 1985 (Proceedings not published).

(93) Schweite., H.E. et. al. "Neubildungen bei der hydration von hochfenschlacken" Zement - Kalk - Gips 4 1969 pp.154 - 161

(94) Mascolo., G. & Marino., O "MgO - bearing phases in the hydration products of slag cement". Proc. 7th. ICCC., Paris, 1980. III pp. 58 - 62.

(95) Satarin., V.I. "Slag - Portland Cements" Proc. 6th. ICCC., Moscow, 1974. I pp. 1 - 51.

(96) Ben - Dor., L. "Electron and optical microscopy" pp. 733 - 792 in - "Advances in cement technology" ed. Ghosh., S.N. publ. Pergamon, Oxford, 1983. 751pp.

(97) Regourd., M. et al. "Microstructure of slag cements" Cim. betons, platres, chaux, 699 1976 pp. 83 -86.

(98) Sersale., R. et. al. "Microstructure and properties of hydrated cements with different slag contents" Proc. 7th. ICCC, Paris, 1980. III pp. 63 - 68.

(99) Lou., Z. "On ettringite modification of slag cement" Proc. 7th. ICCC, Paris, 1980. III pp. 82 - 87.

(100) Kondo., R. & Ohsawa., S. "Studies on a method to determine the amount of granulated blast furnace slag and the rate of hydration of slag in cements" Proc. 5th. ICCC, Paris, 1968. IV Supplementary paper IV-106 pp. 255 - 262.

(101) Daimon., M. "Mechanism and Kinetics of slag cement hydration" Proc. 7th. ICCC, Paris, 1980. III pp. 1 - 9.

(102) Demoulian., E. et. al. "Détermination de la teneur en laitier dans les ciments par dissolutions sélectives" Proc. 7th. ICCC, Paris, 1980. III pp. 151 - 156.

(103) Luke., K. & Glasser., F.P. "Selective dissolution of hydrated blast furnace slag cements" Cem. Concr. Res. 17 (2) 1987. pp. 273 - 282

(104) Luke., K. & Glasser., F.P. "Internal chemical evolution of th constitution of blended cements" Cem. Concr. Res. 18 1988. pp. 495 - 502

(105) Voinovitch., I.A. & Dron., R. "Action des différents activants sur l'hydration du laitier granulé" Bull. Liason Labo. Ponts. et Chauss. 83 mai - juin 1976 Réf 1810 pp. 55 - 58

(106) Voinovitch., I.A. & Dron., R. "Action des différents activants sur l'hydration du laitier granulé". Silicates Ind, 41 1976 pp. 209 - 212

(107) Vernet., C. et. al. "Cinetique de l'hydration des ciments au laitier" Proc. 7th. ICCC., Paris, 1980. III pp. 128 - 133.

(108) Masson., C.R. "Ionic equilibria in liquid silicates" J. of the Amer. Ceram. Soc. 1968. 51 (3) pp. 134 -143

(109) Stade., H. & Wieker., W. "On the strucures of ill crystallized calcium hydrogen silicates. I - Formation and proerties of an ill crystallized calcium hydration disilicate phase." Z. anorg. allg. chem., 1980 466 pp. 55 - 70

(110) Glasser F.P. et. al. "Immobilization of radioactive waste in cement based matrices" DOE report June 1985 144pp. DOE-RW-85.063

(111) Longuet., P et. al. "La phase liquide du ciment hydraté" Rev. des materiaux et des travaux publics. Ciment et bétons, 1973 676 pp. 35 - 41

(112) Penguin., P. et. al. "l'étude de la corrosion des aciers et metaux dans le béton" Cahirs du centre scientifique et technique du baitment 130 1972 pp. 1 -9

(113) Marr., J. & Glasser., F.P. "Effect of silica, PFA and slag additives on the composition of cement pore fluids" Proc 6th International conference on alkalis

in concrete. 1983. ed. Idorn., G.M. & Rustam., S. Publ. DBF, Copenhagen pp. 239 - 242.

(114) Glasser., F.P. et. al. "Analysis of slag - cement blends and the internal environment in slag cements" Presentation No.12 at "Workshop on Blastfurnace Slag Cements, York, 14-17 October 1985 (Proceedings not published).

(115) Poubaix, M "Atlas of electrochemical equilibriua in aqueous solutions. Pergamon press, Oxford, 1966. 271 pp.

(116) Angus., M.J. and Glasser., F.P. "The chemical environment in cement matrices" Conference on the chemistry of cement, Stockholm, 1985, unpublished.

(117) Glasser., F.P. et. al. "Solubility modelling of cements: Implications for radioactive waste immobilisation." Materials Research Society symposium, Boston, Mass. 1987. SBNWM vol X pp.331 -342 Publ. Materials Research Society. Pittsburgh, Penn. Ed. Bates., J.K. 827pp.

(118) Glasser., F.P. et. al. "DOE long term studies at Aberdeen" 1986 DoE report No. RW86.084

(119) Glasser., F.P. et. al. "The chemical environment in cements" 1985. SBNWM vol VIII pp.849 -858 Publ. Materials Research Society. Pittsburgh, Penn. Ed. Stone., J.A. & Ewing., R.C. 860pp.

(120) Glasser., F.P. et. al. "Slag cement blends - properties and performance" BNFL seminar on radioactive waste encapsulation 28 - 30 October 1986 London. Unpublished.

(121) Luke., K. et. al. 'Studies of Portland - Blastfurnace slag cement by selective dissolution' Unpublished presentation at a "Conference on the microstructure and chemistry of cement" Leeds, 1985. (First report of results for ref. 103)

(122) Tutti., K. "Corrosion of steel in concrete" Publ. Swedish Cement and Concrete Research Institute, 1982, 289pp. Report Fo4 (ISSN 0346 - 6906)

(123) Berner., U.R. "Modelling pore water chemistry in hydrated Portland cement" Materials Research Society symposium, Boston, Mass. 1987. SBNWM vol X pp.319 -330 Publ. Materials Research Society. Pittsburgh, Penn. Ed. Bates., J.K. 827pp.

(124) Kittl., P. et. al. "A study on the evaporation products of the liquid phase of a cement paste" Proc. 7th. ICCC., Paris, 1980. II pp. 7 - 11.

(125) Dron., R. & Brivot., F "Approach to the problem of the reactivity of granulated slag" Proc. 7th. ICCC., Paris, 1980. III pp134 - 139.

(126) Hinrichs., W & Odler., I "Investigation of the hydration of Portland blast furnace slag cement: hydration kinetics" Adv. Cem. Res. 1989. 2 (5) pp. 9 - 13

(127) Odler., I & Hinrichs., W. "Investigation of the hydration of Portland blast furnace slag cement: composition, structure and properties of the hydrated material" Adv. Cem. Res. 1989. 2 (5) pp. 15 - 20

(128) Roy., D.M. et. al. "Effects of early heat of hydration and exposure to elevated temperatures on properties of mortars and pastes with slag cement" Temperature effects on concrete ASTM STP 858. Ed. Naik., T.R. Publ. American Society for Testing and Materials, Philadelphia, 1985, pp. 150 - 167.

(129) Feldman., R.F. "Significance of porosity measurement on blended cement performance" Proc. 1st. CANMET/ACI conference, Montebello, 1983 pp. 415 - 433

(130) Bakker., R. "On the cause of increased resistance of concrete made from blast furnace cement to the alkali-silica reaction and to sulphate corrosion" Dissertation to the Mining and Metallurgy Faculty of the R.W.T.H. Aachen, for Doctor of Sciences degree: Holland 1980 pp. 94

(131) Roy., D.M. "Hydration, microstructure and chloride diffusion of slag cement pastes and mortars". Proc. 3rd. CANMET/ACI conference, Trondheim, 1989. pp.1265 - 1281

(132) Silsbee., M. et. al. "Composition of pore fluids extruded from slag cement pastes." Proc . 8th. ICCC., Rio, 1986. III pp. 263 - 269

(133) Roper., H. "Composition, morphology, hydration and bond characteristics of some granulated slags." Proc. 7th. ICCC., Paris, 1980. III pp.13 - 18.

(134) Taylor., H.F.W. et. al. "Analytical study of pure and extended Portland cement systems" J. Am. Ceram. Soc. 68 1985 pp. 685 - 690

(135) Uchikawa., H. "Effects of blending components on hydration and structure formation" Proc . 8th. ICCC., Rio, 1986. I pp. 249 - 280

(136) Daimon., M. "Mechanism and kinetics of slag cement hydration." Proc. 7th. ICCC., Paris, 1980. III pp.2 - 14.

(137) Uchikawa., H. "Effect of character of amorphous phase in blending

components on their reactivity in calcium hydroxide mixture" Proc . 8th. ICCC, Rio, 1986. III pp. 245 - 250

(138) Nicolosi., N.L. "A generalized model for the analysis ground water radiolysis" SBNWM 44 1985 pp. 631 - 640

(139) Christensen., H. & Bjergbakke., E "Radiloysis of concrete" (Report STUDSVIK: SKBF / KBS 1984 - 03 - 16 pp 1- 30

(140) Palmer., J.D. & Smith., D.L. "The incorpoation of low and medium level radioactive wastes (solids and liquids) in cements" Report United Kingdom Atomic Energy Authority, Chemistry Division, Winfrith, 1985 AEEW - R 1951 118pp.

(141) Geiker., M. & Knudsen., T. "Chemical shrinkage" Engineering conference, Henniker, USA, Aug, 1985, Offprint 19pp (Proceedings unpublished)

(142) Cook., D.J. et. al. "Volume changes in Portland - blast furnace slag cement concrete" Proc. 2nd. CANMET/ACI conference, Madrid, 1986 Supplementary paper 10, pp 1 - 10

(143) Hansen., T.C. "Physical structure of hardened cement paste. A classical approach." Mater. & Struct. v19 (114) 1986 pp. 423 - 436

(144) Taylor., H.F.W. "Bound water in cement pastes and its significance for pore solution compositions" in "Microstructural development during hydration of cement" Eds. Strudle., L.J. & Brown., P.W., Publ. 1987 Materials Research Society, Pittsburgh, Penn.

(145) Wendlandt., W.W. "Thermal methods of analysis" Publ. Wiley Interscience, 1974, New York. 543pp

(146) Ramachandran., V.S. "Thermal analysis in cement chemistry" Publ. Arnold, London. 1974 pp. 266

(147) Bragg., W.L. "The crystalline state" volume 1 G. Bell & Sons London 1949

(148) Bogue., R.H. "Hydration of Portland cement compounds" Industrial and Engineering Chemistry 8 1934 pp. 837 - 847

(149) Bloch., F. et. al. "Nuclear Induction" Phys. Rev. 69 1946 pp. 127

(150) Purcell., E.M. et. al. "Resonance absorption by nuclear magnetic moments in solids" Phys Rev 69 1946 pp. 37

(151) Nixon., P. & Page., C.L. "Pore solution chemistry and alkali aggregate reaction" Katherine & Bryant Mather International Conference on Concrete Durability, ACI Special pubjication SP100. Ed. Seadon., J.M. 1987 2 pp. 1833 - 1862

(152) Brightman., M.A. "Pore fluids from the Argillaceous Rocks of the Harwell Research Site." Brit. Geol. Surv. 1985. Rep No: FLPU - 85 - 6.

(153) Richardson., I.G. et. al. "The hydration of blastfurnace slag cements" Adv. Cem. Res. 1989. 2 (8) pp. 147 - 157

(154) Marsmann., H. "^{29}Si-NMR Spectroscopic results" Springer-Verlag book series "NMR basic principles and progress." 1981 vol17 pp. 66 - 235

(155) Marsmann., H "Si - 29" Springer-Verlag book series "NMR basic principles and progress." 1981 vol17 pp. 66 - 235

(156) Lippmaa., E. et. al. "Structural studies of silicates by solid state high resolution 29-Si NMR" J. Amer. Chem. Soc. 102 pp. 4889 - 4893

(157) Magi., M. "Solid state high resolution Si-29 chemical shifts in silicates" J. Phys. Chem. 88 (8) pp. 1581 - 1522

(158) Shaw., D. "Fourier Transform NMR Spectroscopy. Elsevier, 1976, Oxford. 421 pp

(159) Mc.Whinnie., W.R. "Electron spin resonance and nuclear magnetic resonance applied to minerals" Chapter 6 in Berry., F.J. & Vaughan., D.J. "Chemical bonding and spectroscopy in mineral chemistry" Chapman & Hall, London, 1985, 325pp.

(160) Fyfe., C.A "Solid state NMR for Chemists" CFC Press, Guelph, Ontario, Canada, 1985. 388pp.

(161) Richards., Sir Rex, & Packer., K.J. (Eds.) "Nuclear Magnetic Resonance Spectroscopy in Solids" Phil. Trans. Roy. Soc Lond A-299 pp. 475-686 1981 (14 contributions)

(162) Lippmaa et. al. "A high resolution ^{29}Si study of the hydration of tricalcium silicate." Cem. Concr. Res. 12 1982 pp. 597 - 602

(163) Harris., R.J. et. al. "Two dimensional Si-29 NMR studies of aqueous silicate solutions." J. Mag. Res. 1984 57 pp. 115 - 121

(164) Murdoch., J.B. et. al. "High resolution Si-29 NMR study of silicate and aluminosilicate glasses: The effect of network modifying cations." Amer. Mineral. 70 pp.332 - 343

(165) Schneider., E. et. al. "Speciation and local structure in alkali and alkaline earth glasses: Constraints from silicon-29 NMR spectroscopy." J. Non Cryst. Solids 89 1987 pp. 371 - 383

(166) Nofz., M. et. al. "Effect of the network modifying cation an the silicon-29 NMR chemical shift in alkali and alkaline earth aluminosilicate glasses." Z. Chem. 26 1986 pp. 221 - 222

(167) Fraser., D.G. & Clayden., N.J. "A high resolution silicon - 29 nuclear magnetic resonance study of qrdering in silicate glasses on the join Ca Mg $Si_2 O_6$ - Na Al $Si_3 O_8$ " Chem. Geol. 62 1986 pp. 43 - 47

(168) Klinowski., J. "Solid State NMR" Royal Society of Chemistry Specialist publication NMR vol 16. Ch.6 pp. 153 - 190

(169) Komarneni., S. et. al. "Naturally occuring Jennite: Characterization by ^{27}Al and ^{29}Si MASNMR spectroscopy and cation exchange properties." Cem. Concr. Res. 17 1987 pp.891 -895

(170) Komarneni., S. et. al. "Al substituted Tobermorite - The co-ordination of aluminium as revealed by solid state ^{27}Al Magic Angle Spinning (MAS) NMR. Cem. Concr. Res. 15 1985 pp. 723 - 728

(171) Wieker., W. et. al. "Solid state high resolution silicon-29 NMR

spectroscopy of synthetic 14, 11 and 9Å tobermorites" Cem Concr. Res. 12 (3) 1982 pp. 333 - 339.

(172) Grimmer, A.R. et. al. "High resolution solid - state ^{29}Si NMR of polymorphs of Ca_2SiO_4" Cem. Concr. Res. 15 1985. pp. 467 - 473

(173) Lippmaa., E. et. al. "A High resolution ^{29}Si study of the hydration of tricalciumsilicate. Cem. Concr. Res. 12 1983. pp. 597 - 602

(174) Barnes., J.R. et. al. "Hydration of Portland cement followed by 29Si solid state NMR spectroscopy" J. Mater. Sci. Lett. 4 1985 pp. 1293 - 1295

(175) Clayden, N.J. et. al. "The application of solid state nuclear magnetic resonance spectroscopy techniques to the study of the hydration of tricalcium silicate" Proc . 8th. ICCC, Rio, 1986. III pp. 51 - 56

(176) Clayden., N.J. et. al. "Hydration of tricalcium silicate followed by solid - state ^{29}Si NMR spectroscopy" J. Chem. Soc. Chem. Commun. 1984 pp. 1396 - 1397

(177) Clayden., N.J. et. al. "Solid State NMR Studies of Cement Hydration" Proc. Brit. Ceram. Soc. 35 1984 pp.55 - 64

(178) Lambert., P "Corrosion and passivation of steel in concrete" Ph.D thesis, University of Aston in Birmingham, UK. 1983. 273pp

(179) Justnes., H. et. al. "The Utilization of Nuclear Magnetic Resonance (NMR) in cement and concrete Research" SINTEF Report No: STF65 A89071 Forskninginstituttet for Cement og Betong, 1989, The Norwegian Institute of Technology, Trondheim, Norway.

(180) Bailey., J.E. and Stewart., H.R. "Relationships between microstructural development and the physico-chemical Nature of OPC pastes" Proc. Brit. Ceram. Soc. 35 1984 pp. 193 - 205.

Appendix

Graphical stages in calculating kinetic parameters using the chemical shrinkage method.

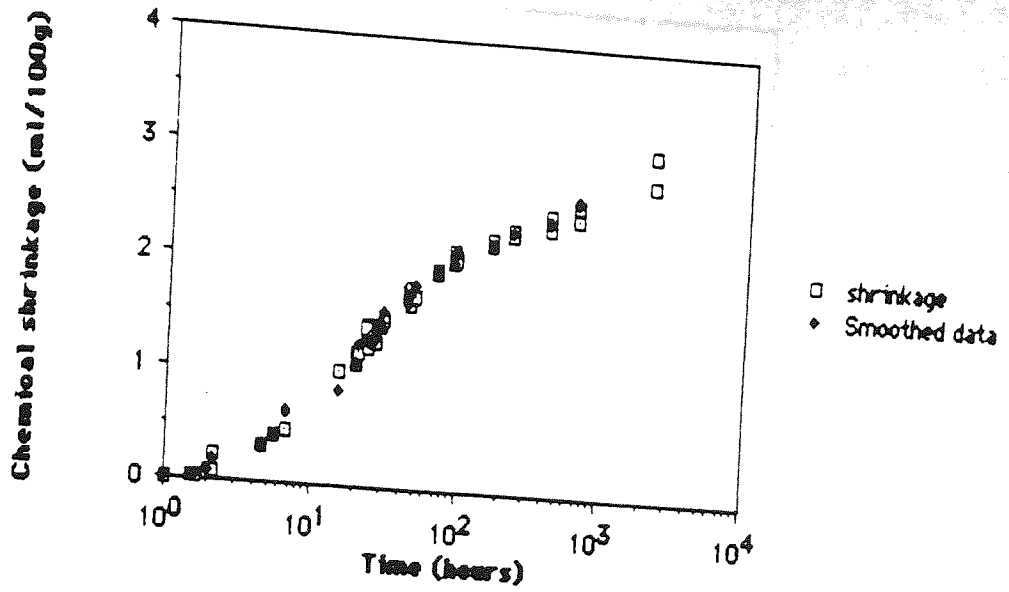

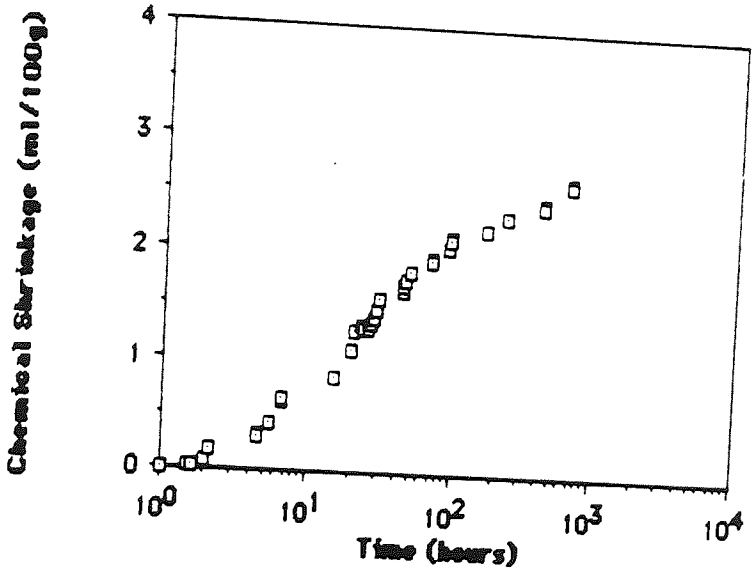

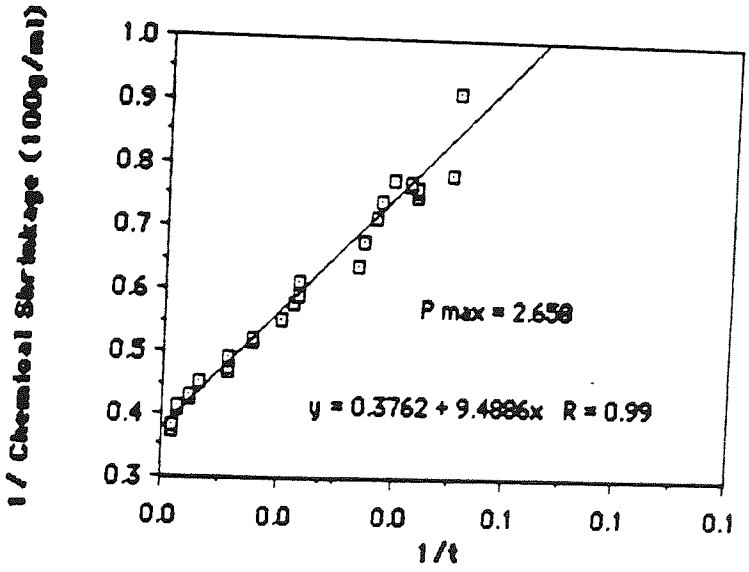

Data for samples 50% BFS, 0.3 w/s ratio cured at 25°c

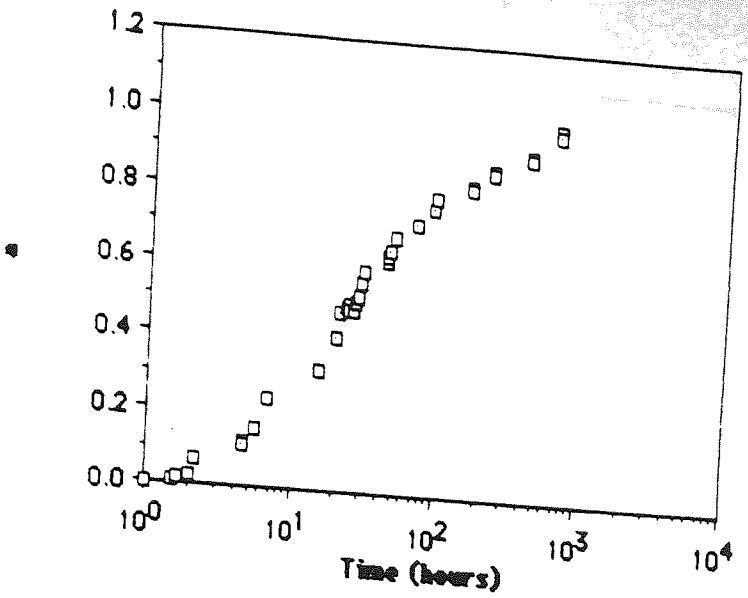

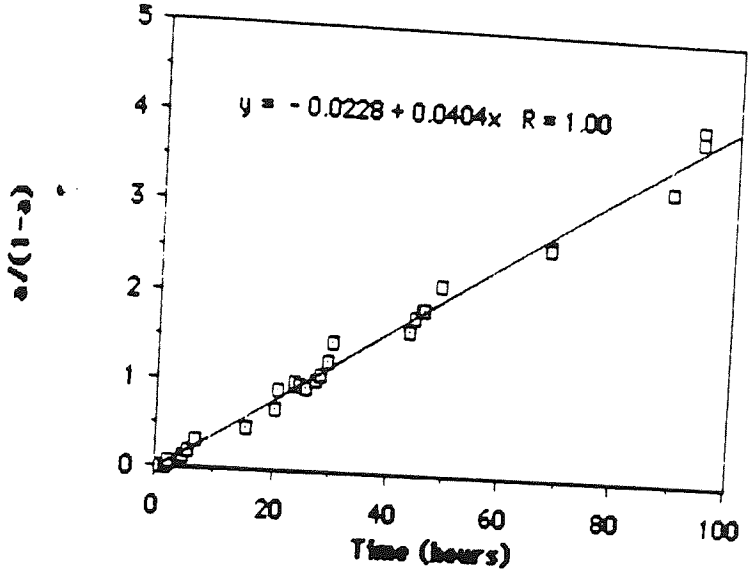

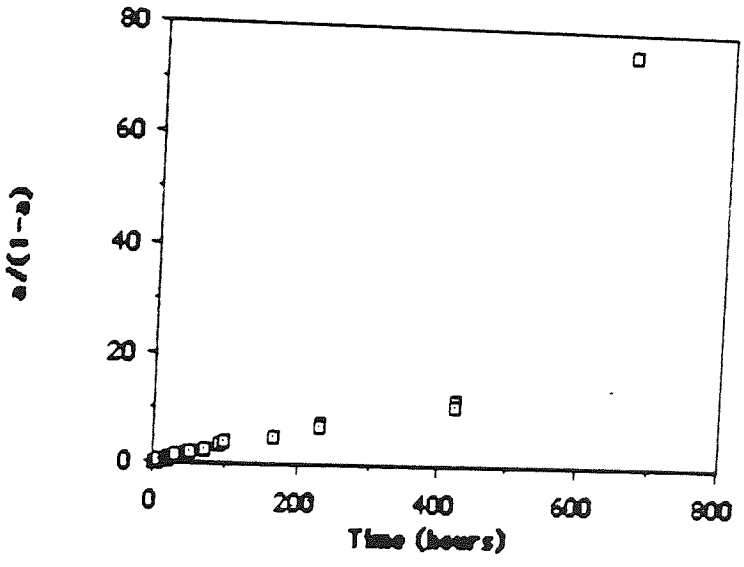

Data for samples 50% BFS, 0.3 w/s ratio cured at 25°c

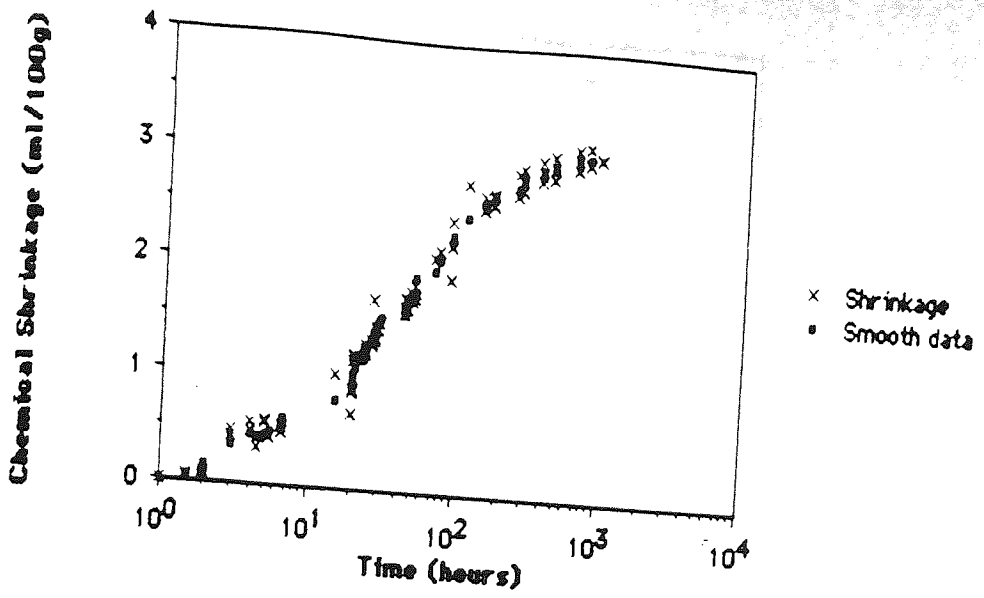

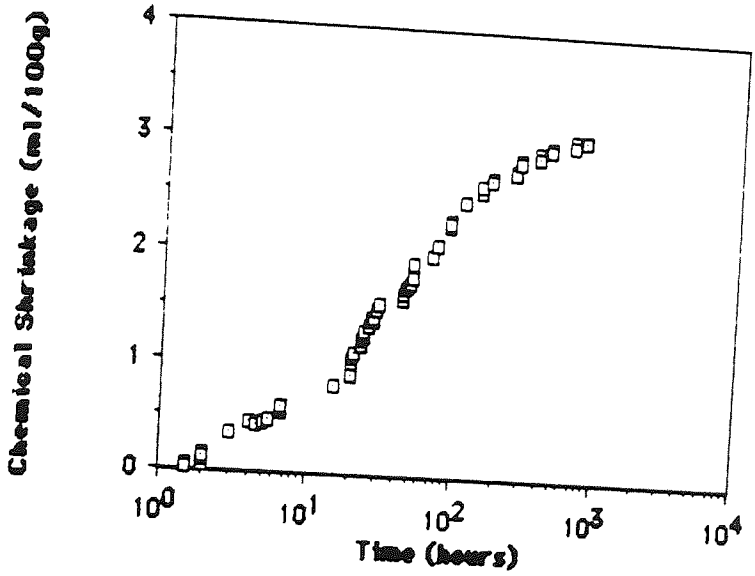

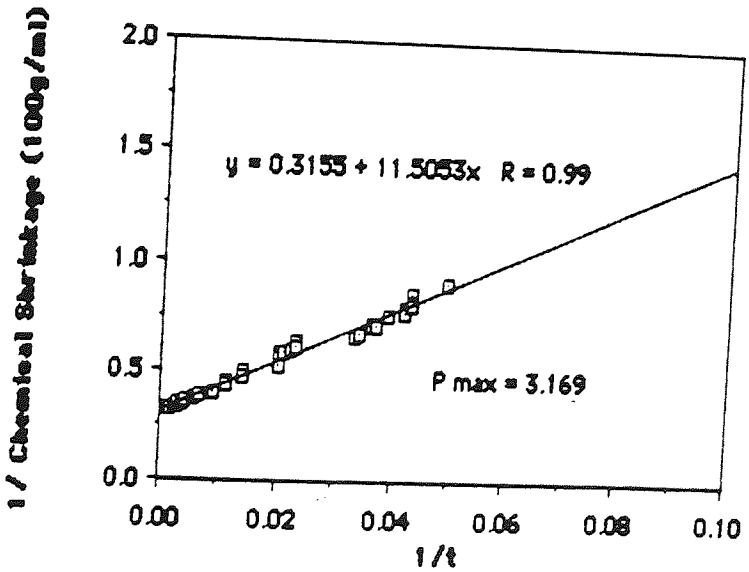

Data for samples 50% BFS, 0.4 w/s ratio cured at 25°c

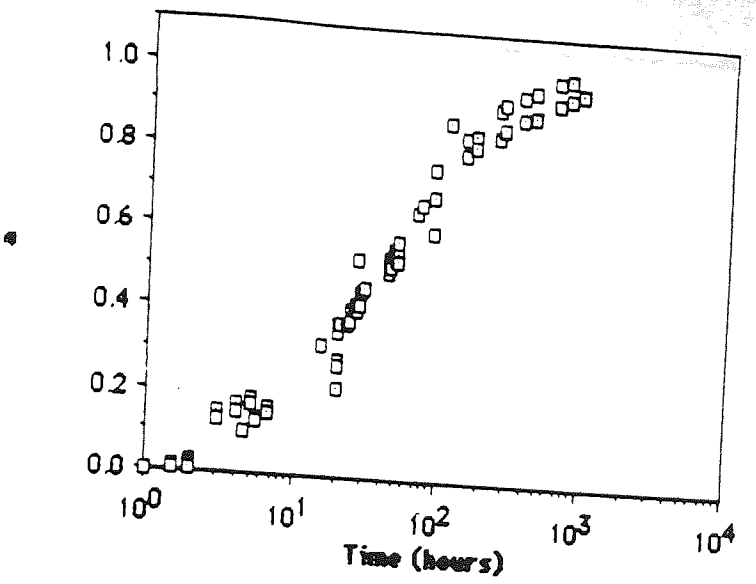

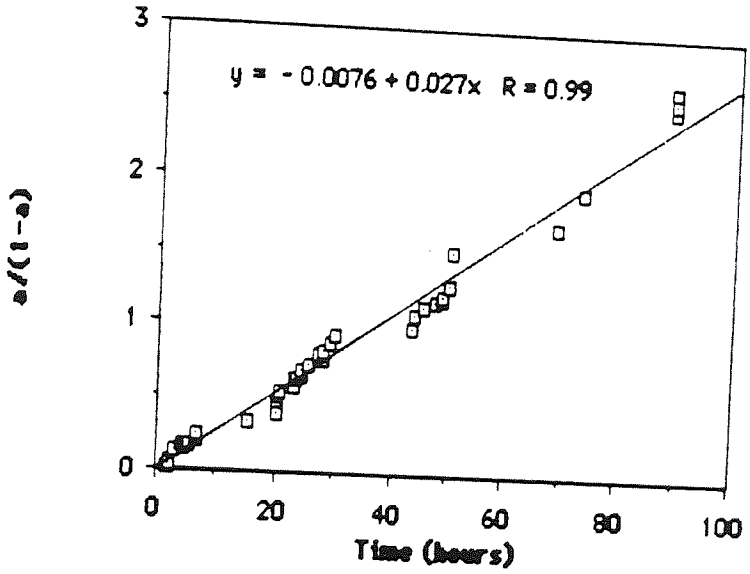

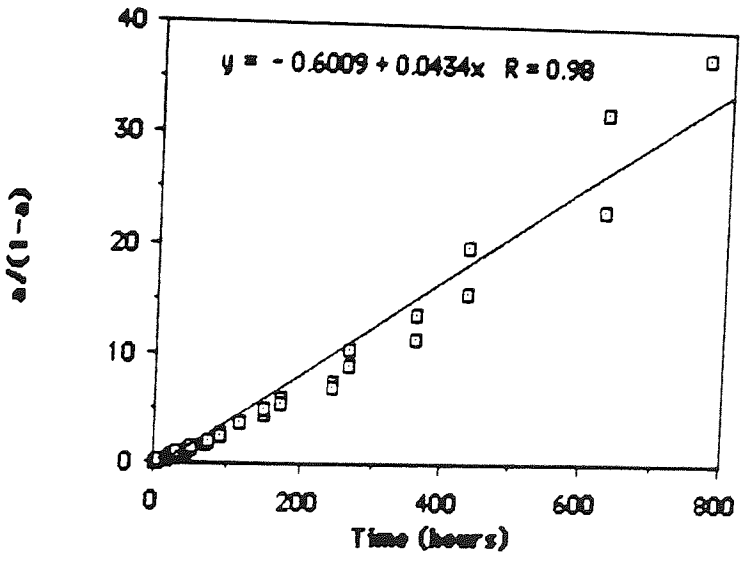

Data for samples 50% BFS, 0.4 w/s ratio cured at 25°c

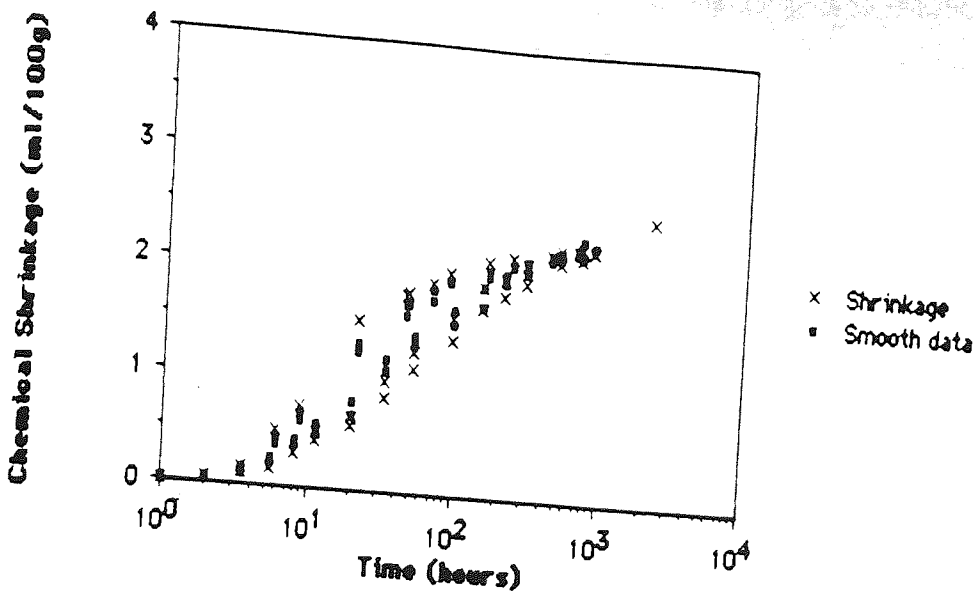

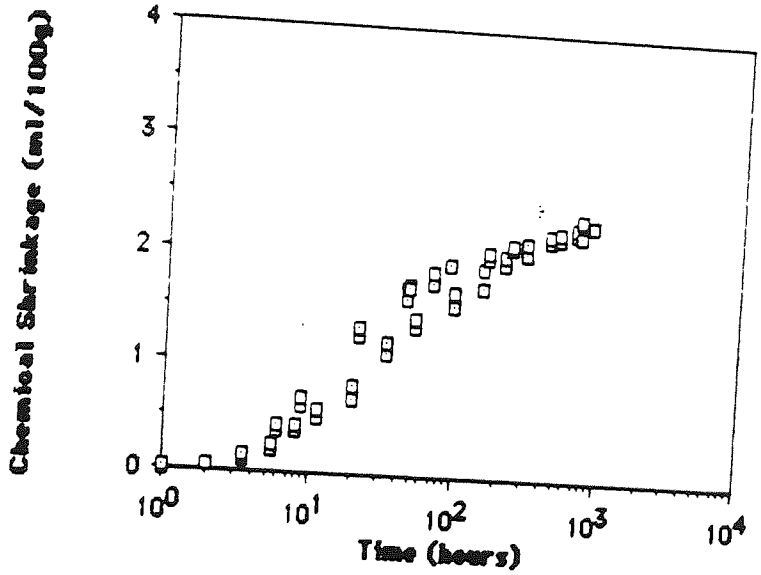

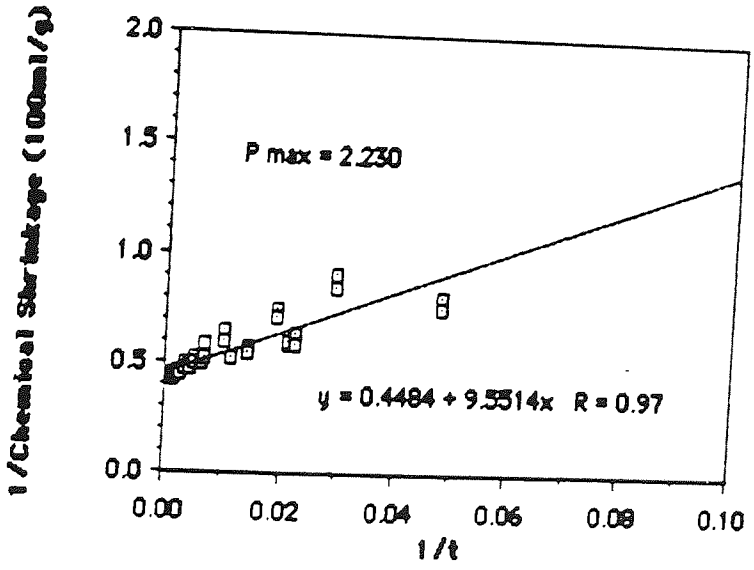

Data for samples 70% BFS, 0.3 w/s ratio cured at 25°c

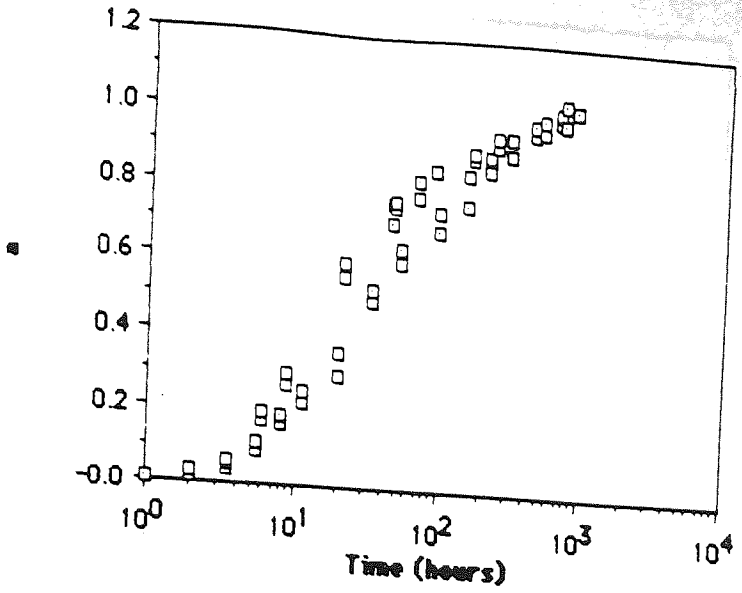

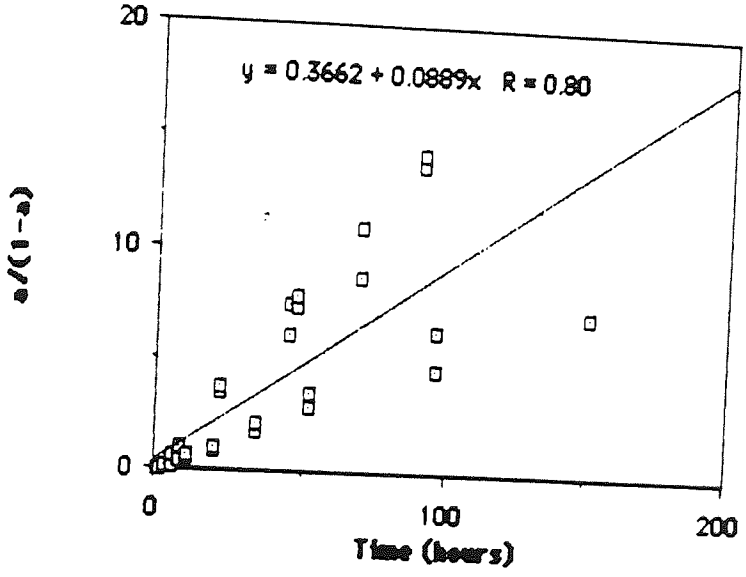

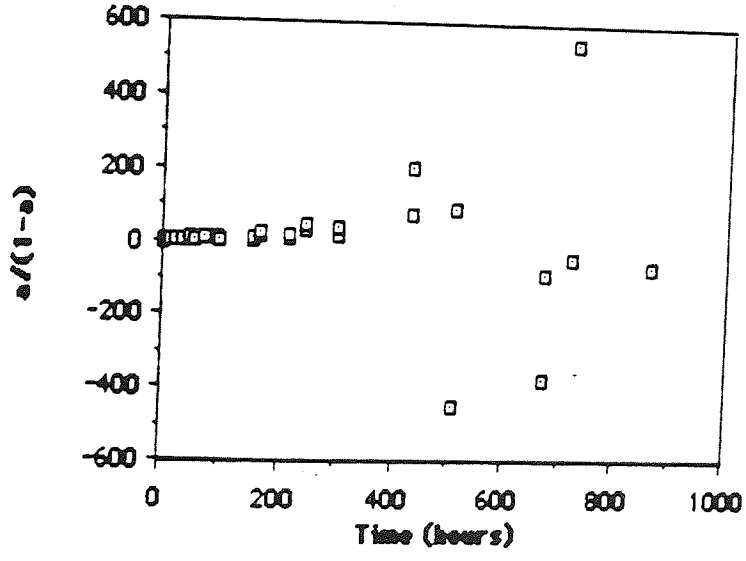

Data for samples 70% BFS, 0.3 w/s ratio cured at 25°c

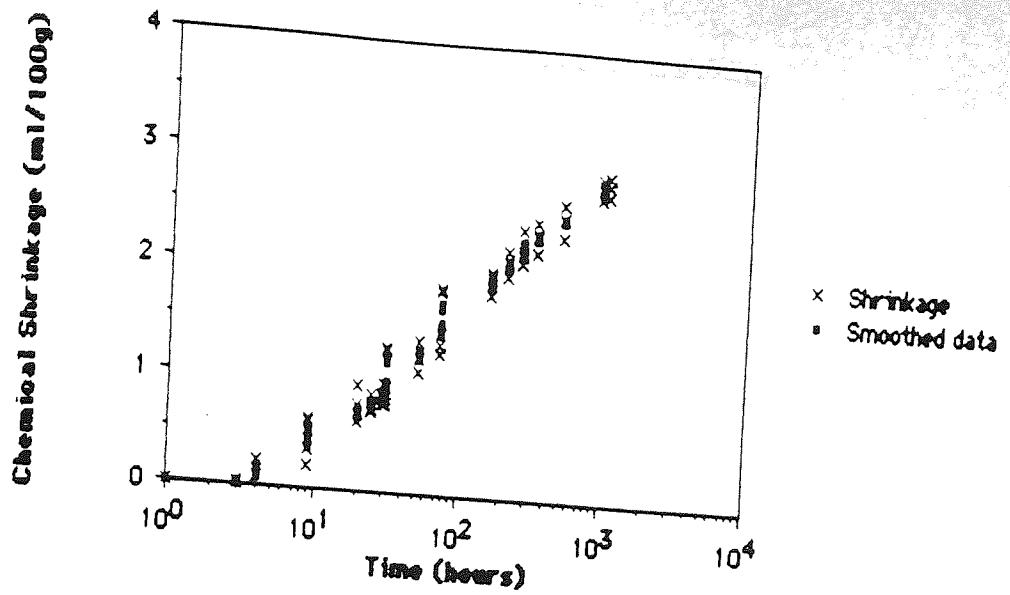

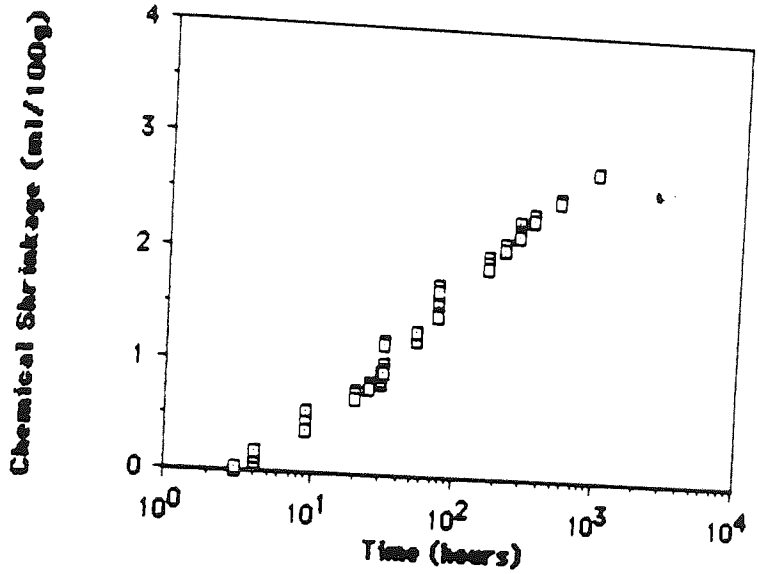

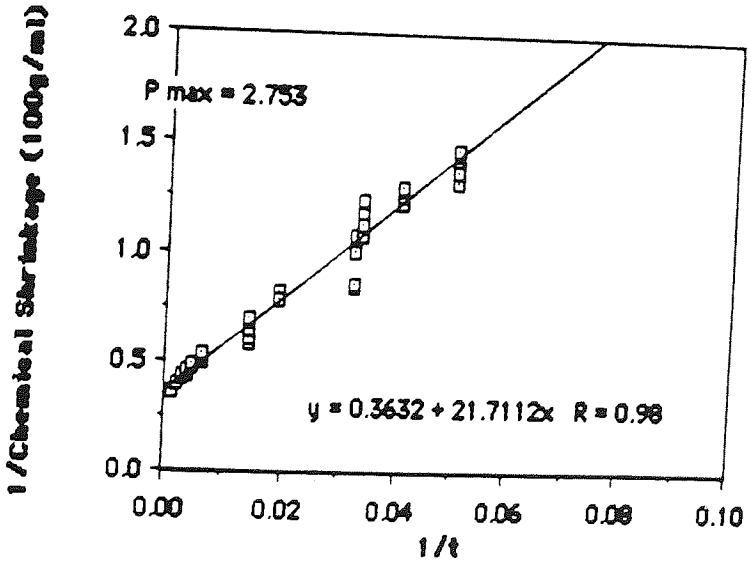

Data for samples 70% BFS, 0.4 w/s ratio cured at 25°c

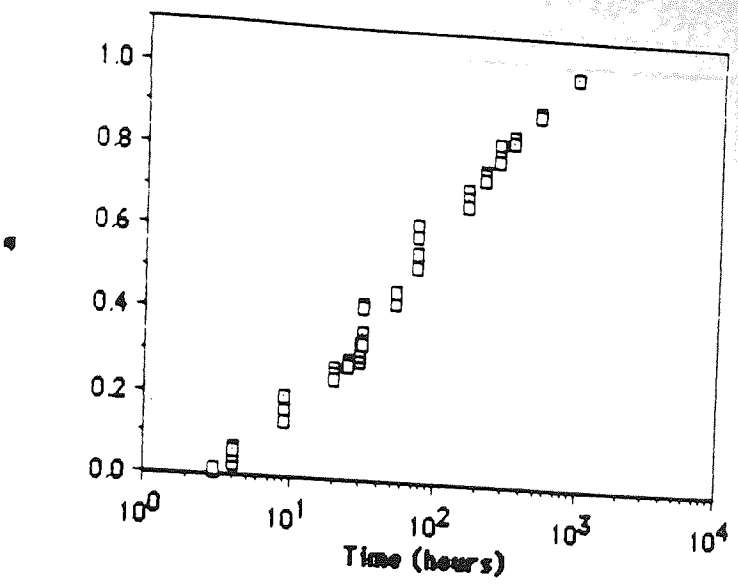

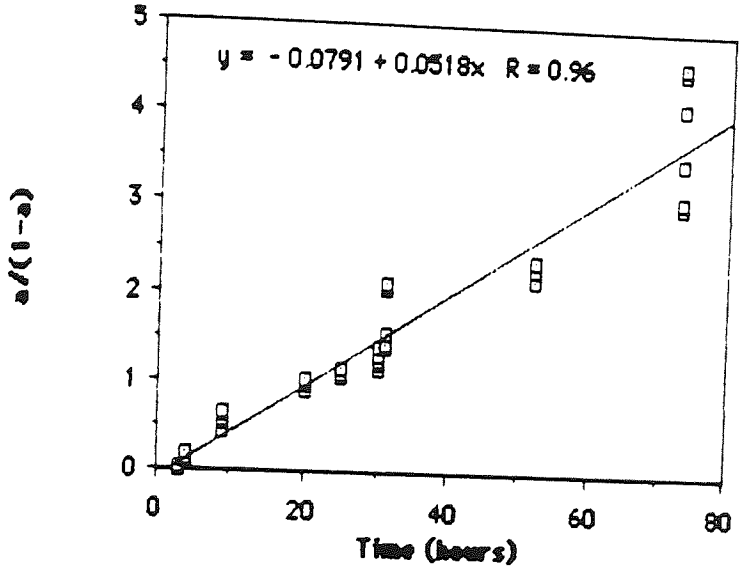

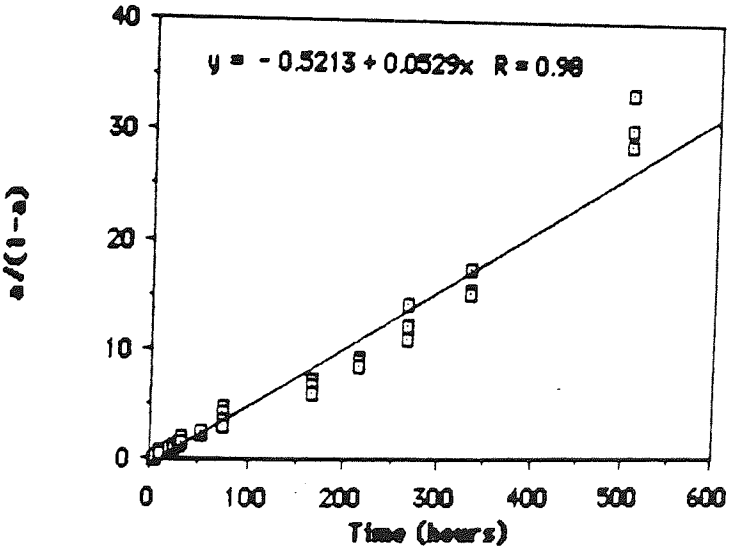

Data for samples 70% BFS, 0.4 w/s ratio cured at 25°c

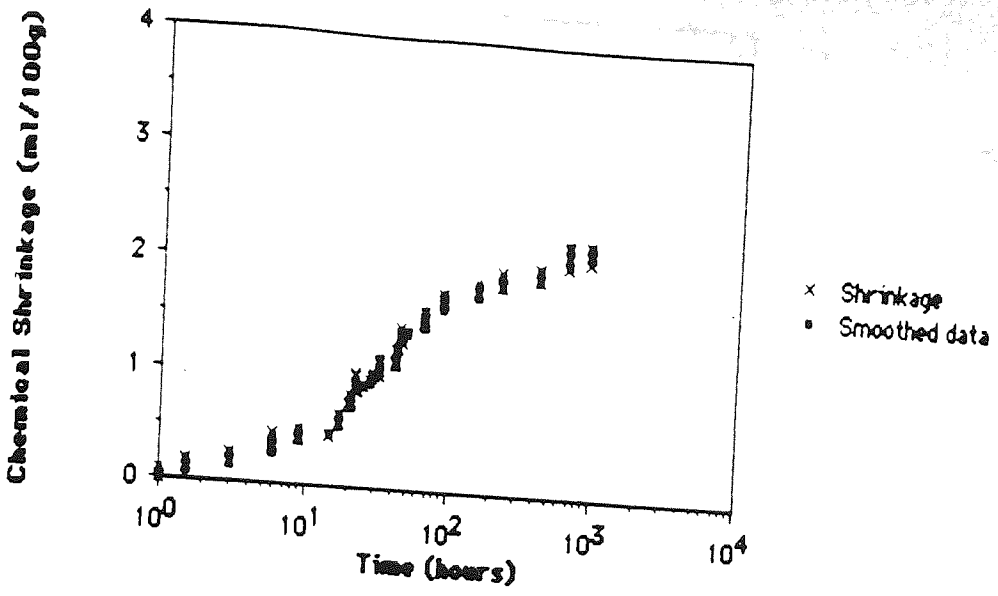

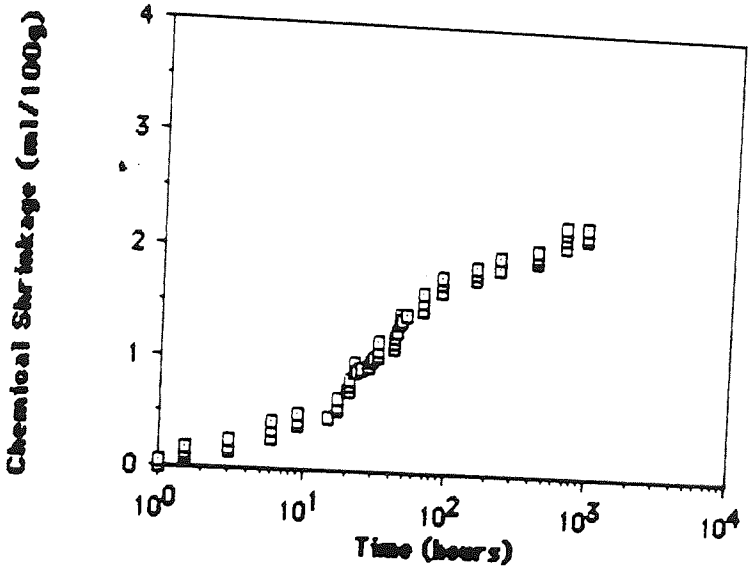

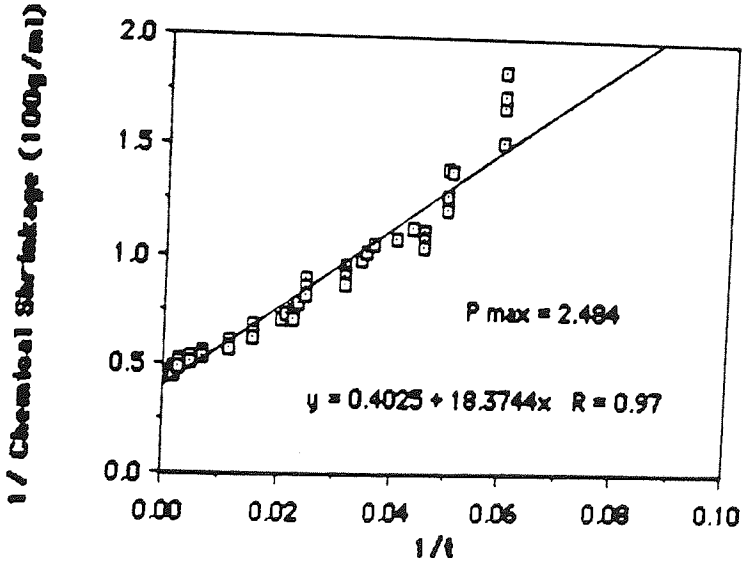

Data for samples 90% BFS, 0.3 w/s ratio cured at 25°c

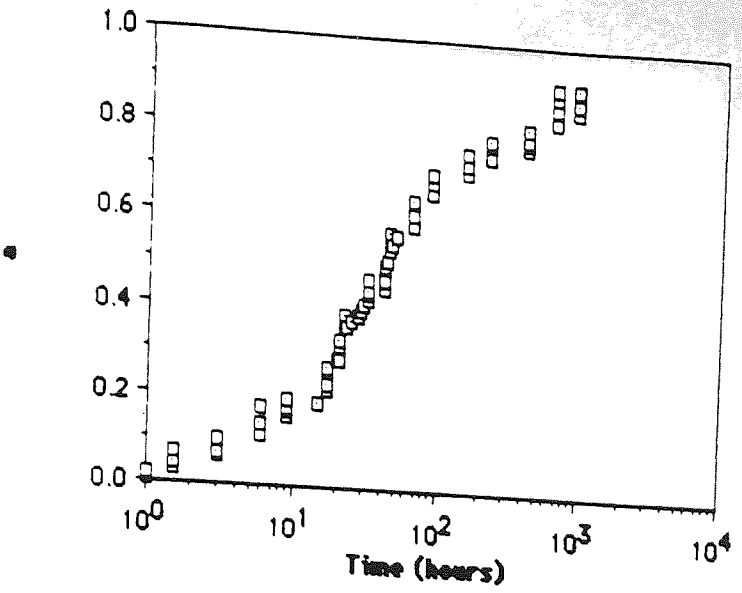

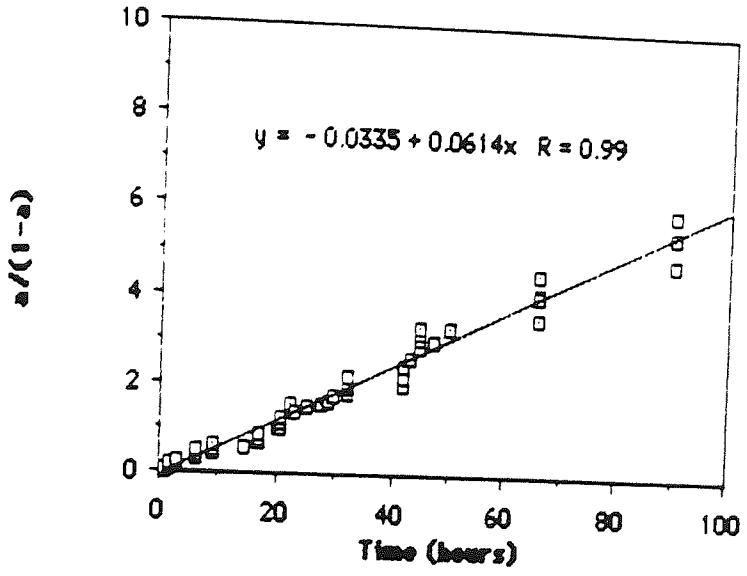

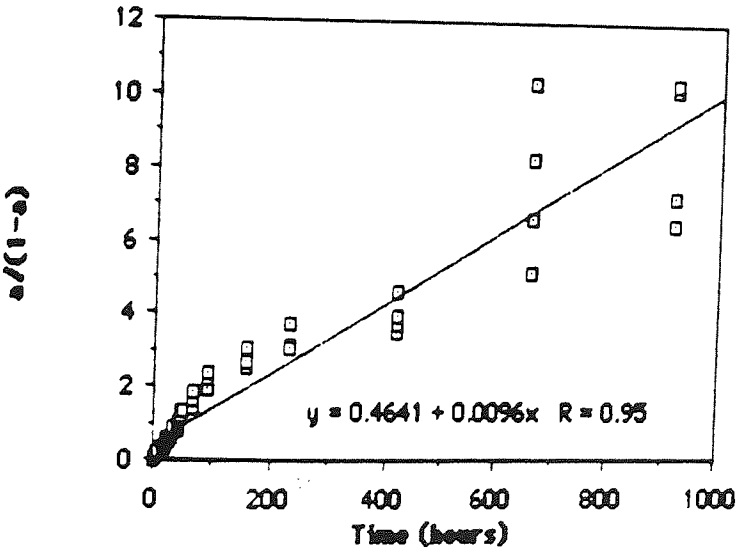

Data for samples 90% BFS, 0.3 w/s ratio cured at 25°c

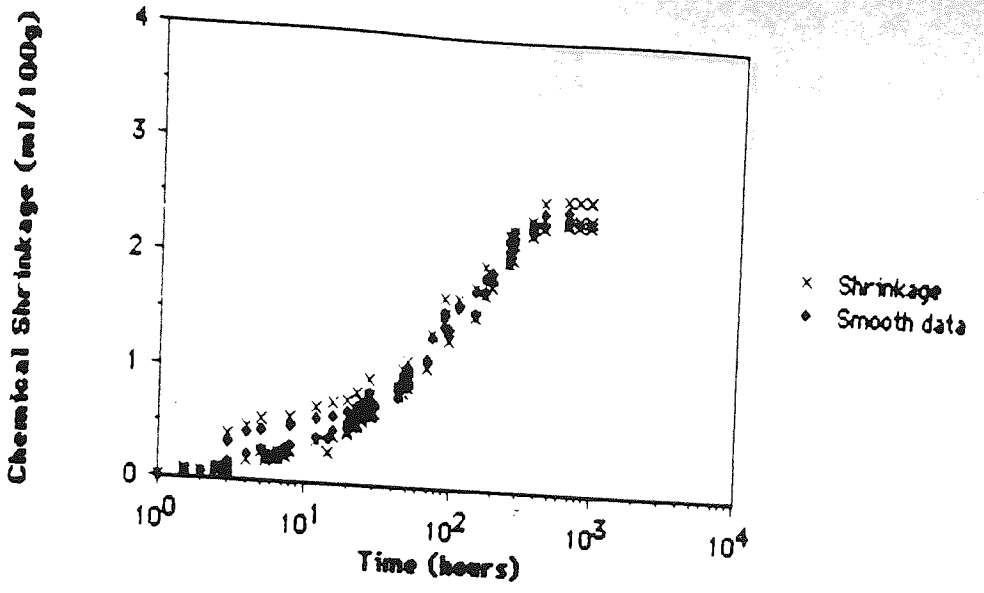

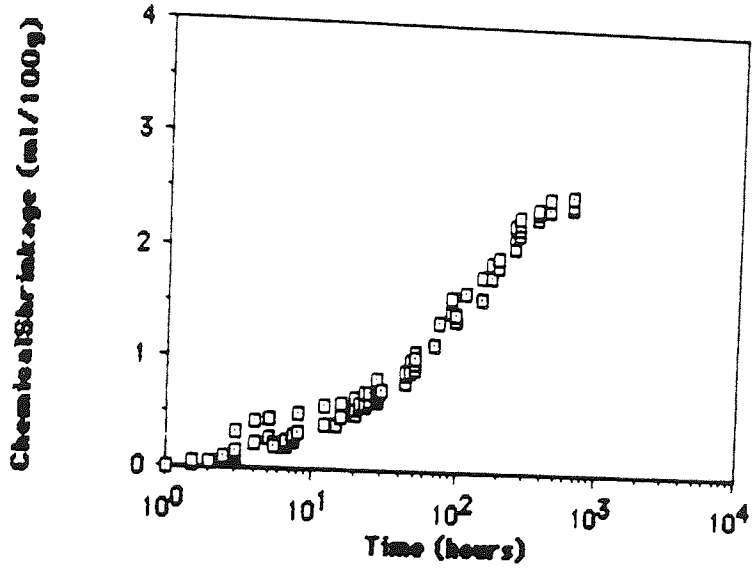

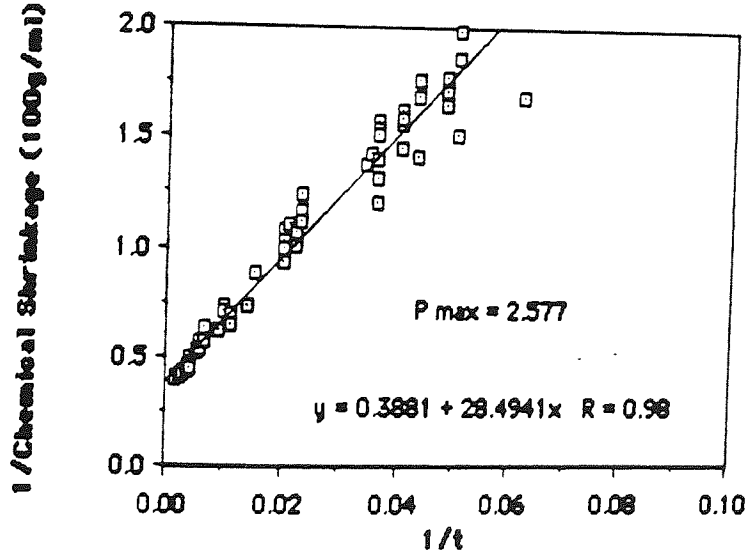

Data for samples 90% BFS, 0.4 w/s ratio cured at 25°c

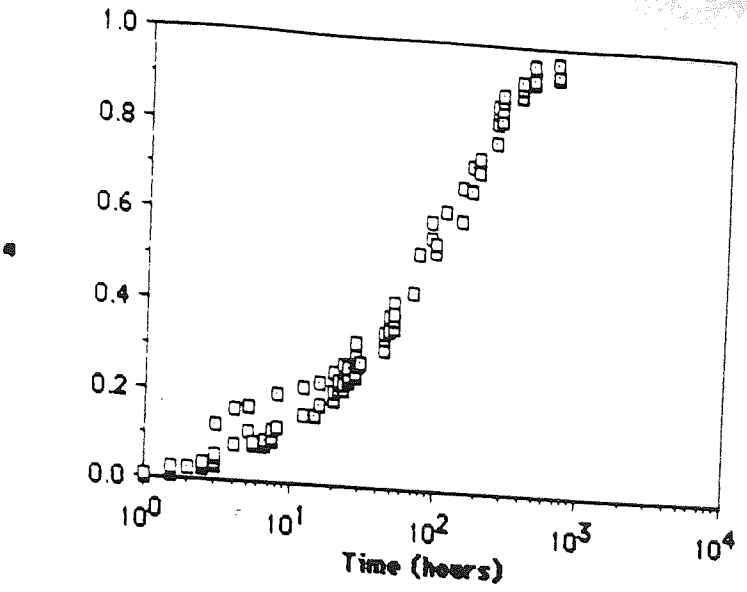

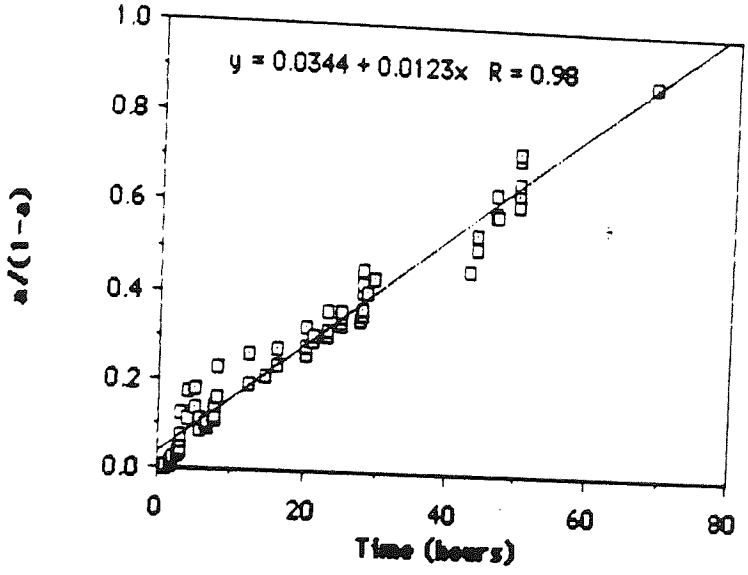

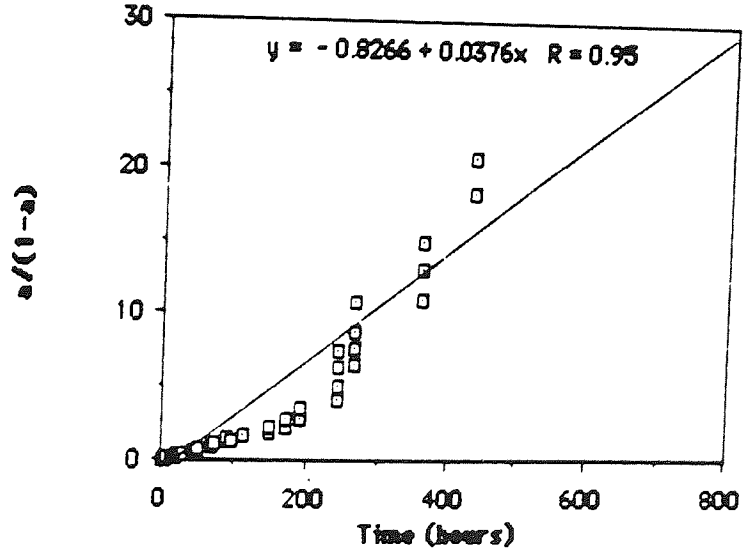

Data for samples 90% BFS, 0.4 w/s ratio cured at 25°c

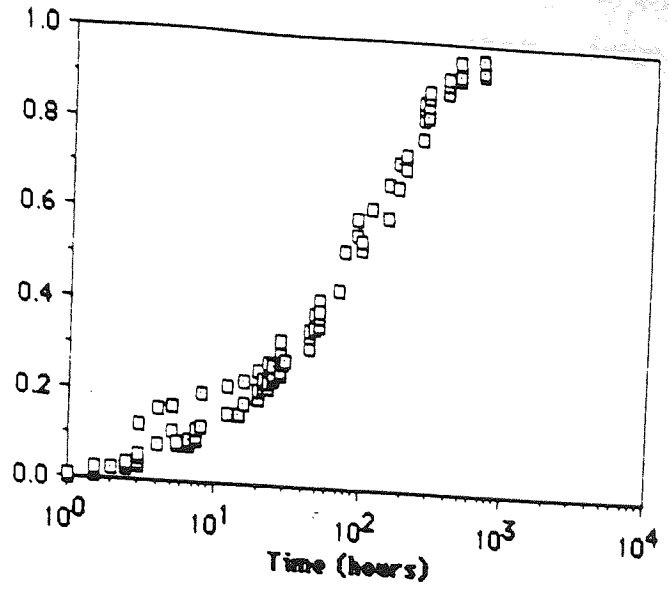

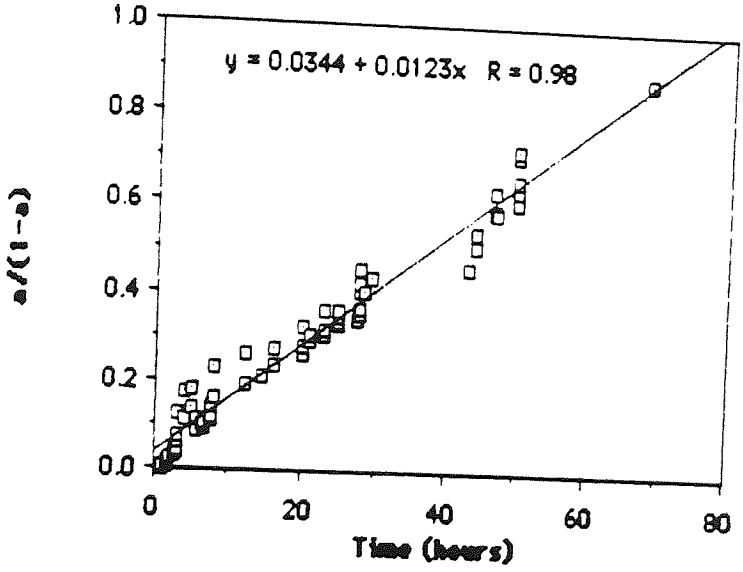

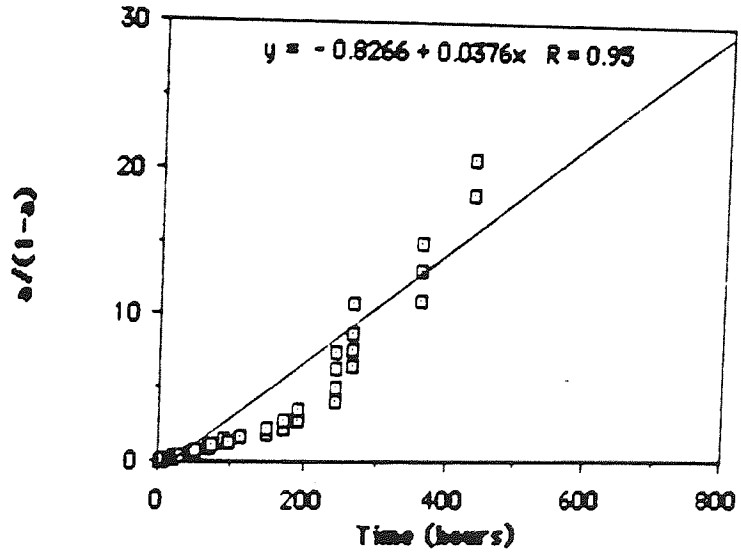

Data for samples 90% BFS, 0.4 w/s ratio cured at 25°c

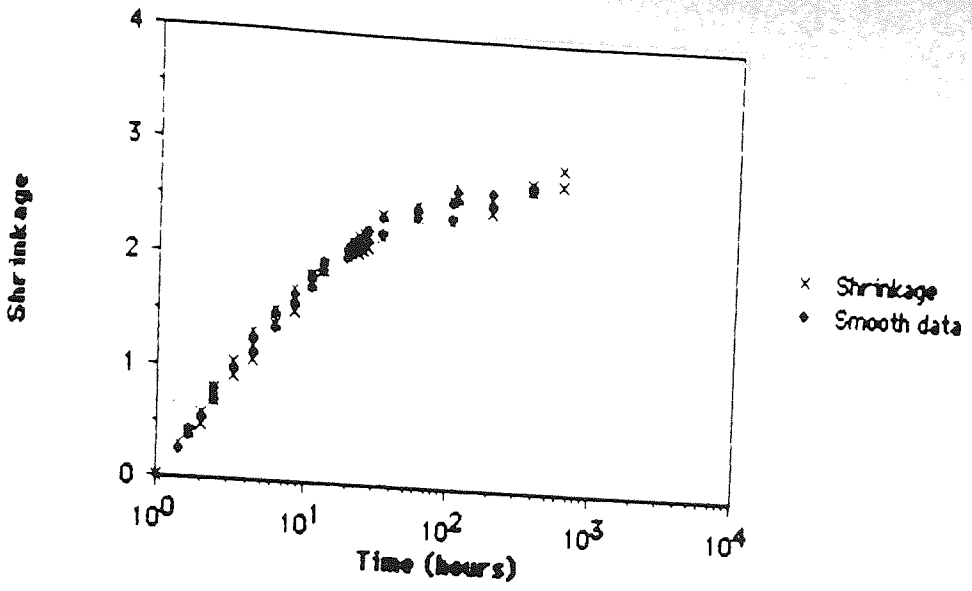

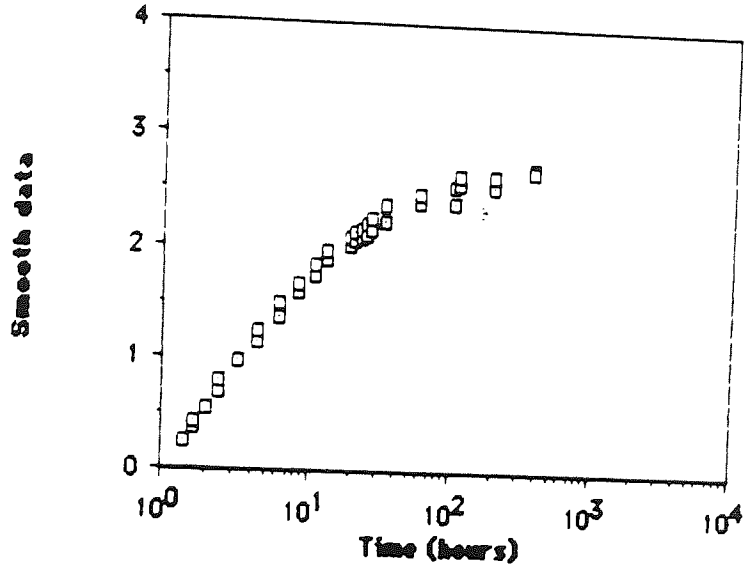

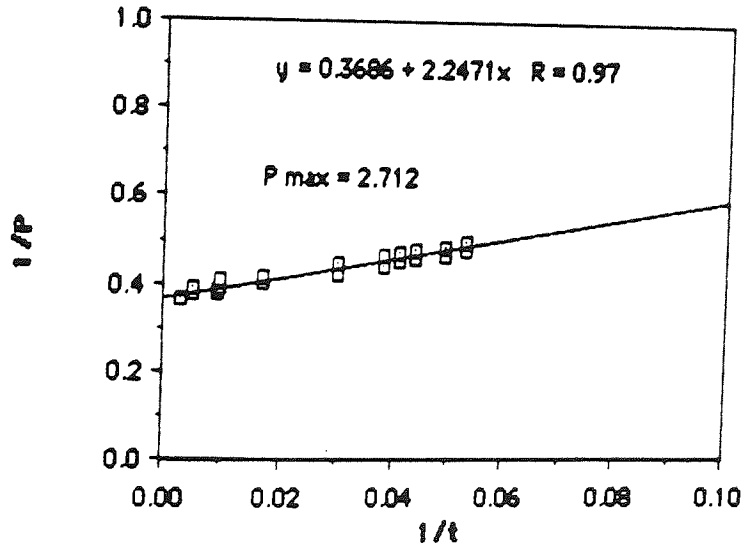

Data for samples 50% BFS, 0.3 w/s ratio cured at 50°c

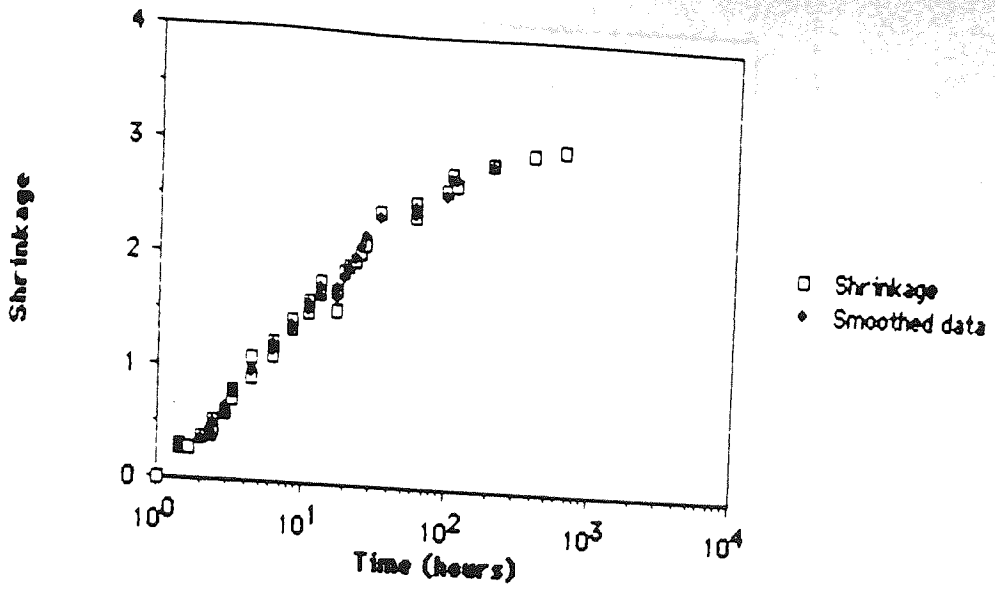

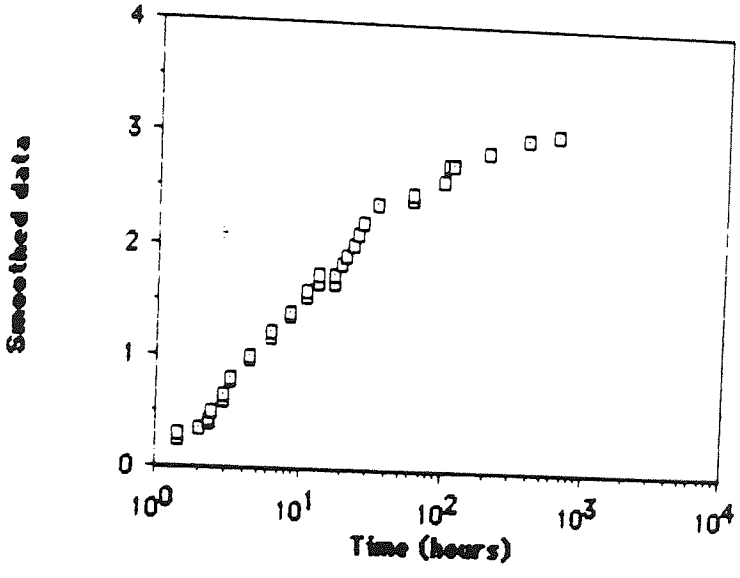

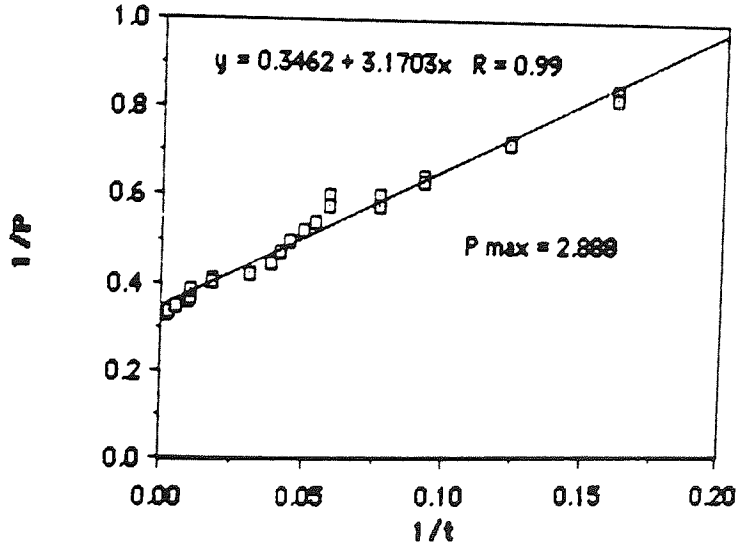

Data for samples 50% BFS, 0.4 w/s ratio cured at 50°c

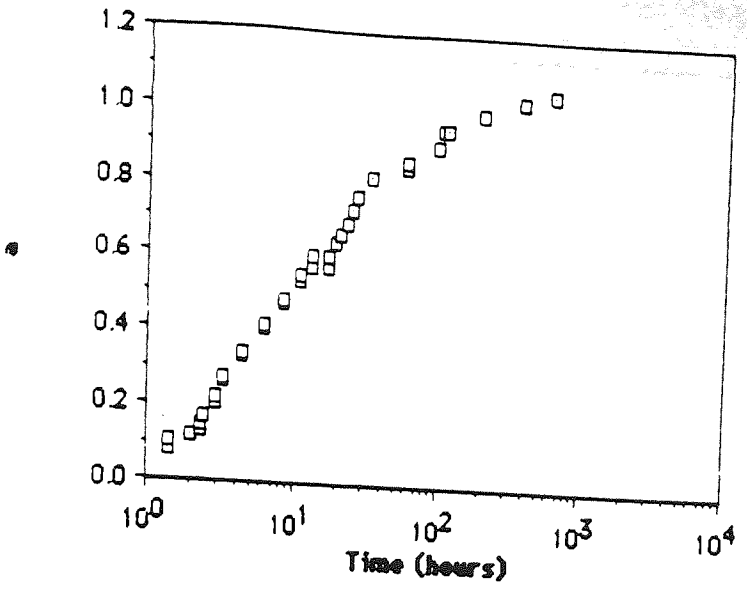

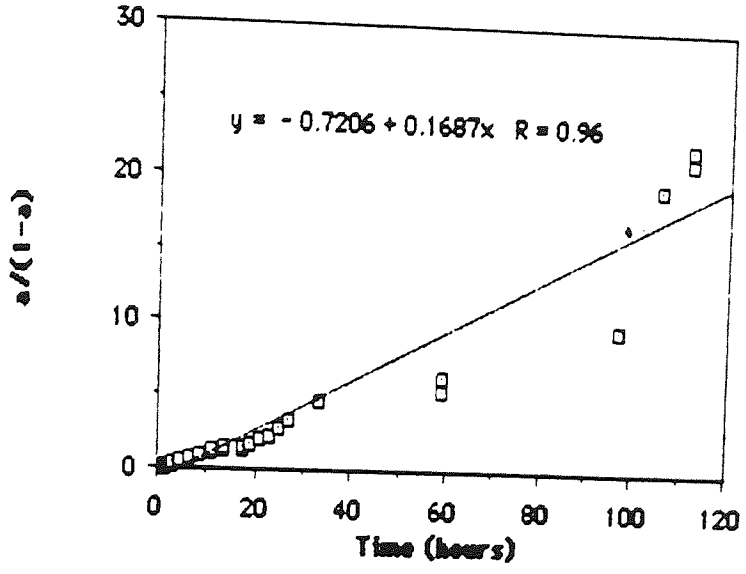

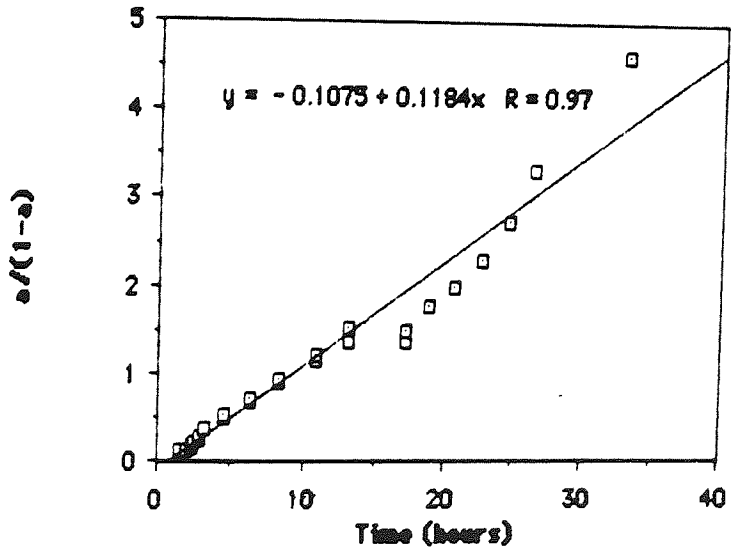

Data for samples 50% BFS, 0.4 w/s ratio cured at 50°c

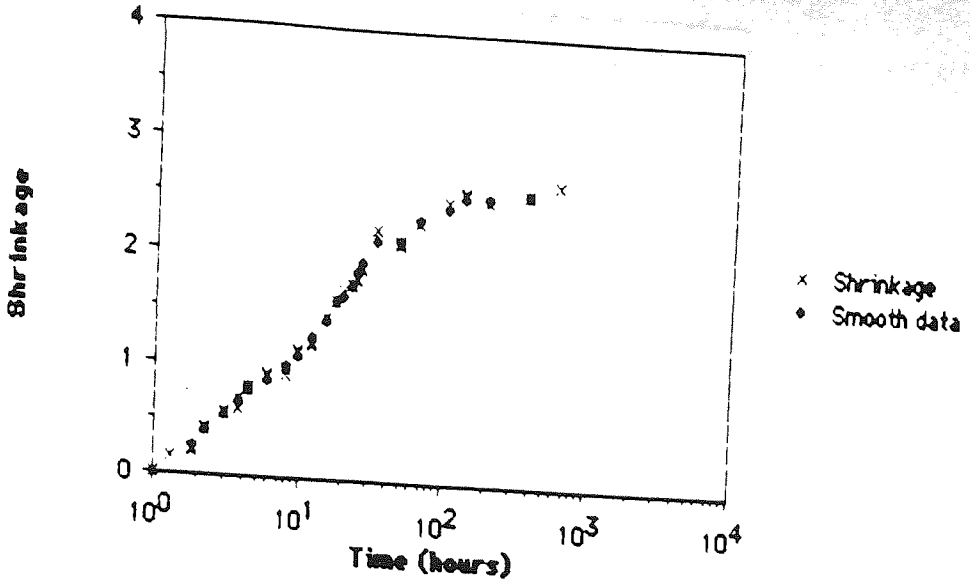

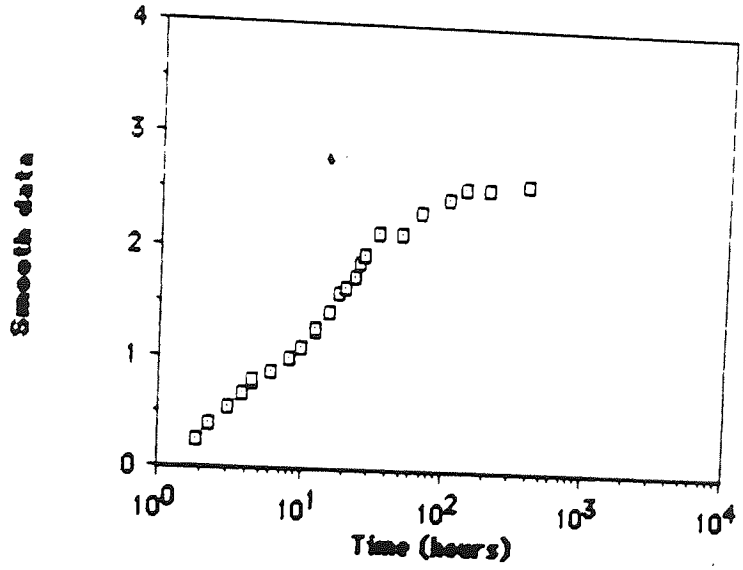

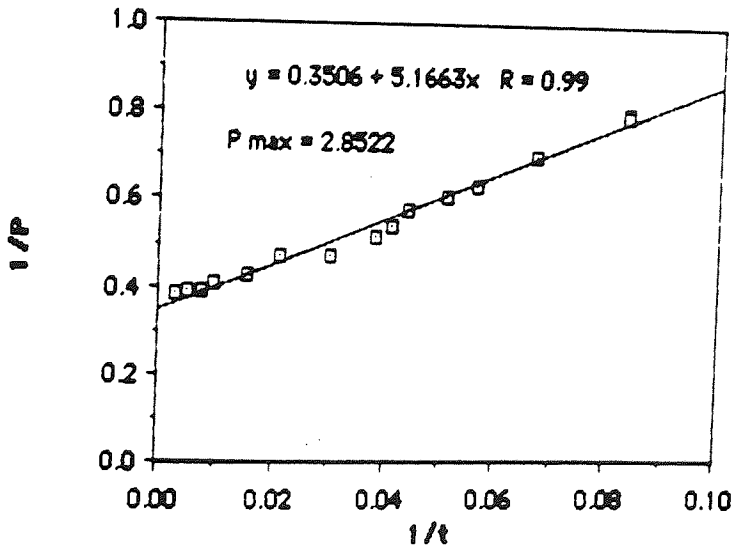

Data for samples 70% BFS, 0.3 w/s ratio cured at 50°c

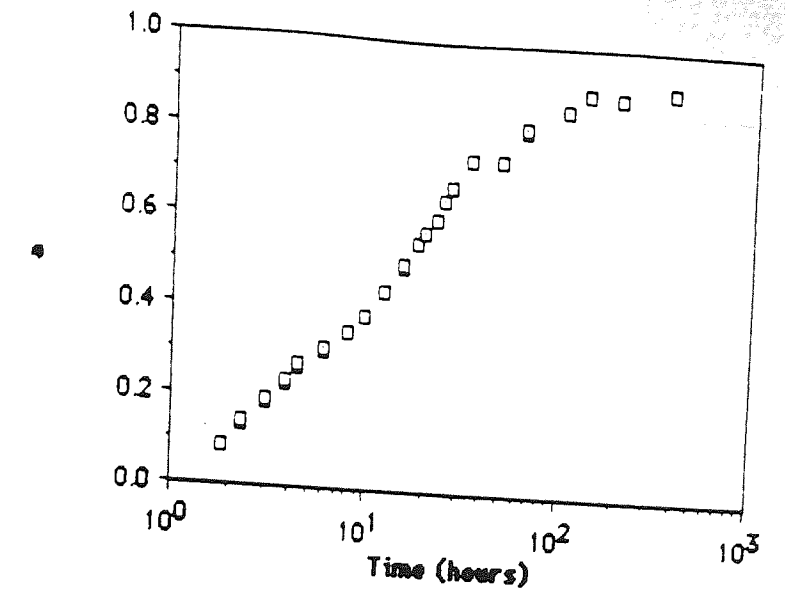

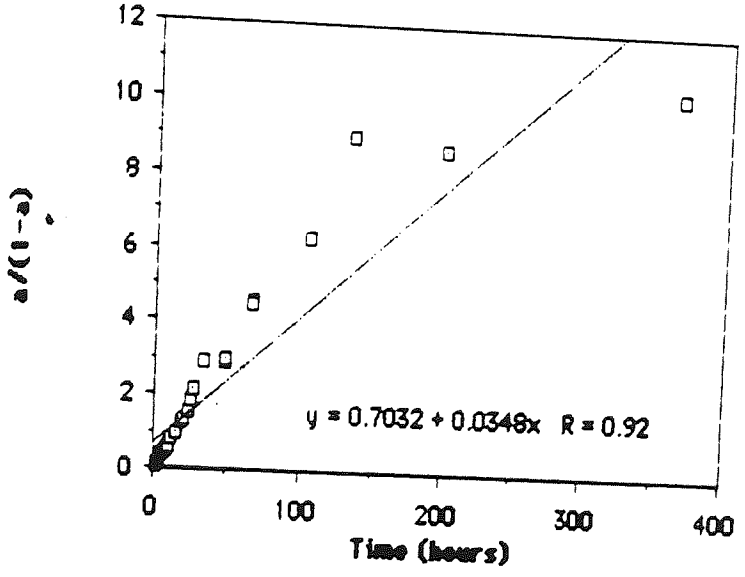

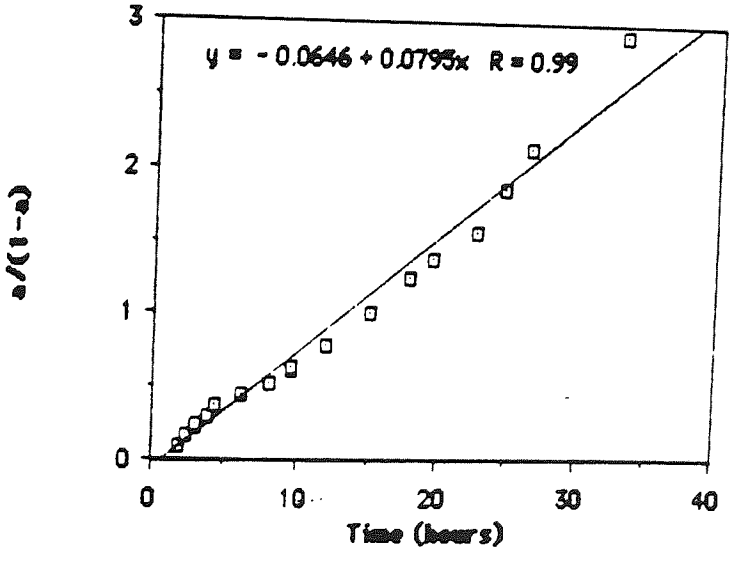

Data for samples 70% BFS, 0.3 w/s ratio cured at 50°c

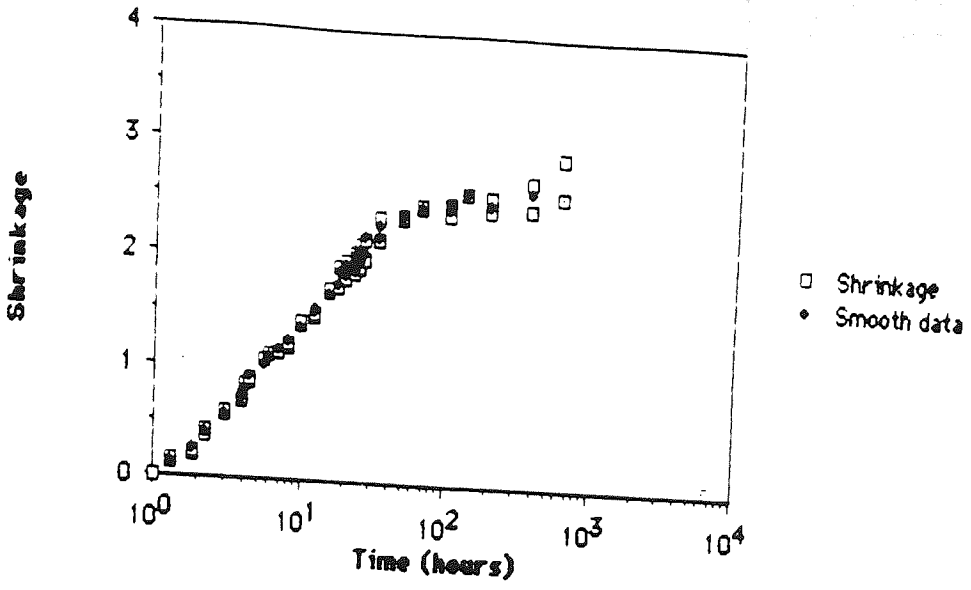

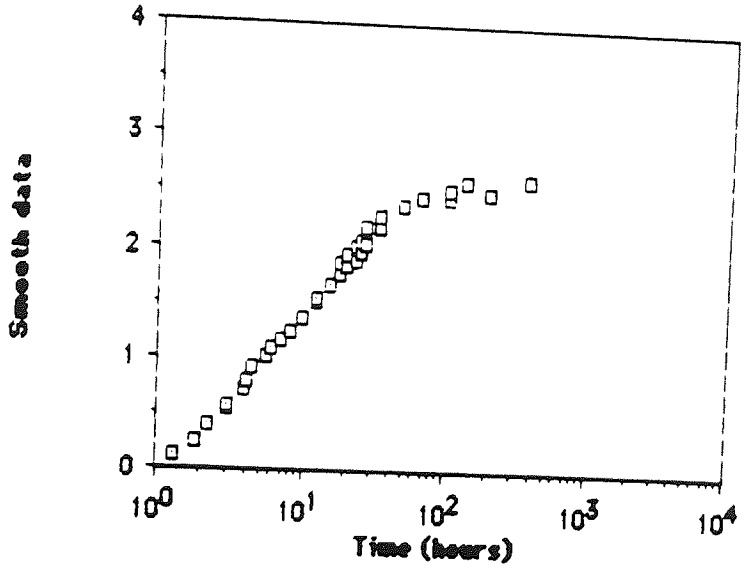

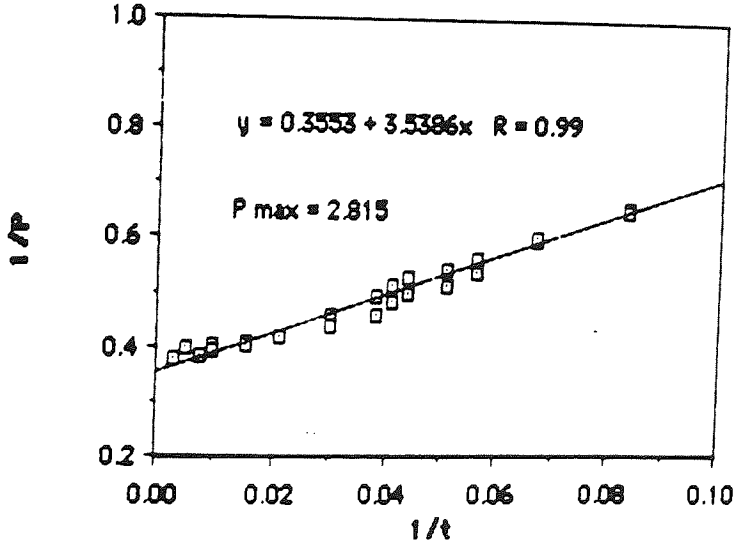

Data for samples 70% BFS, 0.4 w/s ratio cured at 50°c

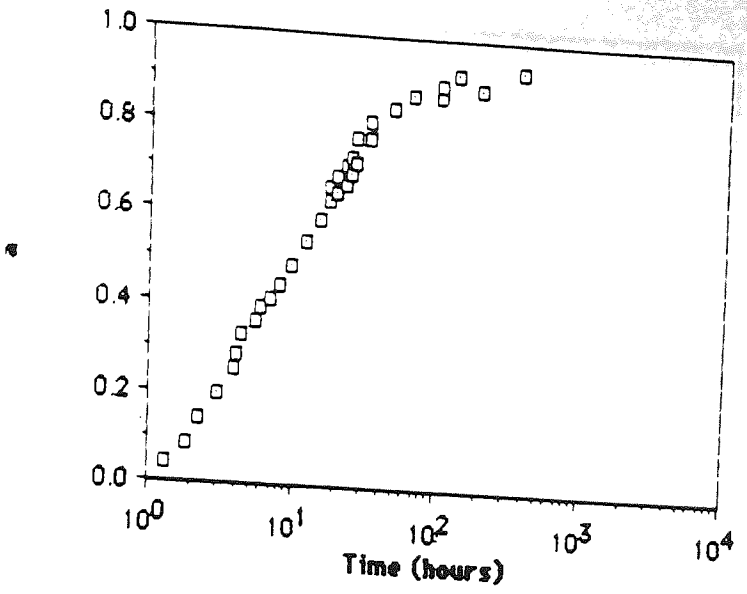

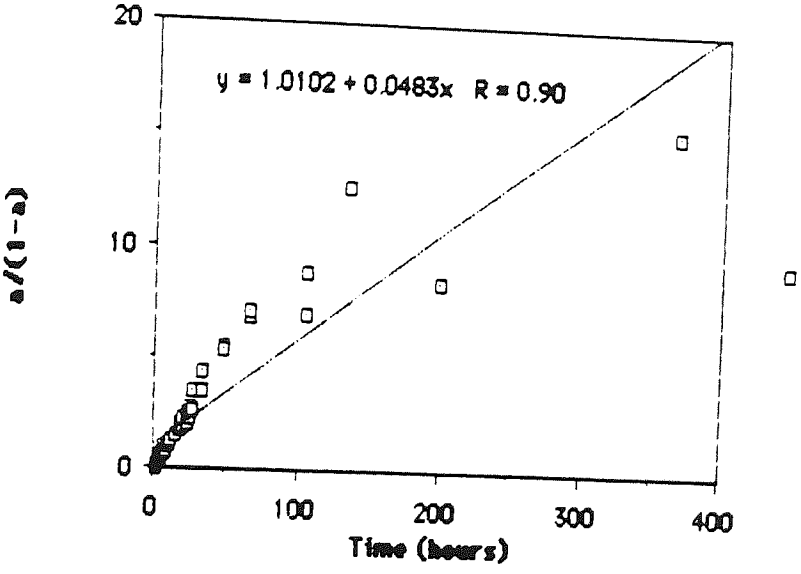

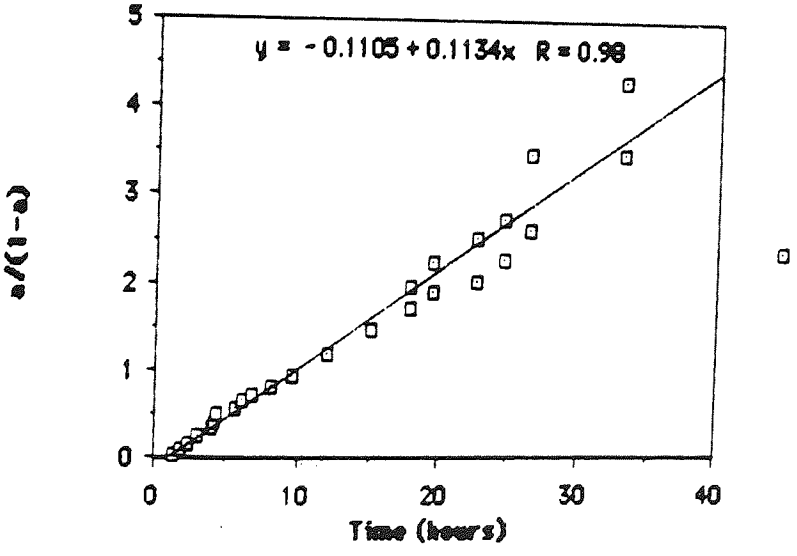

Data for samples 70% BFS, 0.4 w/s ratio cured at 50°c

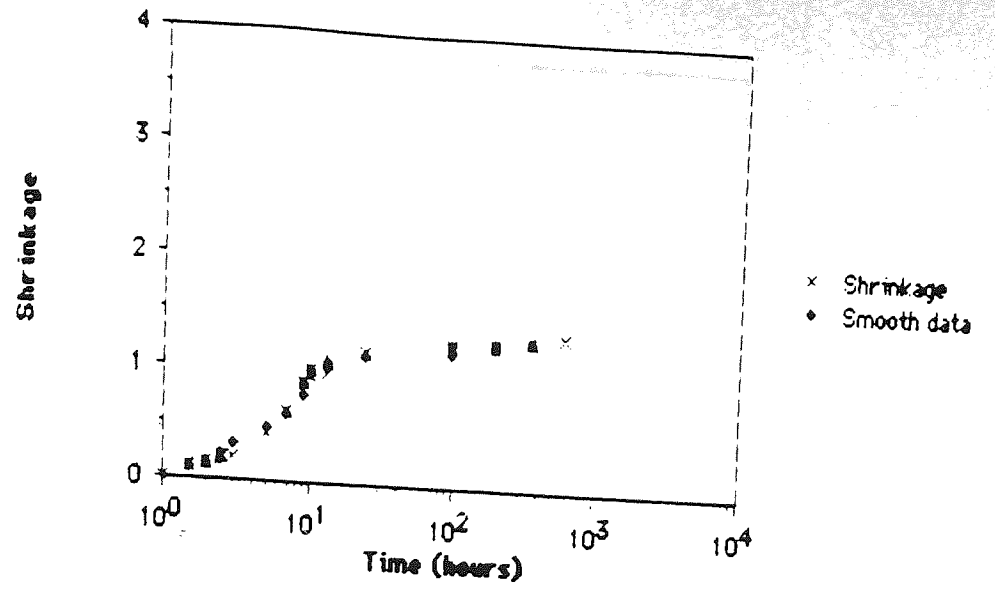

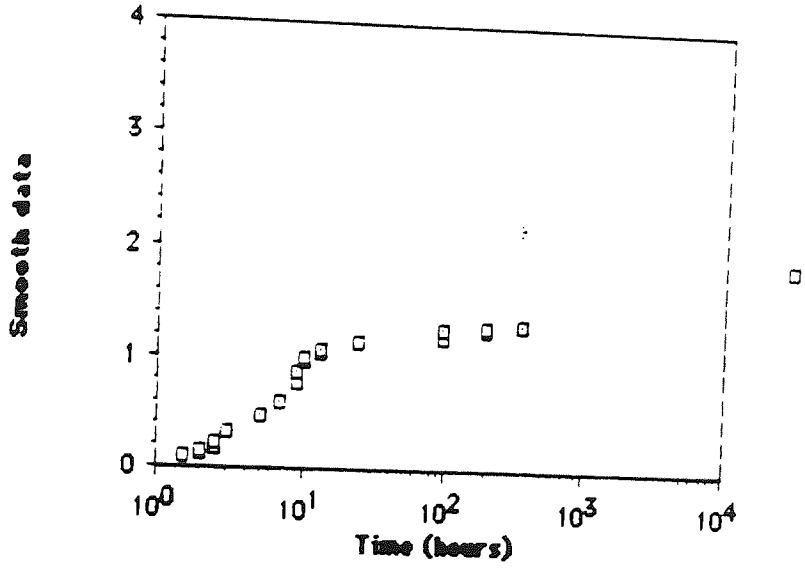

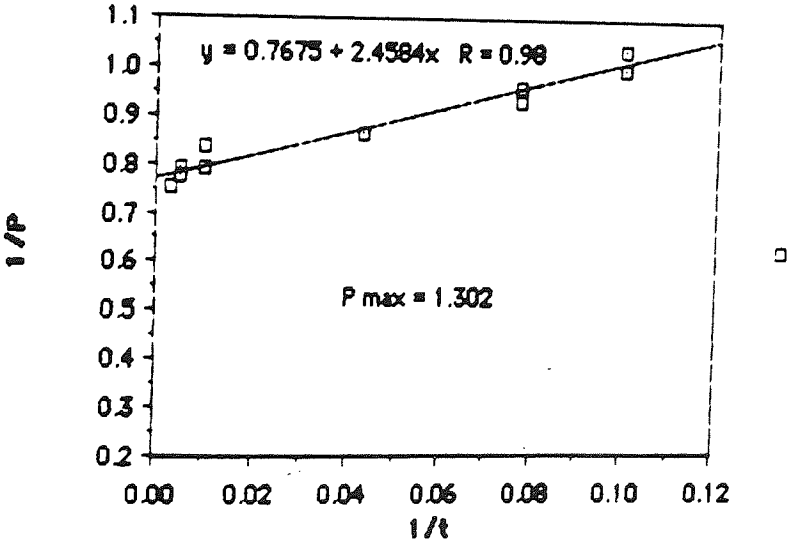

Data for samples 90% BFS, 0.3 w/s ratio cured at 50°c

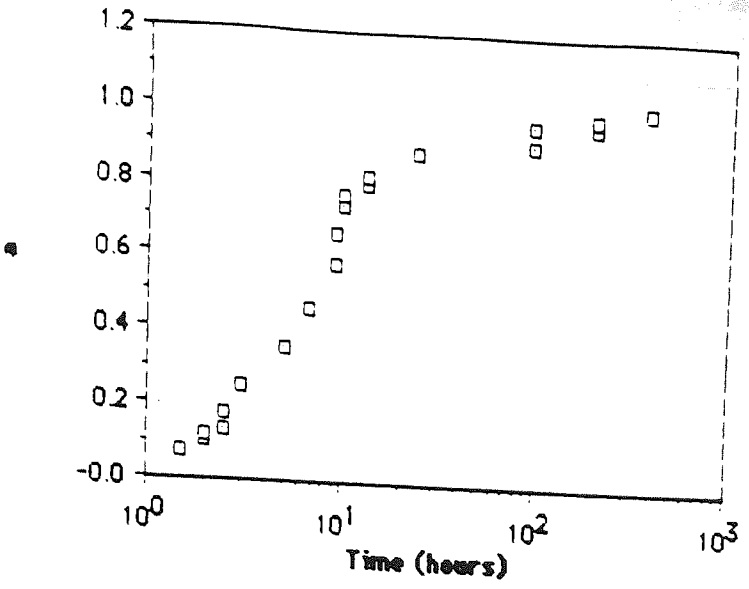

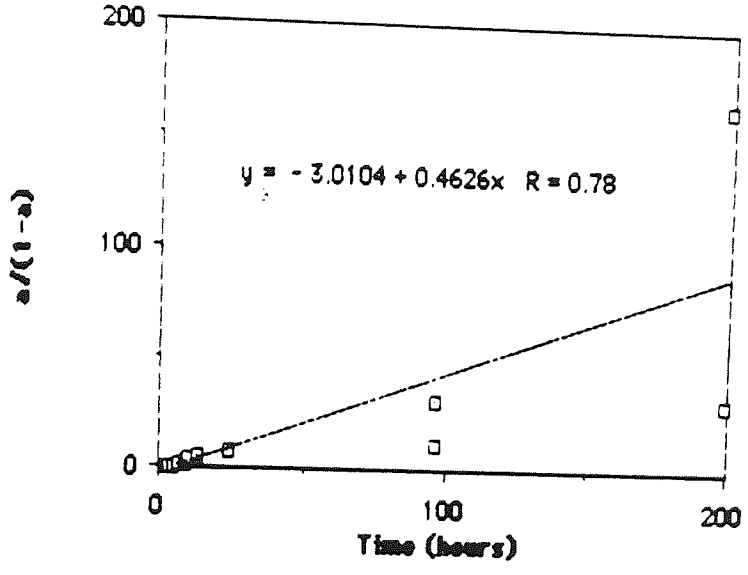

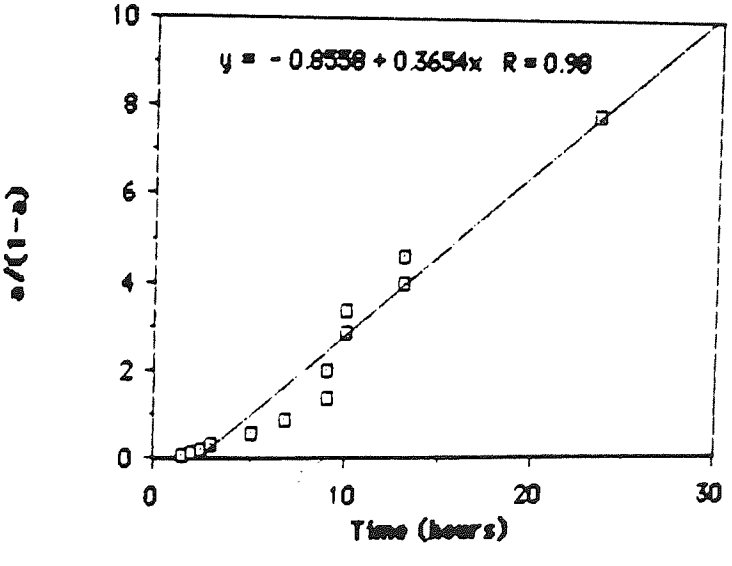

Data for samples 90% BFS, 0.3 w/s ratio cured at 50°c

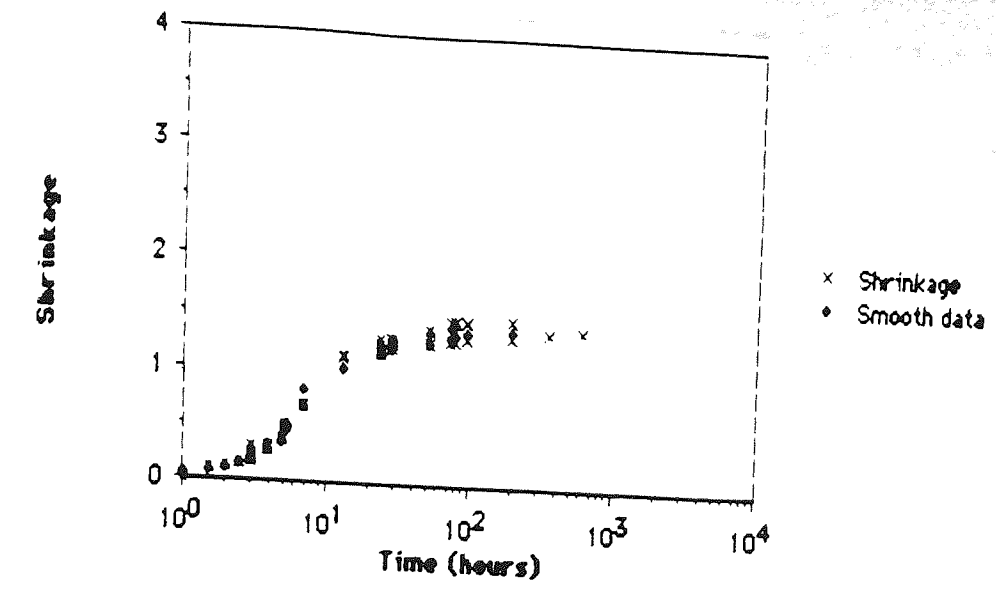

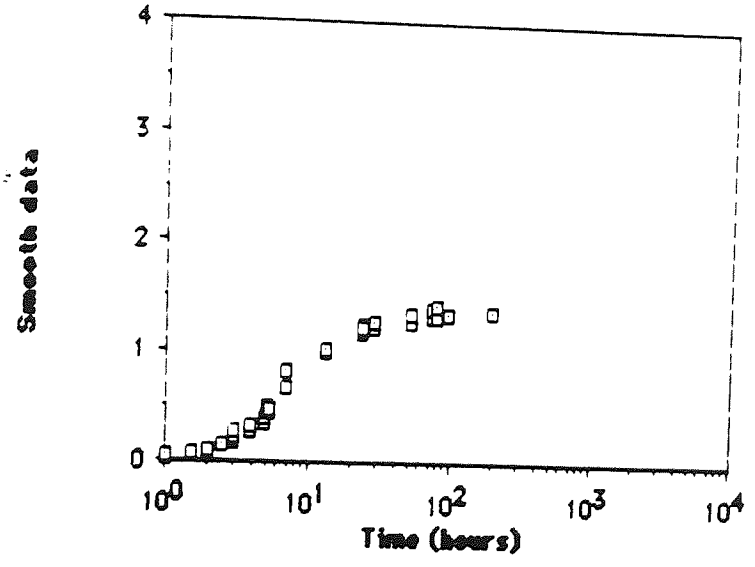

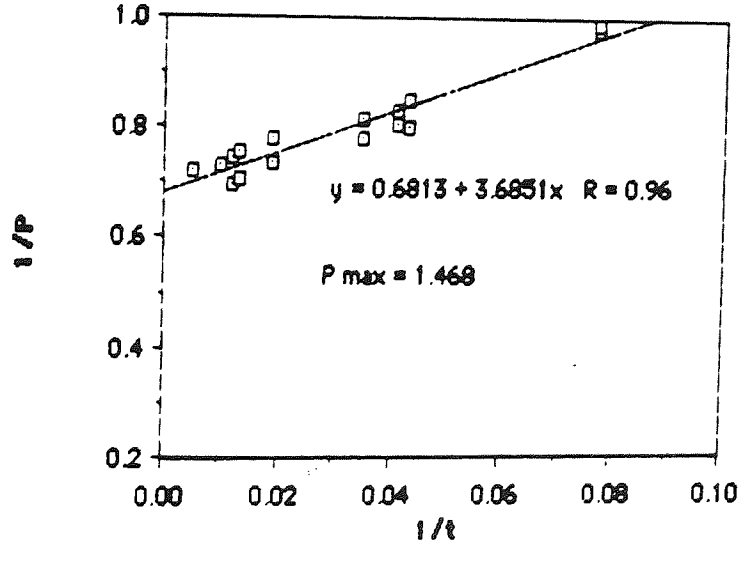

Data for samples 90% BFS, 0.4 w/s ratio cured at 50°c

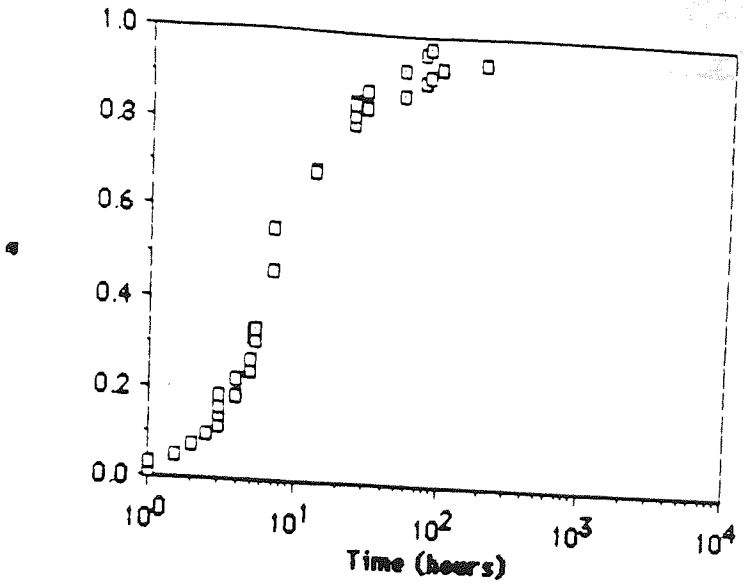

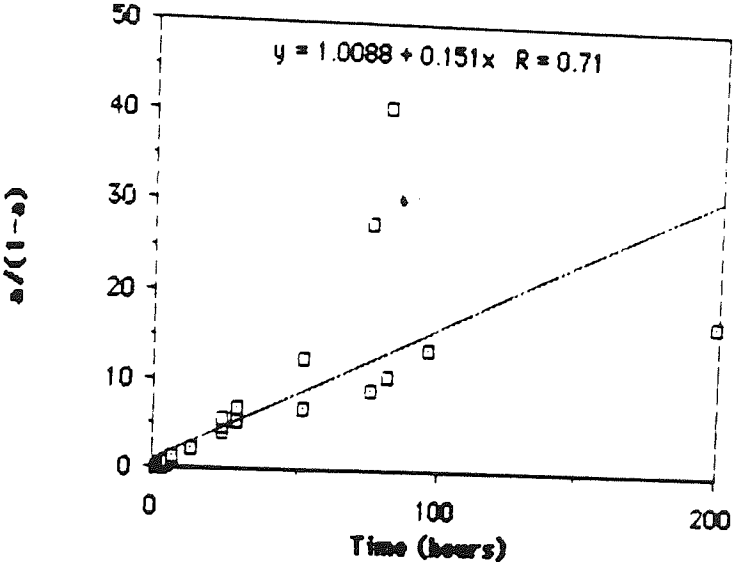

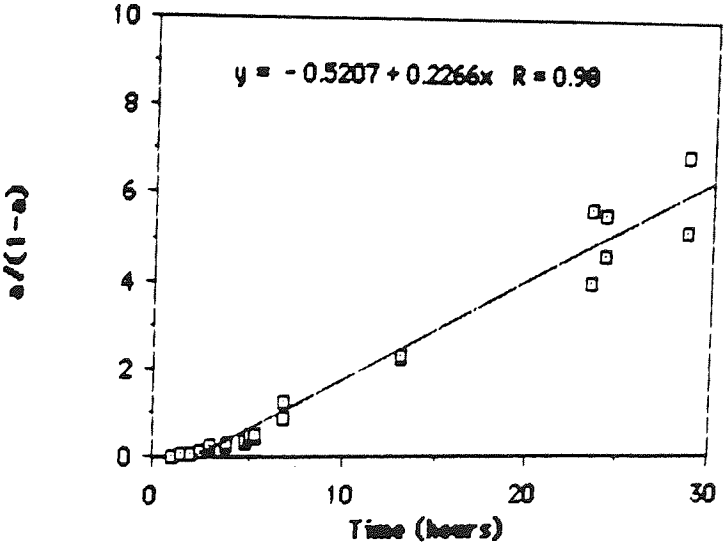

Data for samples 90% BFS, 0.4 w/s ratio cured at 50°c

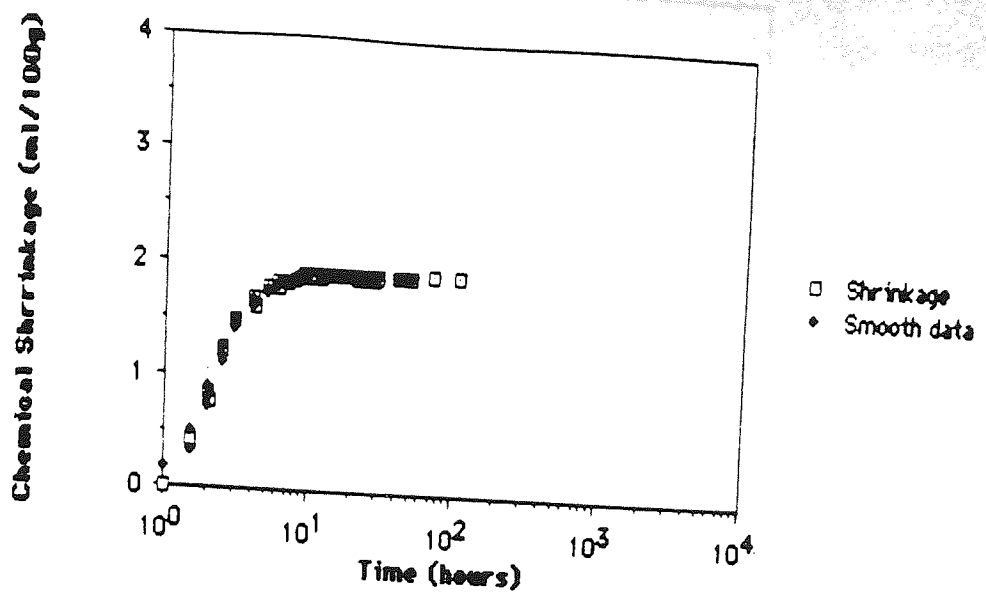

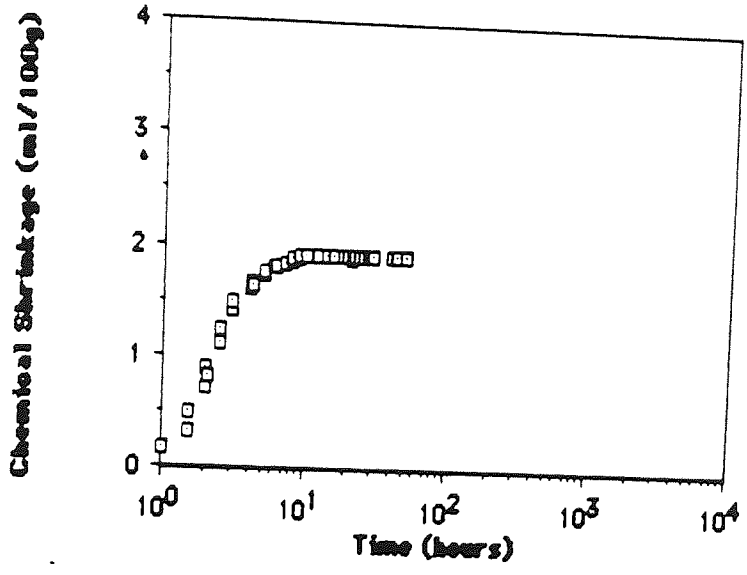

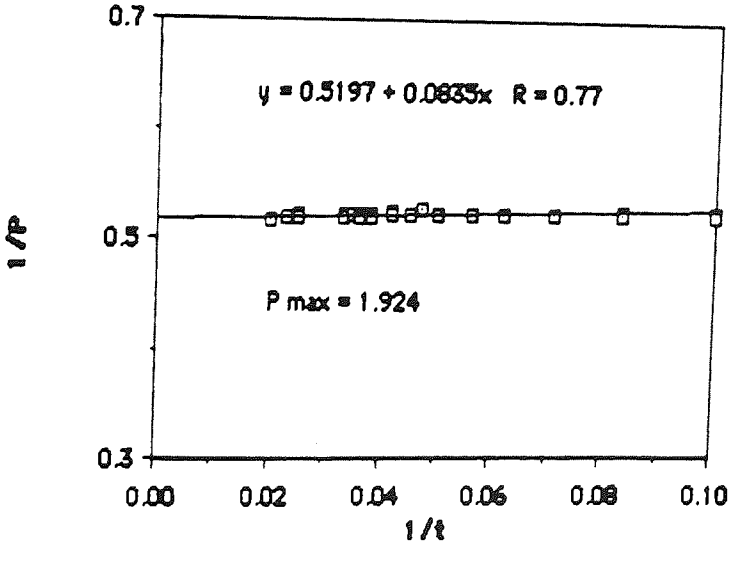

Data for samples 50% BFS, 0.3 w/s ratio cured at 70°c

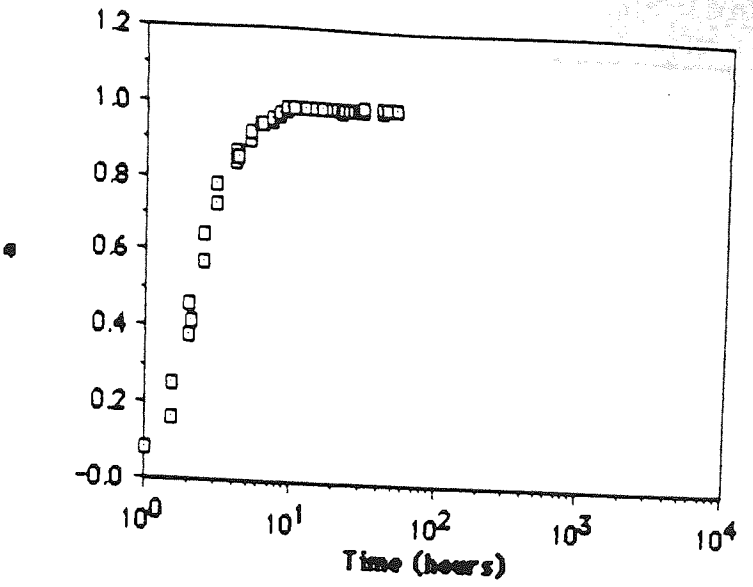

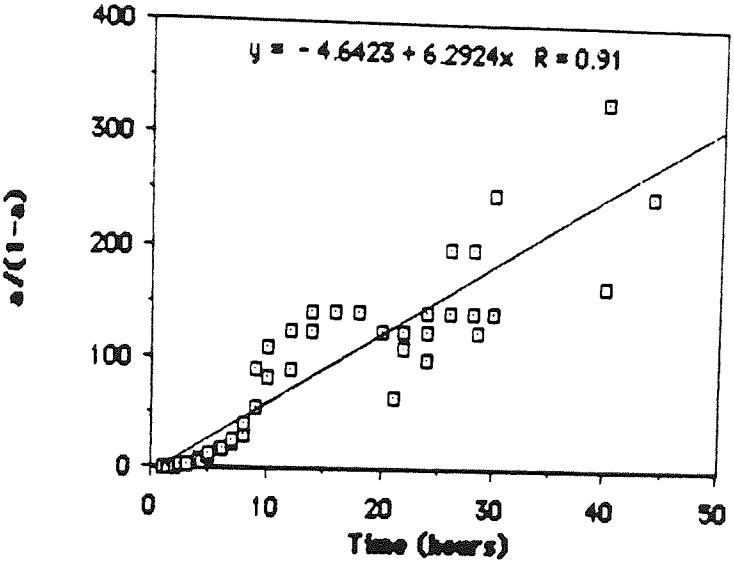

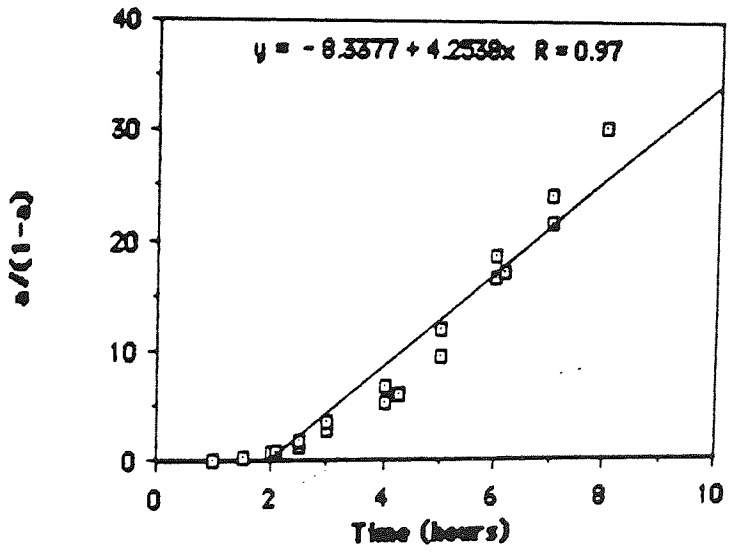

Data for samples 50% BFS, 0.3 w/s ratio cured at 70°c

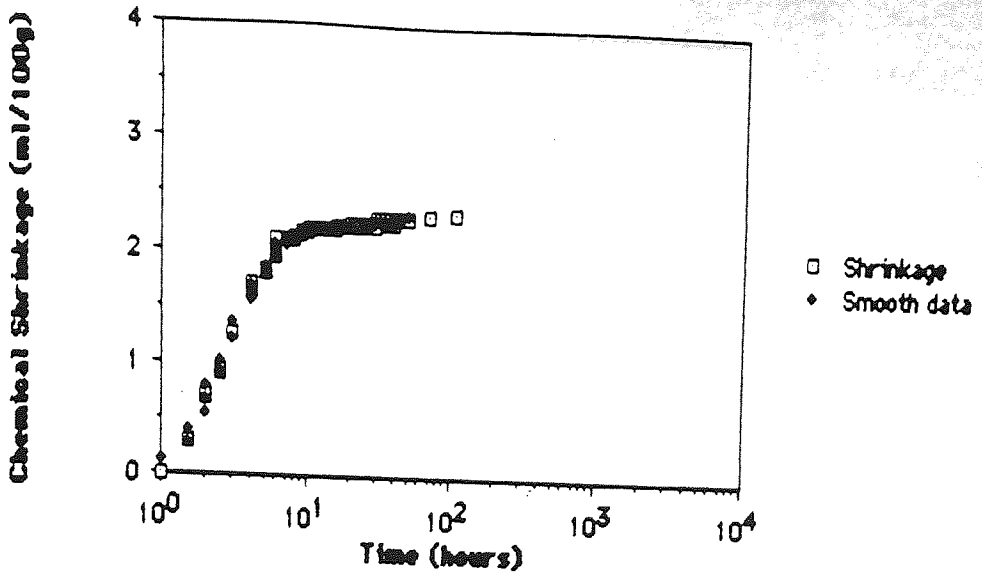

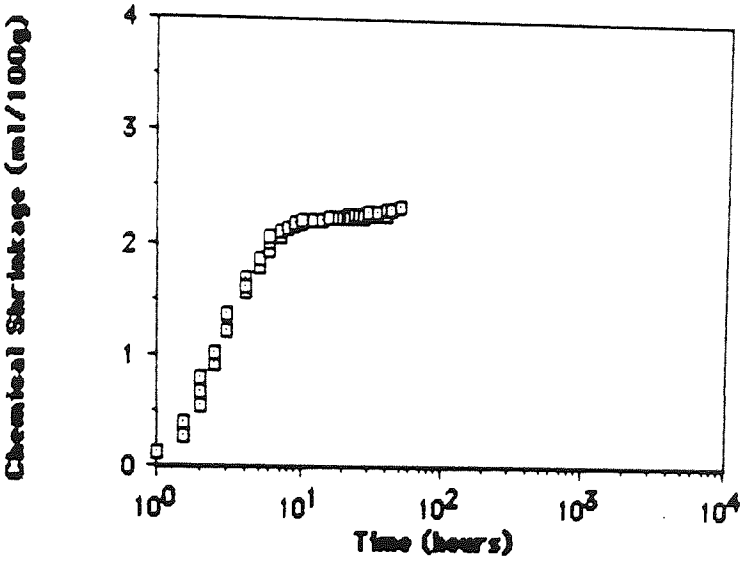

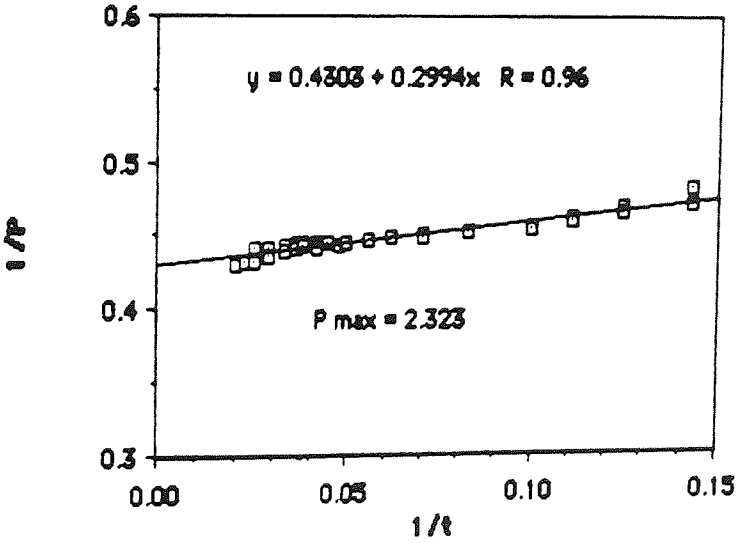

Data for samples 50% BFS, 0.4 w/s ratio cured at 70°c

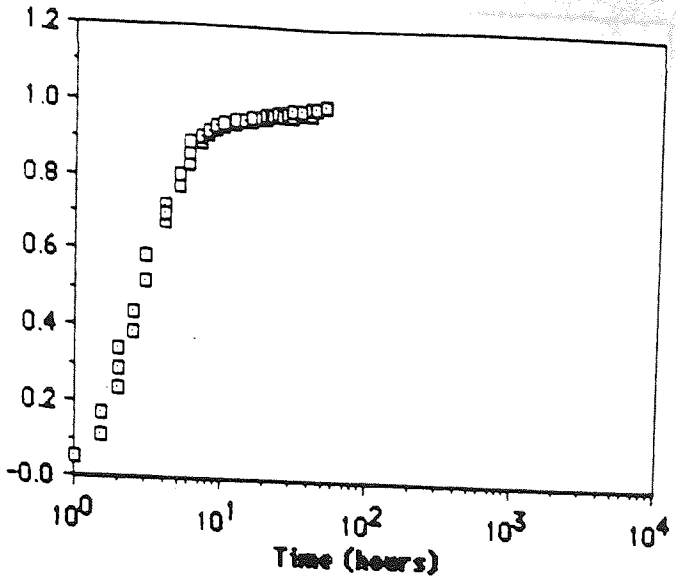

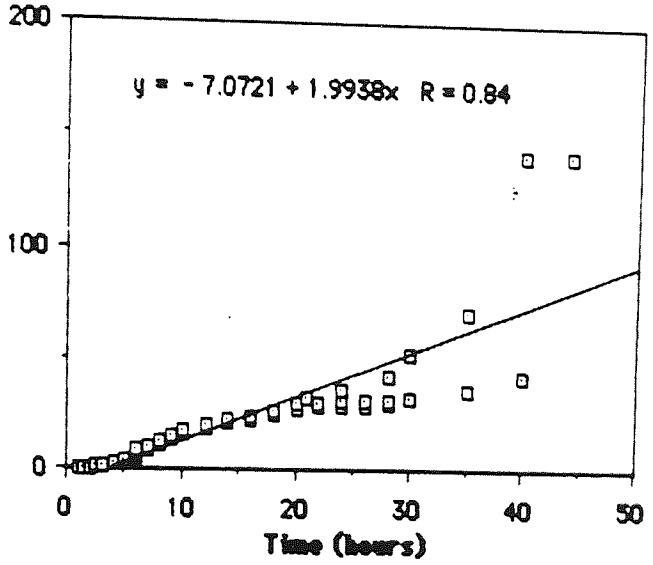

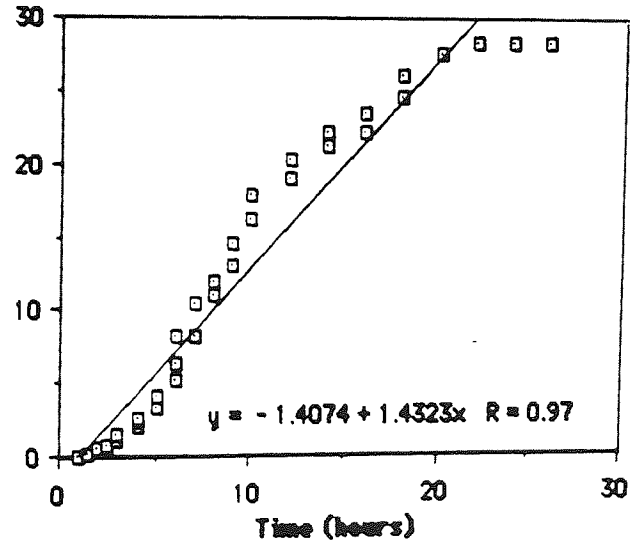

Data for samples 50% BFS, 0.4 w/s ratio cured at 70°c

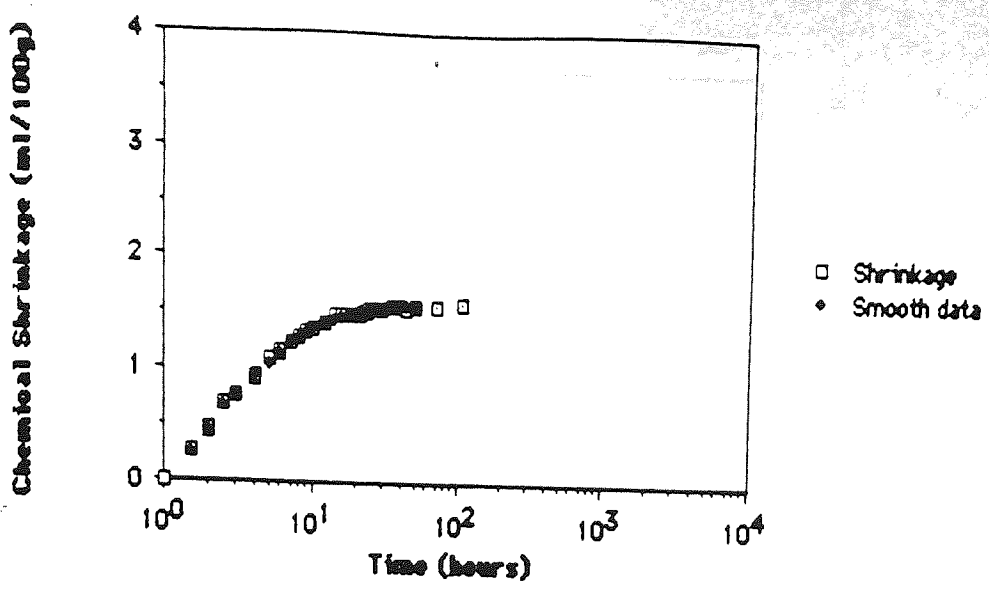

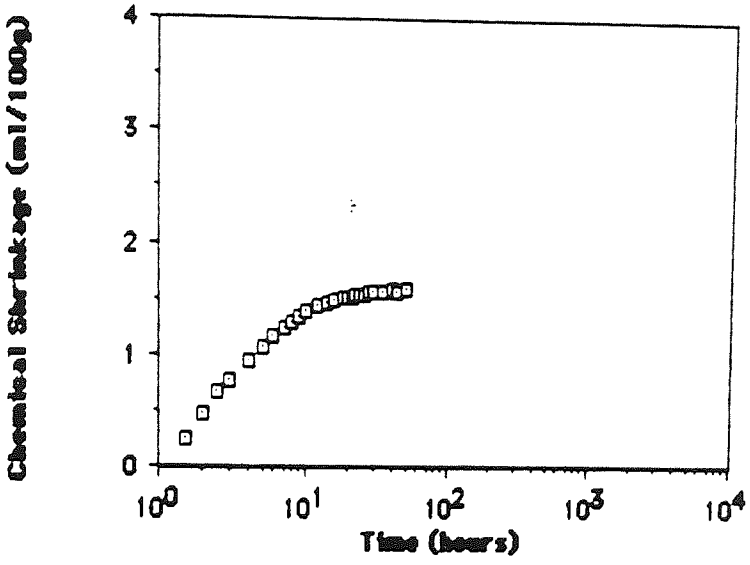

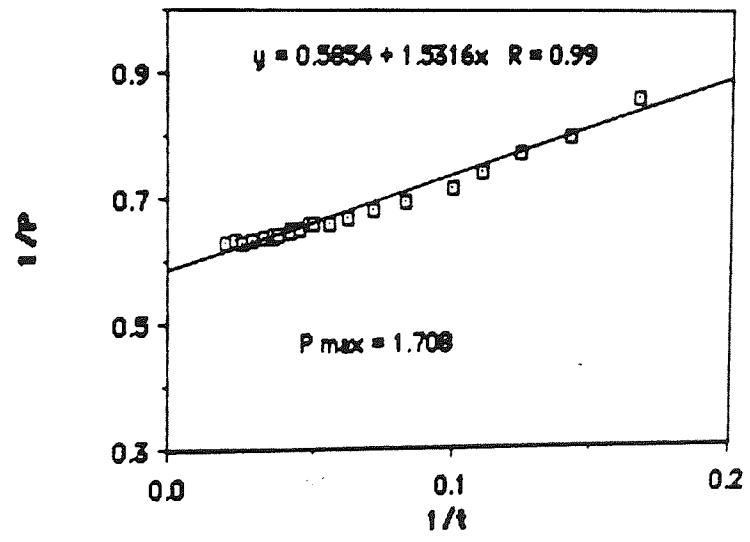

Data for samples 70% BFS, 0.3 w/s ratio cured at 70°c

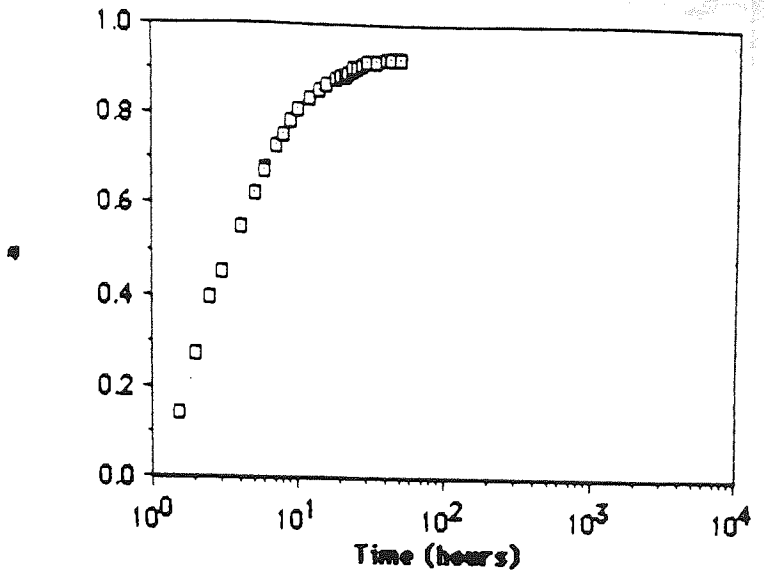

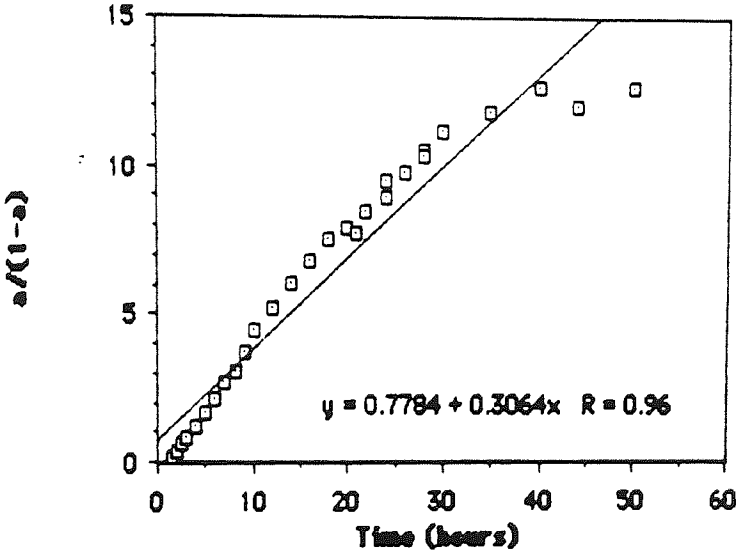

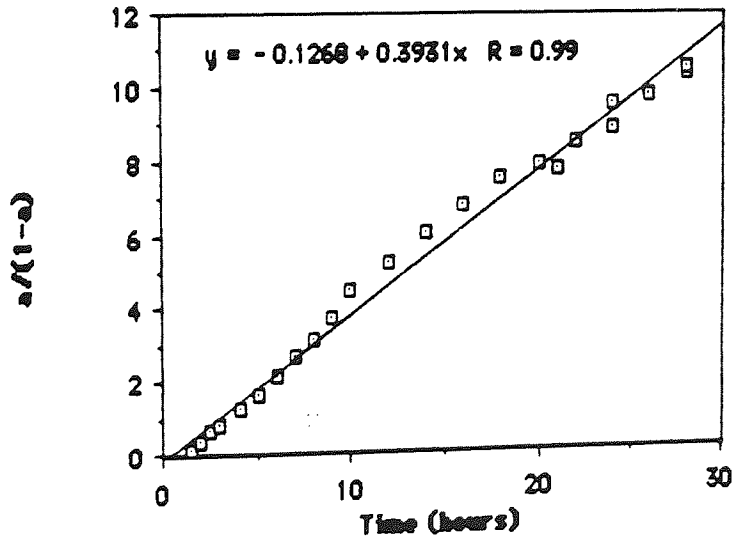

Data for samples 70% BFS, 0.3 w/s ratio cured at 70°c

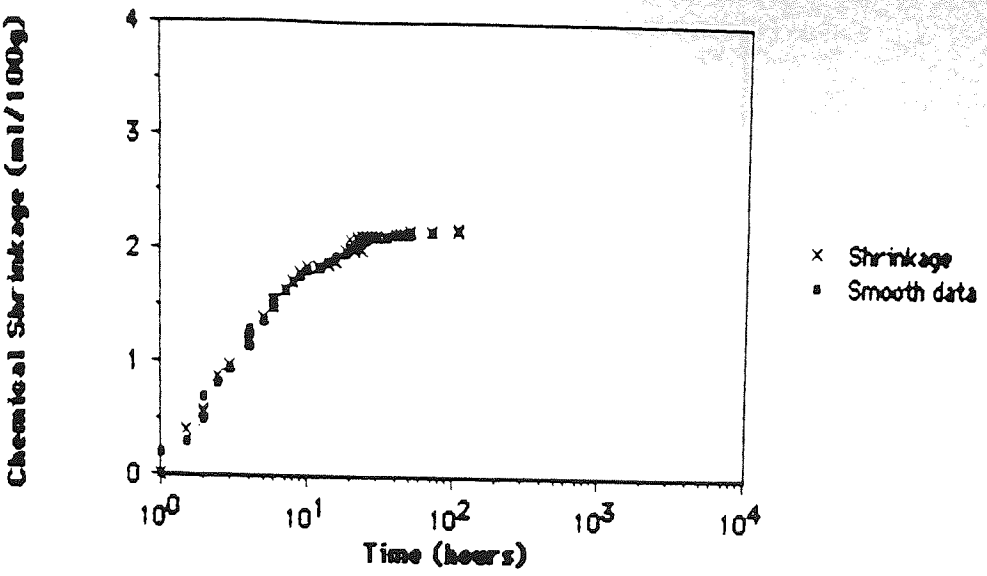

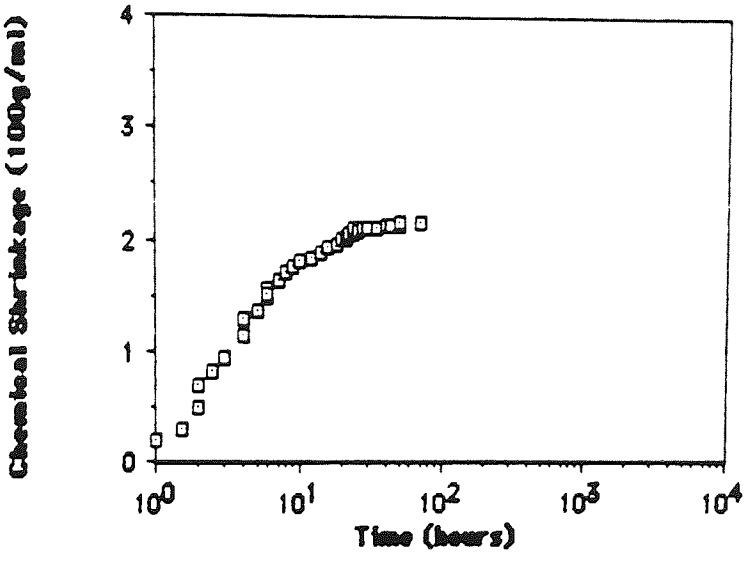

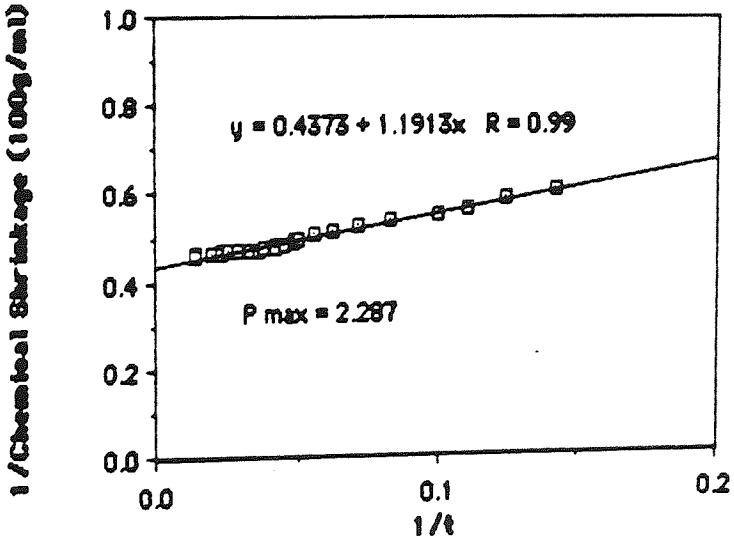

Data for samples 70% BFS, 0.4 w/s ratio cured at 70°c

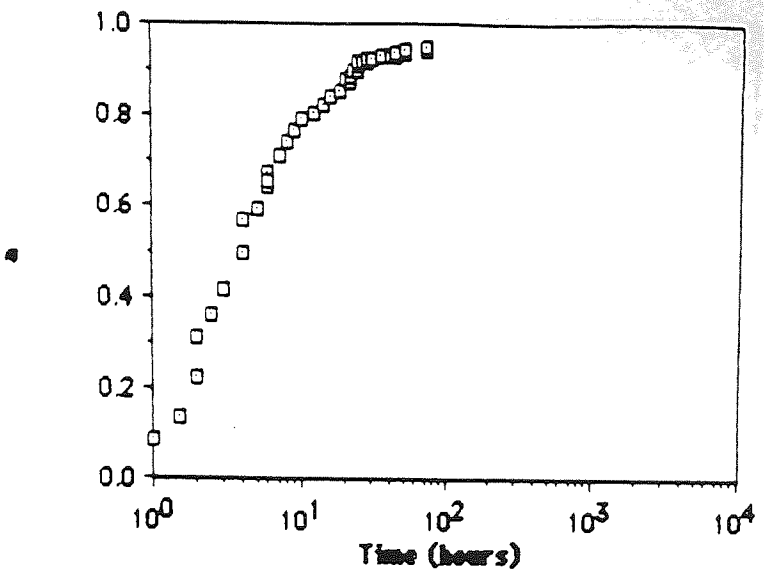

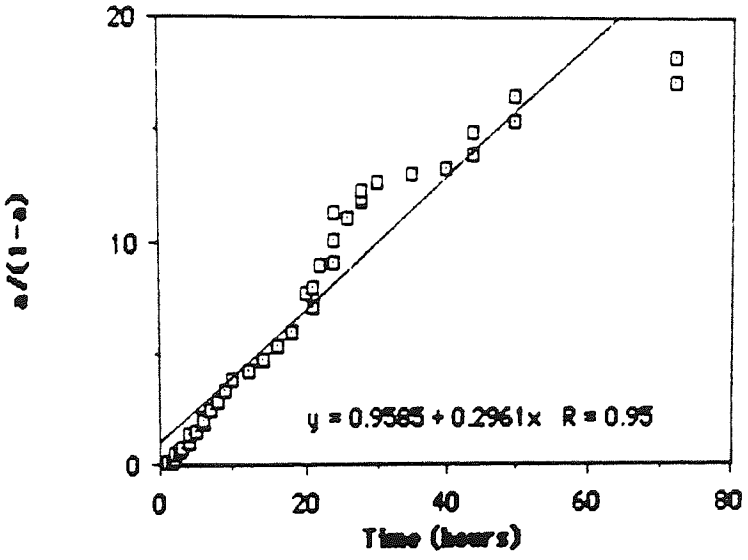

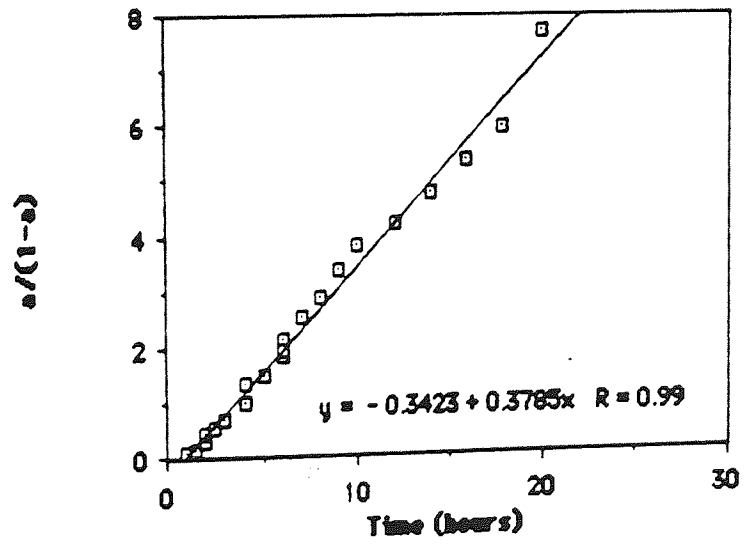

Data for samples 70% BFS, 0.4 w/s ratio cured at 70°c

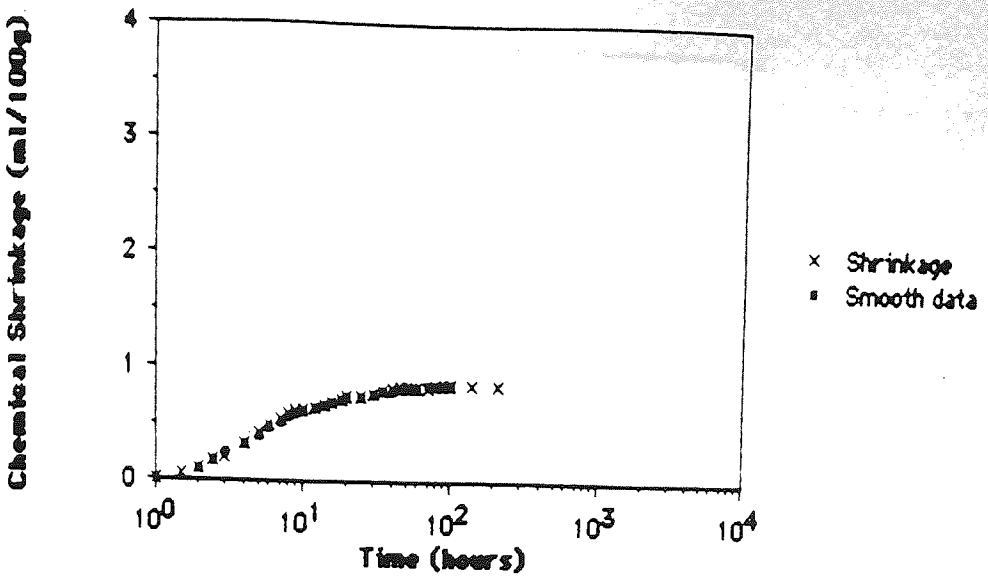

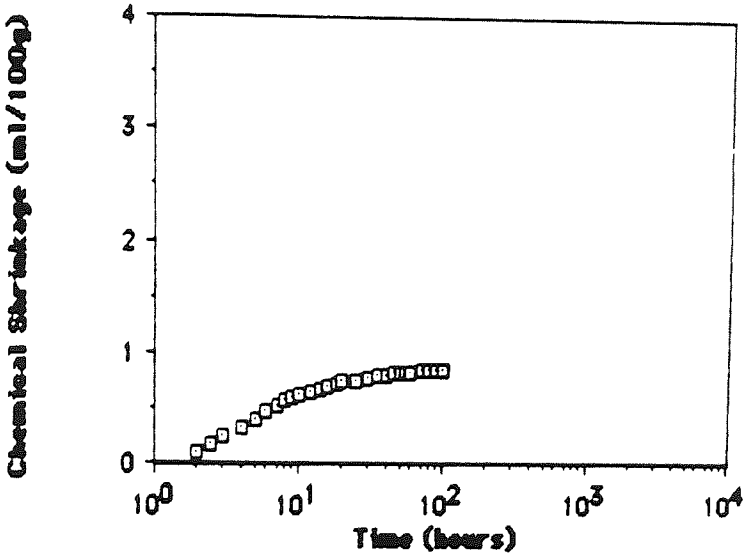

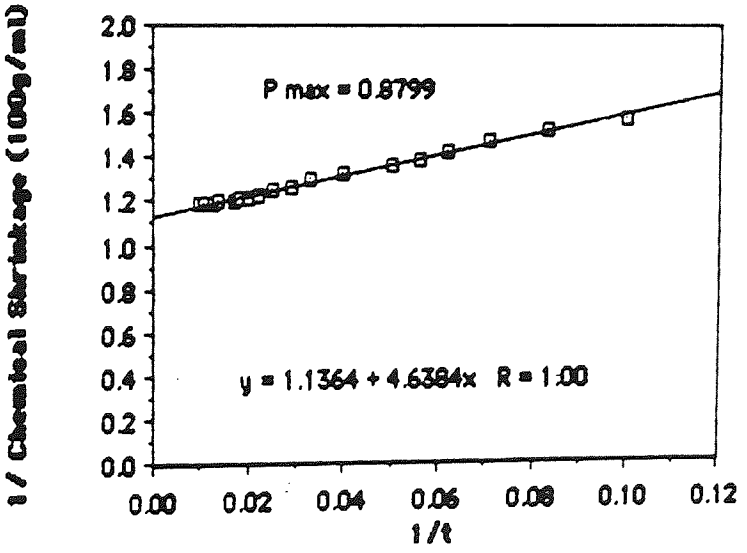

Data for samples 90% BFS, 0.3 w/s ratio cured at 70°c

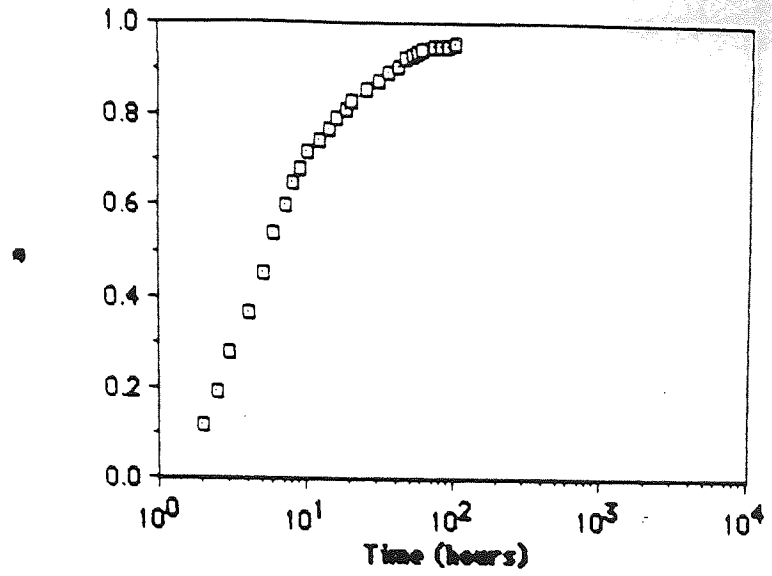

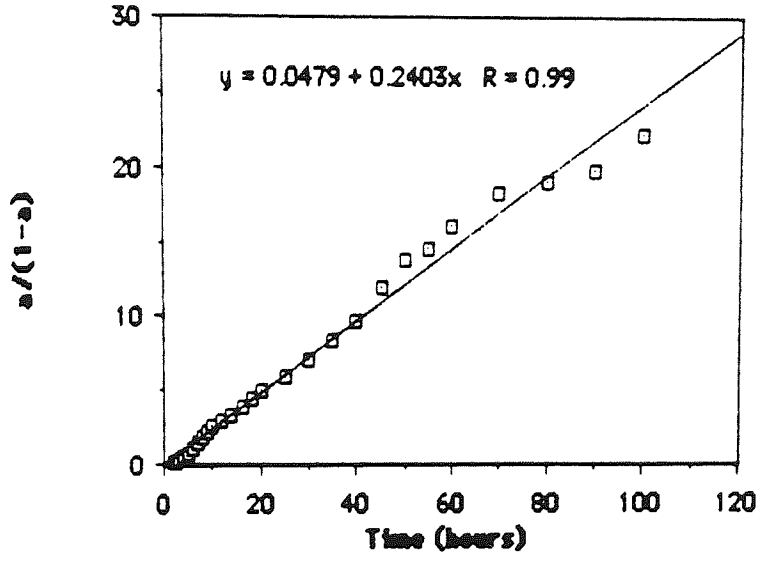

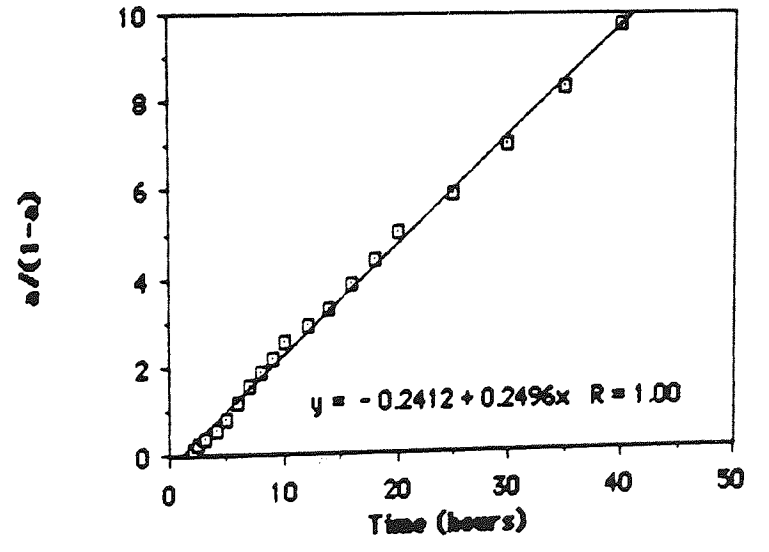

Data for samples 90% BFS, 0.3 w/s ratio cured at 70°c

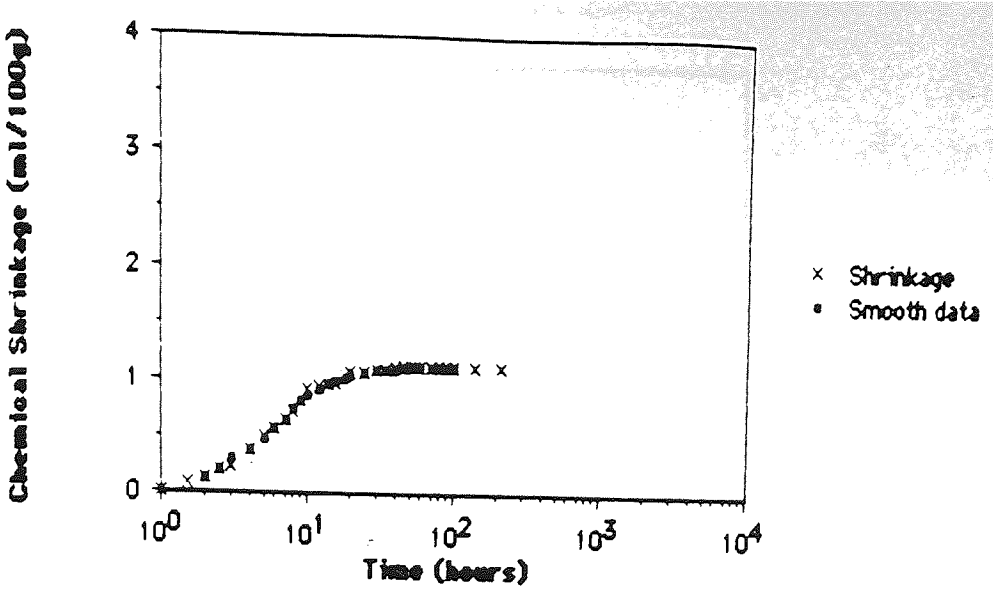

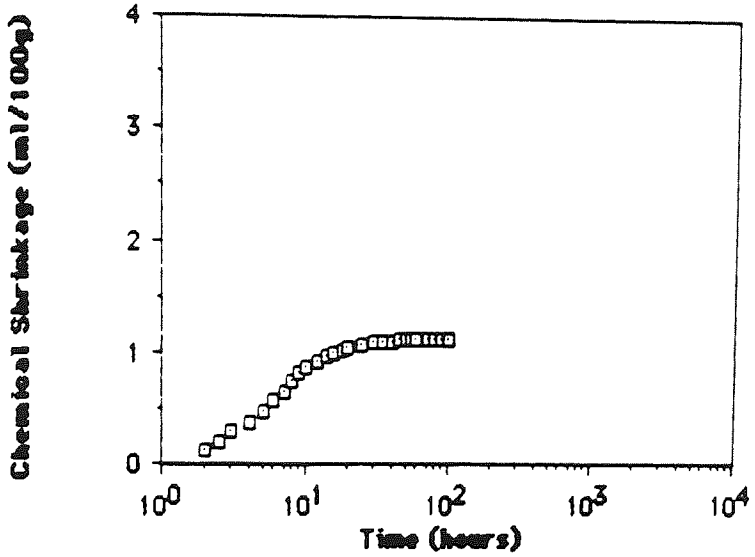

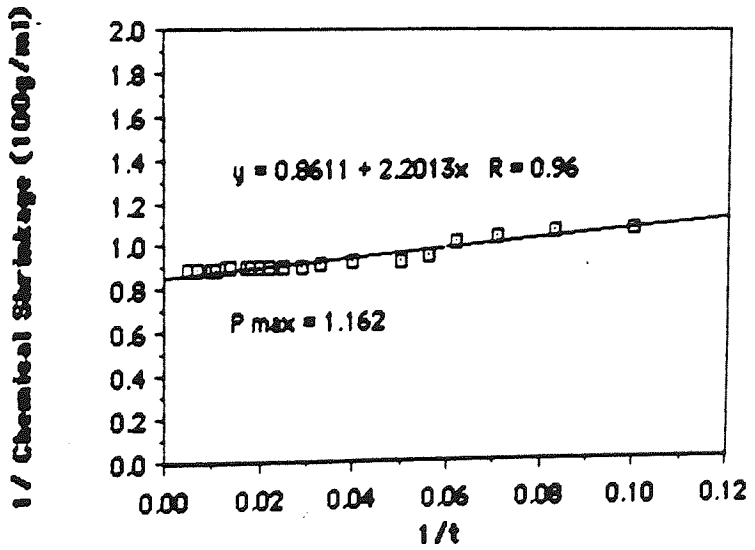

Data for samples 90% BFS, 0.4 w/s ratio cured at 70°c

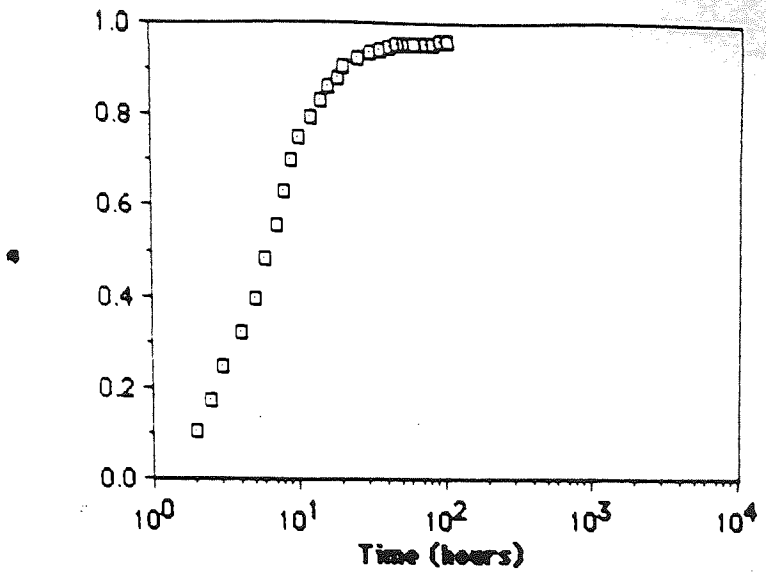

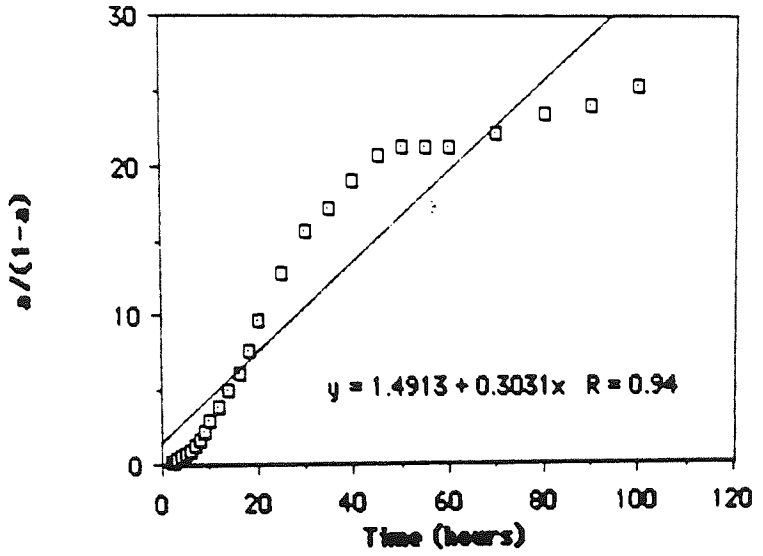

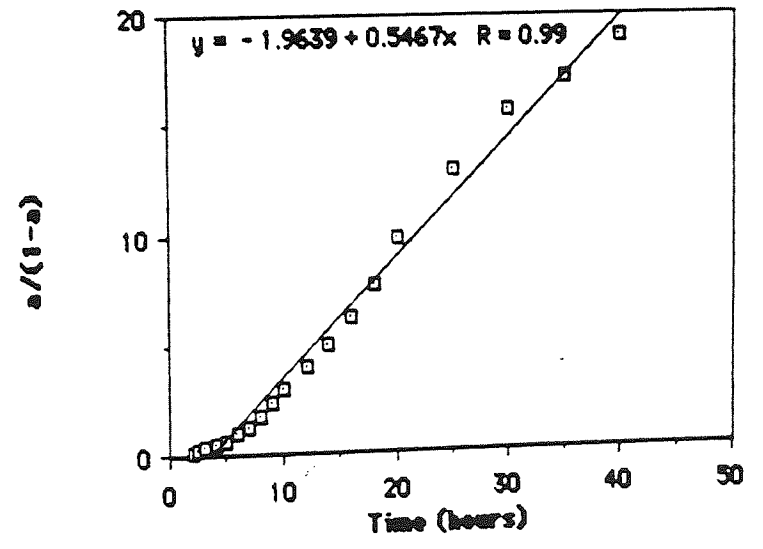

Data for samples 90% BFS, 0.4 w/s ratio cured at 70°c